Anthracene and Aminothiazole Based Organo-Cations Guiding Ionic-Cocrystals, Hydrates of Pyridinedicarboxylic Acids and Selected Metal Complexes

A Dissertation

Submitted in partial fulfillment for the Degree of

Doctor of Philosophy

Submitted by
Abhay Pratap Singh

(Roll No. 196122001)

Thesis Supervisor: Prof. Jubaraj B. Baruah

Department of Chemistry

Indian Institute of Technology Guwahati

Guwahati-781039, Assam, India

December, 2024

TH-3622_196122001

Dedicated to My Parents

And family…

TH-3622_196122001

TH-3622_196122001

Indian Institute of Technology Guwahati

Department of Chemistry

Declaration

I do hereby declare that this thesis entitled "***Anthracene and aminothiazole based organo-cations guiding ionic-cocrystals, hydrates of pyridinedicarboxylic acids and selected metal complexes***" is the outcome of research work carried out by me under the supervision of **Prof. Jubaraj B. Baruah**, at the Department of Chemistry, Indian Institute of Technology Guwahati, India.

In keeping with the general practice of reporting scientific observations, due acknowledgements have been made, and references to the original sources have been cited whenever the work is based on findings by other researchers.

IIT Guwahati
December, 2024

Abhay Pratap Singh
Roll No. 196122001

TH-3622_196122001

TH-3622_196122001

Prof. Jubaraj B. Baruah
Department of Chemistry
Indian Institute of Technology Guwahati
Guwahati, 781039, Assam, India

Phone no. +91-361-258-2311(O)
Fax no. +91-361-269-0762
Email: juba@iitg.ac.in

CERTIFICATE

This is to certify that the research work presented in this thesis entitled "***Anthracene and aminothiazole based organo-cations guiding ionic-cocrystals, hydrates of pyridinedicarboxylic acids and selected metal complexes***" is an authentic record of the results obtained from the research work carried out by **Mr. Abhay Pratap Singh** (**Roll No. 196122001**) under my supervision in the Department of Chemistry, Indian Institute of Technology Guwahati, India. This work is original and has not been submitted elsewhere for a degree or award.

IIT Guwahati
December, 2020

Prof. Jubaraj B. Baruah
(Thesis Supervisor)

TH-3622_196122001

Acknowledgements

I would like to acknowledge all the people who have contributed to this thesis in many ways.

I would like to express my deepest gratitude to my supervisor, **Prof. Jubaraj B. Baruah**, whose invaluable guidance has been a cornerstone of my research journey. I have been profoundly inspired by his vast knowledge, logical acumen, and unwavering support. This thesis would not have been possible without his steadfast encouragement and insightful direction. His mentorship has been a source of immense strength for me. In moments of success, his heartfelt congratulations uplifted me, and in times of failure, his comforting words and encouragement reignited my confidence. As a mentor and guide, he possesses an exceptional ability to illuminate the path forward, solving challenges with remarkable clarity and patience. His kindness, optimism, and tireless dedication have been instrumental in shaping my doctoral studies. I am especially grateful for the countless hours he devoted to my project and his meticulous efforts in bringing this thesis to completion. For all of this and more, I owe him my deepest thanks.

I am highly indebted to "**Indian Institute of Technology Guwahati** and **Ministry of Education (Govt. of India)"** for financial support and resources throughout my tenure.

I would like to acknowledge my sincere gratitude to all my doctoral committee members **Prof. Subhas Chandra Pan**, **Dr. Kalyan Raidongia**, and **Dr. Akshai Kumar A. S.** for their insightful advices and valuable suggestions during progress of my research work.

I am grateful to all faculty members in the Department of Chemistry, IIT Guwahati for their help and encouragement and also the non-teaching staff of the Department for their technical support. I am thankful to the Central Instrument Facility (CIF) and NECBH, IIT Guwahati for various characterization facilities.

- Thanks to, Dr. Kulakamal Senapati, Mr. Aniruddha Gogoi, Mr. Basab Bhattacharjee, Mr. Imdadul Islam, Mr. Diganta Kumar Hira, Mrs. Abhilasha M. Baruah, and other staff for their support at instrumental laboratory during the research work.
- Thanks to, **Dr. Manish Kumar** and MD. Saddam Hussain (BSBE Department) for Antibacterial activity assay.
- I express my sincere thanks to my seniors and lab mates; Dr. Babulal Das, Dr. Munendra Pal Singh, Dr. Rinki Brahma, Dr. Jitendra Nath and Satyendra Verma for their advice, well wishes, encouragement and constant support during the research period at IIT Guwahati.
- I am thankful to my friends; Supriya Singh, Deepak Kumar Prajapati, Sujeet Kumar Gupta, Rameshwar Kumar, Rohitesh Pradhan, Shaurya Rastogi, Manoj Shukla,

TH-3622_196122001

Akshara Bisarya, Dr. Aakash Santra, Abhisek Metya, Amar Kumar, Dr. Paltan Laha, Parminder Singh, Himani Narjinari for constant support and motivation to keep going during the time of downcast. Also, I consider myself lucky and blessed to have some amazing friends at IITG, with whom I have had some of the most amazing moments during my stay at IITG. I would like to name a few, Ravinder Chahal, Dr. Jagnyesh Kumar Satpathy, Sourav Kumar, Maitery Yadav, Vishnu G., Shubhangini Singh, Sreekanth Y., Jagpreet Singh, Avikash Singh, Dr. Jitesh Singh, Harsh Baliyan, Akash Dev Roshan and the list goes on. These are some of the most amazing people, who have given me cherished memories of fun, exploring, and playing cricket together. I am truly grateful to them. The cricket ground at IITG was my sanctuary, where I could escape the routine and release the stresses of research. Therefore, I am thankful to the sports board for providing the necessary resources.

- I would like to acknowledge my teachers; Mr. Devendra Pandey and Mr. Awadhesh Prajapati for their excellent teaching, motivation, love and blessing. I extend my gratitude to Dr. Srikanta Patra and Prof. V. R. Pedireddi for developing my interest towards research.

Finally, my Ph. D. endeavor could not be completed without the endless love, unending support, tolerance and blessings from my family. I wish to express my sincere gratitude to my parents (Mr. Ram Kunwar Singh and Mrs. Sheela Singh), my brothers (Prateek Kumar Singh and Navneet Pratap Singh), sister-in-law (Shivangi Singh) and my sister Sheetal Singh. They are the main soul and inspiration for each and every step that I achieve in my life.

I would like to thank everyone who contributed in some way or the other to the successful completion of this thesis. Your support and encouragement have been essential.

Thank you all for being part of this journey.

TH-3622_196122001

Abstract

The research presented in this thesis is based on the synthesis, structural characterization, and self-assemblies of salts, ionic-cocrystals and hydrates. Series of 2,6- and 3,5-pyridinedicarboxylate ionic-cocrystals were investigated to show newness in their compositions by complete or partial deprotonations. Different multi-component cocrystals with novel photoluminescence properties are demonstrated in the thesis. Multiple numbers of hydrates from different anionic cobalt(II), copper(II), and zinc(II) pyridinedicarboxylate complexes possessing anthracene-based organo-cations and their interconversions are depicted. The focus on the hydrates is to identify their polymorphic and metastable forms, as well as providing in-depth insights into their thermal and spectroscopic characteristics. The contribution highlights diverse non-covalent assemblies formed through weak interactions such as hydrogen bonds, halogen bonds, π-stacking, and chelate-chelate interactions. The study was extended to zinc(II) pyridinedicarboxylate complexes containing sulfathiazolium cations to demonstrate variations in the bioavailability of a drug molecule derived from the same components in each case but with different compositions. The thesis could provide a systematic study to reveal the complexities to have pre-designed synthetic procedures and pointed towards the necessities for case by case study on each assembly formed under slight changes on the crystallization conditions. It has opened scopes for newer avenues to explore assemblies of ionic-cocrystals as well as solvated metal complexes to observe new properties and transformations among the ionic forms within an assembly by stimuli such as concentration gradient or additives. The thesis has five chapters, which included an introduction and analysis results and experimental section.

The introductory chapter 1, describes non-covalent interactions, such as chelate-chelate and π-stacking among ligands that play crucial role in constructing supramolecular assemblies. The emergence of ionic cocrystals has expanded research on molecular recognition and self-assembly. Based on the literature, the scopes of the research was proposed to study metal 2,6-pyridine-dicarboxylate (26pdc) complexes with organo-cations of three ditopic amines, namely 9-N-(3-imidazolylpropylamino)methylanthracene (H**anthraimmida**), N-{(10-chloroanthracen-9-yl)methyl}-3-(1H-imidazol-1-yl)propan-1-amine (**Chloroanthaimmida)** and 4-amino-N-(thiazol-2-yl)benzene sulfonamide (sulfathiazole) were envisaged.

TH-3622_196122001

The chapter 2 explores the synthesis, structural characterization, and photoluminescence properties of ionic-cocrystals formed between Hanthraimmida and Hchloroanthraimmida with 2,6- or 3,5-pyridinedicarboxylic acid (pdc), highlighting the influence of different pdc isomers on self-assembly and hydrogen bonding interactions. Hanthraimmida formed various ionic-cocrystals and salts with interesting compositions. One such example, $2[(H_3anthraimmida)^{2+}][(26pdc)^{2-}\cdot 2(H26pdc)^{-}]\cdot(H_226pdc)\cdot CH_3OH$, demonstrated a unique assembly containing neutral, mono-ionic, and di-ionic forms of 26pdc linked via hydrogen bonds. Another, $[(H_3anthraimmida)^{2+}][(35pdc)^{2-}]\cdot 4H_2O$, exhibited encapsulated water clusters formed by hydrogen bonding networks. Additionally, ionic-cocrystals with resorcinol showed diverse structural formations, including one where ditopic Hanthraimmida stabilized an anionic template with resorcinol and water, and another featuring two resorcinol guest molecules; one stabilizing the ionic assembly and the other encapsulated within it indicating potential for multi-component system design. Similarly, Hchloroanthraimmida formed salts and ionic-cocrystals with distinctive structural characteristics. As an example, $[(H_2chloroanthraimmida)^{2+}][2(H35pdc)^{-}]\cdot 4H_2O$, displayed hydrogen-bonded chain-like water arrangements. Moreover, ionic-cocrystals with 1,4-diiodotetrafluorobenzene (IFbenz) revealed charge-transfer interactions between the chloroanthracenyl ring and the π-clouds of IFbenz, alongside notable N…I halogen interactions and Z-shaped cationic arrangements. Photoluminescence studies further demonstrated that certain salts exhibited dual fluorescence emissions due to the presence of different ionic species within the structures.

In chapter 3, the hydrates of H_3anthraimmida cobalt, copper, and zinc-26pdc complexes were presented. Three cobalt hydrates $[(H_3anthraimmida)Co(26pdc)_2]\cdot 4H_2O$, $[(H_3anthraimmida)Co(26pdc)_2]\cdot 4.5H_2O$ and $[(H_3anthraimmida)Co(26pdc)_2]\cdot 2H_2O\cdot 2CH_3OH$ were presented. Similarly, two polymorphs of $[(H_3anthraimmida)Cu(26pdc)_2]\cdot 4.5H_2O$ were formed under different crystallization conditions along with intermediate methanol solvate, $[(H_3anthraimmida)Cu(26pdc)_2]\cdot 2.5H_2O\cdot 2CH_3OH$, quickly converted to the stable form. In the case of zinc hydrates, two forms $[(H_3anthraimmida)Zn(26pdc)_2]\cdot 4H_2O$ and $[(H_3anthraimmida)Zn(26pdc)_2]\cdot H_2O\cdot 1.5CH_3OH$ exhibited transformations due to reductions in unit cell volume. Fluorescence studies further revealed aggregation-induced emission enhancement upon water addition, which correlated with π-stacking modifications. Overall, this chapter highlights the structural diversity, self-assembly, and interconversion of metal-organic

TH-3622_196122001

hydrates, emphasizing the role of hydrogen bonding, π-stacking, and electrostatic interactions in determining their stability and transformation mechanisms.

The chapter 4 has the crystallization and structural studies of cobalt(II), copper(II), and zinc(II) 2,6-pyridinedicarboxylate (26pdc) complexes. Two types of hydrates were observed for cobalt and copper, while zinc formed only a stable hydrate. In the case of cobalt hydrates, the metastable form crystallized in a triclinic $P\bar{1}$ space group as a methanol-water solvate, while the stable form adopted a monoclinic C2/c space group as a pentahydrate. These two forms underwent reversible transformation upon recrystallization. The copper hydrates showed reversible transformations driven by solvent interactions. Overall, the study demonstrated that a chloro-substitution reduced the number of hydrates than the unsubstituted cation by minimizing Cl...Cl and C-H...Cl repulsions.

The chapter 5 explores the modulation of sulfathiazolium (HSTZ) cations in different 2,6-pyridinedicarboxylate complexes, focusing on four distinct structures. The first, a salt $[(HSTZ)(H26pdc)]\cdot 0.5H_2O$, was formed by mixing 2,6-pyridinedicarboxylic acid ($H_2$26pdc) with sulfathiazole in methanol, driven by their pKa differences. The second structure, a zinc complex $(HSTZ)[Zn(H26pdc)(26pdc)]\cdot 2H_2O$, was synthesized using zinc(II) acetate with $H_2$26pdc in the presence of HSTZ. Additionally, two ionic-cocrystals were obtained by reacting $(HSTZ)[Zn(H26pdc)(26pdc)]\cdot 2H_2O$ with resorcinol or 3-nitrophenol, stabilizing the $[Zn(26pdc)_2]^{2-}$ species through aromatic stacking and hydrogen bonding. Overall, this chapter highlights the critical role of self-assembly in controlling drug proportions and underscores its potential applications in targeted drug delivery.

The experimental section is provided at the end of each chapter. The spectra and the crystal parameters along with CCDC numbers are listed in appendices. The thesis is concluded with a summary and list of published papers from the research.

TH-3622_196122001

Table of Contents

TH-3622_196122001

TH-3622_196122001

TH-3622_196122001

ABBREVIATIONS

DNA: Deoxyribonucleic acid

Cp: Cyclopentadienyl

NMR: Nuclear magnetic resonance

API: Active Pharmaceutical Ingredients

ICCs: Ionic-cocrystals

CH_3CN: Acetonitrile

DMF: Dimethyl formamide

POMs: Polyoxometalates

DMSO: Dimethyl sulfoxide

AIE: Aggregation induced emission

THB: Trihydroxy benzene

Å: Angstrom

DFT: Density functional theory

H_2O: Water

DSC: Differential Scanning Calorimetry

TGA: Thermo-gravimetric analysis

DLS: Dynamic light scattering

EtOH: Ethanol

ESIPT: Excited state intramolecular proton transfer

FESEM: Field emission scanning electron microscope

FRET: Forster resonance energy transfer

HOMO: Highest occupied molecular orbital

FTIR: Fourier Transform Infrared

LUMO: Lowest unoccupied molecular orbital

MeOH: Methanol

µM: Micromolar

CIF: Crystallographic Information File

TMS: Tetramethylsilane

PET: Photo-induced electron transfer

TH-3622_196122001

ESI-MS: Electrospray Ionization Mass spectrometry

EPR/ESR: Electron Paramagnetic Resonance/ Electron Spin Resonance

UV-vis: Ultraviolet-visible

TH-3622_196122001

Chapter 1

Introduction

1.1. Self-assemblies

Functional behavior of life is based on an assembled unit functioning with synergy, allowing progress and performance at a time scale required for life.[1] The collective properties associated from macroscopic level connected with statistics have provided the correlation of the properties from microscopic to macroscopic level.[2] Assembling from atomic and molecular level have provided understandings of material properties.[3] Similarly, the colligative properties of molecules originate from same or different kinds of molecules interacting in collective manner. On the other hand, self-assemblies of polymeric materials have contributed to new properties[4] corroborating to nano-dimension. The classical self-assembling processes were envisaged through examples such as proteins,[5] nucleic acids,[6] and all kinds of biomolecules. These have helped in medical forensic sciences significantly. The emergence of composites as applied materials their activities in various facets have ensured the necessity to study self-assemblies as future materials. Starting from water harvesting,[7] purification,[8,9] water splitting,[10] hydrogen productions,[11] fertilizers,[12] drug delivery[13] and as materials with novel properties,[14] they have necessitated exploring self-assemblies. In these directions, the hybrid composites of inorganic and organic materials have shown urgency to look at the discrete features contributing to properties. The self-assemblies constructed with non-covalent interactions provide reversibility from reconstructions. These have been the boon of the biological sciences.[15,16] Many synthetic supramolecular assemblies used as biological models are inspired by natural systems. In the last century, It has seen a tremendous boom on the assemblies with non-covalent interactions. In inorganic chemistry, limitations in multiple possibilities from the metal and ligands tendency to provide or build modified supramolecular architectures from the parent ion or ligand provide challenges to targeted design of assemblies. The lower yield, purification processes and having larger difference in properties in solution than in solid state possess difficulties in their studies. To deal with weak metal–ligand interactions than stable covalent bonds of carbon compounds the equilibrium and energetic gets higher priority. The weak interactions in inorganic complexes sets multiple paths to reduce selectivity in target product. So there is need to identify mesoscopic supramolecular structures inorganic assemblies to take

TH-3622_196122001

advantages of weak metal bonds to design new inorganic assemblies. In the following section the selected aspects of non-covalent assemblies are introduced.

1.2. Non-covalent assemblies

The non-covalent assemblies are systematic ensemble of one or more components of molecules or ions or reactive species formed by non-covalent interactions.[17]Each self-assembly has systematic directional arrangements and are with own replicating signature. These signatures are the replica as assembling units and are generally used to describe the assembly as well as replicating properties.[18]The physical properties of self-assemblies are guided by their structures and in general, these are much different from their parent discrete units. Many properties of host molecules are modulated by guest via conformational changes. The principal component of a supramolecular assembly providing the space to accommodate another smaller or relataively same sized molecule through corresponding shape, size and electronic requirement are termed as host.[44-46] They serve as the pivotal point to guide the directionality of a self assembly. Hydrogen bond is one of the most important weak interactions that contribute to supramolecular host-guest self-assemblies. There are various types of hydrogen bonds classified based on the energy varying from 4 to 120 kJ/mol as weak, moderate and strong (Figure 1.1).

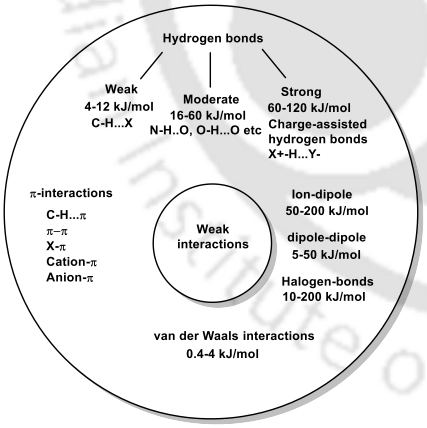

1.1.1

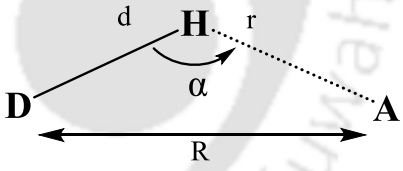

1.1.2

Parameters	Type of hydrogen bonds		
	Strong	Moderate	Weak
Bond energy ($kJmol^{-1}$)	60-120	16-60	<12
H···A (r Å)	1.2-1.5	1.5-2.2	2.2-3.2
D···A (R Å)	2.2-2.5	2.5-3.2	3.2-4.0
<D-H···A (α°)	175-180	130-180	90-150

Figure 1.1: Some prominent and commonly observed weak-interactions **1.1.1**, the hydrogen bond parameters in different types of hydrogen bonds **1.1.2**.

There is also another class of hydrogen bond, known as charge-assisted hydrogen bond[19] that occurs through proton-transfer or as electrostatic interactions. Each of these have characteristic hydrogen-bond parameters. In general, the hydrogen bond donor···acceptor distances and angle

TH-3622_196122001

between the hydrogen bond donor and acceptor taking the hydrogen atom as the center as illustrated in the Figure 1.1.2 is considered to demarcate between the classes. Moreover, depending on the number of hydrogen bond donor or acceptor sites utilized by one central-atom with multiple atoms, they are classified as bifurcated, trifurcated hydrogen bonds.

The non-covalent self-assemblies of unsaturated compounds or aromatic rings or molecules having unsaturated functional groups may have various π-interactions involving the π-clouds of an unsaturated or aromatic part. There are different types of π-interactions, such as π-π (<50 kJ/mol),[20] C-H···π,[21] cation-π,[22] anion-π interactions[23] (5 to 80 kJ/mol) etc. Furthermore, ion-dipole (50-200 kJ/mol), ion-ion (200-300 kJ/mol), dipole-dipole (5-50 kJ/mol), electrostatic interactions contribute to stabilize a self-assembled structure. The halogen bonds[24] play important role in the self-assemblies which contributes from 10 to 200 kJ/mol. Beyond all these, van der Waals interactions[25] from 0.4 to 4 kJ/mol has significant role in self-assemblies.

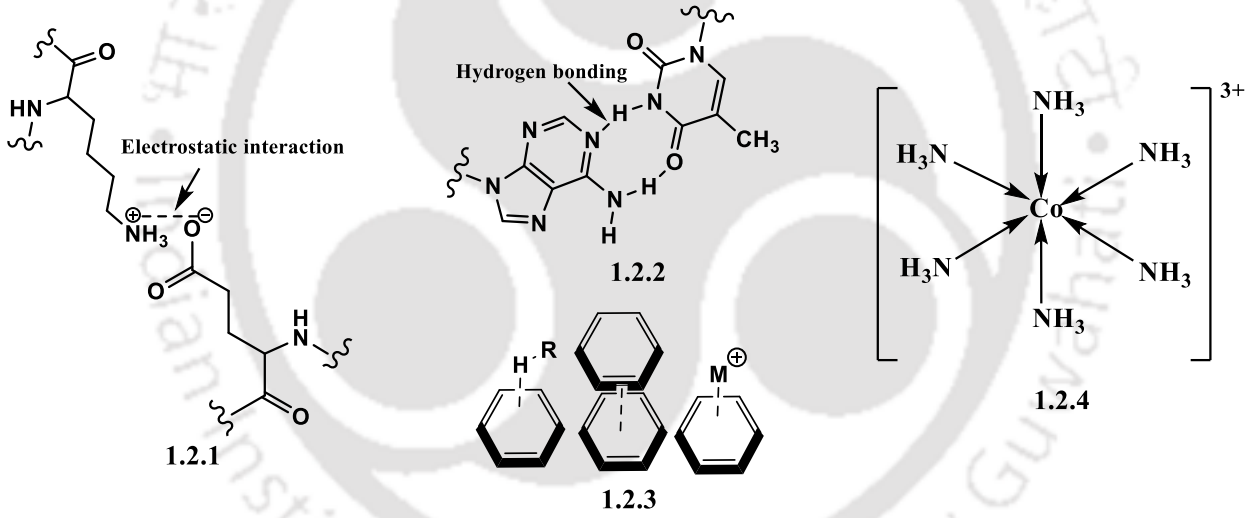

Figure 1.2: Depiction of several non-covalent interactions.

From the energy values, it is clear that each of these interactions are relatively weak, but collectively they contribute to increase stability, change physical properties and chemical reactivity. The influence of directional weak interactions and stereo electronic effects helps in shaping the final structure and depicts their collective behavior much different from discrete units. The roles played by hydrogen-bonds in controlling structures of DNA base pairs in self or cross-associations of biological molecules such as adenine, thymine, guanine, uracil and cytosine are classical examples to illustrate the complexity forming self-assemblies. As an illustration, Figure 1.3 shows hydrogen bonds between different base pairs: guanine-cytosine **1.3.1**, adenine-thymine

TH-3622_196122001

1.3.2, adenine-uracil **1.3.3** and guanine-uracil **1.3.4**. Each hydrogen bonded base pair associates in different manners and have different energies, provide multi-faceted avenues to explore model systems and also to understand biological systems.[15]

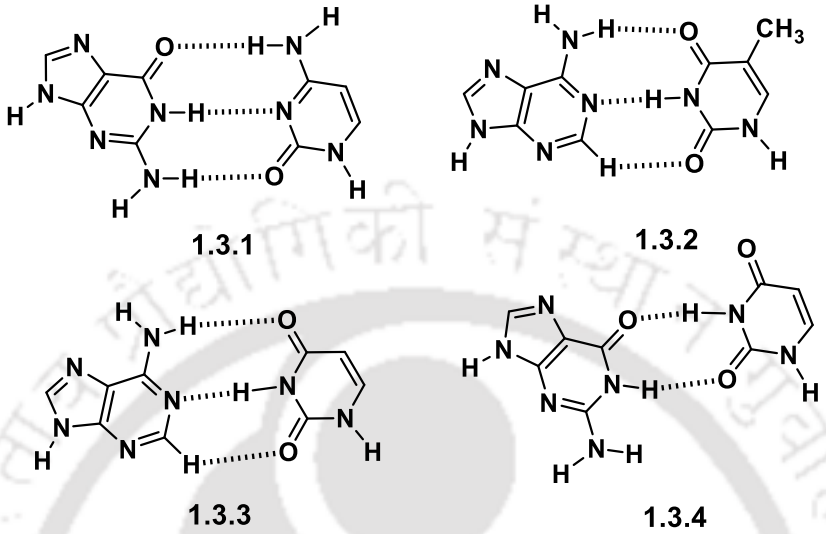

Figure 1.3: Hydrogen bonds among different nucleic acid base pairs.

Guanosine in water with Na^+ or K^+ ions have interesting structures. In each case the alkali metal ions are embedded within the central cavity of the hydrogen-bonded quartet assembly (known as G-quartet). Each quartet (**1.4.1**) is composed of four guanosine molecules linked by N-H···O and N-H···N hydrogen bonds. There is also π-π interaction between the aromatic planes and cation-dipole interactions. These provide columnar structure of the approximate length 8-30 nm. Similarly, analogous compound isoguanosine exhibits a similar hydrogen-bonded quartet structure around alkali metal cations forming planar cyclic pentamer, depicted as **1.4.2**. The differences between the assembling of the isoguanosine arises from the functional groups on the indole ring. In the former case the nitrogen of indole ring participated in hydrogen bonds whereas in the latter case it was not. Hence the hydrogen bonds being similar, the packing patterns in each case have large differences. These non-covalent self-assemblies are replica of ionophores and are easily synthesized. They show dynamic behaviors caused by solvent, temperature or pH which are reversible, hence makes them important to study as biological model systems.[16] The foregoing aspects of self-assemblies are dealt through structural studies and thermodynamics backed up by theoretical calculations, which are part of a subject crystal engineering. The crystal engineering is a subject that explores specific design aspects through understanding of crystal structures of molecules or reactive species,[26] assemblies of specified topology,[27] cocrystals, polymorphs,

TH-3622_196122001

solvates.[28] Basically, it provides the design and building principles to observe structure property relations.[29] The aspects on weak interactions are unearthed through analysis of the inter- and intra-molecular weak interactions, and also by analysis of the inter-play of weak interactions.

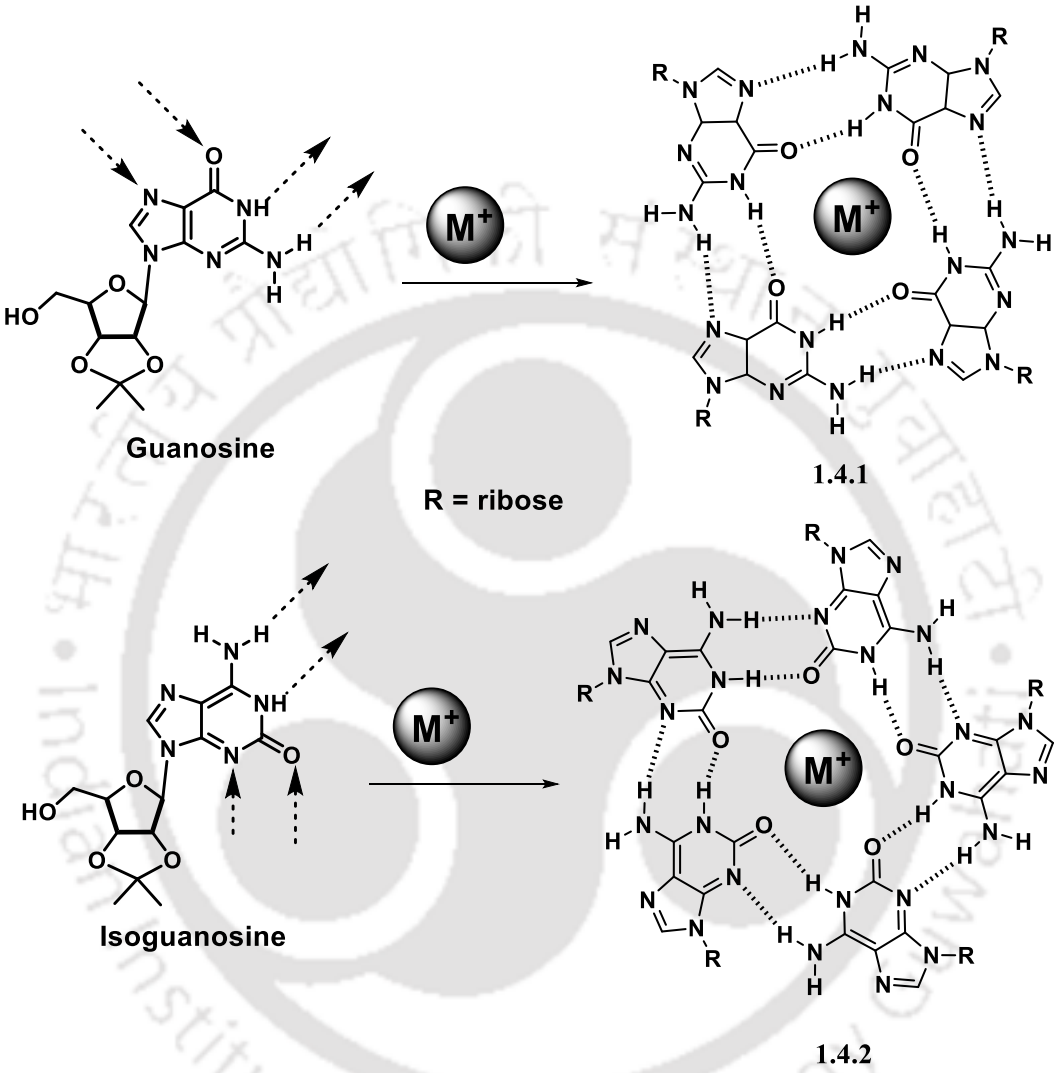

Figure 1.4: Hydrogen bonded self-assembly of guanosine **1.4.1** and isoguanosine **1.4.2** in the presence of metal ions (M^+).

In this venture, the crystal engineering has been helping to explore predefined architectures to observe and study specific properties. It has also provided systematic reasoning in correlating structure-property relationships. Keeping aside the contribution of crystal engineering to the biological aspects, the crystal engineering as a subject has emerged as a key-player to understand matters that relate different day to day activities. The scheme 1.1 is showing the realm of crystal engineering in everyday sciences. Its application in molecules to materials, specifically in pharmaceutical,[30] energetic-materials,[31] multi-component reactions,[32] catalysis,[33] solid-state

TH-3622_196122001

reactions,[34] devices and sensors [35] are immense. The crystal engineering helps to find out the replica of self-assemblies to help in predesign non-covalent synthesis. The topological, physical and chemical properties associated with non-covalent assemblies are understood by analyzing the structures and various interaction through a comparative manner.

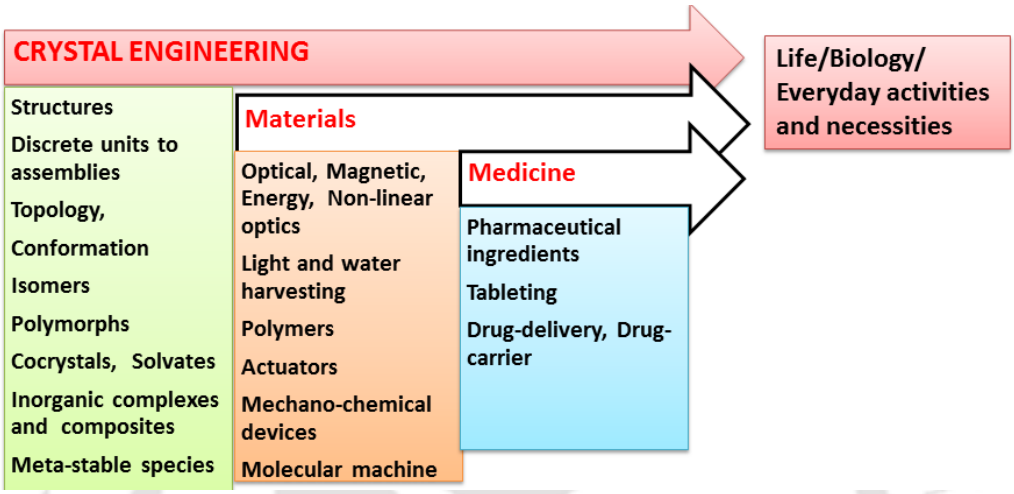

Scheme 1.1: Versatile use of crystal engineering in self-assemblies.

Furthermore, impetus to design multi-component systems and analyzing the directional aspects and various resonating structures stabilized in assemblies had contributed to material design and eco-friendly synthetic paths. In the next sections some of those aspects that get revealed through crystal engineering are depicted.

1.3. Supramolecular synthons

The weak interactions guiding the directional properties of non-covalent assemblies necessitates a retrosynthetic approach that is similar to retro-analysis of structural backbone of a complex molecule to design appropriate synthetic strategies. Crystals encompassing non-covalent interactions are dependent on the chemical and geometrical factors, from individual molecules. To implement new design of non-covalent self-assemblies the retro-analysis is done through identifications of supramolecular synthons.[36] The rational approaches towards solid-state assemblies observed from crystal-structures provide an essence to implement crystal engineering.[37] By definition "Supramolecular synthons are structural units within supramolecules which can be formed and/or assembled by known or conceivable synthetic operations involving intermolecular interaction." Identifications of sub-structural units of a target supramolecule that is used to assemble it from logically chosen precursor molecules, are the supramolecular synthons.

TH-3622_196122001

They provide the conceptual building units for self-assemblies,[38] which are generally demonstrated through crystal engineering. Alternatively, retro-synthesis of crystal structures are done by analyzing supramolecular synthons. Hence, synthons stem from the functional groups involved in hydrogen-bonding or other weak interactions originating from the molecular structure. On the other hand, the synthons that are from the assembling of same type of functional groups are called homo-synthon; whereas, the ones with different types of functional groups are called as hetero-synthon.

Table 1.1: Some common homo and hetero-synthons and their graph set notation.

Entry No	Synthons	Interactions	Graph-set notation
1	acid-acid	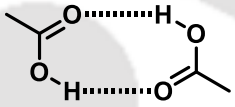	R_2^2 (8)
2	amide-amide	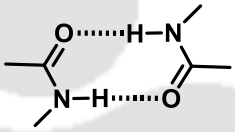	R_2^2 (8)
3	acid-amide	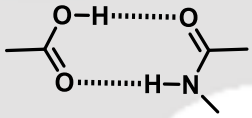	R_2^2 (8)
4	acid-pyridine	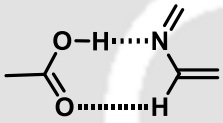	R_2^2 (7)
5	amide-pyridine	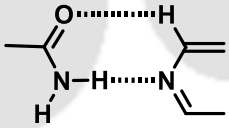	R_2^2 (7)
6	amide-N-oxide	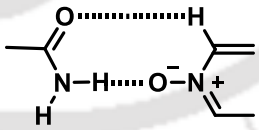	R_2^2 (8)

Some of the common synthons are listed in the table 1.1. The entry 1 and 2 are the examples of homo-synthons, rest of the entries 2-6 of table 1.1 are examples of hetero-synthons. The entry 6 is an example of charge-assisted hydrogen bonds and a very weak C-H···O interactions. It may be noted that a self -assembly of one molecule with different functional groups may be associated with homo-synthons only or combination of homo and hetero-synthons. These provide different structure from same molecule in different polymorphic forms. As the synthons contribute to

TH-3622_196122001

stability, attentions are required on the energetic of synthons are very important and for predesigning a supramolecular synthesis. The energy associate with a synthon allows to correlate the feasibility to have or not an alternative synthon within an assembly. They also help to reconstruct as well as transform to another form in reversible manner by stimuli. For example, 1-(n-methylthiazol-2-yl)-3-naphthalen-1-yl-thiourea[39,40] had different synthons formed by rotation of carbon and nitrogen bond, which provide two polymorphs, each having independent synthon. Graph set notations are used as descriptors of the synthons. According to graph-set notation, graph set designator 'G' is assigned into four different notations, R for ring, D for discrete, C for chain and S for self or intramolecular hydrogen bonded systems.

$$G_d^a(n)$$

Where G = Graph set designator C/R/D/S, d = Number of donor atoms, a = Number of acceptor atoms, n = Total number of atoms present in hydrogen-bonded motifs

Figure 1.5: A generic graph-set descriptor.

The total number of atoms involved in hydrogen bonding is denoted in brackets and the number of donors and acceptors present in the assemblies are designated as subscript and superscript respectively as shown in table 1.1. A systematic analysis of the structures by Margaret Etter and colleagues to put forward hydrogen bonding design rules known as Etter's rules.[41] It states that

1. All good proton donors and acceptors are involved in hydrogen bonding.
2. Six-membered-ring intramolecular hydrogen bonds form in preference to intermolecular hydrogen bonds.
3. The best proton donor and acceptor remaining after intramolecular hydrogen bond formation will form intermolecular hydrogen bonds.

The Etter's rules are followed by most of the hydrogen bonded assemblies, but there are exceptions when steric factors and packing requirement do not allow participation of the good donor or acceptor bonds to participate in hydrogen bonding scheme. More precisely, the introduction of the concepts of supramolecular synthons, and study on the packing and energetics of hydrogen-bonded building blocks in crystal structures, have enhanced their applications towards materials and

TH-3622_196122001

medicinal compounds.[42] The contribution has also widely recognized by the Green-chemists to appreciate the principles based on which the subject Green-chemistry has evoloved.[43]

1.4. Host-guest complexes and Cocrystals

The supramolecular chemistry based on non-covalent interactions between host and guest molecules have evolved from the later part of nineteenth century. It received due accolades through Nobel Prize, received by J.-M. Lehn, D. J. Cram, and C. J. Pedersen in the year 1987. A host refers to large molecules that possess significant space to accommodate a guest.[44] On the other hand, a guest includes cation, anion, ion pairs, or complex molecules which readily fits into those spaces of a host. For effective host-guest binding, compatible binding sites as well as electronic properties, such as polarity, hydrogen bonds, and hardness or softness should complement with that of the guest molecule. Therefore, a pre-organized host has advantage over the one where significant reorganization of structure to adopt a guest is required.[45] Various capsular structures are created by self-assembled ligands that have supramolecular parts to further bind guest such as metal cages of urea derivatives.[46]

The cocrystals are assemblies of two or more neutral or combination of neutral or ionic components held together by weak non-covalent interactions. They are indispensable part of supramolecular chemistry and have contributed to modulate property of parent partner molecules. Crystal engineering of cocrystals help to select partner molecules/ions to form engineered supramolecular structures through utilization of the principles of molecular recognition and self-assembly.[47] The cocrystals have contributed significantly to pharmaceuticals, so methodology for large-scale cost-effective synthesis in eco-friendly manner is important. Traditional crystallization methods, such as solvent evaporation, layering, cooling, or the addition of foreign substances, have limitations for industrial applications. An alternative to these methods is the use of mechanochemistry through solid-state milling,[48] as this process is simple, efficient, and environmentally friendly. In addition, mechanochemistry allows the investigation of rare crystal forms that cannot be achieved as single components, while also promoting atom economy. The use of mechanochemical means in crystal engineering was there in literature since 1844, when Friedrich Wöhler discovered the first organic cocrystal, quinhydrone.[49] It is a cocrystal of *p*-benzoquinone and hydroquinone in equimolar amounts, that can be prepared by grinding an

TH-3622_196122001

equimolar amount of the two compounds.[50] The realm of host-guest chemistry and cocrystals in recent years have emerged as interdisciplinary and indispensable to all branches of chemistry. Simple inorganic complexes with second coordination spheres featuring uncoordinated sites, ready for supramolecular interactions, or templates created through ligand coordination, are utilized to form various self-assemblies.[51] For example, oxime–oxime hydrogen-bonded synthons or amide amide synthons enables supramolecular assembly of $[Ag(3\text{-acetoximepyridine})_2]PF_6$,[52] and $[Pt(L)_2(\text{isonicotinic acid})_2]\cdot 2H_2O$ complexes.[53] The bis-cyclic amidinium dications have been extensively used and such cations form self-assemblies with anionic species like $[Ni(CN)_6]^{4-}$.[54] To predesign a supramolecular assembly or to form cocrystals there are several design principles often used. These are based on the factors such as ΔpKa,[55] selection of complementary heterosynthons,[56-60] and based on the application of Hansen solubility parameters.[61]

The different facets of the self-assemblies of two or more components is too broad, hence, in this thesis the discussion is limited to self-assemblies of ionic-cocrystals and metal-complexes. In the latter sections the aspects required for understanding non-covalent assembling of inorganic complexes that encompasses the thesis is described.

1.5. π–stacking and metal chelates

The π-interactions are widely observed in biological systems as well as assemblies of small molecule.[62] π-Stacking has significance as important as the hydrogen bonding in non-covalent assemblies of units having unsaturated and aromatic building blocks. As an illustration a six-membered aromatic rings can be organized in arrangements such as face-to-face, off-set (slipped parallel displaced) and face-to-edge (T-shaped or C-H···π interaction) evident as shown in the Figure1.6. All these interactions are often observed in self-assemblies and have contributed to directionality of self-assemblies. The most commonly observed π-interaction is from the off-set or slipped stacking arrangement, in which the displacement of the parallel rings takes place. In those cases, effective interactions occur when the ring centroid vector and the ring normal forms an angle of about 20º and centroid to centroid distances of around 3.8 Å. In the case of benzene, edge-on arrangement is more stable than face-to-face stacking.[63]This phenomenon due to repulsion between negatively charged electron clouds of π system in the face-to-face stacking orientations. Whereas, in edge-to-face arrangement attractive interaction between positively charged H-atom

TH-3622_196122001

and π-electrons occur (Figure 1.7). Such arrangement leads to herringbone structure[64a] of crystalline benzene. Structural analysis from crystal structure database of Cambridge Crystallographic Database Center,[64b] had suggested that the face-to-face stacking is preferred arrangements and commonly observed, when donor is electron rich and acceptor is electron deficient aromatic system.

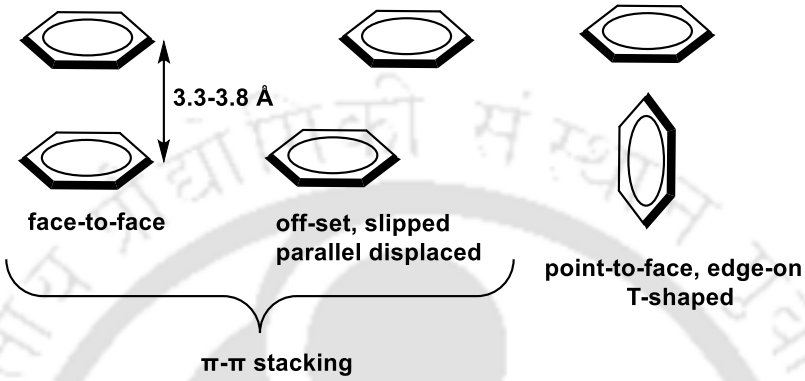

Figure 1.6: Different π-interactions between two benzene rings.

The stacking between coordinated and uncoordinated benzene provide lowering of energy about −4.40 kcal/mol. But, the stacking between two coordinated benzenes causes a gain by −4.01 kcal/mol. These are comparable, hence, the inclusion of benzene by stacking is a favorable process. The net gain from such interactions was about double the amounts that was gained by stacking among two benzene molecules (−2.73 kcal/mol). Stacking between coordinated benzene and coordinated cyclopentadienyl anion usually have horizontal displacements (> 4.5 Å). Presence of methyl group in aryl and Cp ligands shows both stacking and C–H···π interactions.[65]

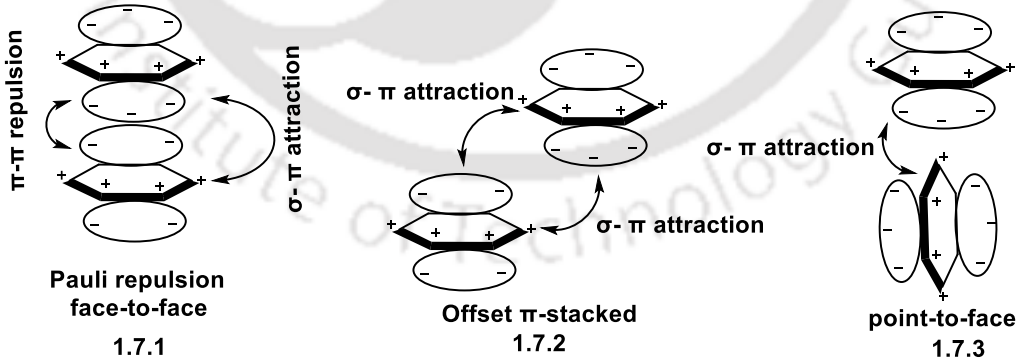

Figure 1.7: Attractive and repulsive forces between electron clouds of different types of π- stacking arrangements (reproduced from ref 62a).

There are large numbers of examples of metal complexes where chelate π-interactions contribute in their self-assemblies.[66]These interactions are not only limited to organic and biomolecules but

TH-3622_196122001

have extensively contributed to self-assemblies of inorganic complexes. The stacking of a portion of ligand have also contributed to self-assemblies. For example, di-chloride-bis-(2-{(*E*)-[(2-methoxyphenyl)azaniumylidene]methyl}phenolato-κ*O*) zinc(II), complex has extensive π-stacking to provide dimers, which further assembles to provide 1D-chain like structure (Figure 1.8). The self-assembled dimers has not only the π–stacking interactions but also the hydrogen bonds. The dimers had −33.0 kcal mol^{-1} gain in energy over the discrete molecules.[67]

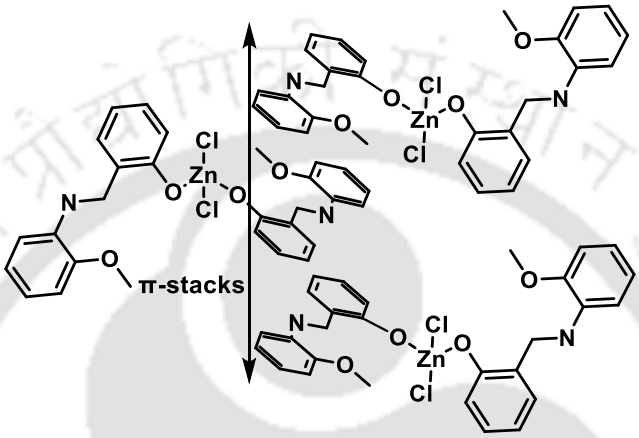

Figure 1.8: The π-stacks forming extended chain-like arrangements (along the arrow) in a zinc complex.

A 1D coordination polymer of the imine ligand (E)-2-(4-(1-methyl-1H-imidazol-2-yl)but-3-en-1-yl)pyridine (2amp) complex with copper(II) $[Cu(2amp)Cl](PF_6)$ showed face-to-face interactions between the imidazole rings. The interaction shown in the Figure 1.9, was suggested to influence the magnetic interactions among the copper(II) sites to show ferromagnetic property by the corresponding copper(II) complex.[68a] Another examples[68b] of complex having strong intramolecular hydrogen bond is $[Cu(bzmal)(phen)(H_2O)]\cdot 3H_2O$ (where bzmal = benzylmalonate, and phen = 1,10-phenanthroline). In this complex, the phenyl group attached to malonate has π-interaction with the π-clouds ring of the coordinated 1,10-phenanthroline.

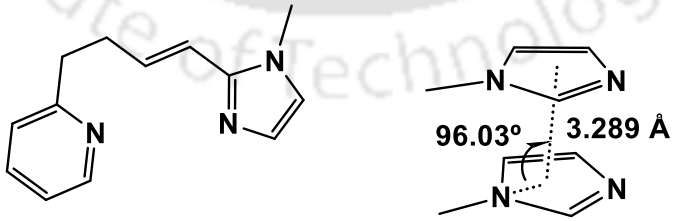

Figure 1.9: The structure of the ligand (E)-2-(4-(1-methyl-1H-imidazol-2-yl)but-3-en-1-yl)pyridine (left) and its stacking between imidazole rings (right) in a copper complex.

The stacking among the ligands were used to synthesize new complex by changing/modulating stacking interactions by another components. For example, A 2×2 complex with a flexible ligand

TH-3622_196122001

having π-aromatic part may be changed to another type of stacks as illustrated in Figure 1.10. A third ligand can be incorporated to have interactions with the stack.

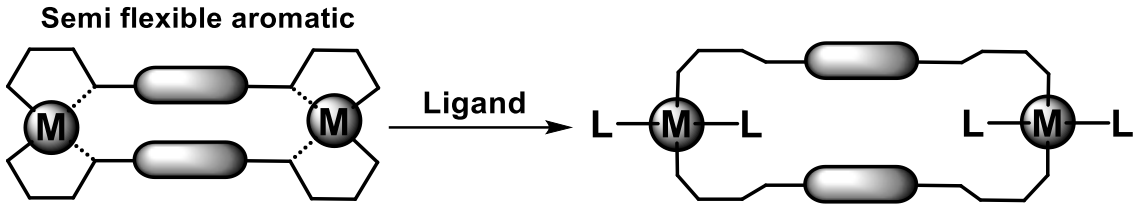

Figure 1.10: The change of binding patterns by introducing ligands to a bimetallic complex affecting the stacking between aromatic units.

The 2 × 2 type rhodium complex **1.11.1** transforms after introduction of an additional ligand such as the one shown in **1.11.2**. This introduction was facilitated by the electron donor and acceptor ability between the ligand.[69]

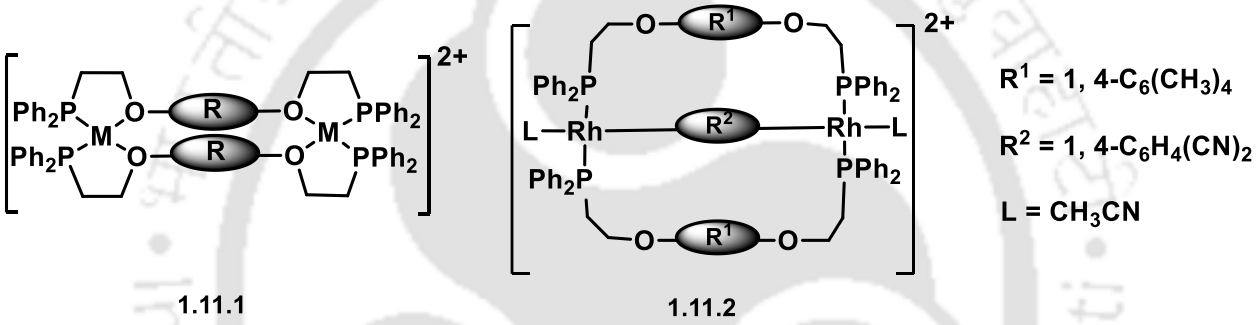

Figure 1.11: Incorporation of a new ligand to a Rh-bimetallic complex to change the original stacking pattern.

The cross-over of ligation patterns are also observed in metal complexes, an example in which temperature dependent changes were observed is shown in the Figure 1.12. Equilibrium with different forms of the complex by changing coordination and stacking arrangements was established.

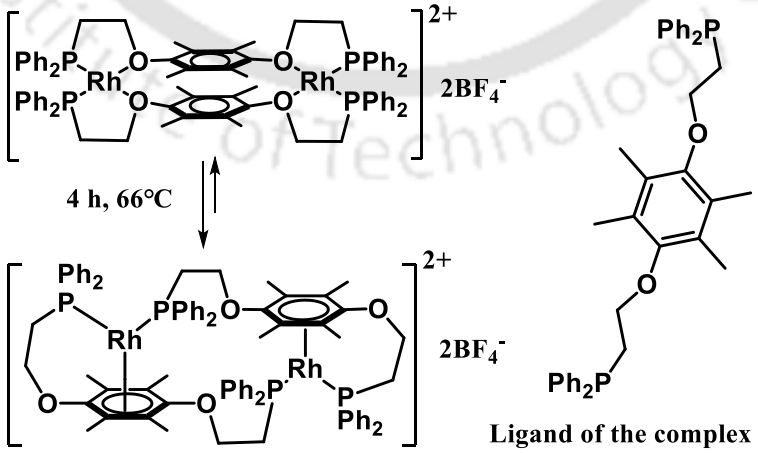

Figure 1.12: Equilibration in bimetallic Rh-complexes: Presence or absence of stacking interactions.

TH-3622_196122001

Several studies related to self-assembling using inorganic templates had been demonstrated in literature includes utility of anionic, cationic metal template for hydrogen bonding as well as the one suitable for stacking interactions. Those templates includes tetranuclear cobalt,[70] metal-phenanthroline,[71] penta-ammino copper complexes[72] as well as metal complexes with naphthalimide and 2,6-pyridinedicarboxylate complexes.[73] The utility of tris-phenanthroline nickel(II) in binding to nitro-phenolic compounds[74] are shown in the Figure 1.13.

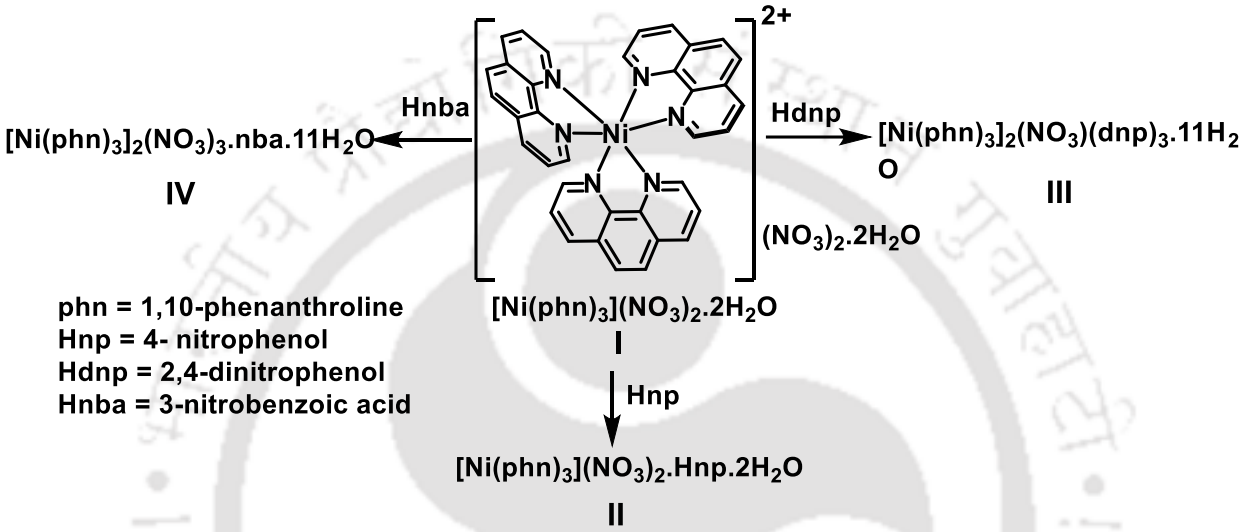

Figure 1.13: The ionic-cocrystal of tris-1,10-phenanthroline nickel(II) nitrate with nitro-phenolic compounds.

The second sphere of zinc carboxylate with amide based ligands were shown that supramolecular interactions had played roles in guiding the crystalline products.[75] The assembling of bis aqua, ethylene diamine copper complexes with benzoate groups as free ions have provided assemblies guided by the substituents and directional properties of the benzoates.[76] Recently, the second coordination sphere of $[Ni(ethylenediamine)_2(H_2O)]^{2+}$ was utilized in assembling of complexes.[77] The complex $[Ni(1,10\text{-phenanthroline})_3](NO_3)_2.2H_2O$ formed an assembly that had stacking among the chelates and the molecule served as template for different nitrophenols. The interesting feature is that the amounts nitrophenol accommodated per nickel complex varied, specially the ability to accommodate three molecules of 2,4-dintrophenol was significant to prepare energetic compounds. The aromatic stacking among fluorophoric molecules provide control on their photo physical properties.[78]

The dimeric π-stacked coronene of a neutral Eu(III) complex **1.14.2** of the ligand **1.14.1** has intramolecular stacking interactions between two coronene units. The stacking had helped in energy transfer from the low-energy triplet state to the energy acceptor.

TH-3622_196122001

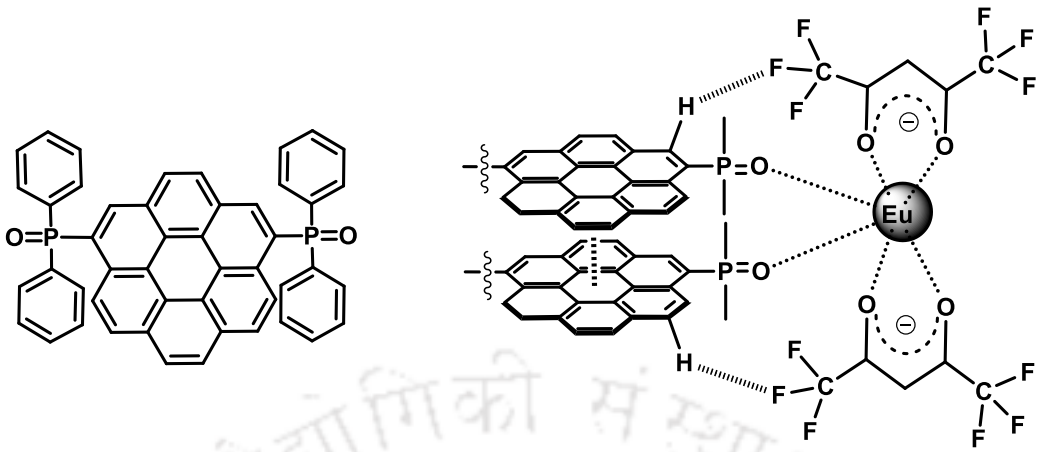

Figure 1.14: The structure of **1.14.1** and its intra-molecular coronene-coronene stacking in a europium complex.

Similarly, the π-stacking in the pyrene-based complex shown in the Figure 1.15, had two *tris*-hexafluoro-acetylacetonate bridged by two intervening pyrene-based phosphine oxide ligands. The population of localized electron on the stacked pyrenes had influenced the photophysical properties of the lanthanide ions.[79]

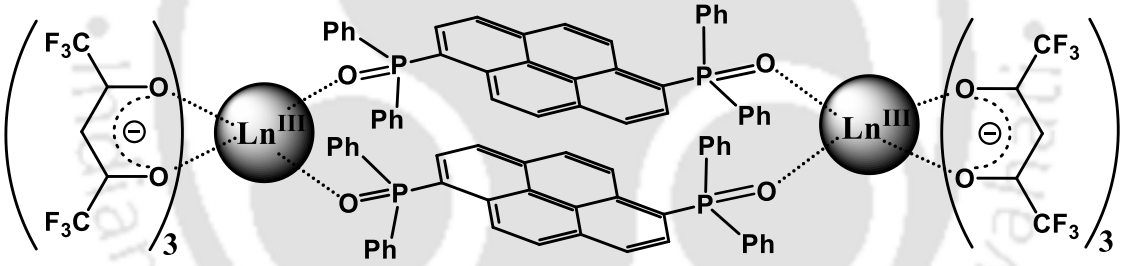

Figure 1.15: A phosphine oxide bridged binuclear *tris*-hexafluoro-acetylacetonate-lanthanum complex with pyrene-pyrene stacking.

In another example, a lutecium complex **1.16.1** had C-H···F interactions to provide a rigid and planar structure. The complex self-assembles through the stacking among the planar parts and it showed blue fluorescence due to the rigidity and stacking.[80]Some mononuclear complexes have intramolecular and intramolecular stacking among the polynuclear aromatic part affecting photophysical properties, one such example is the europium complex **1.16.2**. The complex had high luminescence due to effect on Eu ions of the electronically isolated stacked aromatic ring systems.[81]

TH-3622_196122001

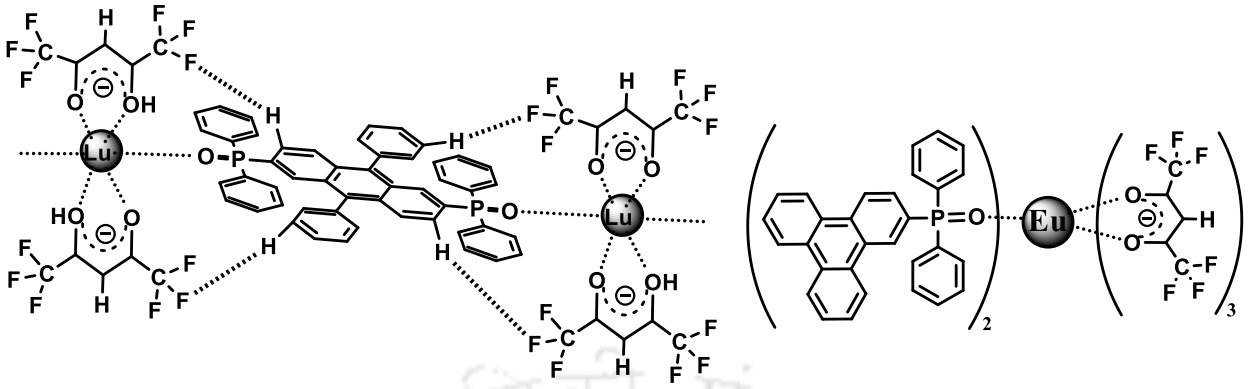

1.16.1 **1.16.2**

Figure 1.16: The effect of C-H···F interactions providing planarity and rigidity to complex 1.16.1 and a mono-nuclear complex that had extensive stacking in self-assembly.

The complexes $Tp^{Py}Ln(CH_3CO_2)_2(H_2O)$ (Ln = Eu, Tb) form extensive π-stacking interactions. Due to π-stacking interactions intense photoluminescence were observed from the two complexes. They had analogous stacking patterns which was complemented also in the respective crystal packing.[82] In a mixture of complexes having $[Tp^{Py}Eu]^{2+}$ or $[Tp^{Py}Tb]^{2+}$ with small amounts of isostructural gadolinium complex, there was efficient energy transfer from the gadolinium complex to the $[Tp^{Py}Eu]^{2+}$ or $[Tp^{Py}Tb]^{2+}$ centers effecting the intensity of emission spectra from the parent compounds (Figure 1.17).

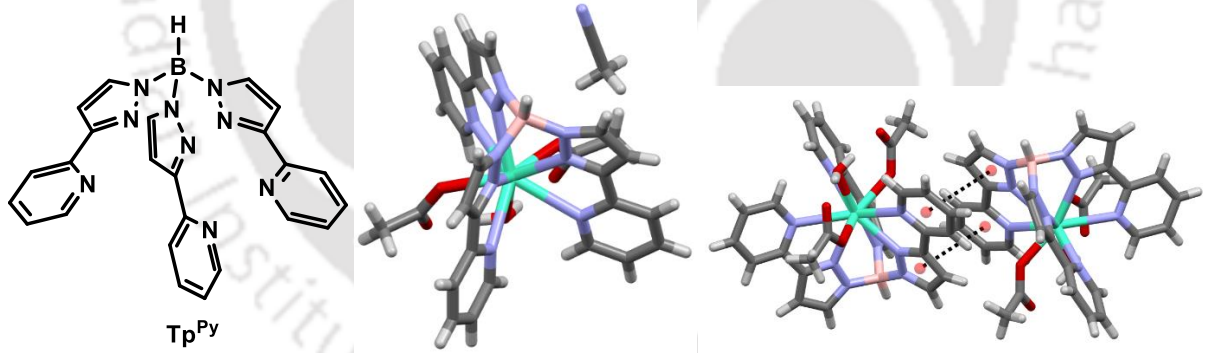

Tp^{Py}

1.17.1 **1.17.2** **1.17.3**

Figure 1.17: The ligand Tp^{Py} **1.17.1**, complex $\{Tp^{Py}Gd(CH_3CO_2)_2(CH_3CN)\}$**1.17.2** and stacking between heterocyclic ligands (**1.17.3**) (color code: cyan = gadolinium, blue = nitrogen, red = oxygen, grey = carbon, pink = boron).

Other than the π-π stacking interactions, there are other π-interactions that have important roles to guide supramolecular assemblies of metal complexes. Anion···π interaction is one such interaction found in assembling of certain complexes. As an example, the copper complex of the polydentate ligand 2,4,6-tris(dipyridin-2-ylamino)-1,3,5-triazine (dpyatriz) **1.18.1**; $[Cu_3Cl_3(dpyatriz)_2](ClO_4)_3$ has two dpyatriz ligands bridged via coordination to Cu(II) and disposed either face-to-face or in

TH-3622_196122001

an eclipsed manner (**1.18.2**). The ionic perchlorate had anion···π interactions with the triazine rings of the complex.[83]

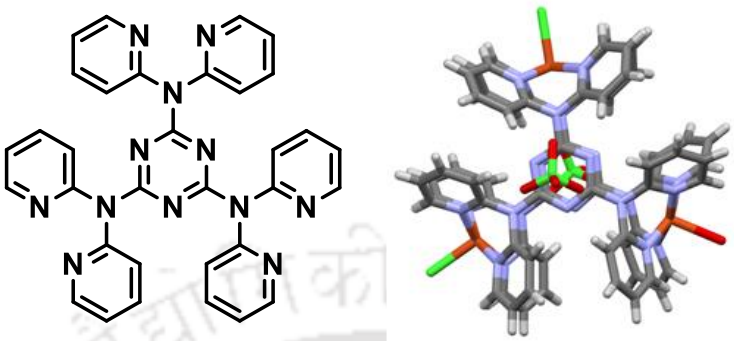

1.18.1 **1.18.2**

Figure 1.18: Structure of ligand (dpyatriz = 2,4,6-tris(dipyridin-2-ylamino)-1,3,5-triazine) **1.18.1**, and **1.18.2** is the stacked structure of $[Cu_3Cl_3(dpyatriz)_2](ClO_4)_3$ showing anion···π interactions.

The iron(II) complex $[Fe_4(bptz)_4(CH_3CN)_8.BF_4]^{7+}$ (**1.19.2)** of 2,4-dipyrazolyl-1,3,5-triazine (bptz) had a grid-like structure. Within the voids of the grids the one BF_4^- anion was included. This complex shows anion···π interaction between fluorine atom of the tetrafluoroborate with the triazine part of the ligand. Similar encapsulation of SbF_6^- anion also showed such interactions. These interactions as well as the competitive binding of different analogous ions were monitored by NMR spectroscopy. The effect of the anion on the chemical shifts of neighboring ring protons and fluorine atoms in proton NMR and fluorine NMR spectroscopy can distinctly indicate relative binding.[84]

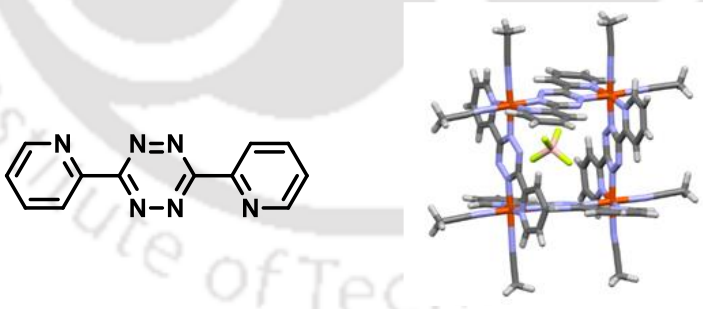

1.19.1 **1.19.2**

Figure 1.19: The ligand bptz **1.19.1** and anion-π interactions in its iron complex **1.19.2**.(Color code: grey = carbon, blue = nitrogen, red = oxygen, pink = boron, neon = fluorine)

Anion π-interactions were observed in coordination polymer hexa(4-cyano-phenyl)[3]-radialene **1.20** with silver ion. The anion of the polymeric complex $\{[Ag(hexa(4\text{-}cyanophenyl)[3]radialene)](PF_6)\cdot 2(CH_3NO_2)\}_n$ were located in the pockets above and below the

TH-3622_196122001

[3]-radialene ligands. Anions had weak anion···π interactions with the electron-deficient [3]-radialene cores.[85]

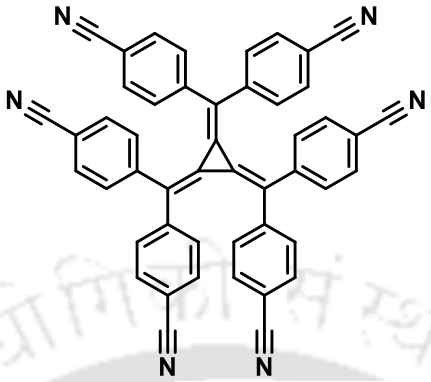

Figure 1.20: Structure of hexa(4-cyanophenyl)[3]-radialene.

The stacking influences the circular dichroism of chiral assembly. For example, the two systems shown in Figure 1.21, labeled as **1.21.1** and **1.21.2**, involve two anions: one with a coordinated anion and the other with two anions, one of which is in a hydrogen-bonding environment. These systems exhibit significant differences in their respective properties. The assembly of these anions and ion pairs of chiral anions with planar triazatriangulenium cations independently exhibited distinct chirality and circularly polarized luminescence properties. Those optical properties were opposite of each other.[86]

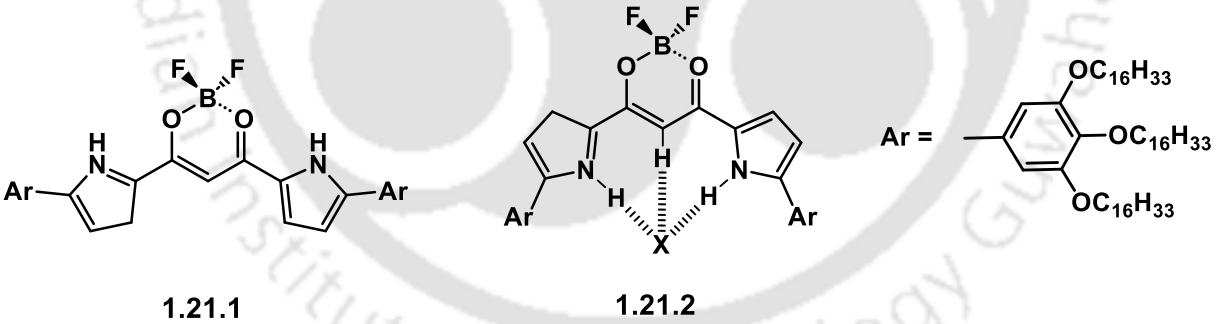

Figure 1.21: An anion and ion-pair of the anion that show different chiralities.

Besides stacking interactions typical of organic molecules, ligands forming planar geometries with metal ions often exhibit π-interactions as part of their coordination behavior. Aggregation among the ligands of number of complexes, where chelates or ligand are capable of π-stacks among them have profound interest. Carboxylates, imines, β-diketones are common chelating ligands studied for chelate-chelate stacking effects.[87,88] Chelate-chelate interactions among square planar bis(2,4-pentanedionato)palladium (II) provides the example of chelate-chelate π-stacked interactions. As

TH-3622_196122001

shown in the Figure 1.22, the two chelate rings in neighbor complexes may be organized in parallel or antiparallel fashion. According to angles between the chelate planes there are three feasible orientations close differences in energies, which are shown in the Figure 1.22. These are parallel eclipsing with linearly arranged metal ions, or through an eclipsing orientation is in a crossed manner with the metal ions at 90º with respect to the diketonate units. The third possibility is the partly translated parallel orientation, which is referred to as anti-parallel orientation. In the palladium complex this antiparallel arrangement of chelate-chelate stacking was observed (Figure 1.22).[87]

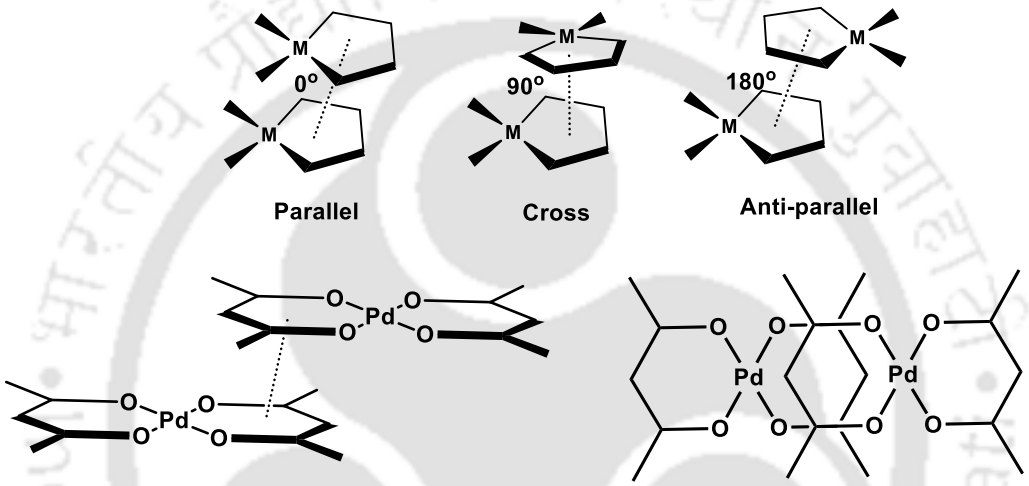

Figure 1.22: Different Chelate-Chelate stacking in square-planar complexes.

The above examples have shown that the stacking among chelates or with π-aromatics of a ligand provide large avenues to design new inorganic non-covalent assemblies. They have contributed to ion and molecular recognition. The stabilities of those assemblies are influenced by other weak interaction schemes also then a prominent contribution by stacking interactions in a competitive manner or as subsidiary interactions contributing to stability.

1.6. Ionic-cocrystals

Ionic-cocrystals are cocrystals that have at least one ion pair and a variable number of coformers. Supramolecular assembly that are related to host-guest chemistry of ion pairs, they belong to an important class of supramolecular systems referred as ionic-cocrystals. The term 'ionic-cocrystal' was introduced by Braga and his coworkers.[89]They are generally stabilized by charge-assisted hydrogen bonds or coordination bonds. Due to polymeric structures, some ionic-cocrystals are referred also under the classification of coordination polymers. The ionic-cocrystal of sodium

TH-3622_196122001

chloride with urea were observed in the year 1783.[90] The structure was confirmed after it was crystalized by slow evaporation of an equimolar solution of sodium chloride and urea.[91] The structure was confirmed by single-crystal X-ray crystallographic study as 1:1:1 complex of sodium chloride, urea and water molecule (Figure 1.23). With progress of research, cocrystals of calcium salts with glucose,[92] benzoic acids with potassium carboxylate salt were characterised.[93]

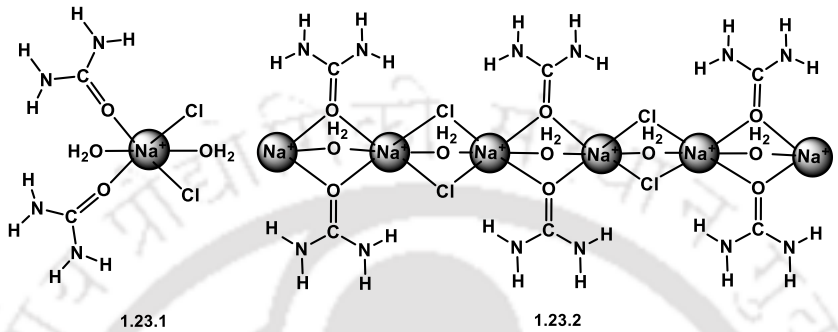

Figure 1.23: Environment of sodium ion **1.23.1,** and **1.23.2** is the self-assembly of hydrated urea sodium chloride ionic-cocrystal.

The organic acid and amine groups have higher propensity to form ionic-cocrystals as they themselves remain as hydrogen bonded assembly. As an example, benzoic acid remains as hydrogen bonded dimer in aromatic solvents and a hydrogen bonded dimer has the possibility to ionize without dissociating. One such example of ionic-cocrystal of aromatic carboxylic acid with an organic amine dimethylamine pyridine is shown in Figure 1.24.

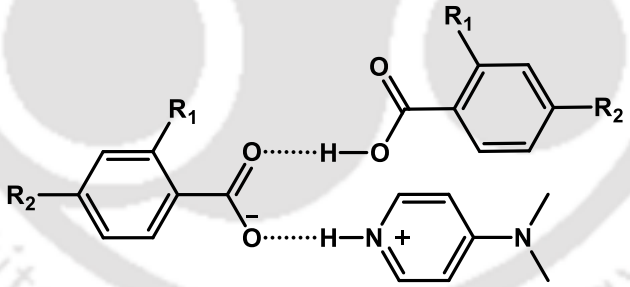

Figure 1.24: An example of ternary ionic-cocrystal of carboxylate, carboxylic acids and pyridine.

In early stage of development of ionic-cocrystals, the ionic-cocrystals of acid and its salt were studied by X-ray and neutron diffraction by Speakman.[94] He categorized those into two categories as, type A and B. The type A includes salts that had the proton distributed across the carboxylates (**1.25.1)**, while type B had the proton localized at one of the oxygen atoms (**1.25.2**). Many ionic-cocrystals originated from conjugate acid/base.[95,96] A representation of a ternary ionic-cocrystal is shown in the Figure 1.25. Several ionic-cocrystals were known much before the term ionic-cocrystals was introduced in literature.

TH-3622_196122001

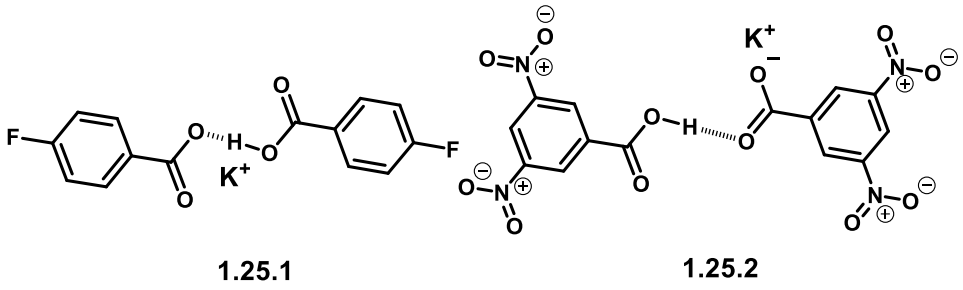

1.25.1 **1.25.2**

Figure 1.25: Type A: Potassium hydrogen bis(4-flourobenzoate) **1.25.1,** and Type B: potassium hydrogen bis(3,5-dinitrobenzoate) **1.25.2**, ionic-cocrystals.

These includes, phenylquinoline carboxylic acid with pyrazolones;[97] streptomycin acid salts with alkaline earth metal halides[98] and theophylline with sodium acetate, sodium salicylate, and sodium glycinate salts. The ionic-cocrystal of the fluoxetine hydrochloride with benzoic acid[99] was used to modulate dissolution rate of fluoxetine hydrochloride. Stahly and coworkers had analyzed cocrystals from Cambridge crystallographic database, such analysis provided scope to systematically analyze the synthons.[100]

Table 1.2: Some phenolic and hydroxyl compounds.

Phenols	Ionic-cocrystal
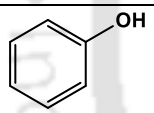 pKa = 9.95 Phenol	Tetramethylammonium·phenol·phenolate
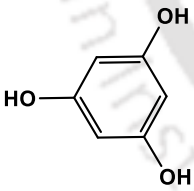 pKa = 8.5, 8.9 1,3,5-benzezentriol	Tetraethylammonium ·1,3,5-benzentriol·1,3,5-benzentriolate Tetraethylammonium· 1,3,5-benzentriol·1,3,5-benzentriolate
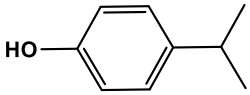 pKa = 10.28 4-Isopropylphenol	Potassium·4-isopropylphenol·4-isopropylphenolate, Tetrapropylammonium·4-isopropylphenol·4-isopropylphenolate Tetrabutylammonium ·4-isopropylphenol·4-isopropylphenolate

Among the various functional groups, phenolic part is abundant in natural and synthesized organic compounds. This units provide scope to prepare ionic-cocrystals having phenol-phenolate

TH-3622_196122001

interactions. These were observed in different ionic-cocrystals of phenol, resorcinol, phloroglucinol, 4-methoxyphenol, and 4-isopropylphenol.[101] It was suggested to be a strategy to solubilize phenolic derivatives. Some of biologically active phenols suffer from low aqueous solubility. The hydrogen-bond strength of PhOH···PhO$^-$ was found to be about 3 times stronger than the phenol–phenol hydrogen bond. Some examples of ionic-cocrystals of phenolic compounds are listed in table **1.2**. It may be noted that the pK_a value of these phenols are 8-10 and the pK_b of the hydroxide of each cationic parts are about 13. Thus, the cationic part remains in one form being highly ionic nature of the parent compound, whereas the phenols having weak acidity hydrogen bonds to remain in neutral as well as anionic form in the cocrystal.

Ternary ionic-cocrystal of quinoline-4-carbaldoxime with 2-nitrobenzoic acid and 2-nitrobenzoate. The neutral 2-nitrobenzoic acid was accommodated due to a senary sub-assemblies. The quinoline-4-carbaldoxime with several other carboxylic acids did not provide ionic-cocrystal but hydrated salts with several other carboxylic acid such as 2-hydroxybenzoic acid, 3-nitrobenzoic acid, 4-nitrobenzoic acid, 2,3- or 2,4-dihydroxybenzoic acid were formed. They had senary sub-assemblies different from the ionic-cocrystal, these were quaternary sub-assemblies connected by hydrogen bonding with water molecules. In such senary sub-assemblies, water molecules were held in the hydrophobic junctions of the hydrogen bonded oximes and carboxylic acids.[102] Crystals derived from simple amino acid glycine with sulfamic acid (Figure 1.26) are piezoelectric having prospects in devices used in edge computing.[103a] N-phthaloyl glycine also form ionic-cocrystals with N-aminoquinoline.[103b]

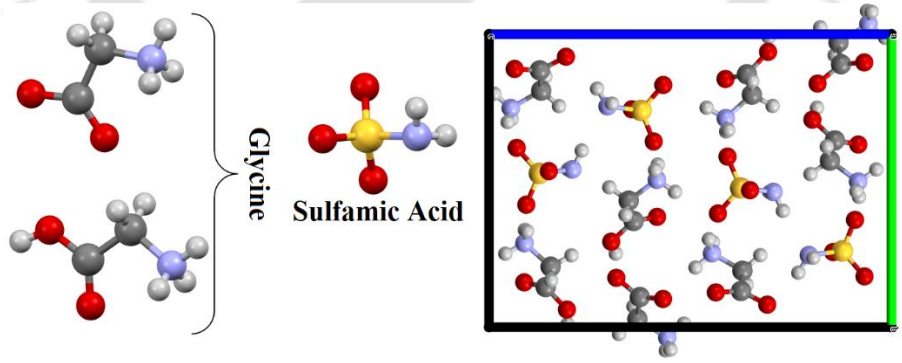

Figure 1.26: Self-assembly of the ionic-cocrystal of glycine with sulfamic acid viewed along *bc*-crystallographic plane. (Color code: grey = carbon, red = oxygen, blue = nitrogen, yellow = sulfur)

Aakeröy et al[104] demonstrated that ditopic bases are effective templates for the crystallization of ternary cocrystals. Seaton et al.[105] had used a combination of charge-assisted and conventional

TH-3622_196122001

hydrogen bonds to construct multi-component assemblies.[106] Stoichiometric quaternary molecular solids were synthesized through structural non-equivalences, combined with a homologation of synthetic approach by Desiraju[107] and coworkers. Braga and coworkers had reported that the solubility of barbituric acid (**1.27.1**) in water was affected by the addition of charge neutral but ionic salt such as alkali halides. They also isolated several ionic-cocrystals of barbituric acid with alkali bromides (LiBr, NaBr, KBr, RbBr and CsBr) and cesium iodide.[108]

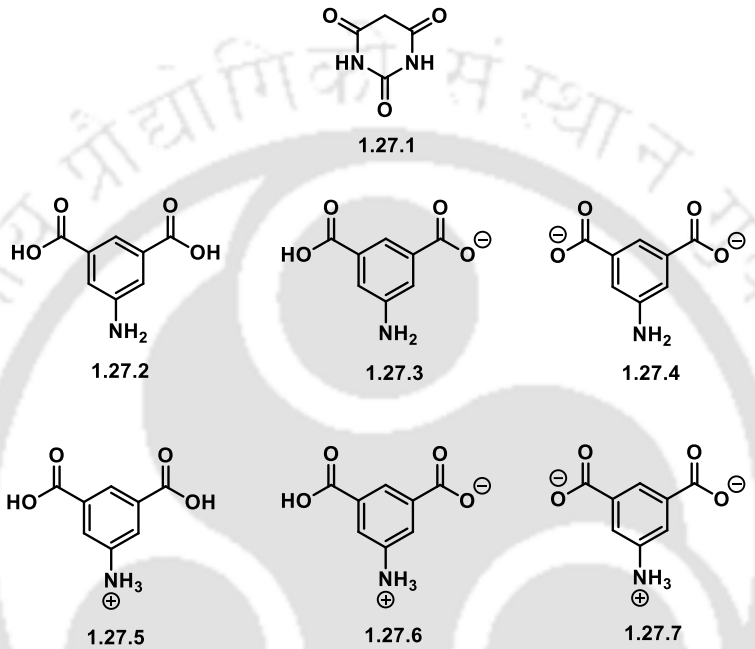

Figure 1.27: Structure of barbutiric acid **1.27.1** and **1.27.2-1.27.7** are different ionic forms of 5-aminoisophthalic acid.

5-Aminoisophthalic acid is an amphoteric acid (**1.27.2** to **1.27.7**), the neutral, ionic and zwitterionic forms of it could be stabilized in different self-assemblies of salts or ionic-cocrystals. Dianion **1.27.4** of the acid was observed in hydrated 1:2 salt with 6-methylpyridin-2-amine, whereas the salt of it with 5-methylthiazol-2-amine had the zwitterionic anion form **1.27.7** of the acid. The mono-anion **1.27.3** of the 5-aminoisophthalic acid was observed in the salt of 4,6-dimethylpyrimidin-2-amine.[109] The self-assembly of the 1:1 cocrystal of caffeine with 5-aminoisophthalic acid had neutral form **1.27.2** of the acid and the cationic form **1.27.5** of the acid was observed in the perchlorate and bromide salts.

The ionic-cocrystals formed by partial proton transfer was observed in the ionic-cocrystal squaric acid (H_2squ) with 4,4′-bipyridine (4bpy). The formation of such crystals was dependent on crystallization. Slow crystallization at room temperature provided the 1:1 salt $[H\text{-}4bpy]^+[Hsqu]^-$, (**1.28.1**).Whereas, crystallization from solution treated at higher-temperature provided a di-salt

TH-3622_196122001

$[H_2\text{-4bpy}]^{2+}[squ]^{2-}$ **1.28.2a** and another form (**1.28.2b)** of the salt that had proton disorder across intermolecular hydrogen bonds in which the shared protons had 0.82:0.18 occupancy for $^{+}$N–H···O^{-} and N···H–O forms. Each of these salts had distinguishable shape and color of the crystals.[110]

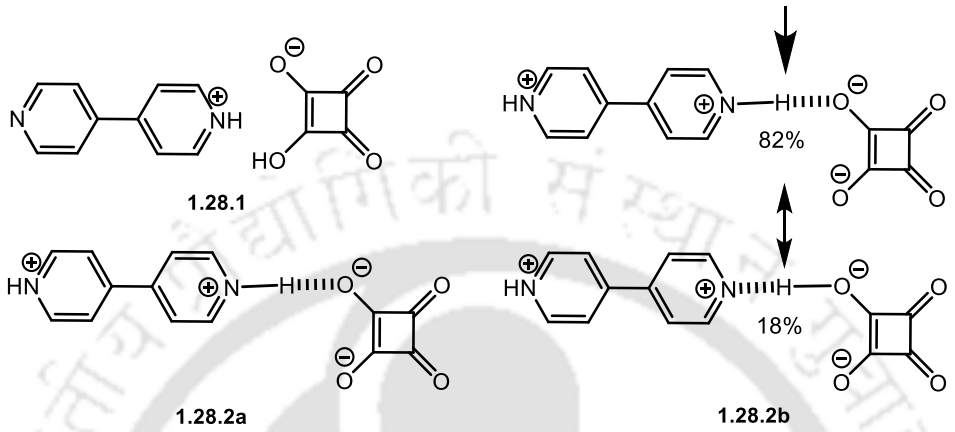

Figure 1.28: Two different salts of squaric acid with 4,4′-bipyridine , in a second form of the dianionic salt proton disorder was observed.

The foregoing discussion have suggested that ionic-cocrystals of simple organic compounds based on the acid-base principle and the accommodation of neutral molecules with the ion pair, are not limited to organic ionic counter parts but neutral organic molecules form assemblies with ionic salts. The modulation of solubility and release of different components have applications in adsorptions to provide remediation of contaminants, release of fertilizers to soil. These necessitates developing newer assemblies through hierarchy and understanding of relative proton-transfer between different components and extend to diverse possibilities. In the next section the ionic-cocrystals of drug molecules are discussed.

1.6.1. Ionic-cocrystals with drug molecules

Primary benefit of formulating drugs as ionic-cocrystals is to have multiple chemical units in a drug to decreases the numbers of pills to be taken by patients and enhances one or more physicochemical properties. Recent studies on ionic-cocrystals have indicated to improve various solid-state properties, particularly solubility,[111] melting point,[105] and dissolution rate. [112,113] The ionic-cocrystals have emerged as an important topic of research in chemistry of formulating effective drugs. For a drug modulation of active component in a formulation and their easy release from an assembly are prerequisites, which can be take care by ionic-cocrystals of drug molecules.

TH-3622_196122001

Many insoluble drugs have been improved to have greater solubility and performance without an adverse effect. In fact, some drug molecules were modified to provide dual roles and to control release. The ionic-cocrystals of 5-amino-2-naphthalene sulfonate with ammonium ions have pharmaceutical applications and they show non-linear optical properties.[114]

The salt/ionic-cocrystal forms of Pefloxacin[115] with succinic acid had easier dissolution at pH 1.2 (acidic, like gastric environment) and pH 7 phosphate buffer media (neutral, like intestinal passage). Lithium based drugs are very efficient for treatment of maniac episodes in bipolar disorder, however their utility is limited due to hygroscopicity. Ionic-cocrystals of lithium chloride

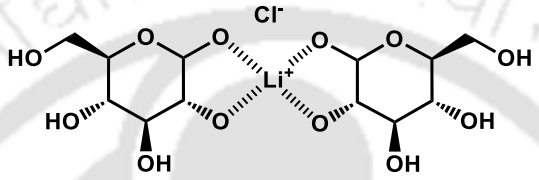

Figure 1.29: Ionic-cocrystal of glucose with lithium chloride.

with glucose[116] shown in the Figure 1.29 have been utilized to overcome this. The ionic-cocrystal caused improvement on the drug action in blood and brain pharmacokinetics. The stability of the ionic-cocrystal and no adverse effect in vivo performance, has given higher scopes for its applications. Many active pharmaceutical ingredients (APIs) are formulated in solid forms have ICCs as active ingredients. As an example, fluoxetine hydrochloride is used as antidepressant. Prozac was co-crystallized with benzoic acid, succinic acid and fumaric acid in different ratios, it had altered the physiochemical properties of the parent API.[111]

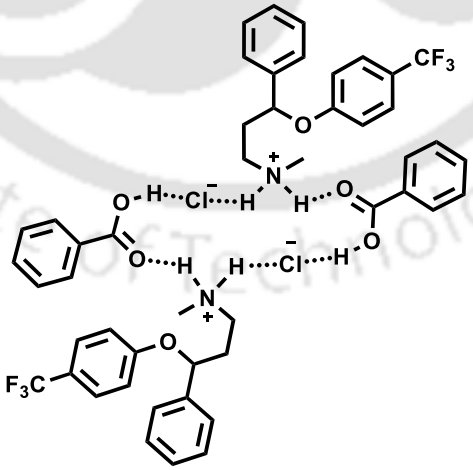

Figure 1.30: The assembly fluoxetine hydrochloride–benzoic acid ionic-cocrystal.

Divalproex sodium, is an anticonvulsant used for treatment of epilepsy, it consists of sodium valproate and valproic acid.[117] The ionic-cocrystals of drugs such as ciprofloxacin (cip),

TH-3622_196122001

norfloxacin (nor), and enrofloxacin (enro) with α,ω-dicarboxylic acids listed in Figure 1.31 adopt any of the forms out of A^+B^-, $A^{2+}B^{2-}$, $A^{2+}B^{2-}B$, and A^+B^-A. From glutaric acid, adipic acid, pimelic acid, suberic acid, azeliac acid, and sebacic acid the cocrystals were guided by $R_2NH_2^+\cdots^-OOC$ or $R_3NH^+\cdots^-OOC$ hydrogen bonds but each had different supramolecular synthons and certain assemblies formed gels.[118a] Some ionic-cocrystals with multicomponent compositions are [(enro$^+$)$_2$(adipate^{2-})·adipic acid·CH_3CN] and [(nor$^+$)$_2$(azeliacate^{2-})·azeliac acid ·$4H_2O$]. The salts like fumarate, oxalate, tartrate and malonate salts of these drugs have 30 to 110 times higher solubility than the parent drug molecules.[118b,c]

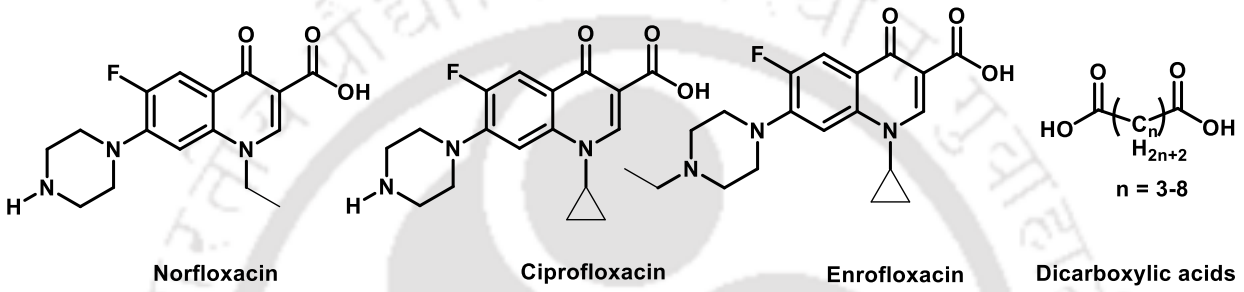

Figure 1.31: The structures of ciprofloxacin, norfloxacin, and enrofloxacin and coformer α,ω-dicarboxylic acids.

Ionic-cocrystal of isoniazid with carboxylic acid such as 2,5-dihydroxybenzoic acid, 2,4-dihydroxycinnamic acid together with water molecule were studied for their change in the API properties from the parent drug molecule.[119] Sulfonated Schiff bases were reported to form ionic-cocrystals with bipyridyl and bipyridyl ethane. They had higher solubility than the single component and each had sulfonamide-pyridine synthon.[120]

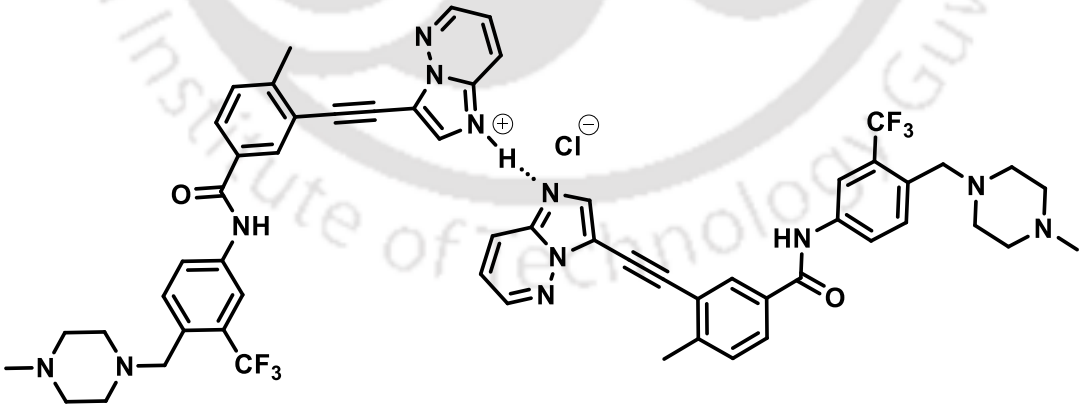

Figure 1.31: Assembling of ponatinib hydrochloride with ponatinib.

The active pharmaceutical ingredient ponatinib hydrochloride, shown in Figure 1.31, forms an ionic-cocrystal due to differences in hydrogen bond donor sites within the molecules, as well as interactions involving the assembly of mono-cations, di-cations, water molecules, and chloride

TH-3622_196122001

ions. Hydrogen bond between the ponatinib mono-cations and di-cations were held together by hydrogen bonds, the chloride ion was located between the square voids created within by assembled cations.[121]

The antimalarial drug pyrimethamine (pyr) varieties of multicomponent ionic-cocrystals with conformer such as barbituric acid (Hbar), succinimide (suc), benzoic acid (Hben), sorbic acid (Hso), glutarimide (glu), such as $Hpyr^{+}\cdot bar^{-}\cdot pyr$, $(H^{+}pyr\cdot sac^{-})_2\cdot glu$, $(Hpyr^{+}\cdot ben^{-})\cdot pyr\cdot suc$ and $(H^{+}pyr\cdot sac^{-})_2\cdot sor$. The drug molecules also provided binary salts with glutarimide and nicotinic acid. The structure of the 2:1:1 ionic-cocrystal of pyrimethamine with succinimide, benzoic acid is shown in the Figure 1.32. The assembly was comprised of N-H…O and N-H…N hydrogen bonds. The synthetic procedure of these cocrystals were dependent on the reaction conditions; for example, the mechanochemical synthesis yielded first two ionic salts, solution crystallization yield the third and fourth one, whereas the salts were prepared by sublimation. The advantages of the ball milling technique were shown in this study; where it was shown that the $(H^{+}pyr\cdot sac^{-})_2\cdot glu$ cocrystal was prepared by adding the coformers in a step wise manner under milling conditions.[122]

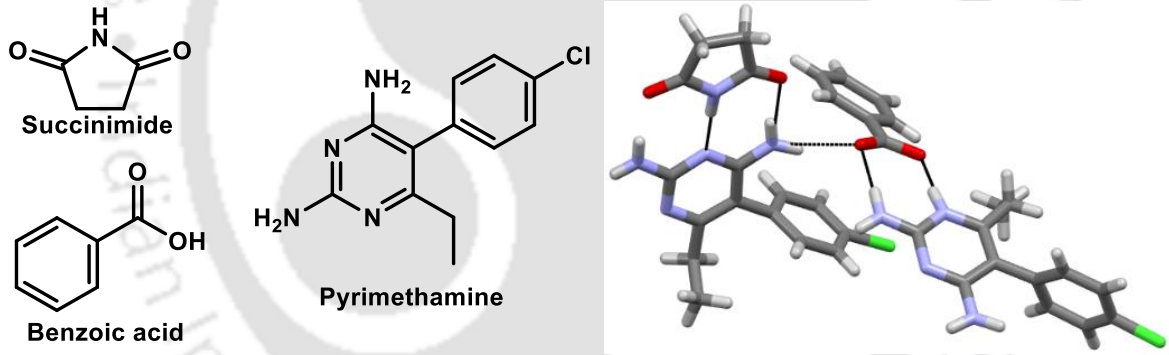

Figure 1.32: An 2:1:1 ionic-cocrystal of pyrimethamine with succinimide, benzoic acid.

The *cis* as well as the *trans* butenedioic acid form ionic-cocrystals with marbofloxacin (mbf) {**1.33.1**}. *Trans* isomer, the fumaric acid (H_2fa) provided ionic-cocrystal (Hmbf·fa·H_2fa) {**1.33.2**}; whereas, the *cis* conformer maleic acid (H_2ma) provided a salt mbf·ma. Each had different types of assembly, in the case of fumaric acid, it adopted a linear geometry whereas the maleic acid had a bent geometry. The salt mbf·ma had higher solubility and permeation rate than the ionic-cocrystal mbf·fa·H_2fa This was due to the balance required to be maintained due to composition differences to control those properties. The salt had higher in-vitro bacterial inhibitory activity assays against Gram-negative and Gram-positive bacterial strains than the ionic-cocrystal and the parent marbofloxacin. Hence, in this case the ionic-cocrystal did not show superior property to a

TH-3622_196122001

salt. The ionic-cocrystal has a layer-like arrangements of anions and neutral dicarboxylic acid molecules on which the cations of the drug molecule were decorated (Figure **1.33)** by charge-assisted hydrogen bonds.[123]

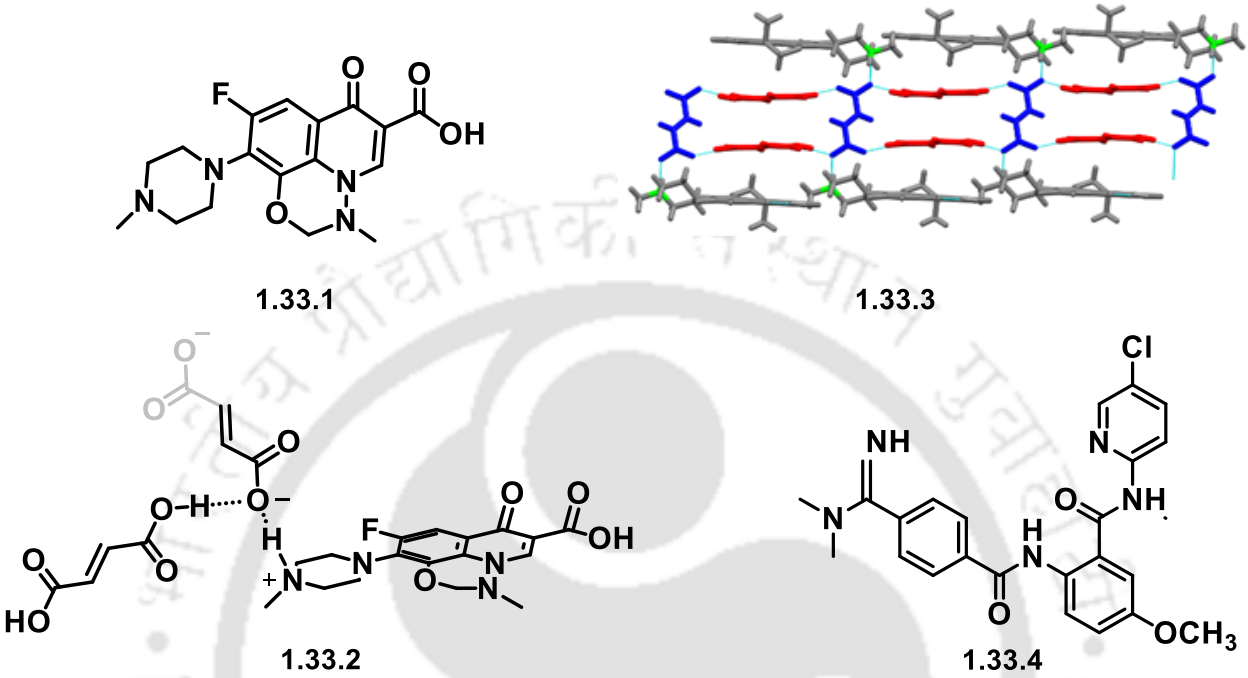

Figure 1.33: The structure of marbofloxacin **1.33.1**, assymetric unit of the assembly Hmbf•fa•H_2fa (half of fa is shown in grey for ease of understanding) **1.33.2** and the packing of the ionic-cocrystal **1.33.3**. The structure of betrixaban **1.33.4**.

Betrixaban (**1.33.4**), is an anticoagulant drug which finds use in venous thromboembolism. The betrixaban forms ionic-cocrystal with maleic acid, which is comprised of the protic-drug maleate maleic acid hydrate (1:1:2:1). The ionic-cocrystal showed a 117°C lower melting difference than salt-cocrystal hydrate of betrixaban.[124] In this example, also the ionic-cocrystal hydrate had 10 times lower solubility as compared to its salt. Based on these results and analysis of the structures it was suggested that the common-ion effect had played the key role in having the lower solubility of the ionic-cocrystal hydrate where drug to coformer ratio was 1:3.

The sulfamethazine drug molecule forms 2:2 ionic-cocrystal with 4-biphenylcarboxylic acid. It crystallized as di-hydrate. The cocrystal has neutral and protonated sulfamethazine molecules.[125] It is a cocrystal of the salt formed by proton transfer between the conjugate acid and base with a cocrystal of the two components. The neutral portion of this ionic-cocrystal had the sulfamethazine hydrogen-bonded to a neutral carboxylic acid, whereas the salt portion had protonated host

TH-3622_196122001

forming charge-assisted hydrogen-bond with the protonated sulfamethazine with the carboxylate ion.

Diclofenac is a commonly used medicine for external healing of wounds. Various compositions and structural variations are observed in assembling of alkali metal complex of the diclofenac.[126] For example, the lithium salt of it having 1,10-phenanthroline ligand is a hydrogen bonded assembly of $[(1,10\text{-phenanthroline})Li(H_2O)_2]^+$ with diclofenac anion (Figure 1.34).

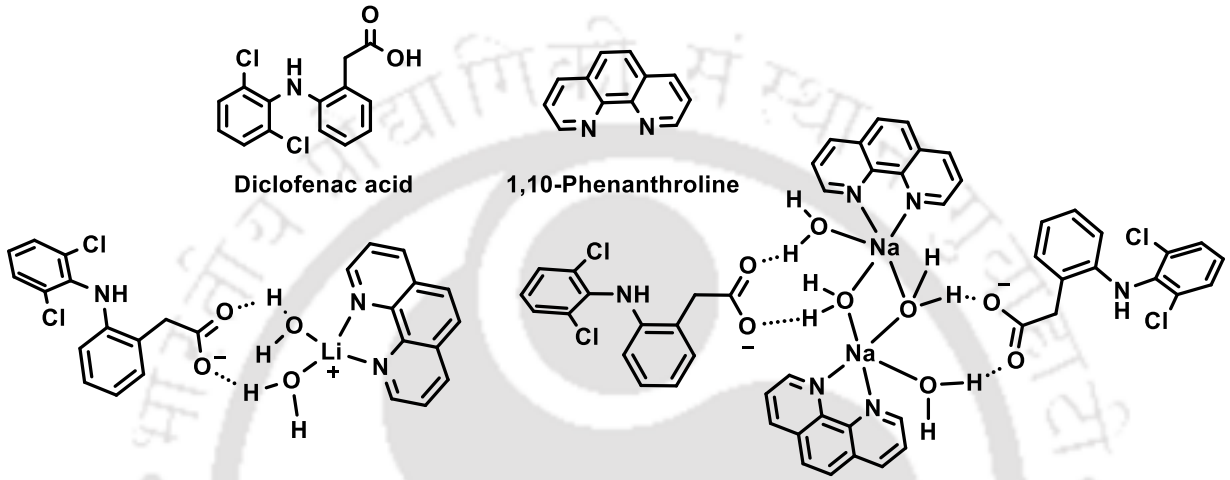

Figure 1.34: The assemblies of lithium and sodium 1,10-phenanthroline complex cations with anion of diclofenac.

Whereas that of the sodium is a binuclear moiety formed by water molecules bridging the sodium ions and coordination of 1,10-phenanthroline, hydrogen bonded with the diclofenac anion. Due to the intrinsic acid base properties of many drugs they form various ionic-cocrystals. These cocrystals have largely contributed to increase availability of active components and modulated solubility. The hydration of certain drugs is controlled to modulate hygroscopicity of drugs. The advantage is that these ionic-cocrystals ability to serve as multi-drugs and dose modulation with modulated activity and release.

The above discussions have revealed the formulation of drug molecules have wide versatility. Depending on the ionic counterpart structural variations and solubility properties and drug availability is enhanced. The ionic-cocrystals of drugs as other material and in waste management requires attention and a systematic approach.

TH-3622_196122001

1.6.2. Ionic-cocrystals having Energetic components

Cambridge crystallographic database analysis also has emerged as a tool to design energetic ionic-cocrystals. One such recent analysis was to find out a rationally predicted ionic-cocrystals of ammonium nitrate. Ammonium nitrate, an energetic compound, showed that several ionic crystals formed varieties of organic nitrogen-based heterocycles. The data-base analysis had enabled one to find out the postulate molecular descriptors which did not tally with the salts and ionic-cocrystal. The important fact observed was that the ionic-cocrystals had high packing coefficiency. The analysis of new intermolecular interaction motifs that drive assembly such as halogen bonding has been also useful in understanding of packing similarities in ionic-cocrystals.[127] The new search of such cocrystals has the purpose to cocrystallize molecules having excess of oxidizing power with oxygen-deficient molecules changes the explosive performance. One of the limitations for such studies over predicting a new combination, inability to predict outcome on properties other than case by case demonstrations on superior or inferior performances as high energy materials. Ammonium perchlorate was also modified to ionic-cocrystal and the modified forms have improved oxidizing properties.[128]

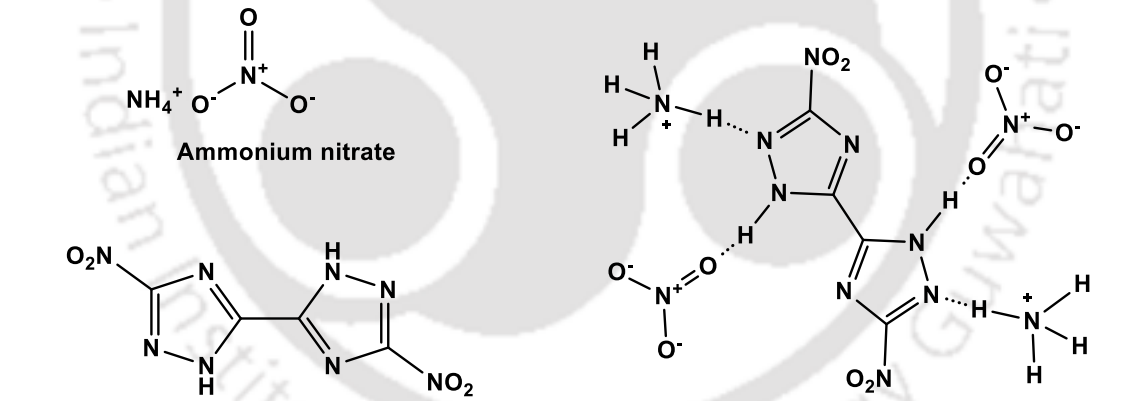

Figure 1.35: The ionic-cocrystal of 5,5′-dinitro-2H,2H′-3,3′-bi-1,2,4-triazole with ammonium nitrate.

Ammonium nitrate as high energy material has prospect as a rocket fuel. The ionic-cocrystals of energetic molecule 5,5′-dinitro-2*H*,2*H*′-3,3’-bi-1,2,4-triazole (Figure 1.35) with ammonium nitrate in a 1:2 molar ration maintained a positive oxygen balance during combustion. This ionic-cocrystal did not undergo solid-state phase transition that was observed with pure ammonium nitrate. Another such example is 2:1 ionic-cocrystal of ammonium dinitride with 5,5′-dinitro-2*H*,2*H*′-3,3″-bi-1,2,4-triazole showed high oxygen balance.[129] The nitro barbituric acid and 7*H*-

TH-3622_196122001

[1,2,4]triazolo[4,3-*b*][1,2,4]triazole-3,6,7-triamine with 1:2 stoichiometry is also studied for the modulation of explosive behavior of parent compounds. It has low impact and high friction sensitivity comparable to trinitrotoluene. There are many ionic-cocrystals of energetic molecules, either as combination of an explosive with non-explosive component or another high energetic component to control the release of energy during explosion and to change the activation required for an explosion.

There are large scopes to modify the compositions explosive properties by utilization of non-covalent interactions of energetic molecules. It allows to modify the explosion process of identified explosive as required for application in specific purpose. The ability to produce stable products allows them to prepare explosive with durable properties for on time requirements.

1.6.3. Ionic-cocrystals of inorganic metal complexes

As in the introductory section of ionic-cocrystals, it was shown that many inorganic salts of alkali and alkaline earth metals form ionic-cocrystals with organic hosts. Essential transition metal containing components as inorganic API such as 1:1 ionic-cocrystal of zinc benzoate with isonicotinamide were prepared and tested for medicinal activities. In such examples the polar groups exposed on its prominent crystalline faces, which provided a strategy reduced hydrophobicity of the parent forms.[130]The use of metal complexes in composites as well as in nano-materials has opened new avenues to study ability of the inorganic complexes in ionic or neutral form to encapsulate an organic compound. Considering the assembling of ionic inorganic complexes provide larger avenues for studying host-guest complexes. Furthermore, assembling of inorganic complexes are guided by electronic factors of central metal ion/s,[131] but significantly influenced by steric factors.[132]

Different properties such as electrochemical, phase-transition change from the individual parent components upon formation of inclusion complexes.[133] On the other hand, common organic compound such as thiourea can be included in ferrocene and its channels.[134] Hence, the inclusion of ionic complex in neutral organic host provide alternative means to study such systems. There are also many studies dealing with cation and anion encapsulations in assemblies.[135]These provide impetus to study the host-guest chemistry of ionic-cocrystals. Voids created by assembling of inorganic compounds helps to cause catalytic reactions.[136] Furthermore, ionic cages are designed

TH-3622_196122001

for inclusion of organic compound,[137] and have application in molecular recognition, self-sorting, catalysis.[138] Having difference in the peripheral part of the ligand causes large difference in the packing leading to modulation of structural patterns. Nano-droplet like structures are produced by aggregation of multiple numbers of metal sites.[139]The vessels like assemblies have been prepared to get specific reactivity to synthesize selective products. For examples inorganic cages have helped to perform diel-Alder reaction in aqueous medium.[140]The discrete metal complexes possessing complementary sites for supramolecular interactions are suitable for generating new assemblies and have potential in biomedicine and optoelectronics.[141]To have molecular understanding there is necessity to have detailed understanding on intermolecular forces within them. Anion coordination have provided large avenues in supramolecular assembly and it has been extended to prepare framework structures.[142a] Supramolecular assembly of ionic coordination complex of platinum shown in Figure 1.36 adopts nano-dimensional structures through different method of preparation.

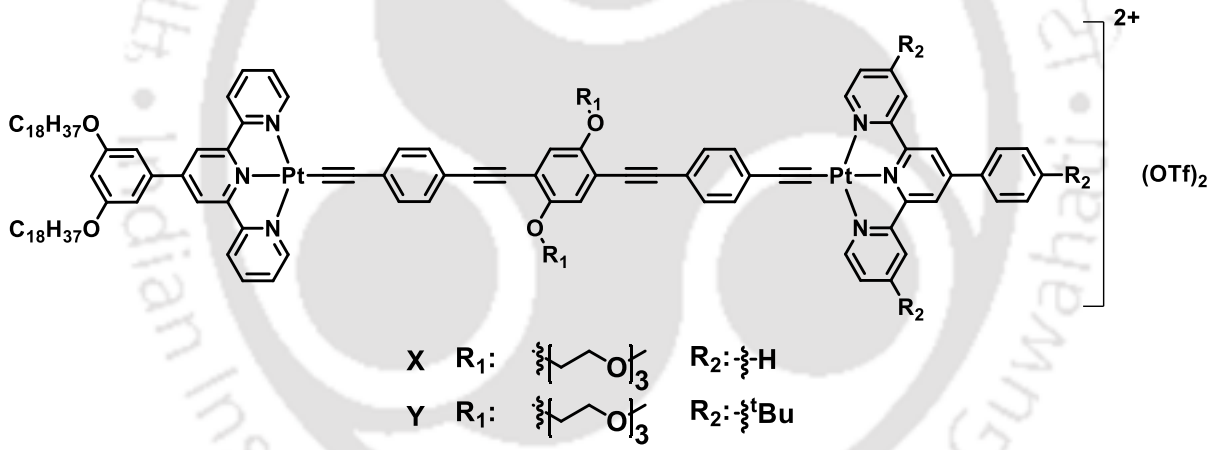

Figure 1.36: Examples of platinum complexes that show stacking among the planar units.

The cation recognitions have been another central point in supramolecular chemistry to build new assemblies and to confer novel properties. Hence, the combined effect of the anionic and cationic part being realized through ionic complexes, hence have prospects for new material properties.

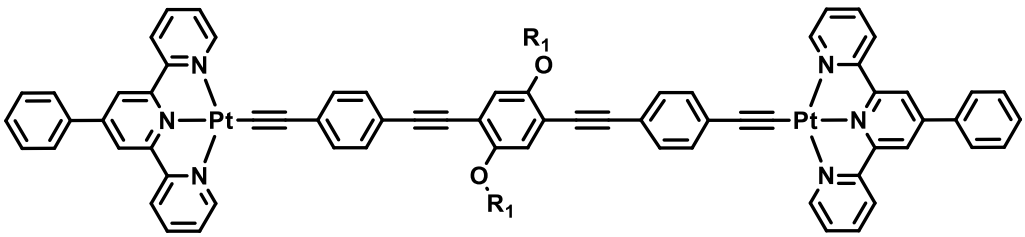

1.37.1

TH-3622_196122001

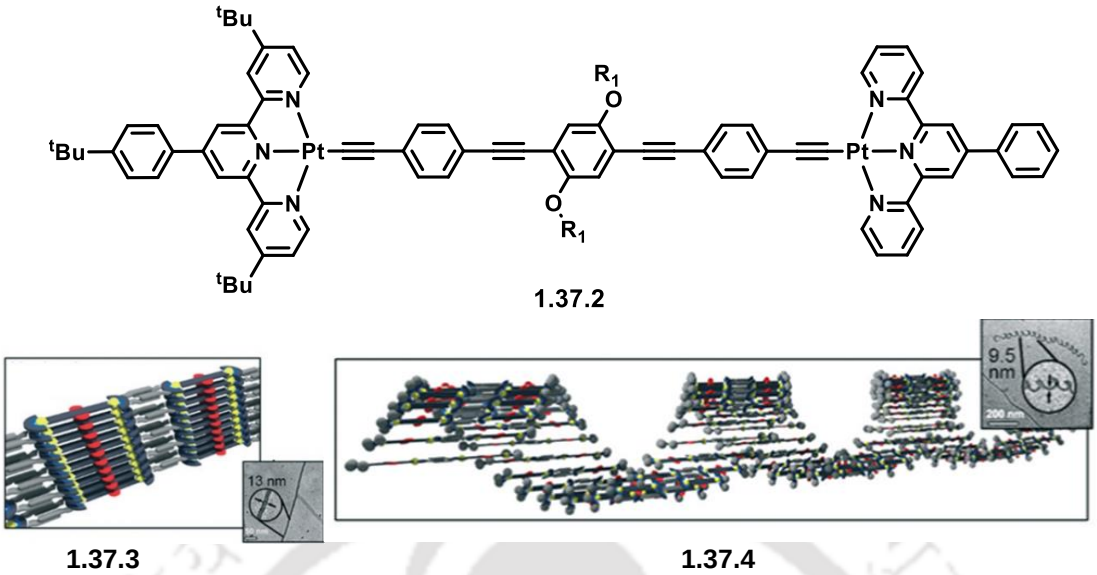

Figure 1.37: Self-assembly of dinuclear complex **1.37.1** and **1.37.2** in DMSO. **1.37.3** and **1.37.4** are the type of assemblies found within the respective assembly.

Cationic self-assemblies of metal complexes are anchored to surface of metal nano-particles (Figure 1.37). The materials have relevance to explore the inherent interactions of the ionic components with a change neutral surface.[142b]

Many self-assemblies having metal-metal interactions may be further assembled by weak interactions to provide multicomponent non-covalent assemblies with structural varieties as well as with new properties. In the Figure 1.38, the dinuclear platinum complex, each platinum site has a square planar geometry. The complex is observed as dimers, which is formed through Pt···Pt interactions.[143] These dimers are assembled through iodine···platimum interactions to provide linear chain like structure by interacting with 4,4′-diiodo octa-fluorobiphenyl as shown in the Figure 1.38. This provided a non-covalently linked polymeric chain-like structure. Though this polymeric complex is not derived from ionic components, yet it has interest to understand role of weak iodine···metal interactions to provide stable non-covalent assemblies of inorganic complexes

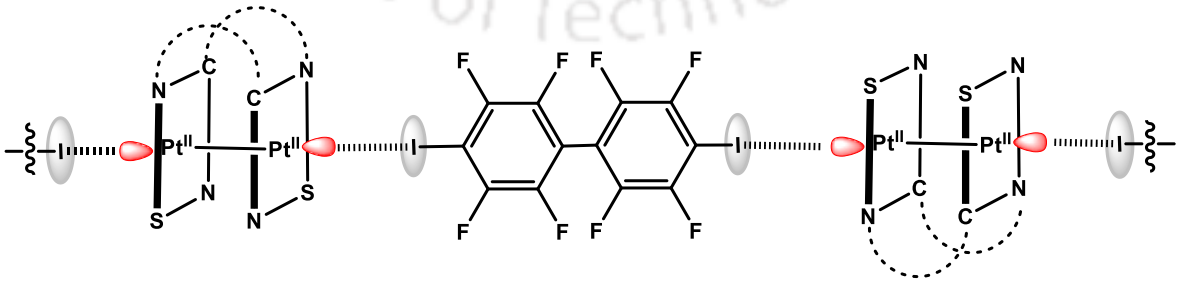

Figure 1.38: supramolecular coordination polymer having platinum···iodine interactions.

TH-3622_196122001

with organic compounds. The nucleobases have multiple sites for protonation and the protonated and neutral molecules get organized in different ways as shown in the Figure 1.39. The hydrogen bonded chains of the protonated adenine (ade) and cytosine (cyt) were stabilized in bis-dipicolinato metal(II) (metal = manganese, copper, zinc at +2 oxidation state) complexes were reported in literature.[144] Protonated adenine were organized as [1H, 9H-ade][3H, 7H-ade] and was stabilized by $[MnL_2]\cdot 3H_2O$; whereas cytosinium cation were found to aggregate with neutral cytosine and hydrogen bond with the seven coordinated manganese (II) complex [1H, 3H-cyt]$_2$[$MnL_2(H_2O)$]·2cyt·$6H_2O$.

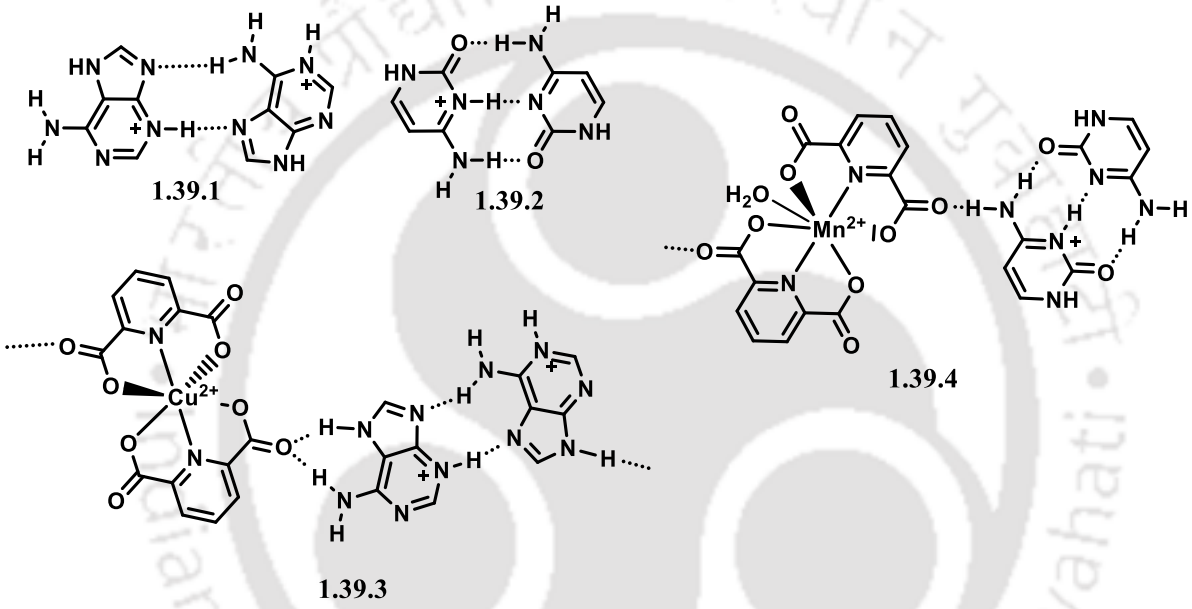

Figure 1.39: The assembling of neutral and protonated base pair of adenines **1.39.1** and cytosine **1.39.2** and their stabilization in metal-2,6-pyridinedicarboxylate complexes **1.39.3** & **1.39.4**.

First row transition metal oxalate (ox) are used for preparation of different assemblies having protonated nucleobase as the organocations. In the complexes having cytosinium cations (1H,3H-cyt) in the complex (1H,3H-cyt)$_2$[M(ox)$_2$(H_2O)$_2$] (M(II) = Mn, Co, Cu and Zn) adopted three-dimensional lamellar structure. These structures had layers of metal–oxalato complexes and hydrogen-bonded one-dimensional (1D) ribbon-like aggregates of the protonated cytosine molecules.[145] Similar complexes where 1H,9H-adeninium were the organocations, also had supramolecular self-assembled structures, but had wide differences in their respective assemblies as compared to the assembly of the analogous complex having cytosinium cations.[146] This difference was due to the changes in the complementary hydrogen bonded schemes and differences in the hydrogen bonding patterns in each case.

TH-3622_196122001

The protonated adenine or thymine, hydrogen bonds with polyoxometalate to provide self-assembled nanostructures. Redox-active functional nano-scale hybrid-materials were prepared from protonated nucleobases, phospho-molybdic acid, tetra-chloroaurate ion with a composition PMA/adenine/$[AuCl_4]^-$ had showed anti-cancer activity.[147] Beside these, mixed-valent tetranuclear oxide-bridged complex of cobalt(II) and cobalt(III) as metal ions $[(\mu_2\text{-Htea})_2(bpy)_2Co_2(\mu_3\text{-O})_2Co_2(bpy)_2]Cl_2.[Co(H_2O)_6]Cl_2.5H_2O$ (Htea = dianion of triethanolamine, bpy =2,2′-bipyridine) is an example of nano-dimensional inorganic ionic-cocrystal. This complex underwent cation exchange upon reaction with chloride salts MCl_2 (M = Zn or Cd) to form new complexes $[(\mu_2\text{-Htea})_2(bpy)_2Co_2(\mu_3\text{-O})_2Co_2(bpy)_2]^{2+}[MCl_4]^{2-}$.[148]

The methylbenzylammonium copper pyridine-2,4-dicarboxylate complex form inclusion complex with of different alcohols. The complexes with composition $[ma]_2Cu(24\text{-pdc})_2(H_2O).ROH$ (ma = methylbenzylammonium, 2,4-pdc = pyridine-2,4-dicarboxylate and ROH = 1-octanol, 2-octanol, cyclohexanol have showed that various alcohol molecules with relatively long hydrophobic alkyl unit could be intercalated to the assembly of coordination polymer.[149]Similar copper (II) complexes also include pyridine and pyridine based molecules such as methylpyridine, 4-t-butylpyridine.[150] Similarly, *bis*-8-hydroxyquinolinium-zinc-2,6-pyridinedicarboxylate complex holds three molecules of 4-nitrophenol in its self-assembly.[151]

In this complex, the 4-nitrophenol molecules were hydrogen bonded to the organo-cation through the water molecules of crystallization. The π-stacked anions provide anionic layers with closest inter-layer separation distance is 18.94 Å. In the complex $[Cu(ppz)_2(NO_3)_2\cdot 0.35H_2O][ppz]_2$ (**1.40.1**) has stacking among the coordinated trans-2-(2-phenylethenyl)pyrazine (ppz) ligand coordinated to copper ions formed layer-like assemblies in which the free trans-2-(2-phenylethenyl)pyrazine molecules were held (**1.40.2**). This complex is an example of self-inclusion of a ligand in a complex.[152]

Sodium metal clusters Na_5O were embedded in metal cage $[Ni(prodicarb)]_9$ to provide $\{(Na_5O)[Ni(prodicarb)]_9(MeOH)_3\}(BF_4)_2\cdot OH\cdot CH_3OH$. The ligand formed different aquated clusters with nickel depending on the type of aquated clusters of alkali-metal cations. The $[Ni(prodicarb)])]_8$ cage was embedded trigonal bipyramidal $[Na_3Li_2O]^{3+}$ cations provided a complex $\{(Na_3Li_2O)[Ni(prodicarb)]_8(CH_3OH)_{1.3}(BF_4)_{0.7}\}(BF_4)_{2.3}\cdot(CH_3OH)_{2.75}\cdot(C_4H_{10}O)_{0.5}$. The complexes with tetrahedral $[Li_4O]^{2+}$ ions had hexanuclear open cage $[Ni(prodicarb)])]_6$ to form a

TH-3622_196122001

complex $\{(Li_4O)[Ni(prodicarb)]\}_6(CH_3OH)_3\}2ClO_4 \cdot 1.85CH_3OH$.[153] These examples have suggested the utility of self-organization of non-covalent assemblies as well as hydrogen bonded networks to adopt suitable geometry as well as to create adequate space for selected cations.

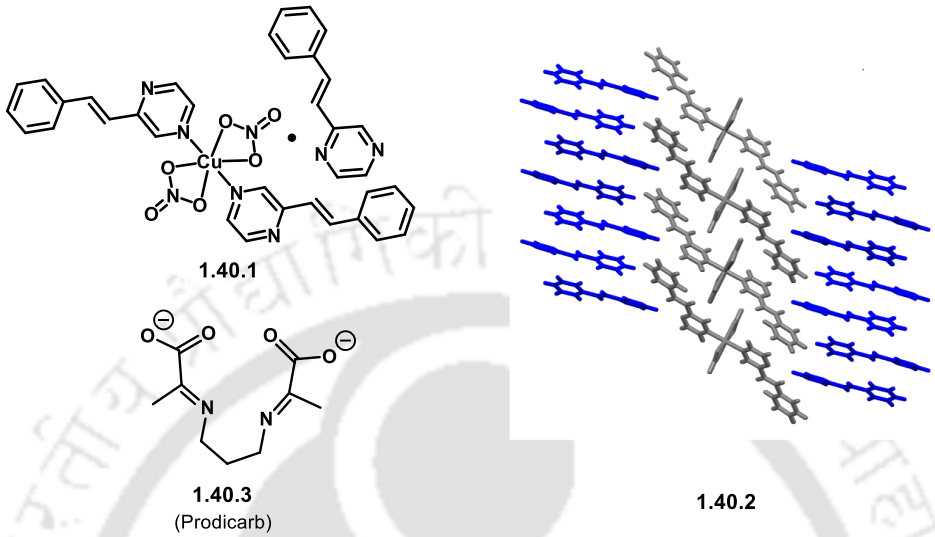

Figure 1.40: Inclusion of 2-(2-phenylethenyl)pyrazine in the trans-2-(2-phenylethenyl)pyrazine copper(II) complex (**1.40.1)** and its self-assembly **1.40.2** along *ac*-crystallographic plane.

The dications of the 1,4-diazacycloheptane (dahc) was involved in the self-assembling of di-aqua bis-malonate copper(II) complex (H_2dahc) $[Cu(mal)_2(H_2O)_2](H_2O)_2$; whereas the dications of the 1,5-diazacyclooctane (daco) were doing a similar role in the self-assembly of similar cobalt(II) complex H_2daco$[Co(mal)_2(H_2O)_2]$. In these complexes the mononuclear $[M(mal)_2(H_2O)_2]^{2-}$ blocks were hydrogen bonded with the help of water molecules to provide 2D-networks which were held by the cationic diamines to provide 3D pillar-layered solids. Here the free as well as coordinated water molecules provided hydrogen bonding sites to stabilize the pillar-like structures[154] There are example of zinc(II) complexes, of 2,4-pyridinedicarboxylate two linear peripheral carboxylate units, together with 3,3′-dimethylbenzidene forming channel-like structures to act as host for small organic molecules. The porous solids had strong, charge-assisted hydrogen bonds and the guests such as *p*-xylene, nitrobenzene, and hexanol were included by the coordination polymer. The important aspect of such assembly was to have retained the hydrogen-bonded framework upon guest loss under vacuum below ~200°C.[155]

The cobalt(II) and copper(II) dibenzoylmethanate were used as template to bind with isonicotinamide, nicotinamide or imidazole. It was found that liquid-assisted grinding provided quantitative inclusion compounds within 20 minutes.[156] In the scheme that shown a linear self-

TH-3622_196122001

assembled structure were formed by involving second coordination sphere of the mononuclear complexes. These assemblies when treated with DMF by liquid assisted grinding, it included DMF molecules as shown in the Figure 1.41. The complexes formed layer where the inclusion of DMF molecules were held by weak C-H···O interactions.

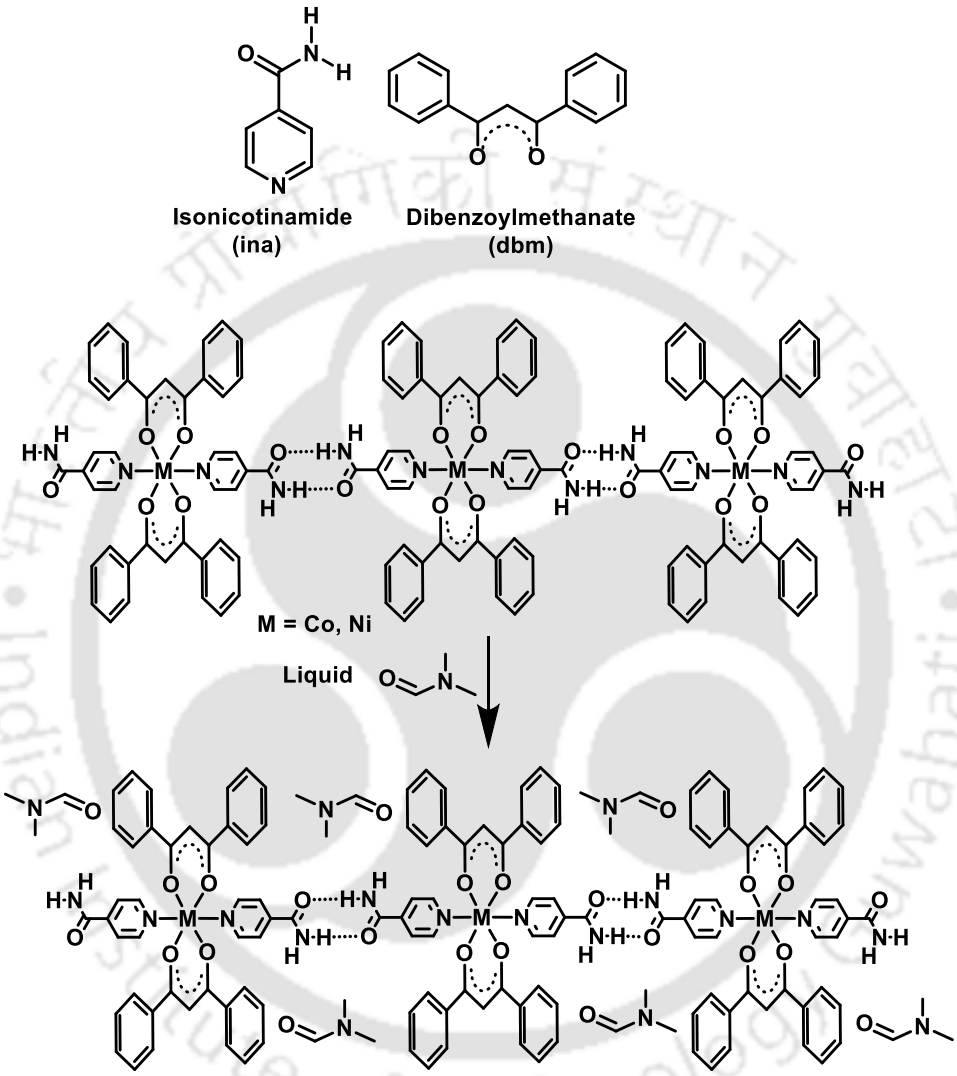

Figure 1.41: Dimethyl formamide included complexes prepared by liquid assisted grinding method.

In $[Ni(im)_6](pfbz)_2$ (im = imidazole, pfbz = penta-fluorobenzoate) complex is an example where the C-H···F hydrogen bonds contribute to generate three dimensional framework.[157] In this example the carboxylate anion of the penta-fluorobenzene carboxylate formed strong N–H···O hydrogen bonds with two imidazoles bound to central nickel ion. The C–H···F bonds had provided the rigidity and directionality to the assembly. These interactions generated a 2D-supramolecular layer which further assemble to provide three-dimensional supramolecular assembly (Figure 1.42.2).

TH-3622_196122001

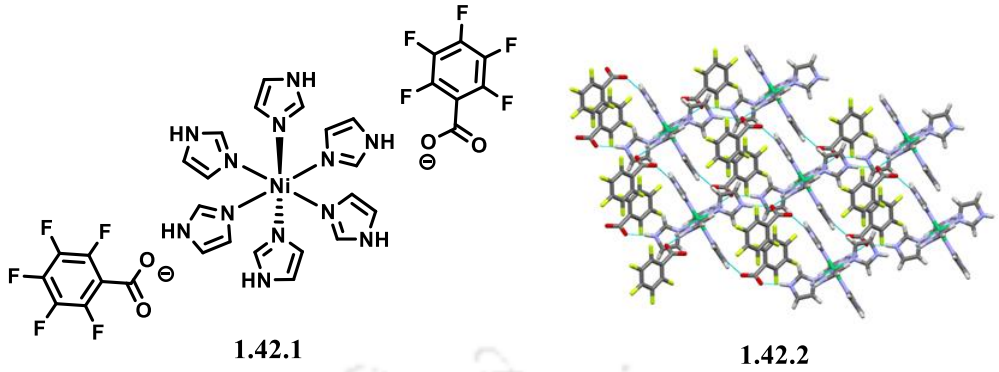

1.42.1 **1.42.2**

Figure 1.42: The $[Ni(imi_6](pfbz)_2$ **1.42.1** and its self-assembly along *bc*-crystallographic plane **1.42.2**.

Zinc ortho-phosphate complex $[Zn(H_2O)_2(H_2PO_4)_2]\cdot 2(paba)$ possess neutral *p*-amino benzoic acid (paba) as partner molecules. It has an assembly pillared by hydrogen-bonded paba with the inorganic portion of the complex. The structure has organic and inorganic chains at alternate positions forming 2-dimensional layer-like structure. This layer has extensive intermolecular hydrogen bonds between the nitrogen atoms of paba with two oxygen atoms from phosphates in the adjacent inorganic chains.[158]

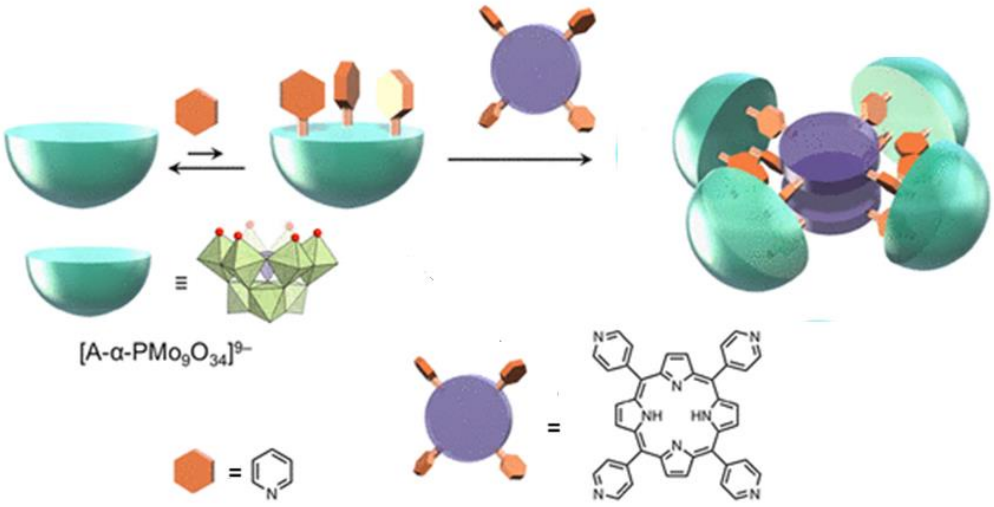

Figure 1.43: Self-assembly of phosphomolybdates and porphyrin based pyridyl ligand.

The supramolecular assemblies extended to lacunary polyoxometalates (POMs) for well-defined coordination sites have large scope to obtain designable properties. The literature being vast and has extensive complexity, hence the discussion is limited to only two examples. The self-assembly of anionic POM comprising multi-vacant lacunary phosphomolybdate $[A\text{-}\alpha\text{-}PMo_9O_{34}]^{9-}$ functionalized with pyridine through weak interactions further gets modified porphyrin based

TH-3622_196122001

pyridyl ligand to form self-assembled structures that intercalate aromatic molecules (Figure 1.43).[159]

The foregoing discussion on the selected examples showed that there are many inorganic complexes self-assemble to modulate their properties. Designing synthetic paths control associative and dissociative equilibriums that are controlled by weak ligation and exchange through weak interactions.The chirality can be changed by careful choice of a third components. Hence, the role of second coordination sphere coupled with electrostatic effect of ions and the weak interactions of guest molecules have scopes to extend to nano-dimensional assemblies or composite designs. Nonetheless, the studying the ionic-cocrystals at molecular level has its fundamental values.

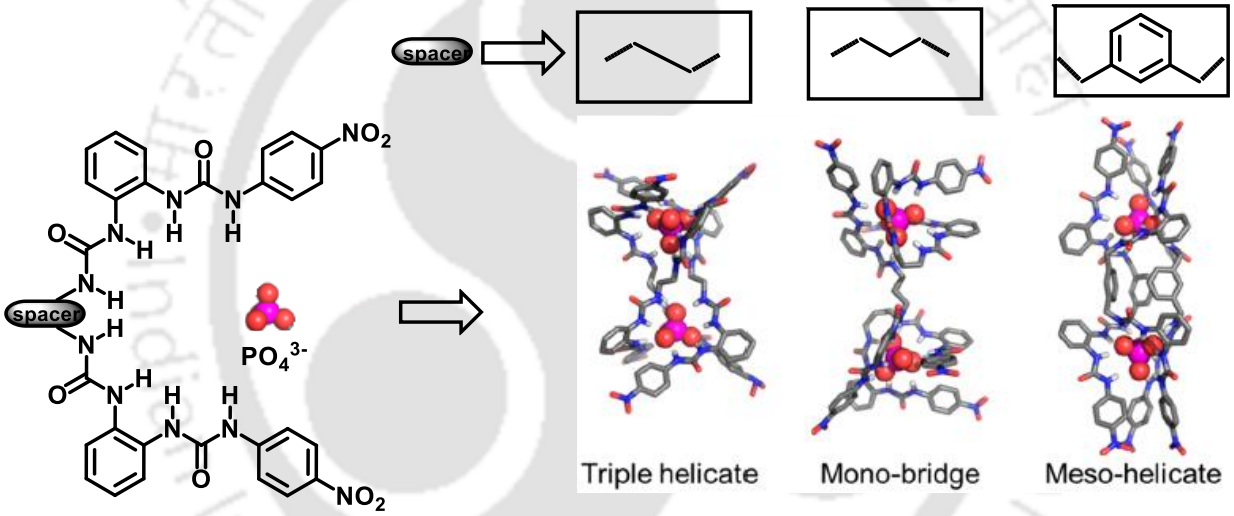

Figure 1.44: (a) Chemical structure of bis-bis(urea) ligands. (b) Different phosphate assisted assemblies based on spacer.

Furthermore, the multiple ion-directed self-assemblies have emerged in recent days. These assemblies make use of structure-directing effects of anions, cations. Depending on the flexibility and binding sites design of molecules for specific purposes are possible. For example, the bis-urea units linked together held through flexible tethers are organized with different helicity by phosphate ions.[170a] For example, when the spacer was $(\text{-CH}_2)_2$- it formed triple helicate, when it was $\text{–(CH}_2)_3$- it formed mono-bridged assembly and in case of $(\text{-CH}_2\text{C}_6\text{H}_4\text{CH}_2)$- it formed a meso-helical assembly (Figure 1.44).

Azobenzene-functionalized bis-bis(urea) ligand is known to assemble by phosphate anion for photoactive $(\text{phosphate})_4(\text{bisurea})_6$-type tetrahedral cage.[170b] The tetrahedral cage binds two

TH-3622_196122001

trimethylammonium cations and one molecule of [18]crown-6 molecule. The complex binds or releases K^+ ion from $[K([18]crown-6)]^+$ under photochemical condition or heating. This demonstrates a reversible transformations of a multi-component assembly by heat or irradiation. The assembly of cyanostar (Figure 1.45), which has multiple binding sites, involved the encapsulation of tetrahedral anions such as tetrafluoroborate and perchlorate. Whereas a coordinating site appends a cationic part derived from triphenylphosphine copper(I) or bis-phosphine-gold(I) complex.[171]

Finally, the overall charge is neutralized by non-coordinating anion such as one derived from tri-fluoromethylsulphonamide or sterically crowded boron-based anion as shown in the Figure 1.45. These assemblies have large prospects as they would provide modulation of properties of multiple component linked to one template. Furthermore, the dynamic assemblies, which equilibrate between stable and usable states, are of interest due to their ability to act as actuators and facilitate transformations of small molecules, such as the utilization of fuels from external sources.

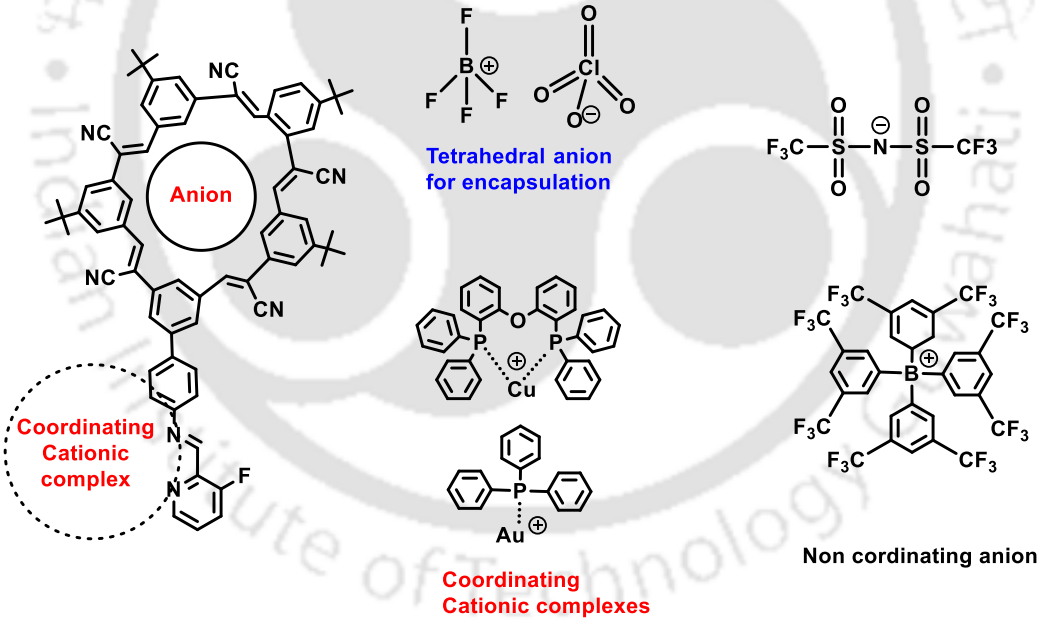

Figure 1.45: A template to prepare multi-component ion-directed self-assembly.

Depending on the organocation, the zinc-2,6-pyridinedicarboxylate forms host for small phenolic molecules such as nitro-phenols, di and tri-hydroxy-aromatics. Anions of the host molecules were assembled differently by different guest which causes variations in the adsorbed amounts and also properties. By adding fluorescent molecule in the cationic part, it was possible to use them for detections of nitro-phenolic complexes.

TH-3622_196122001

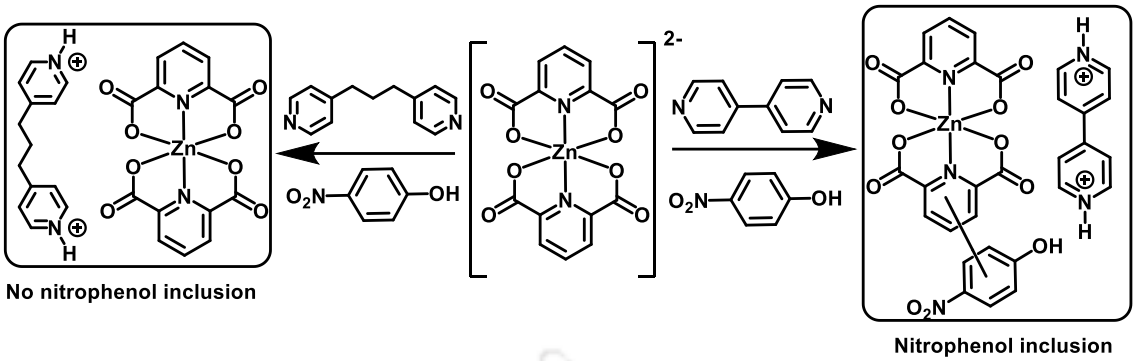

Figure 1.46: Differences caused in the crystallization of nitrophenol inclusion complex by the organocations.

Changing the cationic component alters the ability to include a guest molecule. For example, using 4,4′-bipyridine during the preparation of the cation resulted in the inclusion of 4-nitrophenol, whereas similar inclusion did not occur in complexes containing 1,3-dipyridylpropane (Figure 1.46). On the other hand, the emission properties could be reversible tuned by using rotatable dicarboxylate ligands during hydration and dehydration.[172]

Concomitant polymorphs of aqua-ligand containing cadmium 2,6-pdc coordination polymer have avenues to explore their distinction, but one form in such case was transient and formed in low yield.[173] Further, the polymorphs of hydrate were overserved in ciprofloxacin salicylate monohydrate, in which also one of the polymorph was highly unstable.[174] As such, hydrates of inorganic compounds are important for energy storage,[162] water harvesting[165] and phase transformations.[175,176] Hence these have left large scope to explore different forms of isolable hydrates to make structural comparisons and for studying their interconversion.

The self-assemblies of metal complexes assembled by water molecules are as important as the ones constructed with the aids of cations and anions or neutral molecules. The entire biological world is guided by the weak interactions of water molecules. Their role as hydrogen bond donor and acceptor has contributed to learn a major part of supramolecular chemistry. There are infinite numbers of examples where water molecules act as knitting molecules in assemblies. The association of water molecules with metal complexes contribute to emission,[160] magnetic properties,[161] proton conductors and energy storage.[163] The water-clathrates[164] are used in separation, hydrates of drug molecules have large role and medicinal chemistry.[165] In addition to coordination ability to metal ions the water coordinated anions,[166] ion channels,[167,168] water clusters have their own designated applications. Furthermore, there are many studies on reversible

TH-3622_196122001

and irreversible transformation among hydrates, suggest the requirements of their interconversions.

In addition to that, the complexity in preparation of hydrate of metal complexes of a simple drug molecules is exemplified by the formation of different forms. For example two mononuclear lithium complexes of a commonly used drug diclofenac (dfa), such as $[Li(dfa)(H_2O)_3]$, $[Li(dfa)(H_2O)_2(DMF)]$ by varying solvent of crystallization from water to dimethylformamide (DMF).[169] The aqua-ligands of both the complexes form inter-molecular hydrogen bonds (Figure 1.47) and provide a two-dimensional mono-layered structure along *bc*-crystallographic plane in the respective complex. In each case the hydrophobic sites were located at the outer periphery and the hydrophilic part beneath them. On the other hand, with other alkali metal ions large differences in compositions and structural features were observed from these complexes. Hence, such complexes extended to prepare ionic-cocrystals to accommodate extra drug or guest molecules will have definite interests.

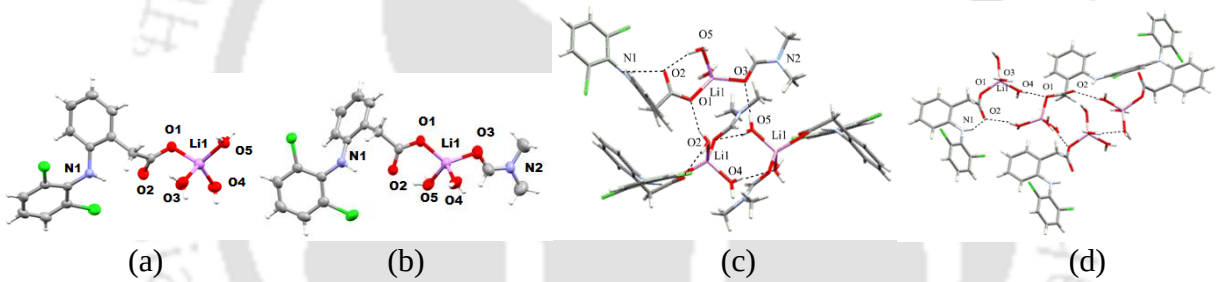

(a) (b) (c) (d)

Figure 1.47: Crystal structure of (a) $[Li(dfa)(H_2O)_3]$ and (b) $[Li(dfa)(H_2O)_2(DMF)]$ and the respective hydrogen bonds contributing to 2D-single layered structures are in (c) and (d).

1.7. Scope of the Research

Based on the above information, there is a large gap to understand supramolecular behavior of polytopic ions in metal containing assemblies. Further to this, the crystal packing between large sized polytopic ions provide avenues for binding to different molecules and molecular ions for recognition. Metal-pdc complexes with organo-cations have been shown from our laboratory[172] with the potential for energetic molecules and polyaromatic hydrocarbons. In our laboratory 9-N-(3-imidazolylpropylamino)methylanthracene (H**anthraimmida)** has been studied to prepare multi-component assemblies. Based on this information, the thesis encompasses utility of larger sized π-based ditopic organo-cations H**anthraimmida** (**1.48.1**), chloro substituted analogue **Chloroanthaimmida** or **Clanth**; N-{(10-chloroanthracen-9-yl)methyl}-3-(1H-imidazol-1-

TH-3622_196122001

yl)propan-1-amine (**1.48.2**) and **sulfathiazole**; 4-amino-N-(thiazol-2-yl)benzenesulfonamide (**1.48.3**) in constructing various non-covalent self-assemblies of salts and ionic-cocrystals with pyridinedicarboxylic acids. The incorporation of other guest molecules like 1,3-dihydroxyphenol, 1,4-diiodotetrafluorobenzen (**1.48.4**) and 3-nitrophenol facilitates the formation of ternary and quaternary salts and ionic-cocrystals. These assemblies give rise to differentiable photoluminescence properties. Some molecules exhibit halogen bonding interactions along with charge assisted hydrogen bonds. The ditopic organo-cations **1.48.1** and **1.48.2** has plethora of scope to form assemblies, which was utilized to form salts and complex hydrates of divalent cobalt, copper and zinc with 2,6-pyridinedicarboxylates. Those compounds formed reversible/irreversible hydrates and polymorphs with metastable intermediates of metal-pdc anion along with imidazole tethered organo-cations. The interconversions between different assemblies assisted by water are being envisaged. The aminothiazole based organo-cationic drug has varied ratio of the molecule during the formation of salt and complexes. This way the concentration of the drug molecules can be modulated through controlled crystal engineering.

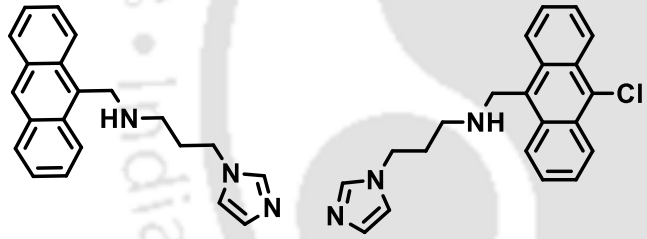

1.48.1 **1.48.2** **1.48.3** **1.48.4**

1.8. References

1. (a) F. M. Gartner, I. R. Graf and E. Frey, The time complexity of self-assembly, *PNAS*, 2022, **119**, e2116373119. (b) J. D. Perlmutter and M. F. Hagan, Mechanisms of virus assembly, *Ann. Rev. Phys. Chem.*, 2015, **66**, 217–239.

2. K. Eftekhari, B. V. Parakhonskiy, D. Grigoriev and A. G. Skirtach, Advances in nano architectonics: a review of "static" and "dynamic" particle assembly methods, *Materials*, 2024, **17**, 1051.

3. (a) J.-M. Lehn, Perspectives in supramolecular chemistry—from molecular recognition towards molecular information processing and self-organization, *Angew. Chem. Int. Ed. Eng.*, 1990, **29**, 1304–1319. (b) J.-M. Lehn, Molecular and supramolecular devices in supramolecular chemistry: concepts and perspectives, *Wiley*, 1995, Ch. 8.

4. D. K. Smith, Supramolecular gels—a panorama of low-molecular-weight gelators from ancient origins to next-generation technologies, *Soft Matter*, 2024, **20**, 10–70.

TH-3622_196122001

5. S. Sivakova and S. J. Rowan, Nucleobases as supramolecular motifs, *Chem. Soc. Rev.*, 2005, **34**, 9–21.
6. F. Zeng and S. C. Zimmerman, Dendrimers in supramolecular chemistry: from molecular recognition to self-assembly, *Chem. Rev.*, 1997, **97**, 1681–1712.
7. (a) W. Xu and O. M. Yaghi, Metal–organic frameworks for water harvesting from air, anywhere, anytime, *ACS Cent. Sci.*, 2020, **6**, 1348–1354. (b) A. Katiyar, J. C. F. Sovierzoski, P. B. Calio, A. A. Vartia and W. H. Thompson, Water plays a dynamical role in a hydrogen bonded, hexameric supramolecular assembly, *Phys. Chem. Chem. Phys.*, 2020, **22**, 6167–6175.
8. (a) W. L. Xu, C. Fang, F. Zhou, Z. Song, Q. Liu, R. Qiao and M. Yu, Self-assembly: a facile way of forming ultrathin, high-performance graphene oxide membranes for water purification, *Nano Lett.*, 2017, **17**, 2928–2933.
9. M. Urso, M. Ussia, X. Peng, C. M. Oral and M. Pumera, Reconfigurable self-assembly of photocatalytic magnetic microrobots for water purification, *Nat. Commun.*, 2023, **14**, 6969.
10. S.-H. Liu and H.-R. Syu, One-step fabrication of N-doped mesoporous TiO2 nanoparticles by self-assembly for photocatalytic water splitting under visible light, *Appl. Energy*, 2012, **100**, 148–154.
11. J. Tian, Y. Zhang, L. Du, Y. He, X.-H. Jin, S. Pearce, J.-C. Eloi, R. L. Harniman, D. Alibhai, R. Ye, D. L. Phillips and I. Manners, Tailored self-assembled photocatalytic nanofibres for visible-light-driven hydrogen production, *Nat. Chem.*, 2020, **12**, 1150–1156.
12. S. Zhang, Y. Yang, Z. Tong, B. Gao, N. Gao, T. Shen, Y. Wan, Z. Yu, L. Liu, X. Ma, Y. Guo, J. Fugice and Y. C. Li, Self-assembly of hydrophobic and self-healing bionanocomposite-coated controlled-release fertilizers, *ACS Appl. Mater. Interfaces*, 2020, **12**, 27598–27606.
13. (a) A. Rosler, G. W. M. Vandermeulen and H.-A. Klok, Advanced drug delivery devices via self-assembly of amphiphilic block copolymers, *Adv. Drug Delivery Rev.*, 2012, **64**, 270–279. (b) V. B. Kumar, B. Ozguney, A. Vlachou, Y. Chen, E. Gazit and P. Tamamis, Peptide self-assembled nanocarriers for cancer drug delivery, *J. Phys. Chem. B*, 2023, **127**, 1857–1871.
14. A. Kadeeja, S. Joseph and J. N. Abraham, Self-assembly of novel Fmoc-cardanol compounds into hydrogels-analysis based on rheological, structural and thermal properties, *Soft Matter*, 2020, **16**, 6294–6303.
15. J. D. Watson and F. H. Crick, Molecular structure of nucleic acids: a structure for deoxyribose nucleic acid, *Nature*, 1953, **171**, 737–738.
16. (a) J. R. Williamson, M. K. Raghuraman and T. R. Cech, Monovalent cation-induced structure of telomeric DNA: the G-quartet model, *Cell*, 1989, **59**, 871–880. (b) V. Abet and R. Rodriguez, Guanosine and isoguanosine derivatives for supramolecular devices, *New J. Chem.*, 2014, **38**, 5122–5128.
17. C. J. T. Cox, J. Hale, P. Molinska and J. E. M. Lewis, Supramolecular and molecular capsules, cages and containers, *Chem. Soc. Rev.*, 2024, DOI: 10.1039/D4CS00761A.
18. Z. Xu, W. Yang, H. Liu and S. Jiang, Guest-induced conformational transformations in tiara[5]arene crystals: a pathway for molecular sieving, *JACS Au*, 2024, **4**, 3475–3483.
19. X.-Y. Chen, L.-H. Cao, X.-T. Bai and X.-J. Cao, Charge-assisted ionic hydrogen-bonded organic frameworks: designable and stabilized multifunctional materials, *Chem. Eur. J.*, 2024, **30**, e202303580.
20. S. K. Burley and G. A. Petsko, Aromatic-aromatic interaction: a mechanism of protein structure stabilization, *Science*, 1985, **229**, 23–28.

TH-3622_196122001

21. A. Gil, V. Branchadell and M. J. Calhorda, A theoretical study of methylation and CH/π interactions in DNA intercalation: methylated 1,10-phenanthroline in adenine–thymine base pairs, *RSC Adv.*, 2016, **6**, 85891–85902.
22. (a) J. C. Ma and D. A. Dougherty, The cation-π interaction, *Chem. Rev.*, 1997, **97**, 1303–1324. (b) P. B. Crowley and A. Golovin, Cation-π interactions in protein-protein interfaces, *Proteins Struct. Funct. Bioinf.*, 2005, **59**, 231–239.
23. (a) D. Quinonero, C. Garau, C. Rotger, A. Frontera, P. Ballester, A. Costa and P. M. Deya, Anion-π interactions: do they exist?, *Angew. Chem. Int. Ed. Eng.*, 2002, **41**, 3389–3392. (b) C. Garau, A. Frontera, D. Quinonero, P. Ballester, A. Costa and P. M. Deya, A theoretical study of anion–π interactions in seven-membered rings, *ChemPhysChem.*, 2003, **4**, 1344–1348. (c) D. Quinonero, A. Frontera, C. Garau, P. Ballester, A. Costa and P. M. Deya, Interplay between cation–π, anion–π and π–π interactions, *ChemPhysChem.*, 2006, **7**, 2487–2491.
24. G. Cavallo, P. Metrangolo, R. Milani, T. Pilati, A. Priimagi, G. Resnati and G. Terraneo, The halogen bond, *Chem. Rev.*, 2016, **116**, 2478–2601.
25. (a) J. P. Sauvage, Transition metal-containing rotaxanes and catenanes in motion: toward molecular machines and motors, *Acc. Chem. Res.*, 1998, **31**, 611–619. (b) M. Fujita, Self-assembly of [2] catenanes containing metals in their backbones, *Acc. Chem. Res.*, 1999, **32**, 53–61. (c) D. L. Caulder and K. N. Raymond, Supermolecules by design, *Acc. Chem. Res.*, 1999, **32**, 975–982. (d) S. Leininger, B. Olenyuk and P. J. Stang, Self-assembly of discrete cyclic nanostructures mediated by transition metals, *Chem. Rev.*, 2000, **100**, 853–908.
26. G. R. Desiraju, Crystal engineering: from molecule to crystal, *J. Am. Chem. Soc.*, 2013, **135**, 9952–9967.
27. R. Custelcean, P. V. Bonnesen, N. C. Duncan, X. Zhang, L. A. Watson, G. Van Berkel, W. B. Parson and B. P. Hay, Urea-functionalized M4L6 cage receptors: anion-templated self-assembly and selective guest exchange in aqueous solutions, *J. Am. Chem. Soc.*, 2012, **134**, 8525–8534.
28. S. Aitipamula, R. Banerjee, A. K. Bansal, K. Biradha, M. L. Cheney, A. R. Choudhury, G. R. Desiraju, A. G. Dikundwar, R. Dubey and N. Duggirala, Polymorphs, salts, and cocrystals: what's in a name?, *Cryst. Growth Des.*, 2012, **12**, 2147–2152.
29. D. S. Reddy, Y. E. Ovchinnikov, O. V. Shishkin, Y. T. Struchkov and G. R. Desiraju, Supramolecular synthons in crystal engineering: solid state architecture and synthon robustness in some 2,3-dicyano-5,6-dichloro-1,4-dialkoxybenzenes, *J. Am. Chem. Soc.*, 1996, **118**, 4085–4089.
30. L. L. Osorno, A. N. Brandley, D. E. Maldonado, A. Yiantsos, R. J. Mosley and M. E. Byrne, Review of contemporary self-assembled systems for the controlled delivery of therapeutics in medicine, *Nanomaterials*, 2021, **11**, 278.
31. (a) O. Dumele, J. Chen, J. V. Passarelli and S. I. Stupp, Supramolecular energy materials, *Adv. Mater.*, 2020, **32**, 1907247. (b) S. R. Valandro, M. Herber, H. Xiang and E. H. Hill, The role of aggregation on energy transfer in layered rare-earth hydroxide/naphthalene diimide hybrid materials, *J. Phys. Chem. C*, 2024, **128**, 2529–2535.
32. T. Ono, M. Sugimoto and Y. Hisaeda, Multi-component molecular puzzles for photofunction design: emission color variation in Lewis acid-base pair crystals coupled with guest-to-host charge transfer excitation, *J. Am. Chem. Soc.*, 2015, **137**, 9519–9522.
33. (a) Z. Feng, T. Zhang, H. Wang and B. Xu, Supramolecular catalysis and dynamic assemblies for medicine, *Chem. Soc. Rev.*, 2017, **46**, 6470–6479. (b) M. J. Wiester, P. A. Ulmann and C. A. Mirkin, Enzyme mimics based upon supramolecular coordination chemistry, *Angew. Chem. Int. Ed.*, 2011, **50**, 114–137. (c) Z. J. Wang, K. N. Clary, R. G. Bergman, K. N. Raymond and F. D.

TH-3622_196122001

Toste, A supramolecular approach to combining enzymatic and transition metal catalysis, *Nat. Chem.*, 2013, **5**, 100–103.
34. L. R. Macgillivray, G. S. Papaefstathiou, T. Friščić, T. D. Hamilton, D.-K. Bucar, Q. Chu, D. B. Varshney and I. G. Georgiev, Supramolecular control of reactivity in the solid state: from templates to ladderanes to metal-organic frameworks, *Acc. Chem. Res.*, 2008, **41**, 280–291.
35. (a) P. D. J. Patil, R. D. Ingle, S. M. Wagalgave, R. S. Bhosale, S. V. Bhosale, R. P. Pawar and S. V. Bhosale, A naphthalimide-benzothiazole conjugate as colorimetric and fluorescent sensor for selective trinitrophenol detection, *Chemosensors*, 2019, **7**, 38. (b) E. A. Meyer, R. K. Castellano and F. Diederich, Interactions with aromatic rings in chemical and biological recognition, *Angew. Chem. Int. Ed.*, 2003, **42**, 1210–1250. (c) A. S. Oshchepkov, R. R. Mittapalli, O. A. Fedorova and E. A. Kataev, Naphthalimide-based polyammonium chemosensors for anions: study of binding properties and sensing mechanisms, *Chem. Eur. J.*, 2017, **23**, 9657–9665.
36. G. R. Desiraju, Supramolecular synthons in crystal engineering—a new organic synthesis, *Angew. Chem. Int. Ed.*, 1995, **34**, 2311–2327. (b) G. R. Desiraju, Designer crystals: intermolecular interactions, network structures and supramolecular synthons, *Chem. Commun.*, 1997, 1475–1482. (c) E. Peresypkina, A. Virovets and M. Scheer, Supramolecular synthons: will giant rigid superspheres do? *Cryst. Growth Des.*, 2016, **16**, 2335–2341.
37. A. K. Nangia and G. R. Desiraju, Crystal engineering: an outlook for the future, *Angew. Chem. Int. Ed.*, 2019, **58**, 4100–4107.
38. B. König, Molecular recognition. The principle and recent chemical examples, *J. für Prakt. Chemie*, 1995, **337**, 339–346.
39. N. Phukan and J. B. Baruah, Conformational adjustments over synthons of urea and thiourea-based assemblies, *CrystEngComm*, 2016, **18**, 7753–7763.
40. J. B. Baruah, *Principles and Advances in Supramolecular Catalysis*, 1st ed., CRC Press, New York, 2019.
41. (a) M. C. Etter, J. C. MacDonald and J. Bernstein, Graph-set analysis of hydrogen-bond patterns in organic crystals, *Acta Crystallogr.*, 1990, **B46**, 256–262. (b) M. C. Etter, Encoding and decoding hydrogen-bond patterns of organic compounds, *Acc. Chem. Res.*, 1990, **23**, 120.
42. R. J. Flood, N. M. Mockler, A. Thureau, M. Malinska and P. B. Crowley, Supramolecular synthons in protein-ligand frameworks, *Cryst. Growth Des.*, 2024, **24**, 2149–2156.
43. (a) P. T. Anastas and J. C. Warner, *Green Chemistry: Theory and Practice*, Oxford University Press, New York, 1998, p. 30. (b) P. Anastas and N. Eghbali, Green chemistry: principles and practice, *Chem. Soc. Rev.*, 2010, **39**, 301–312.
44. J. W. Steed and J. L. Atwood, *Supramolecular Chemistry*, John Wiley and Sons Ltd, 1997, 1–6.
45. D. J. Cram, Preorganization from solvents to spherands, *Angew. Chem. Int. Ed.*, 1986, **25**, 1039–1057.
46. R. Custelcean, P. V. Bonnesen, N. C. Duncan, X. Zhang, L. A. Watson, G. Van Berkel, W. B. Parson and B. P. Hay, Urea-functionalized M4L6 cage receptors: anion-templated self-assembly and selective guest exchange in aqueous solutions, *J. Am. Chem. Soc.*, 2012, **134**, 8525–8534.
47. (a) J. J. Lavigne and E. V. Anslyn, Sensing a paradigm shift in the field of molecular recognition: from selective to differential receptors, *Angew. Chem. Int. Ed.*, 2001, **40**, 3118–3130. (b) J. Rebek, Jr., Model studies in molecular recognition, *Science*, 1987, **235**, 1478–1484. (c) S. H. Gellman, Introduction: molecular recognition, *Chem. Rev.*, 1997, **97**, 1231–1232.

TH-3622_196122001

48. Y. Xiao, C. Wu, X. Hu, K. Chen, L. Qi, P. Cui, L. Zhou and Q. Yin, Mechanochemical synthesis of cocrystal: from mechanism to application, *Cryst. Growth Des.*, 2023, **23**, 4680–4700.
49. F. Wöhler, Untersuchungen über das Chinon, *Eur. J. Org. Chem.*, 1844, **51**, 145–163.
50. (a) A. V. Trask and W. Jones, Crystal engineering of organic cocrystals by the solid-state grinding approach, *Org. Solid State Reactions*, 2005, **254**, 41–70. (b) D. Douroumis, S. A. Ross and A. Nokhodchi, Advanced methodologies for cocrystal synthesis, *Adv. Drug Delivery Rev.*, 2017, **117**, 178–195. (c) S. L. James, C. J. Adams, C. Bolm, D. Braga, P. Collier, T. Friščić, F. Grepioni, K. D. Harris, G. Hyett and W. Jones, Mechanochemistry: opportunities for new and cleaner synthesis, *Chem. Soc. Rev.*, 2012, **41**, 413–447. (d) T. Friščić, C. Mottillo and H. M. Titi, Mechanochemistry for synthesis, *Angew. Chem.*, 2020, **132**, 1030–1041. (e) K. J. Ardila-Fierro and J. G. Hernández, Sustainability assessment of mechanochemistry by using the twelve principles of green chemistry, *ChemSusChem*, 2021, **14**, 2145–2162.
51. (a) L. Brammer, Developments in inorganic crystal engineering, *Chem. Soc. Rev.*, 2004, **33**, 476–489. (b) S. B. Copp, K. T. Holman, J. O. S. Sangster, S. Subramaniam and M. J. Zaworotko, Supramolecular chemistry of [{M(CO)3(μ3-OH)}4](M = Mn or Re): a modular approach to crystal engineering of superdiamondoid networks, *J. Chem. Soc., Dalton Trans.*, 1995, **2233**, 2233–2243.
52. C. B. Aakeröy, A. M. Beatty and D. S. Leinen, The oxime functionality: a versatile tool for supramolecular assembly of metal-containing hydrogen-bonded architectures, *J. Am. Chem. Soc.*, 1998, **120**, 7383–7384.
53. C. B. Aakeröy, A. M. Beatty and D. S. Leinen, A versatile route to porous solids: organic–inorganic hybrid materials assembled through hydrogen bonds, *Angew. Chem., Int. Ed. Eng.*, 1999, **38**, 1815–1819.
54. (a) M. W. Hosseini, Molecular tectonics: from molecular recognition of anions to molecular networks, *Coord. Chem. Rev.*, 2003, **240**, 157–166. (b) O. Félix, M. W. Hosseini, A. De Cian and J. Fischer, Molecular tectonics VIII: Formation of 1D and 3D networks based on the simultaneous use of hydrogen bonding and ionic interactions, *New J. Chem.*, 1998, **22**, 1389–1393.
55. A. J. Cruz-Cabeza, Acid–base crystalline complexes and the pKa rule, *CrystEngComm*, 2012, **14**, 6362–6365.
56. D. R. Weyna, M. L. Cheney, N. Shan, M. Hanna, Ł. Wojtas and M. J. Zaworotko, Crystal engineering of multiple-component organic solids: Pharmaceutical cocrystals of tadalafil with persistent hydrogen bonding motifs, *CrystEngComm*, 2012, **14**, 2377–2380.
57. T. R. Shattock, K. K. Arora, P. Vishweshwar and M. J. Zaworotko, Hierarchy of supramolecular synthons: persistent carboxylic acid pyridine hydrogen bonds in cocrystals that also contain a hydroxyl moiety, *Cryst. Growth Des.*, 2008, **8**, 4533–4545.
58. P. Kavuru, D. Aboarayes, K. K. Arora, H. D. Clarke, A. Kennedy, L. Marshall, T. T. Ong, J. Perman, T. Pujari, Ł. Wojtas and M. J. Zaworotko, Hierarchy of supramolecular synthons: persistent hydrogen bonds between carboxylates and weakly acidic hydroxyl moieties in cocrystals of zwitterions, *Cryst. Growth Des.*, 2010, **10**, 3568–3584.
59. J. A. Bis, P. Vishweshwar, D. Weyna and M. J. Zaworotko, Hierarchy of supramolecular synthons: persistent hydroxyl pyridine hydrogen bonds in cocrystals that contain a cyano acceptor, *Mol. Pharmaceutics*, 2007, **4**, 401–416.
60. N. K. Duggirala, G. P. F. Wood, A. Fischer, Ł. Wojtas, M. L. Perry and M. J. Zaworotko, Hydrogen bond hierarchy: persistent phenol···chloride hydrogen bonds in the presence of carboxylic acid moieties, *Cryst. Growth Des.*, 2015, **15**, 4341–4354.

TH-3622_196122001

61. M. A. Mohammad, A. Alhalaweh and S. P. Velaga, Hansen solubility parameter as a tool to predict cocrystal formation, *Int. J. Pharm.*, 2011, **407**, 63–71.
62. (a) C. Janiak, A critical account on-stacking in metal complexes with aromatic nitrogen-containing ligands, *J. Chem. Soc., Dalton Trans.*, 2000, **3885**, 3885–3896. (b) C. H. Hunter and J. K. M. Sanders, The nature of π-π interaction, *J. Am. Chem. Soc.*, 1990, **112**, 5525–5534.
63. D. P. Malenov, G. V. Janjić, V. B. Medaković, M. B. Hall and S. D. Zarić, Noncovalent bonding: stacking interactions of rings of transition metal complexes, *Coord. Chem. Rev.*, 2017, **345**, 318–341.
64. (a) A. Guijarro, J. A. Verges, E. San-Fabian, G. Chiappe, E. Louis, Herringbone pattern and CH-π bonding in the crystal architecture of linear polycyclic aromatic hydrocarbons, *ChemPhysChem*, 2016, **17**, 3548–3557. (b) C. R. Groom, I. J. Bruno, M. P. Lightfoot, S. C. Ward, The Cambridge Structural Database, *Acta Cryst.*, 2016. **B72**, 171–179.
65. (a) D. P. Malenov and S. D. Zarić, Stacking interactions of aromatic ligands in transition metal complexes, *Coord. Chem. Rev.*, 2020, **419**, 213338. (b) D. P. Malenov and S. D. Zarić, Strong stacking interactions of metal-chelate rings are caused by substantial electrostatic component, *Dalton Trans.*, 2019, **48**, 6328–6332.
66. (a) S. Pramanik, S. Pathak, A. Frontera, S. Mukhopadhyay, Exploration of supramolecular and theoretical aspects of two new Cu(II) complexes: On the importance of lone pair···π(chelate ring) and π···π (chelate ring) interactions, *J. Mol. Struct.*, 2022, **1265**, 133358. (b) S. Maity, T. K. Ghosh, R. M. Gomila, A. Frontera, A. Ghosh, Recurrent π (arene)···π(chelate ring) motifs in four trinuclear CuII2MII (M = Cd/Zn) complexes derived from an unsymmetrical N2O2 donor ligand: structural and theoretical investigations, *CrystEngComm*, 2020, **22**, 7673–7683. (c) S. Mirdya, S. Roy, S. Chatterjee, A. Bauza, A. Frontera, S. Chattopadhyay, Importance of π-interactions involving chelate rings in addition to the tetrel bonds in crystal engineering: a combined experimental and theoretical study on a series of hemi- and holodirected nickel(II)/lead(II) complexes, *Cryst. Growth Des.*, 2019, **19**, 5869–5881. (d) D. P. Malenov, D. Z. Veljkovic, M. B. Hall, E. N. Brothers and S. D. Zarić, Influence of chelate ring type on chelate–chelate and chelate–aryl stacking: the case of nickel bis(dithiolene), *Phys. Chem. Chem. Phys.*, 2019, **21**, 1198–1206. (e) S. L. Tan, S. M. Lee, K. M. Lo, A. O. la Roza and E. R. T. Tiekink, Experimental and computational evidence for a stabilising C–Cl(lone-pair)···π(chelate-ring) interaction, *CrystEngComm*, 2021, **23**, 119–130. (f) R. Gyepes, S. Pacigová, M. Sivák and J. Tatiersky, Experimental and computational evidence of solid-state anion–π and π–π interactions in [VO(O2)(L)(pa)]·xH2O complexes (L = picolinate, pyrazinate or quinolinate; pa = picolinamide), *New J. Chem.*, 2009, **33**, 1515–1522.
67. T. Hajiashrafi, R. Zekriazadeh, K. J. Flanagan, F. Kia, A. Bauzá, A. Frontera and M. O. Senge, The role of π–π stacking and hydrogen-bonding interactions in the assembly of a series of isostructural group IIB coordination compounds, *Acta Crystallogr. C Struct. Chem.*, 2019, **75 (Pt 2)**, 178–188.
68. (a) S. De, M. G. B. Drew, N. Aliaga-Alcalde and D. Datta, Imidazole–imidazole stacking in some inorganic complexes, *Inorg. Chim. Acta*, 2009, **362**, 2879–2883. (b) A. Castineiras, A. G. Sicilia-Zafra, J. M. González-Pérez, D. Choquesillo-Lazarte, J. Niclós-Gutiérrez, Intramolecular "aryl-metal chelate ring" π,π-interactions as structural evidence for metalloaromaticity in (aromatic α,α′-diimine)-copper(II) chelates: molecular and crystal structure of aqua(1,10-phenanthroline)(2-benzylmalonato)copper(II) three-hydrate, *Inorg. Chem.*, 2003, **41**, 6956–6958.

TH-3622_196122001

69. J. R. Farrell, A. H. Eisenberg, C. A. Mirkin, I. A. Guzei, L. M. Liable-Sands, C. D. Incarvito, A. L. Rheingold, C. L. Stern, Templated formation of binuclear macrocycles via hemilabile ligands, *Organometallics*, 1999, **18**, 4856–4868.
70. K. Shankar, A. Mondal, Y. Li, Y. Journaux, J. B. Baruah, Hydroxide-bridged mixed-valence tetranuclear cobalt 4-nitrophenol inclusion complex showing single molecule magnet property, *ChemistrySelect*, 2017, **2**, 7792–7798.
71. V. Russell, M. Scudder and I. Dance, The crystal supramolecularity of metal phenanthroline complexes, *J. Chem. Soc., Dalton Trans.*, 2001, **789**, 789–799.
72. (a) A. A. G. Tomlinson and B. J. Hathaway, The electronic properties and stereochemistry of the copper(II) ion. Part III. Some penta-ammine complexes, *J. Chem. Soc. A*, 1968, **1905**, 1905–1909. (b) A. K. Patela, R. N. Jadejaa, R. J. Butcher, Synthesis and characterization of penta-coordinated copper(II) complexes with hydrazido based ligand and imidazole as auxiliary ligand, *J. Indian Chem. Soc.*, 2021, **98**, 100–182.
73. J. Sendh and J. B. Baruah, Naphthalimide decorated copper(II), cobalt(II) dicarboxylates and tricking turn-ON emission, *Polyhedron*, 2024, **249**, 116792.
74. K. Shankar and J. B. Baruah, Mixed anionic and inclusion complexes of nickel(II) with nitroaromatics showing selectivity in oxygen-π interactions, *Inorg. Chim. Acta*, 2016, **453**, 135–141.
75. R. Brahma and J. B. Baruah, Self-assemblies of zinc-complexes for aggregation induced emission luminogen precursors, *ACS Omega*, 2020, **5**, 3774–3785.
76. K. Shankar and J. B. Baruah, Modulation of fluorescence emissions of copper(II) 2,2′-biquinoline-4,4′-dicarboxylate, *ChemistrySelect*, 2016, **1**, 3038–3044.
77. P. Bansal, A. Saini, P. Kaur, P. Kaur, S. Kumar, P. Kandwal and V. Ferretti, Harnessing of non-covalent interaction in novel $[Ni(en)_3](2\text{-chlorophenylacetate})_2]$ second sphere complex: synthesis, characterization, single crystal structural, DFT, and Hirshfeld surface analysis, *Struct. Chem.*, 2024, **5**, 1493–1507.
78. Z. An, C. Zheng, Y. Tao, R. Chen, H. Shi, T. Chen, Z. Wang, H. Li, R. Deng, X. Liu and W. Huang, Stabilizing triplet excited states for ultralong organic phosphorescence, *Nat. Mat.*, 2015, **14**, 685–690.
79. N. Takuma, S. Kaori, S. Sunao, F. Koji, H. Yasuchika, K. Yuichi, Characteristic stacked structures and luminescent properties of dinuclear lanthanide complexes with pyrene units, *Front. Chem.*, 2023, **11**, 2296–2646.
80. Y. Kitagawa, A. Naito, K. Fushimi, Y. Hasegawa, Bright sky-blue fluorescence with high color purity: Assembly of luminescent diphenyl-anthracene lutetium-based coordination polymer, *RSC Adv.*, 2021, **11**, 6604–6606.
81. Y. Kitagawa, F. Suzue, T. Nakanishi, K. Fushimi, Y. Hasegawa, A highly luminescent Eu(III) complex based on an electronically isolated aromatic ring system with ultralong lifetime, *Dalton Trans.*, 2018, **47**, 7327–7332.
82. E. A. Mikhalyova, A. V. Yakovenko, M. Zeller, M. A. Kiskin, Y. V. Kolomzarov, I. L. Eremenko, A. W. Addison and V. V. Pavlishchuk, Manifestation of π–π stacking interactions in luminescence properties and energy transfer in aromatically-derived Tb, Eu and Gd tris(pyrazolyl)borate complexes, *Inorg. Chem.*, 2015, **54**, 3125–3133.
83. L. A. Barrios, G. Aromí, A. Frontera, D. Quiñonero, P. M. Deyà, P. Gamez, O. Roubeau, E. J. Shotton, S. J. Teat, Coordination complexes exhibiting anion···π interactions: Synthesis, structure, and theoretical studies, *Inorg. Chem.*, 2008, **47**, 5873–5881.

TH-3622_196122001

84. H. T. Chifotides, I. D. Giles and K. R. Dunbar, Supramolecular architectures with π-acidic 3,6-Bis(2-pyridyl)-1,2,4,5-tetrazine cavities: role of anion-π interactions in the remarkable stability of Fe(II) metallacycles in solution, *J. Am. Chem. Soc.*, 2013, **135**, 3039–3055.
85. C. A. Hollis, L. R. Hanton, J. C. Morris, C. J. Sumby, 2-D coordination polymers of hexa(4-cyanophenyl)[3]-radialene and silver(I): anion···π-interactions and radialene C−H···anion hydrogen bonds in the solid-state interactions of hexaaryl[3]-radialenes with anions, *Cryst. Growth Des.*, 2009, **9**, 2911–2916.
86. H. Maeda, W. Hane, Y. Bando, Y. Terashima, Y. Haketa, H. Shibaguchi, T. Kawai, T. Takaishi, M. Uchiyama, A. Muranaka, Chirality induction by formation of assembled structures based on anion-responsive π-conjugated molecules, *Chem. Eur. J.*, 2013, **19**, 16263–16271.
87. D. N. Sredojević, Z. D. Tomić and S. D. Zarić, Evidence of chelate–chelate stacking interactions in crystal structures of transition-metal complexes, *Cryst. Growth Des.*, 2010, **10**, 3901–3908.
88. (a) S. Pramanik, S. Pathak, A. Frontera and S. Mukhopadhyay, Exploration of supramolecular and theoretical aspects of two new Cu(II) complexes: On the importance of lone pair···π(chelate ring) and π···π(chelate ring) interactions, *J. Mol. Struct.*, 2022, **1265**, 133358. (b) G. S. Hammond, D. C. Nonhebel and C.-H. S. Wu, Chelates of β-diketones. V. Preparation and properties of chelates containing sterically hindered ligands, *Inorg. Chem.*, 1963, **2**, 73–76.
89. (a) D. Braga, F. Grepioni, O. Shemchuk, Organic–inorganic ionic co-crystals: a new class of multipurpose compounds, *CrystEngComm*, 2018, **20**, 2212–2220. (b) H.-Y. Gong, B. M. Rambo, V. M. Lynch, K. M. Keller, J. L. Sessler, Neutral and anionic guests and their effect on the formation of pseudorotaxanes by using a flexible tetracationic imidazolium macrocycle, *Chem. Eur. J.*, 2012, **18**, 7803–7809. (c) J. Sendh and J. B. Baruah, Polymorphs, ionic-cocrystal and inclusion complex of N-amino-1,8-naphthalimide, *CrystEngComm*, 2023, **1928**, 1940.
90. J. B. L. De Rome de L'lse, *Crystallographie*, Paris, 2nd ed., 1783.
91. J. H. Palm and C. MacGillavry, Habit modification in the system rock salt-urea-water, *Acta Crystallogr.*, 1963, **16**, 963.
92. F. V. Kobell and J. F. Prakt, D-glucose: sodium chloride monohydrate, *Chemie*, 1843, **28**, 489.
93. C. H. Gerhardt, Untersuchungen über die wasserfreien organischen Säuren, *Annalen der Chemie*, 1853, **87**, 149–179.
94. J. C. Speakman, *Structure and Bonding*, Springer, Berlin, 1972, **12**, 141–199.
95. (a) A. F. Shunnar, B. Dhokale, D. P. Karothu, D. H. Bowskill, I. J. Sugden, H. H. Hernandez, P. Naumov and S. Mohamed, Efficient screening for ternary molecular ionic-cocrystals using a complementary mechanosynthesis and computational structure prediction approach, *Chem. Eur. J.*, 2020, **26**, 4752–4765. (b) D. Musumeci, C. A. Hunter, R. Prohens, S. Scuderi and J. F. McCabe, Virtual cocrystal screening, *Chem. Sci.*, 2011, **2**, 883–890. (c) R. M. Bhardwaj, J. A. McMahon, J. Nyman, L. S. Price, S. Konar, I. D. H. Oswald, C. R. Pulham, S. L. Price, S. M. Reutzel-Edens, A prolific solvate former, galunisertib, under the pressure of crystal structure prediction, produces ten diverse polymorphs, *J. Am. Chem. Soc.*, 2019, **141**, 13887–13897. (d) A. Pulido, L. Chen, T. Kaczorowski, D. Holden, M. A. Little, S. Y. Chong, B. J. Slater, D. P. McMahon, B. Bonillo, C. J. Stackhouse, A. Stephenson, C. M. Kane, R. Clowes, T. Hasell, A. I. Cooper, G. M. Day, Functional materials discovery using energy-structure-function maps, *Nature*, 2017, **543**, 657–664. (e) S. Mohamed and L. Li, From serendipity to supramolecular design: assessing the utility of computed crystal form landscapes in inferring the risks of crystal hydration in carboxylic acids, *CrystEngComm*, 2018, **20**, 6026–6039. (f) A. R. Buist and A. R. Kennedy, Ionic-cocrystals of

TH-3622_196122001

pharmaceutical compounds: sodium complexes of carbamazepine, *Cryst. Growth Des.*, 2014, **14**, 6508–6513. (g) S. Mohamed, A. A. Alwan, T. Friščić, A. J. Morris, M. Arhangelskis, Towards the systematic crystallisation of molecular ionic-cocrystals: insights from computed crystal form landscapes, *Faraday Discuss.*, 2018, **211**, 401–424.
96. T. Alkhidir, Z. M. Saeed, A. F. Shunnar, E. Abujami, R. M. Nyadzayo, B. Dhokale and S. Mohamed, Expanding the supramolecular toolkit: computed molecular and crystal properties for supporting the crystal engineering of higher-order molecular ionic-cocrystals, *Cryst. Growth Des.*, 2022, **22**, 485–496.
97. U. Garg and Y. Azim, Challenges and opportunities of pharmaceutical cocrystals: a focused review on non-steroidal anti-inflammatory drugs, *RSC Med Chem.*, 2021, **12**, 705–721.
98. L. P. Robert, Complex salts of streptothricin, *US Pat.*, 1949, 2474758.
99. S. L. Childs, L. J. Chyall, J. T. Dunlap, V. N. Smolenskaya, B. C. Stahly and G. P. Stahly, Crystal engineering approach to forming cocrystals of amine hydrochlorides with organic acids. Molecular complexes of fluoxetine hydrochloride with benzoic, succinic, and fumaric acids, *J. Am. Chem. Soc.*, 2004, **126**, 13335.
100. G. P. Stahly, A survey of cocrystals reported prior to 2000, *Cryst. Growth Des.*, 2009, **9**, 4212–4229.
101. S. Jin, R. Sanii, B. Q. Song and M. J. Zaworotko, Crystal engineering of ionic-cocrystals sustained by the phenol–phenolate supramolecular heterosynthon, *Cryst. Growth Des.*, 2022, **22**, 4582–4591.
102. A. Tarai and J. B. Baruah, Quaternary and senary sub-assemblies in cocrystals and salts of quinoline-4-carbaldoxime with aromatic carboxylic acids, *CrystEngComm*, 2016, **18**, 9095–9102.
103. (a) S. Guerin, S. Khorasani, M. Gleeson, J. O'Donnell, R. Sanii, R. Zwane, A. M. Reilly, C. Silien, S.A.M. Tofail, N. Liu, M. Zaworotko and D. Thompson, A piezoelectric ionic-cocrystal of glycine and sulfamic acid, *Cryst. Growth Des.*, 2021, **21**, 5818–5827. (b) N. Barooah, R. J. Sarma, A. S. Batsanov and J. B. Baruah, Structural aspects of adducts of N-phthaloylglycine and its derivatives, *J. Mol. Struct.*, 2016, **791**, 122–130.
140. C. B. Aakeröy, J. Desper and M. M. Smith, Constructing, deconstructing, and reconstructing ternary supermolecules, *Chem. Commun.*, 2007, **38**, 3936–3938.
105. C. C. Seaton, N. Blagden, T. Munshi and I. J. Scowen, Creation of ternary multicomponent crystals by exploitation of charge-transfer interactions, *Chem. Eur. J.*, 2013, **19**, 10663–10671.
106. F. Topić and K. Rissanen, Systematic construction of ternary cocrystals by orthogonal and robust hydrogen and halogen bonds, *J. Am. Chem. Soc.*, 2016, **138**, 6610–6616.
107. (a) M. Rajkumar and G. R. Desiraju, Quaternary and quinary molecular solids based on structural inequivalence and combinatorial approaches: 2-nitroresorcinol and 4,6-dichlororesorcinol, *IUCrJ*, 2021, **8**, 178–185. (b) M. Paul, S. Chakraborty and G. R. Desiraju, Six-component molecular solids: ABC[D1−(x+y)ExFy]2, *J. Am. Chem. Soc.*, 2018, **140**, 2309–2315.
108. D. Braga, F. Grepioni, L. Maini, S. Prosperi, R. Gobetto and M. R. Chierotti, From unexpected reactions to a new family of ionic co-crystals: the case of barbituric acid with alkali bromides and caesium iodide, *Chem. Commun.*, 2010, **46**, 7715–7717.
109. M. P. Singh, A. Tarai and J. B. Baruah, Neutral, zwitterion, ionic forms of 5-aminoisophthalic acid in cocrystals, salts and their optical properties, *ChemistrySelect*, 2019, **4**, 5427–5436.
110. J. S. Stevens, Multicomponent complexes with varying degrees of proton transfer: exploring the nature of new form IV in the salt co-crystal continuum, *Cryst. Growth Des.*, 2022, **22**, 779–787.

TH-3622_196122001

111. O. Shemchuk, D. Braga, L. Maini, F. Grepioni, Anhydrous ionic co-crystals of cyanuric acid with LiCl and NaCl, *CrystEngComm*, 2017, **19**, 1366–1369.
112. O. N. Kavanagh, G. Walker and M. Lusi, Graph-set analysis helps to understand charge transfer in a novel ionic-cocrystal when the ΔpKa rule fails, *Cryst. Growth Des.*, 2019, **19**, 5308–5313.
113. A. Gunnam, K. Suresh and A. Nangia, Salts and salt cocrystals of the antibacterial drug pefloxacin, *Cryst. Growth Des.*, 2018, **18**, 2824–2835.
114. I. Ahmad, A. A. Malik, S. Ahmad, A. A. Dar, Sulfonate-pyridinium ionic-cocrystal solvates: improved material and antimicrobial properties, *Cryst. Growth Des.*, 2024, **24**, 4790–4800.
115. A. Gunnam, K. Suresh and A. Nangia, Salts and salt cocrystals of the antibacterial drug pefloxacin, *Cryst. Growth Des.*, 2018, **18**, 2824–2835.
116. N. K. Duggirala, A. J. Smith, Ł. Wojtas, R. D. Shytle and M. J. Zaworotko, Physical stability enhancement and pharmacokinetics of a lithium ionic-cocrystal with glucose, *Cryst. Growth Des.*, 2014, **14**, 6135–6142.
117. C. Delage, M. Palayer, B. Etain, M. Hagenimana, N. Blaise, J. Smati, M. Chouchana, V. Bloch, V. C. Besson, Valproate, divalproex, valpromide: are the differences in indications justified? *Biomedicine and Pharmacotherapy*, 2023, **158**, 114051.
118. (a) C. O'Malley, P. McArdle, A. Erxleben, Formation of salts and molecular ionic-cocrystals of fluoroquinolones and α,ω-dicarboxylic acids, *Cryst. Growth Des.*, 2022, **22**, 3060–3071. (b) Y. Xu, L. Jiang, X. Mei, Supramolecular structures and physicochemical properties of norfloxacin salts, *Acta Crystallogr.*, 2014, **70**, 750–760. (c) A. O. Surov, A. N. Manin, A. P. Voronin, K. V. Drozd, A. A. Simagina, A. V. Churakov and G. L. Perlovich, Pharmaceutical salts of ciprofloxacin with dicarboxylic acids, *Eur. J. Pharm. Sci.*, 2015, **77**, 112–121.
119. S. Muddassir A. Mashhadi, U. Yunus, M. H. Bhatti, Structural characterization and in-situ synthesis of quaternary ionic-cocrystal of isoniazid from un-ionized coformers, *J. Mol. Struct.*, 2021, **1233**, 130015.
120. M. Sangeetha and R. Mathammal, Structure-activity relationship of the ionic-cocrystal: 5-amino-2-naphthalene sulfonate ammonium ions for pharmaceutical applications, *J. Mol. Struct.*, 2018, **1154**, 327–337.
121. A. J. Stirk, S. T. Holmes, F. E. S. Souza, I. Hung, Z. Gan, J. F. Britten, A. W. Rey, R. W. Schurko, An unusual ionic-cocrystal of ponatinib hydrochloride: characterization by single-crystal X-ray diffraction and ultra-high field NMR spectroscopy, *CrystEngComm*, 2024, **26**, 1219–1233.
122. C. O'Malley, C. Bouchet, G. Manyara, N. Walsh, P. McArdle and A. Erxleben, Salts, binary and ternary cocrystals of pyrimethamine: mechanosynthesis, solution crystallization, and crystallization from the gas phase, *Cryst. Growth Des.*, 2021, **21**, 314–324.
123. Y. Li, Y. Zhang, Q. An, J. Shi and L. Liu, Salt cocrystal and salt of marbofloxacin with butenedioic acid: impact of cis-trans isomerism of coformer on the conformation and properties of marbofloxacin, *Cryst. Growth Des.*, 2024, **24**, 1339–1349.
124. R. Devarapalli, A. Indukuri, M. Bollineni, A. Mondal, C. M. Reddy, R. Chennuru, Investigation of poor solubility of a salt-cocrystal hydrate: a case study of the common-ion effect in betrixaban, an anticoagulant drug, *Mol. Pharmaceutics*, 2021, **18**, 1138–1149.
125. (a) M. P. Singh and J. B. Baruah, Combinations of tautomeric forms and neutral-cationic forms in the cocrystals of sulfamethazine with carboxylic acids, *ACS Omega*, 2019, **4**, 11609–11620. (b) J. Nath and J. B. Baruah, Self-assemblies of solvates, ionic-cocrystals, and a salt based on 4-{[(4-Nitrophenyl)carbamoyl]amino}-N-(pyrimidin-2-yl)benzene-1-sulfonamide: study in

TH-3622_196122001

the solid and solution states, *Cryst. Growth Des.*, 2021, **21**, 5325–5341. (c) J. Nath and J. B. Baruah, Polymorphic solvates, ionic-cocrystals and C–N bond formation to form ionic-cocrystals in sulfamethoxazole and sulfathiazole-derived urea, *CrystEngComm*, 2022, **24**, 3394–3408.
126. S. R. Shah, Z. Shah, A. Khan, A. Ahmed, Sohani, J. Hussain, R. Csuk, M. U. Anwar, A. Al-Harrasi, Sodium, potassium, and lithium complexes of phenanthroline and diclofenac: first report on anticancer studies, *ACS Omega*, 2019, **4**, 21559–21566.
127. A. J. Bennett and A. J. Matzger, Progress in predicting ionic-cocrystal formation: the case of ammonium nitrate, *Chem. Eur. J.*, 2023, **29**, e202300076.
128. Q. Ma, S.-L. Huang, H.-C. Lu, F. Nie, L.-Y. Liao, G. J. Fan, J.-L. Huang, Energetic cocrystal, ionic salt, and coordination polymer of a perchlorate-free high-energy density oxidizer: influence of pKa modulation on their formation, *Cryst. Growth Des.*, 2019, **19**, 714–723. (b) J. C. Bennion and A. J. Matzger, Development and evolution of energetic cocrystals, *Acc. Chem. Res.*, 2021, **54**, 1699–1710. (c) A. K. Yadav, V. D. Ghule and S. Dharavath, Thermally stable and insensitive energetic cocrystals comprising nitrobarbituric acid coformers, *Cryst. Growth Des.*, 2023, **23**, 2826–2836. (d) T. Wang, S. Bu, Z. Lu, B. Kuang, Z. Yi, Z. Xie, C. Zhang, Y. Li, J. Zhang, New form of high-energy primary explosive: dual structure composed of ionic salt-based coordination polymers, *Chem. Eng. J.*, 2023, **457**, 141267.
129. A. J. Bennett, L. M. Foroughi and A. J. Matzger, Perchlorate-free energetic oxidizers enabled by ionic-cocrystallization, *J. Am. Chem. Soc.*, 2024, **146**, 1771–1775.
130. S. Ahmadi and S. Rohani, Overcoming the hydrophobic nature of zinc phenylacetate through co-crystallization with isonicotinamide, *J. Pharm. Sci.*, 2023, **112**, 1929–1938.
131. (a) B. J. Holliday and C. A. Mirkin, Strategies for the construction of supramolecular compounds through coordination chemistry, *Angew. Chem. Int. Ed.*, 2001, **40**, 2022–2043. (b) J. B. Baruah, Predominantly ligand-guided non-covalently linked assemblies of inorganic complexes and guest inclusions, *J. Chem. Sci.*, 2018, **130**, 56. (c) M. Ghazzal, Supramolecular assembly in metal complexes: two structural cases, *Pure Appl. Chem.*, 2013, **85**, 397–404. (d) K. Kuroiwa and N. Kimizuka, Self-assembly and functionalization of lipophilic metal-triazole complexes in various media, *Polym. J.*, 2013, **45**, 384–390.
132. S. Fernández-Fariña, M. Maneiro, G. Zaragoza, J. M. Seco, R. Pedrido, A. M. González-Noya, Nickel, copper, and zinc dinuclear helicates: how do bulky groups influence their architecture?, *Dalton Trans.*, 2024, **53**, 5676–5685.
133. A. Famulari and J. Martí-Rujas, Host–guest chemistry of M12L8 poly-[n]-catenanes: inclusion process by switchable “closed–open” dynamic channels, *Cryst. Growth Des.*, 2022, **22**, 4494–4502.
134. (a) E. Hough and D. G. Nicholson, X-Ray crystallographic studies on ferrocene included in a thiourea host lattice, *J. Chem. Soc. Dalton Trans.*, 1978, **15**, 15–18. (b) M. Sorai, K. Ogasahara and H. Suga, Heat capacity and phase transitions of thiourea-ferrocene channel inclusion compound, *Mol. Cryst. Liq. Cryst.*, 1981, **73**, 231–254.
135. Anion Coordination Chemistry, Eds. K. Bowman-James, A. Bianchi and E. García-España, Wiley Online Library, 2011.
136. E. M. Fatila, M. Pink, E. B. Twum, J. A. Karty and A. H. Flood, Phosphate–phosphate oligomerization drives higher-order co-assemblies with stacks of cyanostar macrocycles, *Chem. Sci.*, 2018, **11**, 2863–2872.
137. (a) K. J. Takeuchi and D. H. Busch, Inclusion complex formation by transition-metal complexes containing a void in proximity to a site that can be made catalytically active, *J. Am.*

TH-3622_196122001

Chem. Soc., 1983, **105**, 6812–6816. (b) S. R. Seidel and P. J. Stang, High-symmetry coordination cages via self-assembly, *Acc. Chem. Res.*, 2002, **35**, 972–983.
138. (a) L. Herkert, A. Sampedro and G. Fernández, Cooperative self-assembly of discrete metal complexes, *CrystEngComm*, 2016, **18**, 8813–8822. (b) K. M. Mullen and P. D. Beer, Sulfate anion templation of macrocycles, capsules, interpenetrated and interlocked structures, *Chem. Soc. Rev.*, 2009, **6**, 1701–1713. (c) M. A. Haga, K. Kobayashi, K. Terada, Fabrication and functions of surface nanomaterials based on multilayered or nanoarrayed assembly of metal complexes, *Coord. Chem. Rev.*, 2007, **251**, 2688–2701. (d) M. Fujita, D. Oguro, M. Miyazawa, H. Oka, K. Yamaguchi, K. Ogura, Self-assembly of ten molecules into nanometre-sized organic host frameworks, *Nature*, 1995, **378**, 469–471. (e) K. Matsumoto, S. Kusaba, Y. Tanaka, Y. Sei, M. Akita, K. Aritani, M. Haga, M. Yoshizawa, A peanut-shaped polyaromatic capsule: solvent-dependent transformation and electronic properties of a non-contacted fullerene dimer, *Angew. Chem., Int. Ed. Eng.*, 2019, **58**, 8463–8467.
139. S. Sato, J. Iida, K. Suzuki, M. Kawano, T. Ozeki, M. Fujita, Fluorous nanodroplets structurally confined in an organopalladium sphere, *Science*, 2006, **313**, 1273–1276.
140. M. Yoshizawa, M. Tamura and M. Fujita, Diels-Alder in aqueous molecular hosts: unusual regioselectivity and efficient catalysis, *Science*, 2006, **312**, 251–254.
141. V. W.-W. Yam, V. K.-M. Au and S. Y.-L. Leung, Light-emitting self-assembled materials based on d8 and d10 transition metal complexes, *Chem. Rev.*, 2015, **115**, 7589–7728.
142. C. R. A. do Prado, M. H. de Oliveira Pessoa, L. da S. dos Santos, A. da S. X. da Cruz, L. R. Dinelli, A. L. Bogado, The self-assembly of cationic metal complexes on gold nanoparticle surface, *ACS Omega*, 2024, **9**, 28989–28999.
143. E. A. Katlenok, M. Haukka, O. V. Levin, A. Frontera and V. Yu. Kukushkin, Supramolecular assembly of metal complexes by (aryl)I··[PtII] halogen bonds, *Chem. Eur. J.*, 2020, **26**, 7692–7701.
144. B. Das and J. B. Baruah, Protonated adenine and cytosine ribbons stabilized by dipicolinato metal frameworks, *Cryst. Growth Des.*, 2010, **10**, 3242–3249.
145. J. P. García-Terán, O. Castillo, A. Luque, U. García-Couceiro, G. Beobide and P. Román, Molecular recognition of protonated cytosine ribbons by metal-oxalato frameworks, *Cryst. Growth Des.*, 2007, **7**, 2594–2600.
146. J. P. García-Terán, O. Castillo, A. Luque, U. García-Couceiro, G. Beobide and P. Román, Molecular recognition of adeninium cations on anionic metal-oxalato frameworks: an experimental and theoretical analysis, *Inorg. Chem.*, 2007, **46**, 3593–3602.
147. H. Chhipa, T. S. Reddy, S. K. Soni, P. R. Selvakannan and S. K. Bhargava, Self-assembled nanostructures of phosphomolybdate, nucleobase and metal ions synthesis and their in vitro cytotoxicity studies on cancer cell lines, *J. Mater. Chem. B*, 2020, **8**, 11044–11054.
148. K. Shankar and J. B. Baruah, Tetranuclear cobalt complexes as nano-dimensional template for inclusion of nitrophenols, *ChemistrySelect*, 2016, **1**, 5152–5158.
149. G. J. Beach, C. E. Hogan, B. N. Besong and G. A. Hogan, Inclusion of alkyl alcohol guest molecules into a copper (II)-based hydrogen-bonded metal-organic framework, *J. Mol. Struct.*, 2019, **1195**, 744–746.
150. H. H. Nguyen, C. E. Hogan and G. A. Hogan, Guest inclusion of pyridine molecules into a copper (II)-bilayer hydrogen-bonded metal-organic framework, *J. Chem. Crystallogr.*, 2021, **51**, 82–87.

TH-3622_196122001

151. M. P. Singh, K. Shankar and J. B. Baruah, Study on the interactions of nitrophenols with bis-8-hydroxyquinolinium zinc-2,6-pyridinedicarboxylate, *Inorg. Chim. Acta*, 2019, **489**, 204–210.
152. C.-Y. Xing, Q.-W. Yang, J.-Z. Wang, H.-B. Song, W.-Q. Zhang, Crystal structure and theoretical computation study on a self-inclusion layered discrete Cu(II) and PPz complex, *Inorg. Chim. Acta*, 2013, **394**, 31–35.
153. X. Lin, D. M. J. Doble, A. J. Blake, A. Harrison, C. Wilson, M. Schröder, Cationic assembly of metal complex aggregates: structural diversity, solution stability, and magnetic properties, *J. Am. Chem. Soc.*, 2003, **125**, 9476–9483.
154. X.-J. Zhao, Z.-H. Zhang, Y. Wang, M. Du, Robust anionic building blocks [M(malonate)2(H2O)2]2− for crystal engineering of inorganic–organic hybrid materials, *Inorg. Chim. Acta*, 2007, **360**, 1921–1928.
155. G. A. Hogan, N. P. Rath, A. M. Beatty, A stable hydrogen-bonded coordination network with removable guests, *Cryst. Growth Des.*, 2011, **11**, 3740–3743.
156. T. Friscic, E. Mestrovic, D. S. Samec, B. Kaitner, L. Fabian, One-pot mechanosynthesis with three levels of molecular self-assembly: coordination bonds, hydrogen bonds and host–guest inclusion, *Chem. Eur. J.*, 2009, **15**, 12644–12652.
157. C.-H. Ge, X.-Y. Zhang, F. Yu, Y.-N. Guo, X.-D. Zhang, Q.-T. Liu, C–H···F hydrogen-bonded assembly of Ni(II) and Cu(II) complexes generate 3D supramolecular frameworks, *J. Chem. Crystallogr.*, 2008, **38**, 501–505.
158. L. Li, D. Sun, G. Tian, X. Song, S. Sun, A new photoluminescent supramolecular inorganic–organic hybrid zincophosphate complex pillared by carboxylate ligand through hydrogen bonding interactions, *Cryst. Res. Technol.*, 2009, **44**, 331–335.
159. C. Li, N. Mizuno, K. Yamaguchi and K. Suzuki, Self-assembly of anionic polyoxometalate–organic architectures based on lacunary phosphomolybdates and pyridyl ligands, *J. Am. Chem. Soc.*, 2019, **141**, 7687–7692.
160. (a) A. F. Leung, L. Hayashibara and J. Spadaro, Fluorescence properties of uranyl nitrates, *J. Phys. Chem. Solids*, 1999, **60**, 299–304. (b) Y. Zhang, H.-M. Chen and M.-J. Lin, Chiral self-discrimination induced luminescence vapochromism of binaphthol imides for anti-counterfeiting and data encryption, *Adv. Optical Mater.*, 2024, **12**, 2470075. (c) F. Zhou, P. Gu, Z. Luo, H. K. Bisoyi, Y. Ji, Y. Li, Q. Xu, Q. Li and J. Lu, Unexpected organic hydrate luminogens in the solid state, *Nature Commun.*, 2021, **12**, 2339. (d) T. Kimura and G. R. Choppin, Luminescence study on determination of the hydration number of Cm(III), *J. Alloys and Compounds*, 1994, **213-214**, 313–317. (e) T. Sagami, Y. O. Tahara, M. Miyata, H. Miyake, S. Shinoda, Luminescence sensing of weakly-hydrated anions in aqueous solution by self-assembled europium(III) complexes, *Chem. Commun.*, 2017, **53**, 3967–3970. (f) A. Tarai and J. B. Baruah, Changing π-interactions and conformational adjustments of N-(isonicotinylhydrazide)-1,8-naphthalimide by hydration and complexation affect photophysical properties, *Cryst. Growth Des.*, 2018, **18**, 456–465.
161. (a) Y. Xin, J. Wang, M. Zychowicz, J. J. Zakrzewski, K. Nakabayashi, B. Sieklucka, S. Chorazy, S.-I. Ohkoshi, Dehydration-hydration switching of single-molecule magnet behavior and visible photoluminescence in a cyanido-bridged DyIIICoIII framework, *J. Am. Chem. Soc.*, 2019, **141**, 18211–18220. (b) D.-Q. Wu, L. Shi, D. Shao, M. Xia, Y. Liao, Y. Wu, J. Wen, B. Zhai, Dehydration-actuated single-molecule magnet behavior in a cyanide-bridged [Fe2Co2] cluster featuring zigzag structure, *J. Molecular Struct.*, 2024, **1295**, 136615. (c) Z. Lu, X. Wang, Z. Liu, F. Liao, S. Gao, R. Xiong, H. Ma, D. Zhang, D. Zhu, Tuning the magnetic behavior via dehydration/hydration treatment of a new ferrimagnet with the composition of

TH-3622_196122001

K0.2Mn1.4Cr(CN)6·6H2O, *Inorg. Chem.*, 2006, **45**, 999–1004. (d) W.-X. Chen, Y.-F. Gao, P.-Y. Gao, Q.-P. Liu, G.-L. Zhuang, Ionothermal synthesis, magnetic transformation and hydration–dehydration properties of Co(II)-based coordination polymers, *RSC Adv.*, 2016, **6**, 71952–71957. (e) Z. Skokanova, J. Krocan, M. Rakos, Effect of water of crystallization on magnetic properties of MgSO4, *Czech. J. Phys.*, 1978, **28**, 220–227. (f) M. Heczko and B. Nowicka, Switching of magnetic properties by topotactic reaction in a 1D CN-bridged Ni(II)–Nb(IV) system, *Dalton Trans.*, 2024, **53**, 5788–5795.

162. (a) M. Sadakiyo, T. Yamada and H. Kitagawa, Hydrated proton-conductive metal–organic frameworks, *ChemPlusChem*, 2016, **81**, 691–701. (b) Y. M. Li, M. Hibino, M. Miyayania, T. Kudo, Proton conductivity of tungsten trioxide hydrates at intermediate temperature, *Solid State Ionics*, 2000, **134**, 271–279. (c) T. S. Bjorheim, T. Norby and R. Haugsrud, Hydration and proton conductivity in LaAsO4, *J. Mater. Chem.*, 2012, **22**, 1652–1661. (d) A. Martinelli, M. N. Otero-Mato, K. Garaga, S. M. H. Elamin, J. W. Rahman, U. Zwanziger, J. M. Werner-Zwanziger, L. M. Varela, A new solid-state proton conductor: the salt hydrate based on imidazolium and 12-tungstophosphate, *J. Am. Chem. Soc.*, 2021, **143**, 13895–13907. (e) J.-H. Cha, K. Shin, S. Choi, S. Lee and H. Lee, Maximized proton conductivity of the HPF4 clathrate hydrate by structural transformation, *J. Phys. Chem. C*, 2008, **112**, 13332–13335.

163. K. Maegawa, M. Wlazło, N. H. H. Phuc, K. Hikima, G. Kawamura, A. Nagai, A. Matsuda, Synthesis and structure-electrochemical property relationships of hybrid imidazole-based proton conductors for medium-temperature anhydrous fuel cells, *Chem. Mater.*, 2023, **35**, 7708–7718.

164. (a) C. I. Ratcliffe, The development of clathrate hydrate, *Sci. Energy Fuels*, 2022, **36**, 10412–10429. (b) E. D. Sloan Jr., Fundamental principles and applications of natural gas hydrates, *Nature*, 2003, **426**, 353–363.

165. (a) R. Sanii, E. Patyk-Kaźmierczak, C. Hua, S. Darwish, T. Pham, K. A. Forrest, B. Space, M. J. Zaworotko, Towards an understanding of the propensity for crystalline hydrate formation by molecular compounds. Part 2, *Cryst. Growth Des.*, 2021, **21**, 4927–4939. (b) R. Li, Y. Shi, L. Shi, M. Alsaedi, P. Wang, Harvesting water from air: using anhydrous salt with sunlight, *Environ. Sci. Tech.*, 2018, **52**, 5398–5406. (c) Y. Xu, Q. Wang, C. Shen, Q. Lin, P. Wang, M. Lu, A series of energetic metal pentazolate hydrates, *Nature*, 2017, **549**, 78–81. (d) D. E. Braun, Supramolecular organisation of sulphate salt hydrates exemplified with brucine sulphate, *CrystEngComm*, 2020, **22**, 7204–7216. (e) D. E. Braun, P. G. Karamertzanis, S. L. Price, Which, if any, hydrates will crystallise? Predicting hydrate formation of two dihydroxybenzoic acids, *Chem. Commun.*, 2011, **47**, 5443–5445. (f) D. E. Braun, T. Gelbrich, V. Kahlenberg, U. J. Griesser, The eight hydrates of strychnine sulfate, *Cryst. Growth Des.*, 2020, **20**, 6069–6083.

166. (a) E. Mamontov, Y. Cheng, L. L. Daemen, J. K. Keum, A. I. Kolesnikov, D. Pajerowski, A. Podlesnyak, A. J. Ramirez-Cuesta, M. R. Ryder, M. B. Stone, Effect of hydration on the molecular dynamics of hydroxychloroquine sulfate, *ACS Omega*, 2020, **5**, 21231–21240. (b) R. K. Khankari and D. J. W. Grant, Pharmaceutical hydrates, *Thermochimica Acta*, 1995, **248**, 61–79.

167. (a) D. T. Gomez, L. R. Pratt, D. N. Asthagiri, S. B. Rempe, Hydrated anions: from clusters to bulk solution with quasi-chemical theory, *Acc. Chem. Res.*, 2022, **55**, 2201–2212. (b) J. K. Nath and J. B. Baruah, Water assisted anion chains and anion dependent fluorescence emission in salts of N,N′-bis(3-imidazol-1-ylpropyl)naphthalenediimide, *New J. Chem.*, 2013, **37**, 1509–1519. (c) V. Lopez-Corbalan, A. Fuertes, A. L. Llamas-Saiz, M. Amoriin, J. R. Granja, Recognition of anion-water clusters by peptide-based supramolecular capsules, *Nature Commun.*, 2024, **15**, 6055.

TH-3622_196122001

168. M. J. Ryan, L. Gao, F. I. Valiyaveetil, A. A. Kananenka, M. T. Zanni, Water inside the selectivity filter of a K+ ion channel: structural heterogeneity, picosecond dynamics, and hydrogen bonding, *J. Am. Chem. Soc.*, 2024, **146**, 1543–1553.
169. A. P. Singh and J. B. Baruah, Lithium(I), cesium(I), barium(II) and cadmium(II) [2-(2,6-dichlorophenylamino)phenyl]acetate (diclofenac) complexes and coordination polymers, *Inorg. Chim. Acta*, 2024, **569**, 122131.
170. (a) B. Wu, S. Li, Y. Lei, H. Hu, N. de S. Amadeu, C. Janiak, J. S. Mathieson, D.-L. Long, L. Cronin, X.-J. Yang, The effect of the spacer of bis(biurea) ligands on the structure of A2L3-type (A = anion) phosphate complexes, *Chem. Eur. J.*, 2015, **21**, 2588–2593. (b) Y. Wang, B. Li, J. Zhu, W. Zhang, B. Zheng, W. Zhao, J. Tang, X.-J. Yang, B. Wu, Light-triggered high-affinity binding of tetramethylammonium over potassium ions by [18] crown-6 in a tetrahedral anion cage, *Angew. Chem., Int. Ed. Eng.*, 2022, **61**, e202201789.
171. (a) W. Zuo, Z. Huang, Y. Zhao, W. Xu, Z. Liu, X.-J. Yang, C. Jia, B. Wu, Chirality sensing of choline derivatives by a triple anion helicate cage through induced circular dichroism, *Chem. Commun.*, 2018, **54**, 7378–7381. (b) A. Dhara, R. E. Fadler, Y. Chen, L. A. Kottner, D. VanCraen, V. Carta, A. H. Flood, Orthogonal, modular anion–cation and cation–anion self-assembly using pre-programmed anion binding sites, *Chem. Sci.*, 2023, **14**, 2585–2595.
172. K. Shankar, A. M. Kirillov and J. B. Baruah, A modular approach for molecular recognition by zinc dipicolinate complexes, *Dalton Trans.*, 2015, **44**, 14411–14423.
173. B.-M. Kukovec, G. A. Venter, C. L. Oliver, Structural and DFT studies on the polymorphism of a cadmium(II) dipicolinate coordination polymer, Cryst. Growth Des., 2012, **12**, 456 – 465.
174. A. O. Surov, N. A. Vasilev, A. V. Churakov, J. Stroh, F. Emmerling, G. L. Perlovich, Solid forms of ciprofloxacin salicylate: polymorphism, formation pathways, and thermodynamic stability, Cryst. Growth Des., 2019, **19**, 2979 – 2990.
175. P. Harsha, M. Khan, R. Thakuria and D. Das, Synthesis of a cocrystal hydrate by sublimation and reversible polymorphic transformation through single-crystal to single-crystal fashion, *Cryst. Growth Des.*, 2024, **24**, 3109–3113.
176. D. Das, E. Engel and L. J. Barbour, Reversible single-crystal to single-crystal polymorphic phase transformation of an organic crystal, *Chem. Commun.*, 2010, **46**, 1676–1678.

TH-3622_196122001

CHAPTER 2

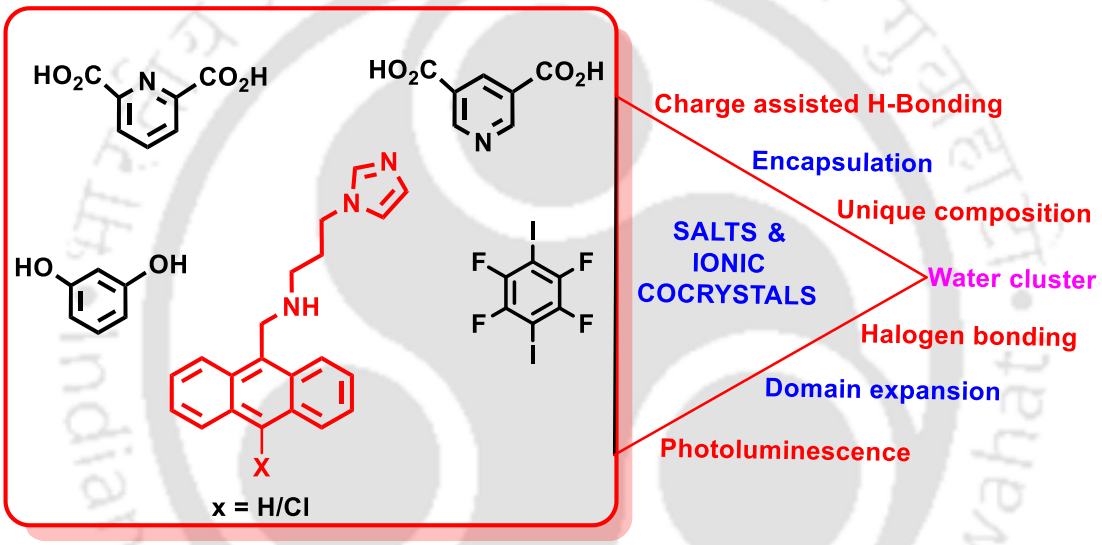

TH-3622_196122001

Chapter 2

Salts and ionic-cocrystals of imidazole tethered anthracene derivative with pyridinedicarboxylic acids

2.1. Introduction

As described in the earlier chapter, the ionic-cocrystals of organic salts are supramolecular associations of the salt with a neutral or another ionic counterpart.[1-4] There are large number of examples of such multi-component cocrystals in literature.[5-10] However, each has own perspective applications and some of their properties such as physical properties and bioavailability in drugs are being continuously explored. In general, to form a salt and cocrystal from a conjugate-acid base pair, one has to rely on the differences of the pKa among partner conjugate acid-base molecules.[11] For example, when the pKa difference is large then proton transfer from the acid to base takes place to provide a salt, on the other hand when difference is very small they form hydrogen bonds and result in cocrystal. There is an intermittent pKa difference region, in which it is difficult to predict whether a cocrystal or salt will be formed. The crystallizations in such cases are very sensitive to conditions used and effect of various other factors such as dielectric of media, solvent, stimuli that are related to crystallization play decisive roles in obtaining a particular form.[11] Thus, in many examples, the explanations on the salt or cocrystal formation from acid-base pairs are based on the pKa differences between the partner acid-base components are valid.[12] While designing a multicomponent cocrystal,[13] a host-guest complex to serve as a host to hold a third and a fourth component is required. In such cases, it would be interesting to utilise the intrinsic acidity or basicity of a poly-acid or poly-base to design host-guest template for preparation of multicomponent cocrystals. Hence, there is a necessity to extend the concepts further to polytopic systems to sort out the different forms of cocrystals through partial or complete proton transfer within the same system.

As a step forward to deal with a combination of ditopic acid and ditopic amine conjugates, we have considered to use a ditopic host such as 9-N-(3-imidazolylpropylamino)methylanthracene {abbreviated as H**anthraimmida** as shown in Figure 2.1(a)} with two distinguishable hydrogen-bond donor or acceptor sites (NH or imidazole N) to utilise for proton-transfer or hydrogen bonding. It was earlier showed that H**anthraimmida,** forms salts as well as cocrystals with phenolic and aromatic carboxylic acids.[14] Therefore, the possibility to utilise such assemblies to

TH-3622_196122001

prepare different ionic-cocrystals as well as multi-component assemblies of this ditopic amine leaves avenue for formation of different ionic-cocrystals. It also provided scope to study the effect of substituent atoms and additional weak interaction schemes arising from such species.

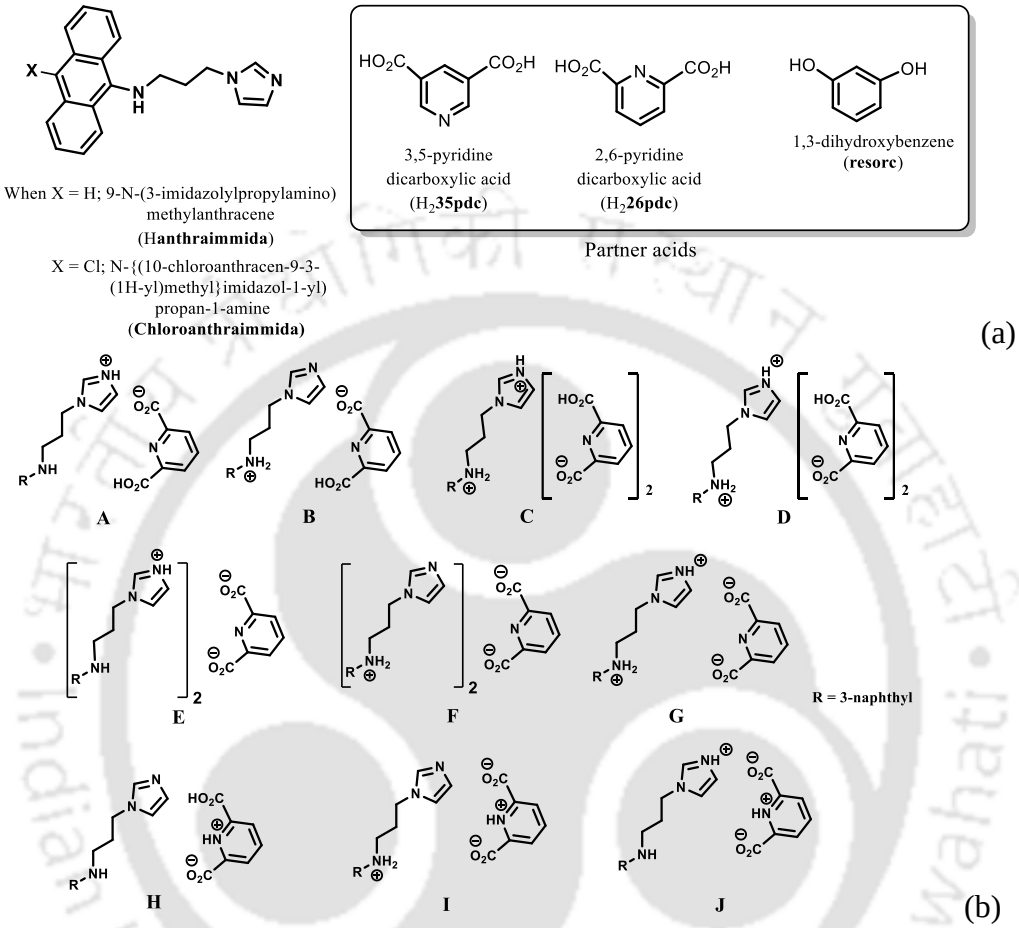

Figure 2.1: (a) Structures of H**anthraimmida** and the partner acid molecules (b) Some probable cocrystals and salts that may be expected from H**anthraimmida** reacting with pyridinedicarboxylic acid.

So we have also chosen another ditopic chloro-substituted analogue, N-{(10-chloroanthracen-9-yl)methyl}-3-(1H-imidazol-1-yl)propan-1-amine (**Chloroanthraimmida** or **Clanth**) to study the steric, electronic effect of chlorine atom in guiding such self-assemblies. Two pyridinedicarboxylic acids were chosen as the partner ditopic acids shown in the Figure 2.1(a) to prepare different cocrystals. These acids are nitrogen containing dicarboxylic acids, and based on the position of the carboxylic acid groups on the respective pyridine ring they are positional isomers. Taking 2,6-pyridinedicarboxylic acid (abbreviated as H_2**26pd**c), as an example with H**anthraimmida**, the different possible forms of mono-cation or di-cation are illustrated as A-D in the Figure 2.1(b). The di-anionic **26pdc**, will provide different compositions such as E-G. Alternatively, assembly

TH-3622_196122001

may be formed by a zwitterion, as illustrated in H-J of the Figure 2.1(b). These aspects get further complicated by having mixed ionic species in salts. For example, a chain like hydrogen bonded carboxylate catemers[15] of neutral, mono-protonated and di-deprotonated anion may bind cations at distinguishable environment as shown in the Figure 2.2(a). Such possibilities will imbibe symmetry independent relation for the distinguishable ions to define their positions in a crystal lattice. This may translate to provide avenue to study them as symmetry non-equivalent[16] cations in the unit cell. Such may be conceived by act of an interaction with or without an additional interacting molecule as depicted in the Figure 2.2 (a)-(b).

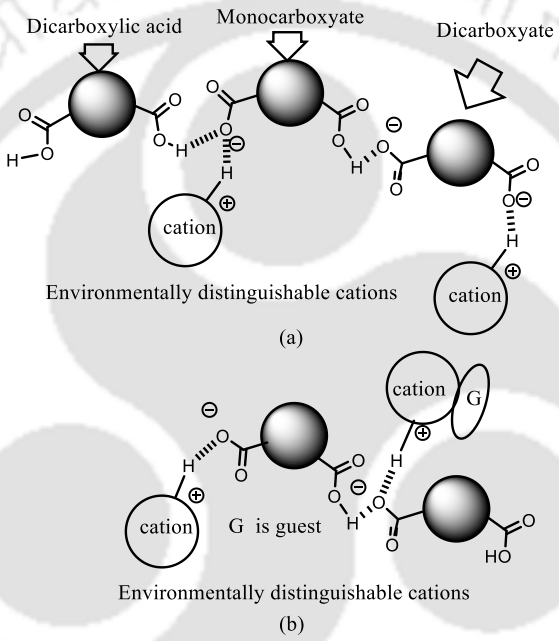

Figure 2.2: Some possibilities to create non-equivalent environment around hydrogen bonded cations attached to assemblies of dicarboxylates: (a) Assembly of neutral acid with different anions, (b) Cation with and without guest held to anionic chain.

It is an established fact that π-stacking within an assembly results in different assemblies such as H and J-type aggregates that show characteristic and distinguishable emission spectra. Hence, understanding the solid-state structures can be of help to understand emission changes taking place due to aggregation.[17] To disseminate the different possibilities and also to explore the properties of new ionic-cocrystals, a series of salts and ionic-cocrystals of H**anthraimmida** and **Chloroanthraimmida** with two positional isomers were synthesized and characterized. The two host compounds were used to prepare various salt, ionic-cocrystals listed in the scheme 2.1. It was also possible to prepare substrate specific ionic-cocrystals with resorcinol and 1,4-diiodotetrafluorobenzene. Their synthesis and characterizations are also presented. The

TH-3622_196122001

compounds H**anthraimmida** and **Chloroanthraimmida** were prepared by reported procedure.[14] Dissolving equimolar amounts of the H**anthraimmida** and H_2**26pdc** in methanol containing about 1% water at room temperature (Scheme 2.1) followed by slow evaporation of solvent provided crystals of the ionic-cocrystal (**2.1**); whereas, similar process with H_2**35pdc** provided a salt (**2.2**). Ionic-cocrystals with resorcinol, **2.3** and **2.4** were prepared in methanol by dissolving equimolar amounts of the three components, namely, H**anthraimmida**, H_2**26pdc** or H_2**35pdc** and resorcinol respectively, followed by slow evaporation to crystallize.

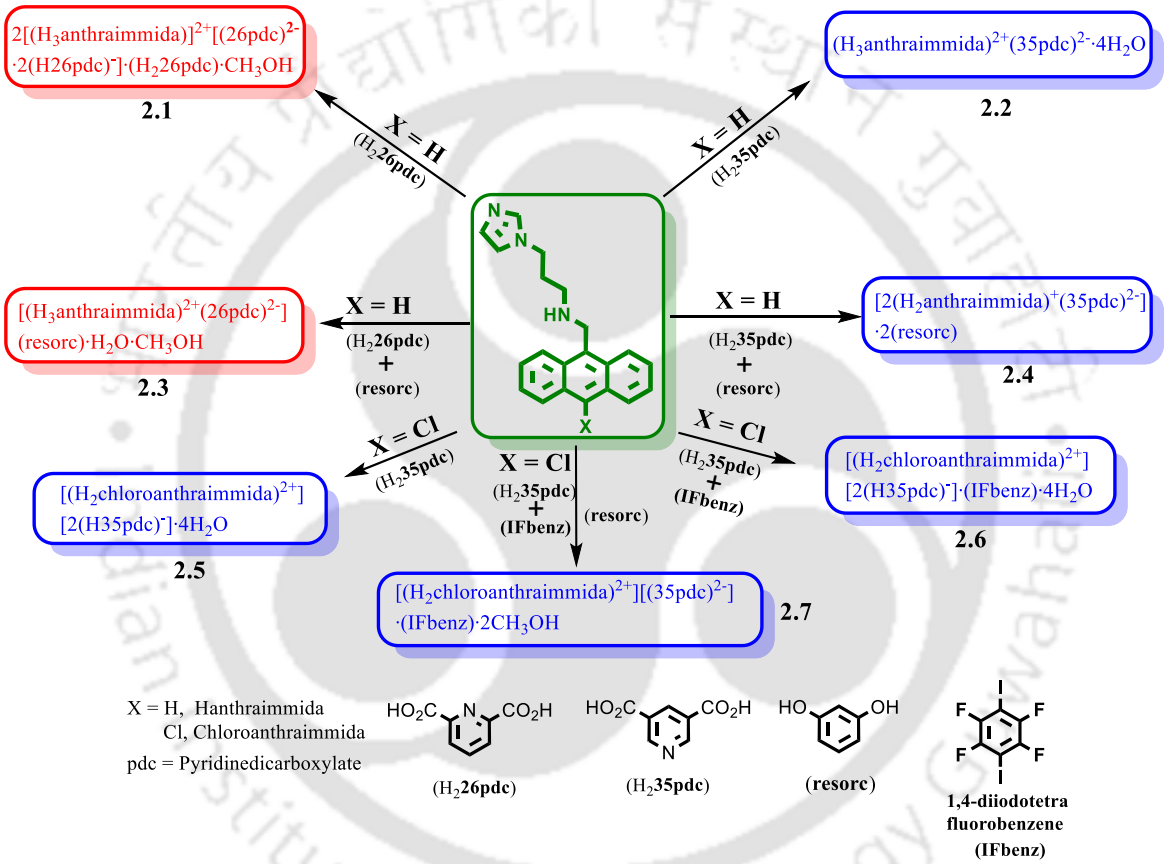

Scheme 2.1: Reactants, products, salts and ionic-cocrystals of the H**anthraimmida** and **Chloroanthraimmida**.

In the similar manner, the ionic-cocrystals **2.5** and **2.6** were prepared using **Chloroanthraimmida** with H_2**35pdc** and 1,4-diiodotetrafluorobenzene (**IFbenz**). While trying to prepare a four component ionic-cocrystal by adding equivalent amount of resorcinol to a solution from which **2.6** could be prepared, a new ionic-cocrystal of **Chloroanthraimmida**, H_2**35pdc** and **IFbenz**, without the incorporation the resorcinol (abbreviated as **2.7**) was serendipitously observed. The spectroscopic details of the salt and the ionic-cocrystals and the hydrogen-bond parameters are listed in the appendix.

TH-3622_196122001

2.2. Structures and self-assemblies of salts and ionic-cocrystals 2.1-2.7

The structures were determined by single crystal X-ray diffraction, the structure of the salt **2.1** had the composition 2[(H_3**anthraimmida)**]$^{2+}$[**(26pdc)**$^{2-}$·2(H**26pdc)**$^{-}$]·(H_2**26pdc)**·CH_3OH (**2.1**), whereas, the salt of H**anthraimmida** with H_2**35pdc** was a conventional tetrahydrate having a composition (H_3**anthraimmida)**$^{2+}$**(35pdc)**$^{2-}$·$4H_2O$ (**2.2**). The structure of **2.1** (Figure 2.3a) has two symmetry independent cations in its unit cell, these are illustrated in the Figure 2.3b. The self-assembly had chains of hydrogen bonded catemers (Figure 2.3c), which were formed among the neutral and anions of the H_2**26pdc**. Each pyridine dicarboxylate of the chain was flanked by two pyridine monocarboxylates. Such units were hydrogen bonded to a neutral H_2**26pdc** forming chain with ··H_2pdc··Hpdc··pdc··Hpdc·· as the repeat units. There are reports on sickle- or concave-shaped species to have symmetry non-equivalent species in their respective unit cell.[25-26] The H_3**anthraimmida**$^{2+}$ had a sickle shaped geometry, possibly due to such a geometry it had two symmetry independent cations in the unit cell of the salt **2.1**. The cations were hydrogen bonded to the catemeric carboxylate-carboxylic acid chain at two distinguishable environments.

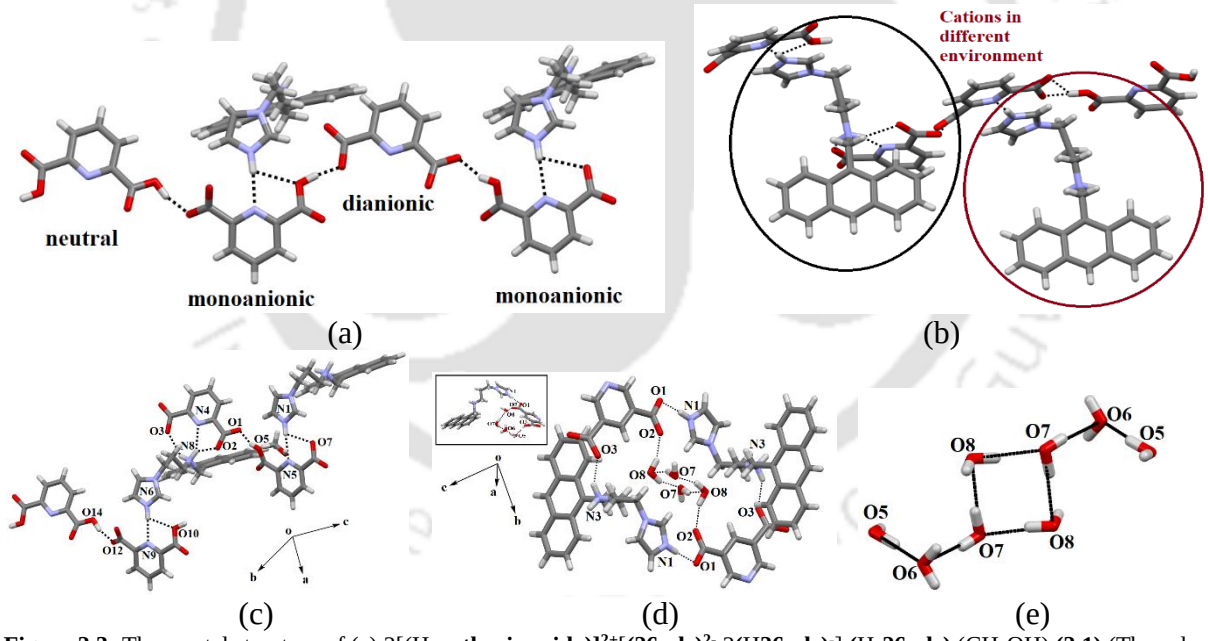

Figure 2.3: The crystal structure of (a) 2[(H_3**anthraimmida)**]$^{2+}$[**(26pdc)**$^{2-}$·2(H**26pdc)**$^{-}$]·(**$H_2$26pdc)**·(CH_3OH) **(2.1)** (The solvent molecules are omitted for clarity) (b) Two distinct environments of the symmetry independent di-cations marked in red and black circles; (c) The prominent hydrogen bonds in the self-assembly. (d) The hydrogen bonded assembly of the (H_3**anthraimmida)**$^{2+}$**(35pdc)**$^{2-}$·$4H_2O$ **(2.2)**, {inset is the crystal structure of **2.2**} (e) Octameric water cluster in **2.2**.

The chains were hydrogen bonded among them, and they were located at translated positions with respect to each other. The spaces in between the chains had accommodated the imidazolium

TH-3622_196122001

portion of the di-cation. The imidazolium N^+-H bond had acted as hydrogen bond donor for an oxygen atom to carboxylate. Whereas, the -NH_2^+- moiety had formed N3$^+$-H···O13 and N3$^+$-H···O12 hydrogen bonds to link another chain (Figure 2.3c).

The self-assembly of the (H_3**anthraimmida)$^{2+}$(35pdc)$^{2-}$·**4H_2O (**2.2**) is shown in the Figure 2.3d, it had self-assembled hydrogen bonded dimers of the salts. Each **35pdc^{2-}** was bridged by di-cations to form the dimers. One of the carboxylate group of the **35pdc^{2-}**, was hydrogen bonded to imidazolium cation. Whereas, the second carboxylate group of the same **35pdc^{2-}** formed hydrogen bond with the NH_2^+ (Figure 2.3d). The di-cation H_3**anthraimmida^{2+}** had sickle shaped geometry. The self-assembled di-cations had the concave faces facing each other. The assembling between two salt molecules, provided the space to accommodate four water molecules in the void. The water molecules were observed as hydrogen bonded octameric water clusters as illustrated in Figure 2.3e. Each water octamer was held in the lattice hydrogen bonds with two dicarboxylates. The water cluster had contributed to form the tight packed structure of the salt by filling the possible voids; and also had provided hydrogen bonds to the self-assembly contributing to the overall stabilization. The presence of water molecule in the salt was also confirmed by themogravimetry; the salt **2.2** losses water molecules upon heating at 70-100°C (Figure 2.9b). Some imidazole derived ligands in metal complexes stabilize different types of water clusters.[27-29] Depending on the geometry of ligands in metal complexes, different geometrical arrangements of octamers of water clusters were observed.[27-28]

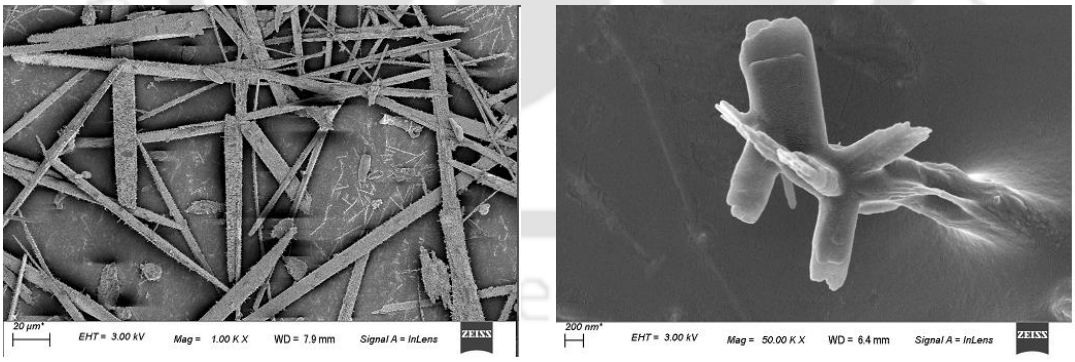

(a) (b)

Figure 2.4: (a) and (b) are the scanning electron micrographs of the crystals of the **2.1** and **2.2** respectively.

In the present case, four water molecules were assembled to form a hydrogen bonded cyclic synthon, which was connected to two pairs of hydrogen bonded water molecules, each pair of water molecules linked at the two terminals of the cyclic synthon. Certain concave shaped

TH-3622_196122001

molecules having water clusters form gel.[30] However in the present case, we did not observe a stable gel, but we found that the salt **2.2** was difficult to crystallize, the crude sample obtained by solvent evaporation was a sticky semi-solid, however, upon re-dissolving, it provided micro-crystals. The micro-crystals grown in different directions with sizes less than 200 nm could be observed in the scanning electron micrograph (SEM) of the **2.2** (Figure 2.4b), whereas, the SEM of the salt **2.1** had micrometer size needle-shaped crystals (Figure 2.4a).

The ionic-cocrystal **2.3**, namely [(H_3**anthraimmida)]$^{2+}$[(26pdc)]$^{2-}$**·resorc·H_2O·CH_3OH (Figure 2.5a) had the 1,3-dihydroxybenzene partner molecule and the solvent of crystallization methanol and water molecules (Fig 2.5a). One of the oxygen atoms (O4) and the nitrogen atom (N4) of one dicarboxylate were hydrogen bonded to two N-H bonds of the NH_2^+. Another carboxylate of the same **26pdc** formed hydrogen bonds with another N-H bond of a neighboring dication. Such assembling provided robust hydrogen bonded $R_4^4(12)$ synthons[31] (Fig 2.5b). Literature suggest that such synthons are useful in generating extended assemblies and contribute to molecular recognition.[32] The synthons were connected to the N^+-H bond of the imidazolium cationic part. One oxygen atom from each of the other carboxylates groups of two independent 35**pdc** ions acted as bridging atoms to two N^+-H of two independent di-cations. Thereby, $R_4^4(8)$ synthons comprising of N^+-H···O bonds were formed (Figure 2.5b). These synthons had knitted the anions with the di-cations through charge-assisted hydrogen bonds.[33] Such interactions have yielded a layer-like arrangements in the self-assembly of the ionic-cocrystal. The resorcinol molecules were hydrogen bonded to O3 oxygen atom of dicarboxylate by O6-H···O3 hydrogen bonds. The structure may thus be explained in a simplified manner as a domain expanded carboxylate catemer by the two aqua bridges. Earlier we reported that depending on the directional hydrogen bonds, the partner provided avenues to construct robust synthons with an expansion of domain.[34] In the present case, the water molecules had played the role in hydrogen bonding to provide the robust $R_4^4(12)$ synthons (Figure 2.5b), each of which holds the 1,3-dihydroxybenzene guests at two sides. In the self-assembly of the **2.3**, the spaces between the self-assembled layers of cations and anions were occupied the **resorc** molecules. The methanol molecules had also occupied the interstitial positions and were weakly associated by C-H···O hydrogen bonds. The crystal structure of 2[(H_2**anthraimmida)]$^+$[(35pdc)]$^{2-}$**·2(resorc) (**2.4)** is shown in Figure 2.5c had hydrogen bonded mono-cations in pairs. The cations were arranged in head to tail orientations with respect to each

TH-3622_196122001

other by hydrogen bonded bridges with two carboxylate anions. These provided robust hydrogen bonded $R_4^4(12)$ synthons (Fig 2.5d).

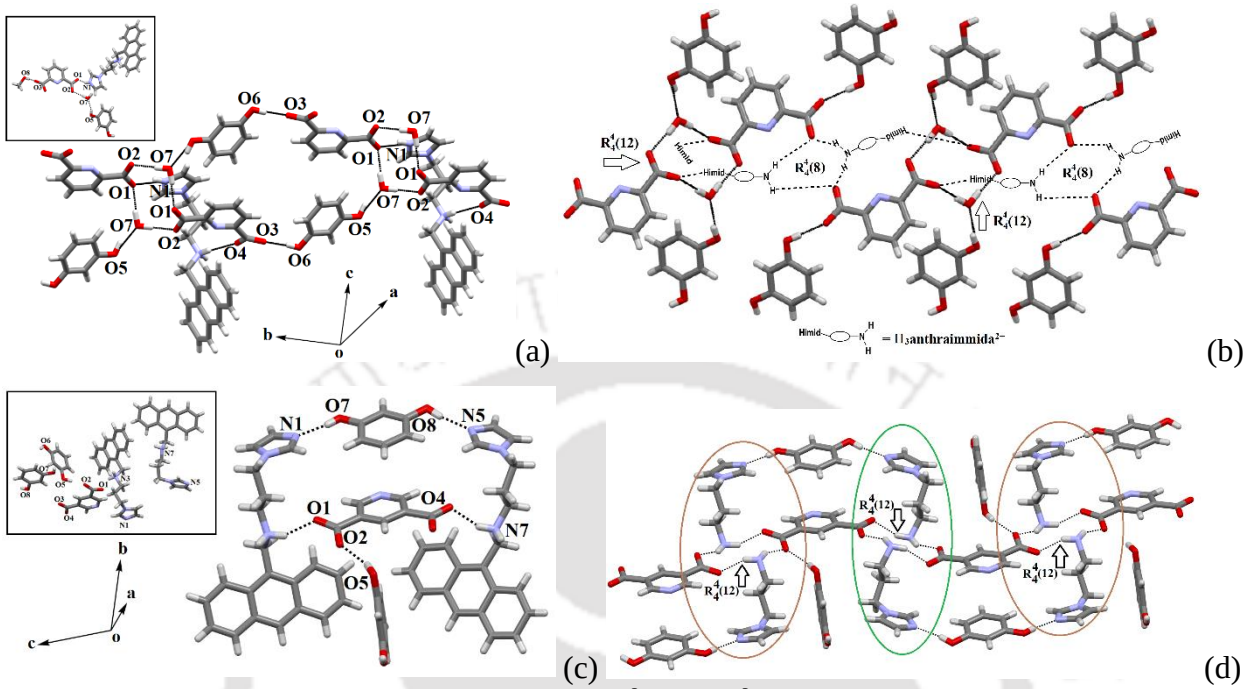

Figure 2.5: The self-assembly of the (a) [(H$_3$**anthraimmida)]$^{2+}$[(26pdc)]$^{2-}$**·resorc·H$_2$O·CH$_3$OH (**2.3**), (b) The aqua-bridged hydrogen bonded carboxylates dimers held together by di-cations in self-assembly of **2.3**, (c) The self-assembly of the 2[(H$_2$**anthraimmida)]$^{+}$[(35pdc)]$^{2-}$**·2(resorc) (**2.4**), and (d) Two distinguishable environments of the cations of **2.4** drawn by omitting the anthracene unit. {Inset in the (a) and (c) are the respective crystals structure}.

A set of **resorc** molecules connected the two such dimers to form cleft-like arrangements. Another set of **resorc** molecules were encapsulated in such a cleft. Thus, one of the **resorc** guests interacted with the dimers to form a secondary host to accommodate the guest, namely another **resorc** molecule. There are examples of assembling of a host with guest to accommodate additional guest molecules.[35-36] The cocrystal **2.4** is an example, where the association of a guest molecule (**resorc**) with the host cations serves as secondary host system to encapsulate an additional guest **resorc** molecule. While the guest resorcinol was present at the alternative positions between the dimeric units, there were two types of surrounding supramolecular environment for the cations as shown in Figure 2.5d. The crystal structures of **2.5**, **2.6** and **2.7** are shown in the Figure 2.6a, 2.6d and 2.6f respectively. These three molecules have hydrogen bonded dication H$_2$**chloroanthraimmida**. In the molecules **2.5** and **2.6**, 3,5-pyridinedicarboxylic acid was found as a zwitterionic anion together with the conventional mono-anionic form, while in the case of **2.7**, it was present in dianionic form.

TH-3622_196122001

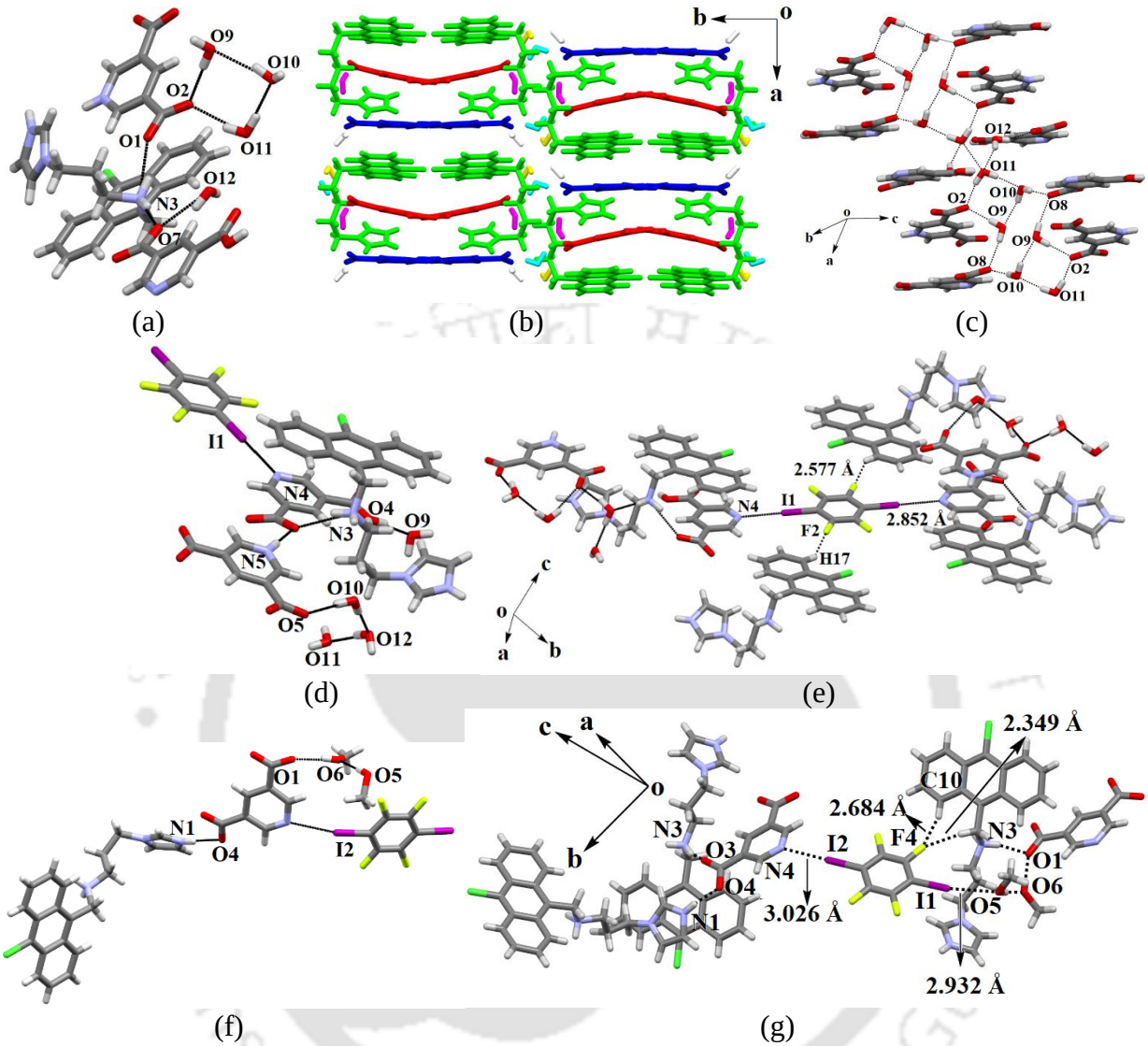

Figure 2.6: (a) Structure of [(H_2**chloroanthraimmida)]**$^{2+}$[2(H**35pdc)**$^{-}$]·4H_2O (**2.5**), (b) U-shaped di-cations in self-assembly of **2.5**, (c) channel of water molecules held by H**35pdc** anions in **2.5**, (d) asymmetric unit of [(H_2**chloroanthraimmida)**$^{2+}$][2(H**35pdc)**$^{-}$]·**(IFbenz)**·4H_2O (**2.6**), (e) halogen bonded **IFbenz** holding different layers of H**35pdc** bonded H_2**chloroanthraimmida**, (f) asymmetric unit of [(H_2**chloroanthraimmida)**$^{2+}$**(35pdc)**$^{2-}$]·**(IFbenz)**·2CH_3OH (**2.7**) and (g) Assembling pattern of **2.7** showing the interactions of **IFbenz**.

In the case of [(H_2**chloroanthraimmida)]**$^{2+}$[2(H**35pdc)**$^{-}$]·4H_2O **(2.5)**, the pyridine···carboxylic acid (N5···H6-O) hydrogen bonds governed the assembly and remained as pairs, while the zwitterionic **35pdc** formed pairs among them via hydrogen bond of $^{+}$N4-H with O4 of carboxylate of the other anion. These dimers were end-capped by hydrogen bonding with four water molecules at two ends. Moreover, the cations adopted U-shape and two such neighbouring cations were in

TH-3622_196122001

face to face arrangements (Figure 2.6b). The anions and water molecules played crucial role in stabilizing the assembly by forming a hydrogen bonded channels (Figure 2.6c).

Introduction of **IFbenz**, as guest to **2.5** provided ionic-cocrystal [(H_2**chloroanthraimmida**)$^{2+}$][2(H**35pdc**)$^-$]·(**IFbenz**)·4H_2O (**2.6**), where the geometry of the dication was changed to Z-shape and the ionic-crystals **2.6** had conventional mono-anion as well as zwitterionic mono-anion of the pyridinedicarboxylic acid. Accordingly, it was a reorganized structure of **2.5**, which served as a template to bind a guest molecule of 1,4-diiodotetrafluorobenzene (Figure 2.6e). The self-assembly of the **2.6** had two pyridine-carboxylate anion, one was conventional and other was zwitterionic. The guest molecules bound by N···I interactions ($d_{N\ldots I}$ = 2.852 Å) via the nitrogen atoms of the pyridine part of the two independent pyridine carboxylate anions. The bond was approximately linear (< C-I···N = 178.9º). The guest **IFbenz** acted as bridging molecule between two layer-like arrangements of guest molecules. Nitrogen-iodine interactions have been widely employed in self-assembly processes, where the N···I distance were typically influenced by the geometry, and were found in the range between 2.2 and 3.1 Å.[52] In this assembly the two independent types of the anions were involved in formation of dimers between them by $^+$N5-H with O2.

The attempt to introduce another guest component (resorcinol) to ionic-cocrystal **2.6** had led to formation of the ionic-cocrystal [(H_2**chloroanthraimmida**)$^{2+}$(**35pdc**)$^{2-}$]·(**IFbenz**)·2CH_3OH (**2.7**). Resorcinol did not participate in the formation of cocrystal, but it guided to form a new ionic-cocrystal. The ionic-cocrystal had dianionic form of **35pdc**, H_2**chloroanthraimmida**, **IFbenz** and two methanol molecules. The methanol molecules participated in the C-I1···O5 interaction (< O5···I1-C = 170.43º, $d_{I\ldots O}$ = 2.932 Å)) at one side along with N···I interactions (< N4···I2-C = 168.75º, $d_{N\ldots I}$ = 3.026 Å) on the other side of the guest. The methanol molecules bonded to the guest were also further hydrogen bonded to another methanol molecule (<O5-H···O6 = 174.63º and $d_{O5\ldots O6}$ = 2.729 Å). As a comparison, in the case of the ionic-cocrystal **2.6** C-H···F interaction ($d_{C\ldots F}$ = 2.577 Å) was observed, while in the case of **2.7**, bifurcated C-H···F interaction was observed with the respective $d_{C\ldots F}$ distances 2.684 Å and 2.349 Å.

From the structural study, it was clear that the charge (extent of protonation) of the constituent cation of the salts of H**anthraimmida** depended on the partner molecules and the dicarboxylic acids used. This suggests that exceptions exist, ranging from conventional salts of an organic

TH-3622_196122001

carboxylic acid to various forms beyond the typical mono-cationic salts[17-18] There are limited examples of assemblies containing conjugate acid or base as guest in organic salts[37-39] and inorganic complexes.[40] Thus, it was interesting to observe that any of the three forms of the pyridinedicarboxylic acids, namely, the neutral, mono-carboxylate or dicarboxylate could get incorporated in the salts either as partner molecule or anions. Having neutral pyridinedicarboxylic acid in ionic-cocrystal is a new observation and suggests that compositions of salt should have priority while dealing with salts of polycarboxylic acids with polytopic base. The pKa of H_2**26pdc** (pKa = 2.16) and that of H_2**35pdc** (pKa = 2.80) are comparable, whereas, the pKa of H**anthraimmida** in DMF and water are 5.9 and 4.1 respectively. From such a small difference of pKa, one would expect similar cocrystal from the two positional isomers of H_2**pdc,**[11-12] but it did not happen. So, it was not possible to make a prior prediction on the composition of the crystalline products observed in this study. A series of independent pH titration with the parent compound with aqueous hydrochloric acid and with the respective H_2**pdc** were carried out. The variation of the pH of the parent compound upon addition of the H_2**pdc** to the solution of H**anthraimmida** or it together with resorcinol, the pH change profiles in each case were similar (Figure A1). This clearly showed that formation of these salt and ionic-cocrystals were not primarily guided by the pKa. The transfers of protons took place to confer a stability by forming tight-packed structures. To support the result of the formation of ionic-cocrystals we conducted the pH titration of Hanthraimmida with different acids shown in Figure A1. It was not possible to forecast the observed compositions, hence one has to depend on the structural and spectroscopic studies to formulate each composition case by case. In general, densely packed cocrystals with stronger hydrogen bonds are more stable,[41] and the ordered π-stacks of aromatic rings in ionic-cocrystals contribute to tight packed structures.[42-43] However, in the present examples, the stacking among the anthracene rings were not observed. Thus, the interplay of hydrogen bonds with electrostatic interactions guided the tight-packed structures in the present case, resulted the partial or complete proton-transfer from the H_2**pdc** to realize the stable structures with varied compositions.

2.3. Powder X-ray diffraction study

In each case of the present examples, only one form of crystals were observed, thus, it was a necessity to find out the bulk purity of the samples after crystallization, to enable suggesting the

TH-3622_196122001

yield of the individual salt or ionic-cocrystals. Accordingly, the powder X-ray diffraction (PXRD) patterns of the crystals after decantation were powdered and the respective PXRD were recorded. As the illustrative example, powder X-ray diffraction of the salt **2.2** and ionic-cocrystal **2.3** is shown in the Figure 2.7 and diffraction pattern of other salts and ionic-cocrystals are in Figure A2. The Miller indices of the major peaks in each case were found to match with the Miller indices of the PXRD generated from the corresponding CIF files by using Mercury software. In certain cases, the exact matching was not there, this was attributed to defects in crystals and loss of some solvent molecules while grinding.

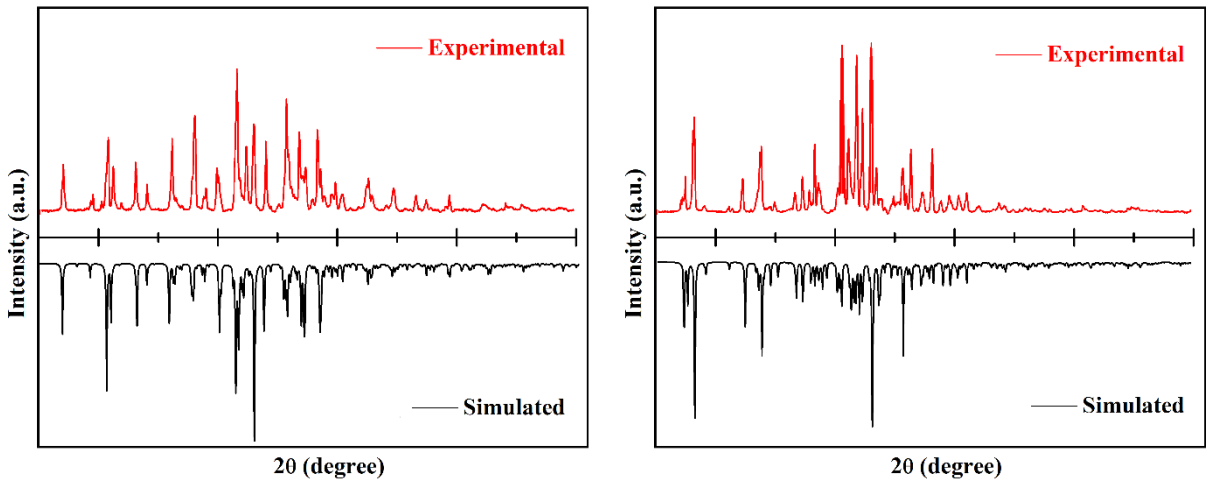

Figure 2.7: Powder X-ray diffraction patterns of the (a) **2.2** and (b) **2.3** (Red = Experimental, Black = Simulated). Simulated pattern generated from CIF file).

2.4. FTIR spectra

The IR spectra of H**anthraimmida** shows N-H stretching peak at 3229 cm^{-1} and a C=C stretching peak at 1505 cm^{-1} {a of Figure 2.8 (i)}. The salt **2.1** shows a broad O-H stretching peak at 3477 cm^{-1}, an aromatic C-H stretching peak at 3049 cm^{-1}, a C=O stretching peak at 1710 cm^{-1}, and a peak at 1563 cm^{-1} likely from aromatic ring vibrations {b of Figure 2.8 (i)}. In case of salt **2.2**, it features peaks at 3456 cm^{-1} (O-H or N-H stretching), 3049 cm^{-1} (aromatic C-H stretching), 1626 cm^{-1} (C=C or C=N stretching), and 1350 cm^{-1} (C-H bending or C-N stretching) {c of Figure 2.8 (i)}. The ionic-cocrystal **2.3** includes peaks at 3371 cm^{-1} (O-H or N-H stretching), 3049 cm^{-1} (aromatic C-H stretching), 1603 cm^{-1} (aromatic C=C or C=O stretching), and 1556 cm^{-1} (aromatic vibrations or N-H bending); and spectrum {d of Figure 2.8 (i)}. The stretching peaks of ionic-

TH-3622_196122001

cocrystal **2.4** presents peaks at 3418 cm^{-1} (O-H or N-H stretching), 3053 cm^{-1} (aromatic C-H stretching), and 1600 cm^{-1} (aromatic C=C or conjugated C=O stretching) {e of Figure 2.8 (i)}.

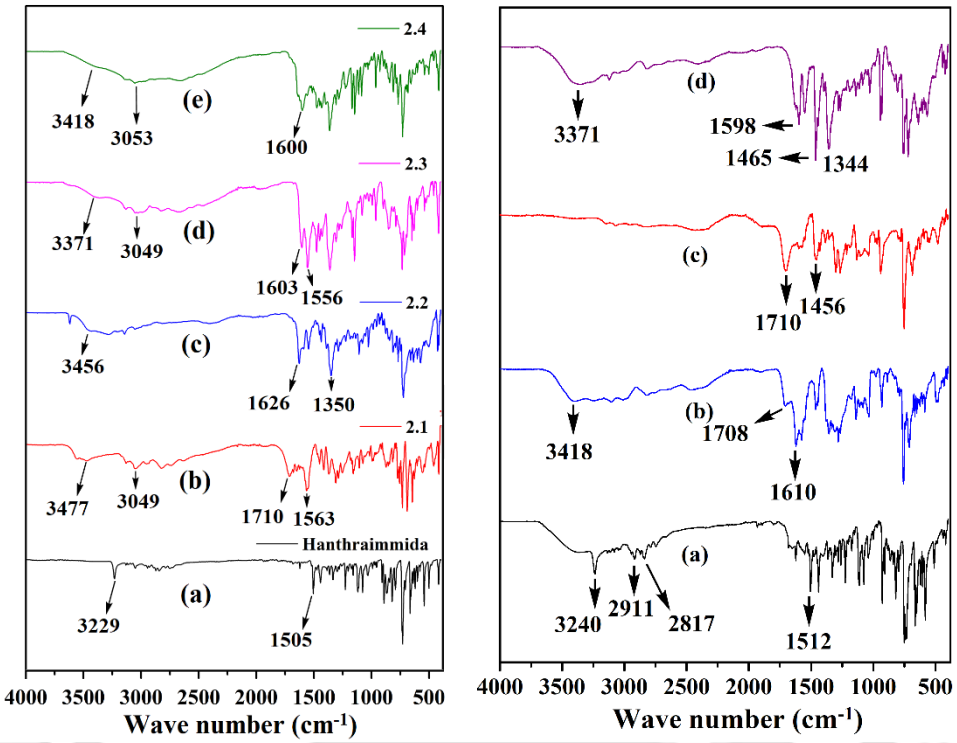

Figure 2.8: IR spectra of (i) (a) H**anthraimmida**, (b) **2.1**, (c) **2.2**, (d) **2.3** and (e) **2.4**; (ii) (a) **Chloroanthraimmida**, (b) **2.5**, (c) **2.6** and (d) **2.7**.

In case of **Chloroanthraimmida** {a of Figure 2.8 (ii)}, the stretching at 3240 cm^{-1} corresponds to N-H stretching The peaks at 2911 cm^{-1} and 2817 cm^{-1} represent C-H stretching vibrations from aliphatic hydrocarbons, while the peak at 1512 cm^{-1} likely corresponds to aromatic C=C stretching or N-H bending. Additionally, the peaks at 1200–1000 cm^{-1} could indicate C-O stretching or aromatic C-H bending. For the salt **2.5**, the peak at 3418 cm^{-1} indicates O-H stretching, likely broadened due to hydrogen bonding it shows the presence of water in the molecule and other peaks in the range of 3000-2900 cm^{-1} are attributed to aliphatic C-H stretching. The sharp peak at 1708 cm^{-1} represents C=O stretching, possibly from carboxylic acids, while the peak at 1610 cm^{-1} could correspond to aromatic C=C stretching or amide N-H bending {b of Figure 2.8 (ii)}. The ionic-cocrystal **2.6** shows weak peaks around 2800–3000 cm^{-1} correspond to C-H stretching vibrations and the peak at 1710 cm^{-1} suggests C=O stretching from a carbonyl group, and the peak at 1456 cm^{-1} is possibly associated with CH_2 bending {c of Figure 2.8 (ii)}. In the case of ionic-cocrystal **2.7**, the broad peak at 3371 cm^{-1} indicates O-H or N-H stretching vibrations. The peaks at 1598

TH-3622_196122001

cm^{-1} and 1465 cm^{-1} correspond to aromatic C=C stretching and CH_2 bending respectively {d of Figure 2.8 (ii)}.

2.5. NMR studies

The compounds **2.1-2.7** were soluble in dimethyl sulfoxide (DMSO), which provided us the scope to study them in the solution phase. The ^{1}H-NMR spectra of the complexes were recorded and compared with the spectra of the parent compounds; the integration of different sets of protons was used to confirm the compositions of the salt and cocrystals.

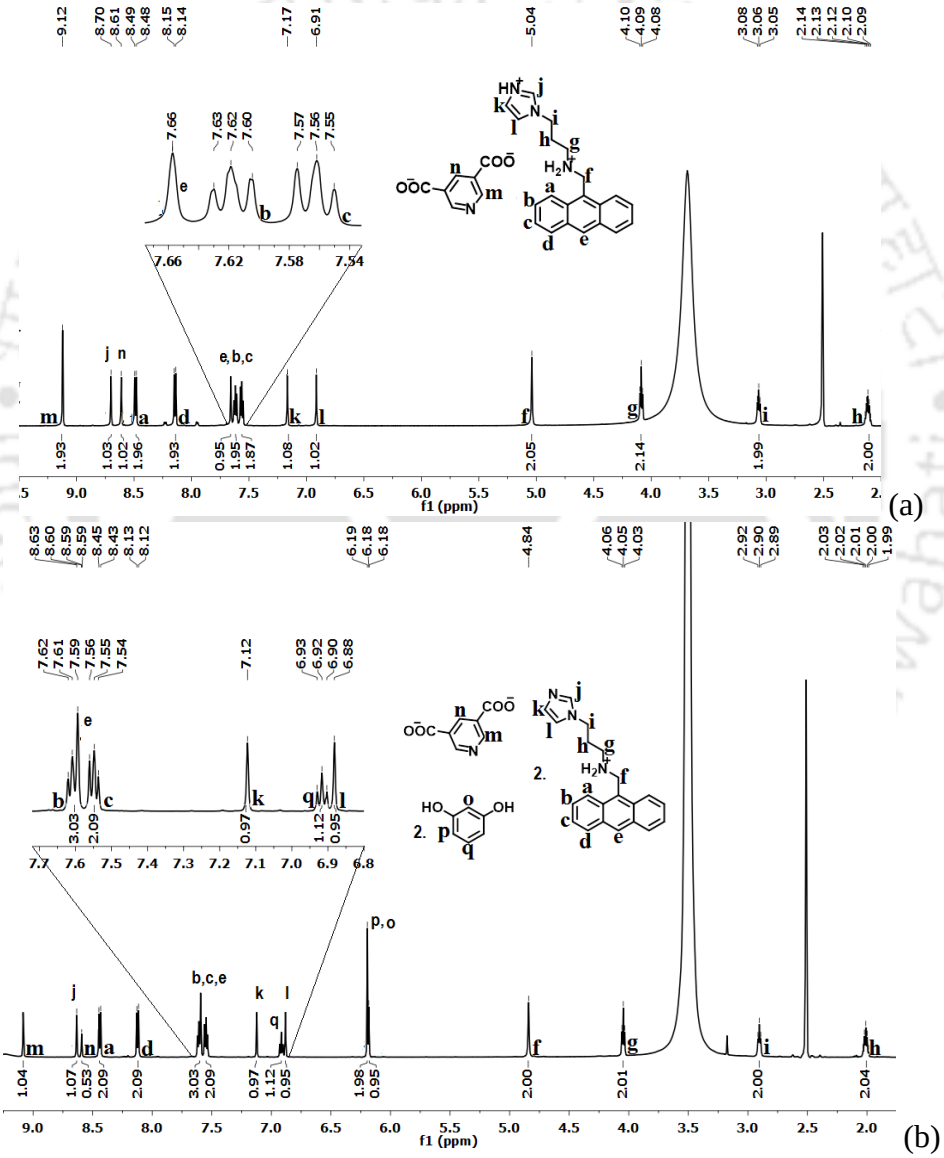

TH-3622_196122001

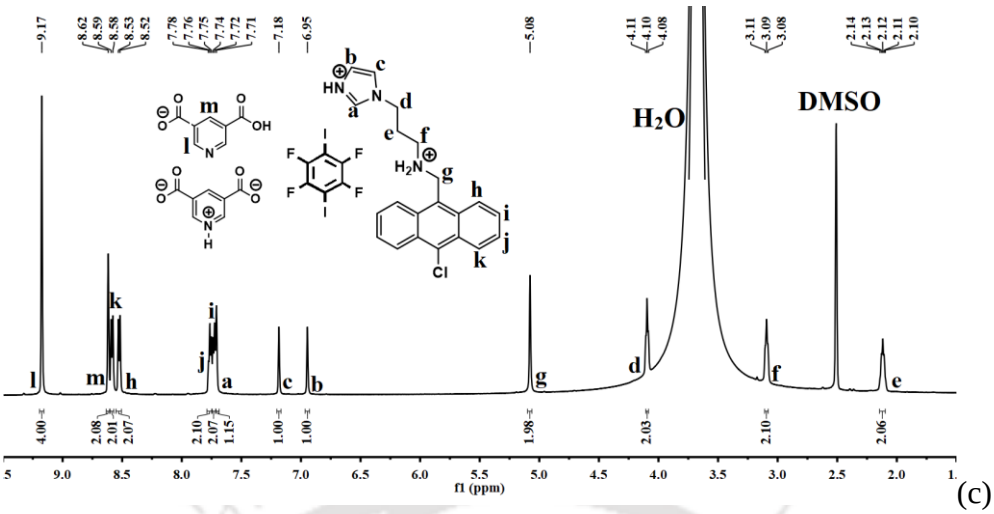

(c)

Figure 2.9: ^{1}H-NMR (600 MHz, DMSO-d_6) spectra of (a) **2.2**, (b) **2.4** and (c) **2.6**.

In the ^{1}H-NMR of salt **2.2**, the integration of peaks tallied to the exact numbers of protons in the salt. The aromatic protons of the salt are present in the range 9.12-6.91 ppm. The singlets at 9.12 ppm (two protons) and 8.61 ppm (one proton) corresponds to the protons of 3,5-pyridinedicarboxylic acid. The signals due to H_3**anthraimmida** cation are as follows; one singlet (one proton) at 8.70 ppm and two singlets at 7.17 ppm and 6.91 ppm. The propyl chain has shown the following characteristic signals, a singlet at 5.04 ppm (two protons), two triplets in the range of 4.10-4.08 ppm (two protons) and 3.08-3.05 and a quintet around 2.14-2.09 ppm (two protons).

The peaks for the protons on the anthracene ring were found at 8.48, 8.14, 7.66, 7.62 and 7.56 ppm (Figure 2.9a). In case of ionic-cocrystal **2.4**, all the other peaks are nearly same except three peaks at 6.92, 6.19 and 6.18 ppm due to protons of resorcinol (Figure 2.9b). In case of ionic crystal **2.6**, H_2**chloroanthraimmida** has almost same peaks as H_3**anthraimmida**. The singlets at 9.17 ppm (four protons) and 8.62 ppm (two protons) corresponds to the peaks due to 35pdc part of the ionic-cocrystal (Figure 2.9c). All the other ^{1}H-NMR spectra and ^{13}C-NMR of the compounds **2.1-2.4** are attached in the Appendix of this chapter (Figure A3-A9).

2.6. Thermogravimetric studies

The thermogravimetric study was carried out to ascertain the amount of solvent loss and the ease of their loss from the respective complexes. The thermograms were also used to compare the thermal stability of the complexes. Compound **2.1** consisted of a methanol molecule of crystallization, which was confirmed by the thermogravimetric analysis. A weight loss of 2.66 %

TH-3622_196122001

was observed, which corresponded to the loss of a methanol molecule (calculated 2.40 %) in the temperature range of 50ºC to 110ºC (Figure 2.10a). It was lost at a temperature close to the boiling point of methanol, that is, 64.7 °C. Further decomposition took place below 228ºC and 332ºC in two steps.

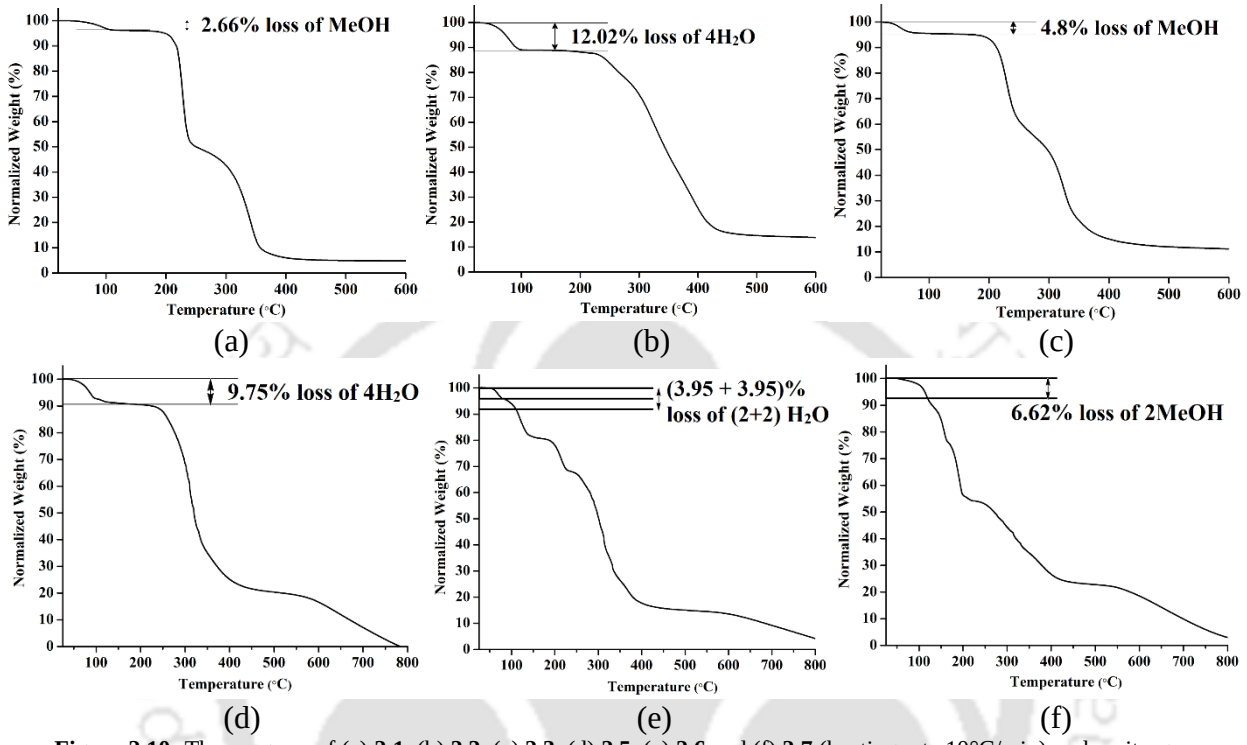

Figure 2.10: Thermogram of (a) **2.1**, (b) **2.2**, (c) **2.3**, (d) **2.5**, (e) **2.6** and (f) **2.7** (heating rate 10°C/min) under nitrogen atmosphere.

Salt **2.2** showed a weight loss of 12.02 % in the temperature range of 44 ºC to 105 ºC (Figure 2.10b). This weight loss corresponded to the loss of four water molecules (calculated 12.98 %). The decomposition of the salt started at 230ºC and lasted up to 436ºC. In **2.3**, a weight loss of 4.8% was observed between 25 ºC to 95 ºC temperature range (Figure 2.10c). This weight loss was equivalent to the loss of one methanol molecules (calculated 4.97 %). The ionic-cocrystal **2.3** took two steps for decomposition one below 228ºC and other around 320 ºC. For **2.5**, four water molecules of crystallization were lost in the temperature range of 50 ºC to 130ºC with a weight loss of 9.75% (calculated 9.52 %) shown in the Figure 2.10d. The decomposition temperature of the compound was 312ºC. In the case of **2.6**, a weight loss of 7.9 % was observed from 50 ºC to 110 ºC, which takes place in the set of two water molecules together that corresponds to the loss 3.95 % each (calculated 7.52 %) (Figure 2.10e). The decomposition of 2.6 takes place below 304ºC. The ionic-cocrystal **2.7** have shown the weight loss of 6.62 %, which corresponded to the

TH-3622_196122001

loss of two methanol molecules (calculated 6.51 %) in the temperature range of 40 ºC to 100 ºC (Figure 2.10f).

2.7. Photoluminescence properties

The detection of pyridinedicarboxylates by fluorescence spectroscopy has interest from biological points of view.[44-46] Varieties on the compositions of the salts discussed above had provided scope to study emission properties of them in solid as well as in solutions. Hence, fluorescence titrations of the H**anthraimmida** with the two positional isomers of H_2**pdc** (λ_{ex}, 365 nm) we carried out. Both titration profile had showed continuous increase in the emission of the conventional vibrational distinct π*-π transitions of H**anthraimmida** occurring at 418 nm, 441 nm and 471 nm (Figure 2.11a). Similarly, in the case of **Chloroanthraimmida** the transitions occur at 428 nm, 450 nm and 482 nm (Figure 2.11b).

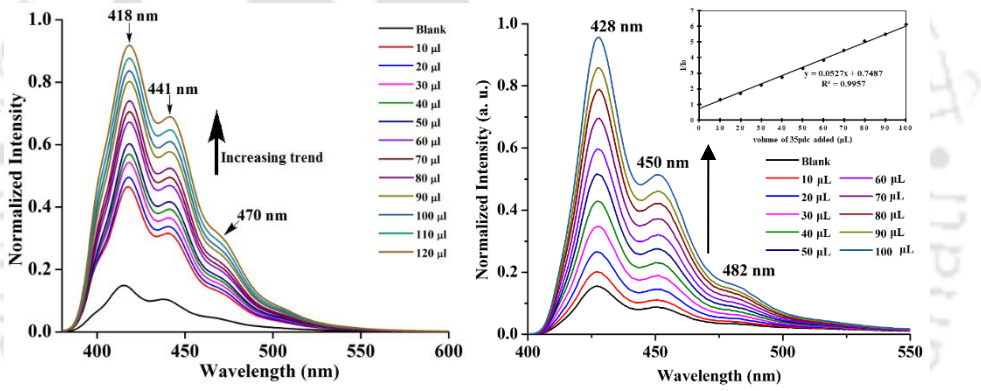

(a) (b)

Figure 2.11: Fluorescence titration (λ_{ex}, 365 nm) of H**anthraimmida** (10^{-5} M in ethanol, 2mL) with (a) H_2**26pdc** (10 µl aliquot of 10^{-5} M in ethanol), (b) Fluorescence titration (λ_{ex}, 300 nm) of **Chloroanthraimmida** (10^{-5} M in methanol, 2mL) with H_2**35pdc** (10 µl aliquot of 10^{-5} M in methanol).

The trends from both complemented the earlier observation caused by other aromatic carboxylic acids or phenolic compounds on the emission spectra of H**anthraimmida**.[14] The observed fluorescence enhancement upon interactions was due to protonation of the N-H group of H**anthraimmida** and **Chloroanthraimmida** by organic carboxylic acids, in these cases by the isomers of H_2**pdc**. This was due to a photo-induced electron transfer (PET) effect that was originally present in the H**anthraimmida**, PET was affected by the protonation. Since the emission changes caused by two positional isomers were identical in the respective emission spectroscopic titration, no selectivity between them was observed.

TH-3622_196122001

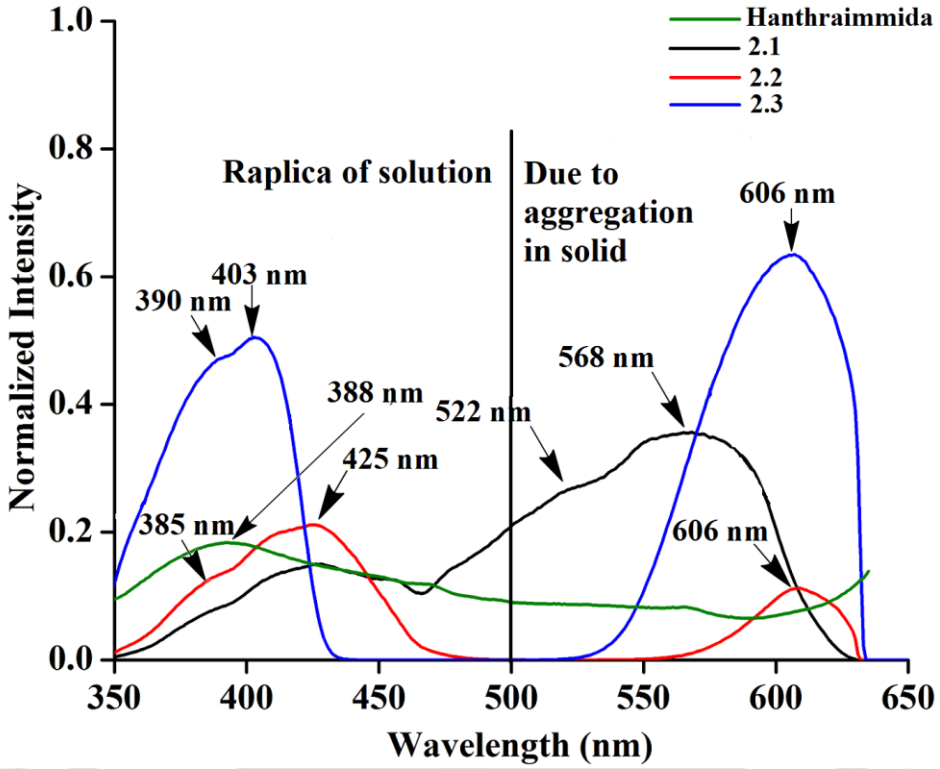

Figure 2.12: Photoluminescence spectra of solid samples of H**anthraimmida**, **2.1-2.3** (excitation at 325 nm).

The solid sample of the H**anthraimmida** had a broad emission at 388 nm (λ_{ex} = 325 nm), this broad emission was due to π* - π transition in accordance with the DFT calculated energy gap of HOMO-LUMO (357.41 nm). Whereas, the solid samples of **2.1-2.3** had shown completely different emission features, showed multiple emission peaks as illustrated in the Figure 2.12. The charge-assisted hydrogen bonds usually modulate π-stacking,[37] and influences photoluminescence properties in solid state, but none of the assemblies of **2.1-2.3** had π-stacking among the anthryl fluorophore. The UV visible spectra of the **2.1-2.3** in solution did not show shift of the peaks from the parent H**anthraimmida** (Fig A12); but the solid samples of the **2.2** and **2.3** clearly showed 32 nm shift of peaks (Figure A13) towards higher side with respect to the absorption peak of the H**anthraimmida**. This suggested a charge transfer in those two examples. In general, the effects of different weak interactions and proton-transfer are averaged out in solution and interactions of solvent molecules at excited and ground states play roles in emission spectroscopy.[47] In the solid state, the structures are rigid; hence, provide scopes to understand the properties from a fixed geometry. The HOMO-LUMO gaps calculated by the DFT have been in use to elucidate different mechanisms such as excited state proton transfer mechanism.[48-49]

TH-3622_196122001

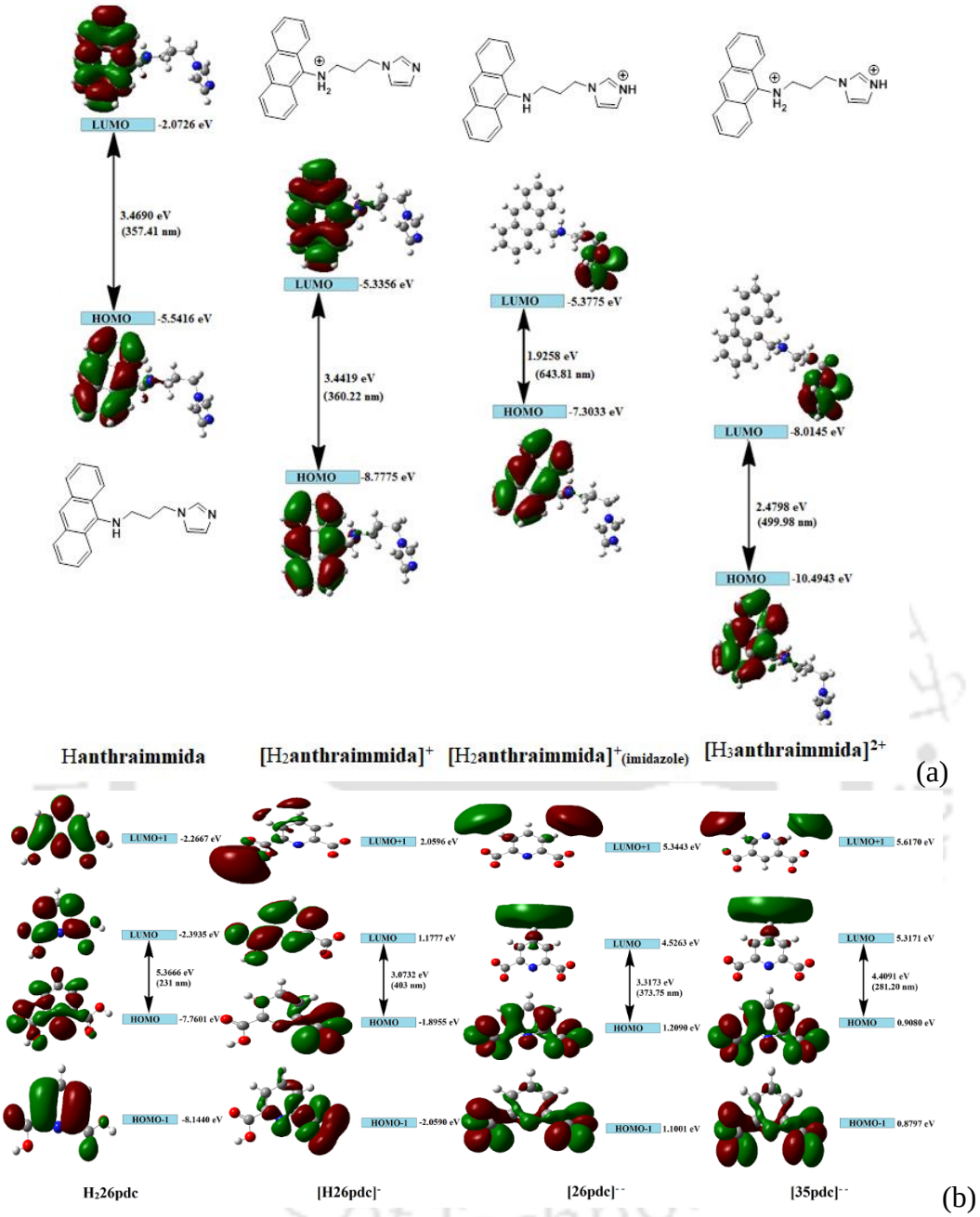

Figure 2.13: Energy details of HOMO and LUMO from DFT calculation with B3LYP functional using 6-311++G (d,p) as basis set of the different species (a) H**anthraimmida**, [H_2**anthraimmida**]$^+$, [H_2**anthraimmida**]$^+$**(imidazole)**, [H_3**anthraimmida**]$^{2+}$ cations, (b) HOMO-1, HOMO, LUMO and LUMO + 1 energy states of the H_2**26pdc,** H**26pdc**$^-$**, 26pdc**$^{2-}$**, 35pdc**$^{2-}$.

So, we examined the molecular orbitals of the cations (Fig 2.13a) and anions (Figure 2.13b) by DFT calculation with B3LYP functional using 6-311++G (d,p) as basis set. There can be two forms of the protonated states of the monocation, namely the anthryl-ammonium form represented as H_2**anthraimmida**$^+$ had a HOMO - LUMO gap 360.22 nm (Figure 2.13a).

TH-3622_196122001

Whereas, the other form having imidazolium cation [H_2**anthraimmida**]$^+$**(imidazole)** had such energy gap of 643.81 nm and the HOMO - LUMO+1 gap of 422.28 nm (Figure 2.13a). Accordingly, the two forms of the mono-cations had large difference in their respective π* to π transition. The H**anthraimmida** and H_2**anthraimmida**$^+$ had orbitals in the HOMO and LUMO were localized at the anthryl group. Hence, in these cases the excitation HOMO to LUMO were for π-π* transition. Whereas, in the form [H_2**anthraimmida**]$^+$**(imidazole)** and in H_3**anthraimmida**$^{2+}$ the respective HOMO was localized at anthryl group, whereas the LUMO was localized at imidazole unit (Figure 2.13a). Thus, the lowest π-π* emission in these species has to be from LUMO + 1 to HOMO. The dication H_3**anthraimmida**$^{2+}$ had the calculated HOMO-LUMO gap 499.98 nm, and the calculated HOMO and LUMO+1 was 365.4 nm. The calculated energy differences between the HOMO and LUMO of the H_2**26pdc,** H**26pdc**$^-$**, 26pdc**$^{2-}$, were 231 nm, 403 nm and 373 nm, respectively (Figure 2.13b). The same gap for **35pdc**$^{2-}$ was 281.20 nm. Thus, the calculated π* to π emission for H_3**anthraimmida**$^{2+}$ at 365.4 nm, was comparable to the one that of the **26pdc**$^{2-}$ (373 nm). The similar energy gaps of these two species of the salts, had suggested the possibility of Fröster resonance energy transfer,[50] and the excitation spectra showed in each case the excitation took place at 325 nm. Hence, by comparing the theoretical π* to π emissions, there was possibility to observe emission from either H_3**anthraimmida**$^{2+}$ or H_2**anthraimmida**$^+$ or **26pdc**$^{2-}$; but the observed emission in each case was at longer wavelengths having large Stoke's shift. The salt **2.1** had two H_3**anthraimmida**$^{2+}$ cations with independent crystallographic symmetry in unit cell, in the solid state it showed emissions at 522 nm and 568 nm. The degenerate HOMO and LUMO of the two symmetry independent di-cations split by mixing of orbitals, leading to emissions at 522 nm, 568 nm, whereas the peak at 385 nm and 425 nm were from π*-π transitions of the H_3**anthraimmida**$^{2+}$ and H**26pdc**$^-$ respectively. The broad unresolved emissions in 390-403 nm were observed for the **2.2** is assigned to the H_3**anthraimmida**$^{2+}$. The salt **2.3** had emission in the region of 385-425 nm from emission of the H_3**anthraimmida**$^{2+}$ and **26pdc**$^{2-}$. The salt and the cocrystal **2.2-2.3** had a common emission at 606 nm. This emission was attributed to the formation of mono-cation by excited state proton transfer from di-cation to **pdc** anion. The path E shown in the Figure 2.14a is one of the possible path. This suggestion is based on the fact that the different cations have small energy barrier and they easily could have transformed to one another by excited state proton transfer. On the other hand, the

TH-3622_196122001

ionic-cocrystal **2.4**, showed a weak emission at 385 nm, and two relatively sharper emissions at 454 nm and 515 nm. The 385 nm emission was from π*-π transition of H_2**anthraimmida**$^+$ and the latter two emissions were due to the mixing of orbitals of the two symmetry independent H_2**anthraimmida**$^+$ represented in Figure 2.14b. In present examples, we have dealt with multi-component cocrystals to observe photoluminescence as a collective effect from the aggregates. Hence, the consistent data on the dual emissions with larger slits are attributed to covering the domain (repeat units in the lattice as discussed in structural analysis) of the aggregate while doing the irradiations. The dual emissions in different materials may occur through different paths, and some of those are reported to violate the Kasha rule.[51] Our systems do violate the Kasha rule in showing the high wavelength emissions. The emission decay profile of **2.1** was tri-exponential and had life-times 0.65 ns, 5.25 ns and 13.70 ns, where second and third paths were followed by about 75 % species. But in the other three cases **2.2-2.4**, each had a short life-time path having life-time in the range of 2.06-3.47 ns, two relatively long life-time paths with 20.95-27.48 ns for one set and 45.25-120.90 ns for another (Figure A14-A17).

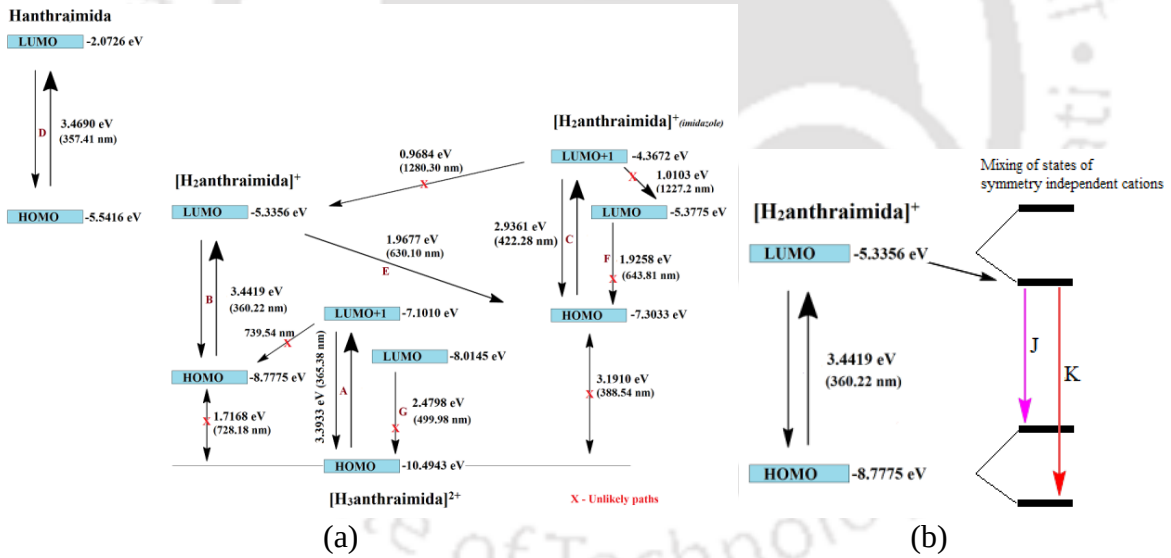

Figure 2.14: (a) Different emission paths in salts having H_3**anthraimmida**$^{2+}$ cation yielding mono-cation through excited state intermolecular proton transfer to anions (assuming the invariant role of the anions to accept proton at excited state). (b) The emission paths of symmetry non-equivalent H_2**anthraimmida**$^+$ cations due to splitting caused by mixing of orbitals.

The relatively longer life-times were followed by a major proportion of species (> 80 %) attributed to the intra-molecular excited state proton transfers. This was due to transfer of protons from dication to anion. As a result of such a transfer the mono-cation transform from one form to another

TH-3622_196122001

as in the path **E** in **2.1**-**2.3** and in the case of **2.4** the splitting of HOMO and LUMO took place. This caused the emissions in the visible region.

2.8. Conclusions

A combined structural and theoretical study on the observed photoluminescence of salts and ionic-cocrystals having different compositions and also having different cationic forms of the same fluorophore have shown emission at longer wavelengths. The salt **2.1** had provided an unusual example on combinations of neutral, and two different anionic forms. Here, the catemeric carboxylic acid-carboxylate had provided the template for the cations at symmetry independent positions. The symmetry non-equivalent cations in lattice in the selected examples were observed due to the different local non-covalent environments. There was a large difference in emission of H**anthraimmida** in the presence of **pdc** in solution than that of the corresponding salt in the solid state. The DFT calculated energy gaps of different forms of ions could explain the emission observed at short wavelength. The multiple fluorescence emissions in the visible-region of the salts in the solid state were attributed to the mixing of degenerate energy-levels of the symmetry independent ions. The two ionic-cocrystal **2.6** and **2.7** originating from same three components had not only distinctions in solvation but also has the following other distinctions (a) **2.6** has two mono-anions, instead **2.7** has a dianion, (b) solvent of crystallization was changed from water to methanol, (c) the guest molecule **IFbenz** in **2.6** was held by two I···N interactions, whereas in the **2.7**, it was held by an I···N and an I···O interactions.

2.9. Experimental Section

The detailed synthetic methodologies for the synthesis of the salt and metal complexes are described. Analytical data are provided with each compound. The instrumental details, crystallographic parameters, and method used are provided in Appendix section at the end of this chapter. The following abbreviations are used for identification of spin multiplicities in 1H-NMR spectra: s = singlet, d = doublet, t = triplet, q = quartet, p = pentet/quintet, m = multiplet; and for FTIR spectra, following abbreviations were used to identify the absorption bands: s = strong, w = weak, br = broad, m = medium.

TH-3622_196122001

2[(H$_3$anthraimmida)]$^{2+}$[(26pdc)$^{2-}$·2(H26pdc)$^{-}$]·(H$_2$26pdc)·CH$_3$OH (2.1): To a well-stirred solution of H**anthraimmida** (63.2 mg, 0.20 mmol) in methanol (10 ml), 2,6-pyridinedicarboxylic acid (33.44 mg, 0.20 mmol) was added. The resulting reaction mixture was stirred for one hour at room temperature. The solution was filtered and kept undisturbed for evaporation. Isolated yield: 71 % ^{1}H-NMR (600 MHz, DMSO-d_6, ppm): 8.73 (s, 1H), 8.43 (d, *J* = 6 Hz, 2H), 8.15 (d, *J* = 6 Hz, 2H), 8.13 (s, 4H), 8.08 (t, *J* = 12 Hz, 2H), 7.73 (s, 1H), 7.64 (t, *J* = 6 Hz, 2H), 7.58 (t, *J* = 6 Hz, 2H), 7.18 (s, 1H), 6.95 (s, 1H), 5.15 (s, 2H), 4.10 (t, *J* = 6 Hz, 2H), 3.20-3.17 (m, 5H), 2.15 (p, *J* = 6 Hz, 2H). ^{13}C NMR (125 MHz, DMSO-d$_6$, ppm): 171.1, 151.4, 150.2, 142.3, 142.2, 136.1, 135.8, 134.9, 134.3, 132.6, 132.3, 132.0, 130.8, 129.6, 124.9, 50.65, 48.9, 47.9, 32.5. IR (Neat, cm^{-1}): 3480 (m), 3049 (m), 2828 (m), 1710 (m), 1563 (m), 1450 (w), 1414 (w), 1369 (w), 1309 (w), 1158 (w), 1105 (w), 1074 (w), 993 (w), 873 (w), 815 (w), 756 (m), 731 (s), 690 (s), 645 (s), 558 (w), 460 (w), 415 (m). Melting point 216.2 ºC

(H$_3$**anthraimmida)$^{2+}$(35pdc)$^{2-}$·4H$_2$O (2.2):** Salt **2.2** was prepared by following the procedure similar to **2.1**, but 3,5-pyridinedicarboxylic acid (33.44 mg, 0.20 mmol) was used in place of 2,6-pyridinedicarboxylic acid. Isolated yield: 73 % ^{1}H NMR (600 MHz, DMSO-d_6, ppm) : 9.12 (s, 2H), 8.70 (s, 1H), 8.61 (s, 1H), 8.49 (d, *J* = 6 Hz, 2H), 8.15 (d, *J* = 6 Hz, 2H), 7.66 (s, 1H), 7.62 (t, *J* = 6 Hz, 2H), 7.56 (t, *J* = 6 Hz, 2H), 7.17 (s, 1H), 6.91 (s, 1H), 5.04 (s, 2H), 4.09 (t, *J* = 6 Hz, 2H), 3.06 (t, *J* = 6 Hz, 2H), 2.12 (p, *J* = 6 Hz, 2H). ^{13}C NMR (125 MHz, DMSO-d$_6$, ppm): 166.9, 153.0, 137.6, 137.6, 135.1, 131.1, 130.9, 129.4, 129.0, 128.6, 127.3, 127.0, 125.8, 125.0, 119.9, 46.1, 44.1, 43.7, 29.0. IR (Neat, cm^{-1}): 3620 (w), 3280 (br, w), 3147 (w), 1626 (s), 1546 (m), 1350 (s), 1288 (w), 1107 (m), 1026 (m), 813 (m), 769 (m), 746 (w), 723 (s), 660 (w), 634 (m), 601 (m), 573 (m), 502 (w), 424 (m). Melting point 232.4 ºC.

[(H$_3$anthraimmida)]$^{2+}$[(26pdc)]$^{2-}$·resorc·CH$_3$OH·H$_2$O (2.3): To a well-stirred solution of H**anthraimmida** (63.2 mg, 0.20 mmol) and 2,6-pyridinedicarboxylic acid (33.44 mg, 0.20 mmol) in methanol (10 ml), 1,3-dihydroxybenzene (resorcinol) (22.02 mg, 0.20 mmol) was added. The resulting reaction mixture was stirred for one hour at room temperature and kept for crystallization of filteration. Isolated yield: 68 % ^{1}H NMR (600 MHz, DMSO-d_6, ppm): 8.67 (s, 1H), 8.44 (d, *J* = 6 Hz, 2H), 8.12 (d, *J* = 6 Hz, 2H), 8.08 (d, *J* = 6 Hz, 2H), 8.03 – 8.00 (m, 1H), 7.66 (s, 1H), 7.59-7.53 (m, 4H), 7.13 (s, 1H), 6.93 – 6.90 (m, 2H), 6.20 – 6.18 (m, 3H), 5.04 (s, 2H), 4.07 (t, *J* = 6

TH-3622_196122001

Hz, 2H), 3.07 (t, *J* = 6 Hz, 2H), 2.11 (p, *J* = 6 Hz, 2H). ^{13}C NMR (125 MHz, DMSO-d_6, ppm): 167.0, 158.9, 150.8, 138.9, 137.6, 131.3, 130.9, 130.2, 129.4, 129.3, 128.5, 127.1, 126.3, 125.8, 124.9, 119.8, 106.7, 102.9, 49.0, 45.7, 44.0, 43.4, 28.71. IR (Neat, cm^{-1}): 3049 (br,w), 1603 (m), 1556 (s), 1476 (m), 1449 (w), 1360 (s), 1167 (w), 1147 (m), 1080 (w), 993 (w), 962 (m), 852 (m), 733 (s), 713 (m), 648 (m), 631 (m), 601 (w), 539 (w), 459 (w), 417 (m). Melting point 181.5 ºC

2[(H_2**anthraimmida)]$^+$[(35pdc)]$^{2-}$·2resorc (2.4):** Ionic-cocrystal **2.4** was prepared by following the procedure similar to **2.3**, but 3,5-pyridinedicarboxylic acid (33.44 mg, 0.20 mmol) was used in place of 2,6-pyridinedicarboxylic acid. Isolated yield: 66 % ^{1}H NMR (600 MHz, DMSO-d_6, ppm) : 9.08 (s, 2H), 8.63 (s, 2H), 8.59 (t, *J* = 2.0 Hz, 1H), 8.45 (d, *J* = 12 Hz, 4H), 8.12 (d, *J* = 6 Hz, 4H), 7.62 – 7.59 (m, 6H), 7.56 – 7.54 (t, *J* = 6 Hz, 4H), 7.12 (s, 2H), 6.93-6.90 (m, 2H), 6.88 (s, 2H), 6.19-6.18 (m, 6H), 4.84 (s, 4H), 4.05 (t, *J* = 6 Hz, 4H), 2.90 (t, *J* = 6 Hz, 4H), 2.01 (p, *J* = 6 Hz, 4H). ^{13}C NMR (125 MHz, DMSO-d_6, ppm): 166.9, 158.9, 152.7, 137.6, 137.5, 131.5, 130.7, 130.2, 129.4, 128.7, 128.2, 126.8, 125.7, 125.0, 119.8, 106.7, 102.9, 46.5, 44.6, 44.3, 40.4, 30.1. IR (Neat, cm^{-1}): 3053 (br, w), 1600 (m), 1513 (w), 1474 (m), 1448 (w), 1432 (m), 1363 (s), 1307 (w), 1283 (w), 1225 (w), 1168 (m), 1146 (m), 1110 (m), 1085 (m), 1050 (w), 1030 (w), 962 (m), 926 (w), 895 (w), 842 (m), 811 (m), 785 (w), 768 (m), 730 (s), 691 (w), 683 (w), 656 (w), 629 (w), 601 (w), 539 (w), 502 (w), 458 (w), 415 (m). Melting point 143.1 ºC.

N-{(10-chloroanthracen-9-yl)methyl}-3-(1H-imidazol-1-yl)propan-1-amine (**Chloroanthraimmida or Clanth**): It was prepared by reductive amination of 10-chloro-9-anthraldehyde with 1-(3-aminopropyl)imidazole in the presence of $NaBH_4$ in methanol by following a procedure similar to the reported procedure with analogous compound.[14] (Isolated yield 62 %). ^{1}H-NMR (600 MHz, DMSO-d_6): 8.50 (d, J = 6Hz, 2H), 8.47 (d, J = 6Hz, 2H), 7.71 (t, J = 6Hz, 2H), 7.66 (t, J = 6Hz, 2H), 7.53 (s, 1H), 7.07 (s, 1H), 6.84 (s, 1H), 4.60 (s, 2H), 3.99 (t, J = 6Hz, 2H), 2.69 (t, J = 6Hz, 2H), 1.89 (p, J = 6Hz, 2H). ESI-MS: m/z [M + H]$^+$: 350.1414. IR (neat, cm^{-1}): 3236 (s), 2943 (m), 2838 (m), 1622 (w), 1551 (w), 1503 (s), 1439 (s), 1363 (m), 1328 (s), 1280 (m), 1259 (m), 1225 (s), 1172 (w), 1112 (s), 1075 (s), 1033 (s), 927 (s), 862 (w), 839 (w), 818 (s), 795 (m), 751 (s), 740 (s), 731 (s), 663 (s), 651 (s). ESI mass found (m/z): 350.1346 (calcd M$^+$ +H) found 350.1414. (Figure A10 and A11)

TH-3622_196122001

[(H_2**chloroanthraimmida)**$^{2+}$][2**(**H**35pdc)**$^{-}$]·4H_2O (**2.5):** Salt **2.5** was prepared by following the procedure similar to **2.1**, but **Chloroanthraimmida** (69.84 mg, 0.20 mmol) was used in place of H**anthraimmida**. Isolated yield: 68 %. ^{1}H NMR (600 MHz, DMSO-d_6): 9.15 (s, 2H), 8.61 (s, 1H), 8.56 (d, J = 6 Hz, 2H), 8.50 (d, J = 6 Hz, 2H), 7.75 (t, J = 6 Hz, 2H), 7.70 (t, J = 6 Hz, 2H), 7.64 (s, 1H), 7.15 (s, 1H), 6.91 (s, 1H), 4.93 (s, 2H), 4.10 (t, J = 6 Hz, 2H), 3.09 (t, J = 6 Hz, 2H), 2.12 (p, J = 6 Hz, 2H). IR (KBr, cm^{-1}): 3093 (w), 1708 (m), 1610 (s), 1578 (s), 1446 (m), 1362 (m), 1278 (m), 1137 (w), 1024 (m), 929 (m), 751 (s), 704 (m), 582 (m), 488 (m).

[(H_2**chloroanthraimmida)**$^{2+}$][2**(**H**35pdc)**$^{-}$]·**(IFbenz)**·4H_2O (**2.6):** Ionic-cocrystal **2.6** was prepared by following the procedure similar to **2.4**, but 1,4-diiodotetrafluorobenzene (**IFbenz**) (80.36 mg, 0.20 mmol) was used in place of resorcinol. Isolated yield: 63 %. ^{1}H NMR (600 MHz, DMSO-d_6): 9.17 (s, 4H), 8.62 (s, 2H), 8.58 (d, J = 6 Hz, 2H), 8.52 (d, J = 6 Hz, 2H), 7.76 (t, J = 6 Hz, 2H), 7.72 (t, J = 6 Hz, 2H), 7.71 (s, 1H), 7.18 (s, 1H), 6.95 (s, 1H), 5.08 (s, 2H), 4.07 (t, J = 6 Hz, 2H), 3.18 (s, 6H), 2.97 (t, J = 6 Hz, 2H), 2.06 (p, J = 6 Hz, 2H). IR (KBr, cm^{-1}): 3117 (w), 3062 (w), 1710 (s), 1578 (w), 1465 (m), 1371 (w), 1305 (m), 1249 (m), 1127 (w), 1043 (w), 939 (s), 751 (s), 680 (m), 582 (m), 479 (m).

[(H_2**chloroanthraimmida)**$^{2+}$**(35pdc)**$^{2-}$]·**(IFbenz)**·2CH_3OH (**2.7):**To the ionic-cocrystal **2.6** resorcinol (22.02 mg, 0.20 mmol) was added that resulted in the formation of **2.7**. Isolated yield: 53 %. ^{1}H NMR (600 MHz, DMSO-d_6): 9.15 (s, 2H), 8.61 (s, 1H), 8.56 (d, J = 6 Hz, 2H), 8.50 (d, J = 6 Hz, 2H), 7.75 (t, J = 6 Hz, 2H), 7.70 (t, J = 6 Hz, 2H), 7.64 (s, 1H), 7.15 (s, 1H), 6.91 (s, 1H), 4.93 (s, 2H), 4.10 (t, J = 6 Hz, 2H), 3.09 (t, J = 6 Hz, 2H), 2.12 (p, J = 6 Hz, 2H). IR (KBr, cm^{-1}): 3371 (br, w), 3108 (w), 2817 (w), 1598 (s), 1549 (s), 1465 (s), 1344 (s), 1259 (w), 1146 (w), 1024 (m), 933 (m), 751 (s), 714 (s), 639 (m), 555 (m), 423 (w).

2.10. References

1. D. J. Berry, J. W. Steed, Pharmaceutical cocrystals, salts and multicomponent systems; intermolecular interactions and property-based design, *Adv. Drug Delivery Rev.*, 2017, **117**, 3 – 24.
2. O. Shemchuk, D. Braga, F. Grepioni, R. Turner, Co-crystallization of antibacterials with inorganic salts: paving the way to activity enhancement, *RSC Adv.*, 2020, **10**, 2146.

TH-3622_196122001

3. O. Shemchuk, F. Grepioni, D. Braga, Co-crystallization of racemic amino acids with $ZnCl_2$: An investigation of chiral selectivity upon coordination to the metal centre, *CrystEngComm*, 2020, **22**, 5613 – 5619.
4. S. Mohamed, A. A. Alwan, T. Friscic, A. J. Morris, M. Arhangelskis, Towards the systematic crystallization of molecular ionic-cocrystals: insights from computed crystal form landscapes, *Faraday Discuss.*, 2018, **211**, 401 – 424.
5. Z. X. Ng, D. Tan, W. L. Teo, F. Leon, X. Shi, Y. Sim, Y. Li, R. Ganguly, Y. Zhao, S. Mohamed, F. García, Mechanosynthesis of higher-order cocrystals: tuning order, functionality and size in cocrystal design, *Angew. Chem. Int. Ed.*, 2021, **133**, 17622 – 17631.
6. A. F. Shunnar, B. Dhokale, D. P. Karothu, D. H. Bowskill, I. J. Sugden, H. H. Hernandez, P. Naumov, S. Mohame, Efficient screening for ternary molecular ionic-cocrystals using a complementary mechanosynthesis and computational structure prediction approach, *Chem. Eur. J.*, 2020, **26**, 4752 – 4765.
7. C. B. Aakeröy, N. C. Schultheiss, A. Rajbanshi, J. Desper, C. Moore, Moore, C., Supramolecular synthesis based on a combination of hydrogen and halogen bonds, *Cryst. Growth Des.*, 2009, **9**, 1, 432 – 441**.**
8. M. Karimi-Jafari, L. Padrela, G. M. Walker, D. M. Croker, Creating cocrystals: a review of pharmaceutical cocrystal preparation routes and applications, *Cryst. Growth Des.*, 2018, **18**, 10, 6370 – 6387.
9. G. R. Desiraju, The supramolecular synthon in crystal engineering in stimulating concepts in chemistry; F. Vögtle, J. F. Stoddart, M. Shibasaki, Eds.; Wiley-VCH: Weinheim, Germany, 2000, pp. 293 – 306.
10. P. Kavuru, D. Aboarayes, K. K. Arora, H. D. Clarke, A. Kennedy, L. Marshall, T. T. Ong, J. Perman, T. Pujari, L. Wojtas, M. J. Zaworotko, Hierarchy of supramolecular synthons: persistent hydrogen bonds between carboxylates and weakly acidic hydroxyl moieties in cocrystals of zwitterions, *Cryst. Growth Des.*, 2010, **10**, 3568 − 3584.
11. S. L. Childs, G. P. Stahly, A. Park, The salt-cocrystal continuum: the influence of crystal structure on ionization state, *Mol. Phramaceutics*, 2007, **4**, 323 – 338.
12. A. J. Cruz-Cabeza, Acid–base crystalline complexes and the pKa rule, *CrystEngComm*, 2012, **14**, 6362 – 6365.
13. N. A. Mir, R. Dubey, G. R. Desiraju, Strategy and methodology in the synthesis of multicomponent molecular solids: the quest for higher cocrystals, *Acc. Chem. Res.*, 2019, **52**, 2210 – 2220.
14. (a) M. P. Singh, A. Tarai, J. B. Baruah, Photo-physical properties of salts of a di-topic imidazole-tethered anthracene derivative in solid and solution, *CrystEngComm*, 2019, **21**, 4898 – 4909. (b) A. Pandith, A. Kumar, H. -S. Kim, 9-N-Alkylaminomethylanthracene probes for selective fluorescence sensing of pentafluorophenol, *RSC Adv.*, 2015, **5**, 81808 – 81816.
15. T. Beyer and S. L. Price, Dimer or Catemer? Low-Energy Crystal Packings for Small Carboxylic Acids, *J. Phys. Chem. B*, 2000, **104**, 2647-2655.
16. N. J. Hestan, F. C. Spano, Expanded theory of H- and J-molecular aggregates: the effects of vibronic coupling and intermolecular charge transfer. *Chem. Rev.*, 2018, **118**, 7069 – 7163**.**
17. K. M. Steed, J. W. Steed, Packing problems: high Z' crystal structures and their relationship to cocrystals, inclusion compounds, and polymorphism, *Chem. Rev.*, 2015, **115**, 2895 – 2933.
18. M. P. Singh, A. Tarai, J. B. Baruah, Neutral, zwitterion, ionic forms of 5-aminoisophthalic acid in cocrystals, salts and their optical properties, *ChemistrySelect*, 2019, **19**, 5427 – 5436.

TH-3622_196122001

19. D. Yan, A. Delori, G. O. Lloyd, T. Friscic, G. M. Day, W. Jones, J. Lu, M. Wei, D. G. Evans, X. Duan, A cocrystal strategy to tune the luminescent properties of stilbene-type organic solid-State materials, *Angew. Chem. Int. Ed.*, 2011, **50**, 12483 – 12486.
20. R. Gui, H. Jin, X. Bu, Y. Fu, Z. Wang, Recent advances in dual-emission ratiometric fluorescence probes for chemo/biosensing and bioimaging of biomarkers, *Coord. Chem. Rev.*, 2019, **383**, 82 – 103.
21. M. L. Cheney, N. Shan, E. R. Healey, M. Hanna, L. Wojtas, M. J. Zaworotko, V. Sava, S. J. Song and J. R. Sanchez-Ramos, Effects of crystal form on solubility and pharmacokinetics: a crystal engineering case study of lamotrigine, *Cryst. Growth Des.*, 2010, **10**, 394 – 405.
22. M. L. Cheney, D. R. Weyna, N. Shan, M. Hanna, L. Wojtas and M. J. Zaworotko, Supramolecular architectures of meloxicam carboxylic acid cocrystals, a crystal engineering case study, *Cryst. Growth Des.*, 2010, **10**, 4401 – 4413.
23. A. Delori and W. Jones, A hydrogen bonded cocrystal with an unusual interweaving between the adjacent triple-helices, *CrystEngComm*, 2011, **13**, 6315 – 6318.
24. Y. Yano, T. Ono, S. Hatanaka, D. T. Grykoc, Y. Hisaeda, Salt–cocrystal continuum for photo function modulation: stimuli-responsive fluorescence color-tuning of pyridine-modified intramolecular charge-transfer dyes and acid complexes. *J. Mater. Chem. C*, 2019, **7**, 8847 – 8854.
25. D. Kalita, R. Sarma, J. B. Baruah, Formation of symmetry non-equivalent molecules in urea and carbamate derivatives: role of anion, *CrystEngComm*, 2009, **11**, 803 – 810.
26. N. Barooah. A. Karmakar, J. B. Baruah, Solvent induced symmetry non-equivalence in crystal lattice of 7-carboxymethyl-1,3,6,8-tetraoxo-3,6,7,8-tetrahydro-1H-benzo[lmn][3,8] phenathrolin-2-yl) acetic acid, *CrystEngComm*, 2008, **10**, 151 – 154.
27. H. –J. Hao, D. Sun, F. –J. Liu, R. B. Huang, L. S. Zheng, Discrete octamer water cluster and 1D T5(2) water tape trapped in two luminescent Zn(II)/1,2-bis(imidazol-1′-yl)ethane/dicarboxylate hosts: from 2D (4,4) net to 3D 5-fold interpenetrated diamond network**,** *Cryst. Growth Des.*, 2011, **11,** 5475 – 5482.
28. N. Kumar, S. Khullar, S. K. Mandal, Encapsulation of a water octamer chain in a chiral 2D sheet like supramolecular coordination network composed of dinickel–dicarboxylate subunits, *ACS Omega*, 2018, **3,** 11062 – 11070.
29. N. Saraei, O. Hietsoi, C. S. Mullins, A. J. Gupta, B. C. Frye, M. S. Mashuta, R. M. Buchanan, C. A. Grapperhaus, Streams, cascades, and pools: various water cluster motifs in structurally similar Ni (II) complexes, *CrystEngComm*, 2018, **20**, 7071 – 7081.
30. A. Karmakar, R. J. Sarma, J. B. Baruah, Structural aspects and properties of salt and inclusion compounds of 8-hydroxyquinoline based amides, *CrystEngComm*, 2007, **9**, 379 − 389.
31. M. C. Etter, J. C. MacDonald, J. Bernstein, Graph-set analysis of hydrogen-bond patterns in organic crystals, *Acta Crystallogr.*, 1990, **B46**, 256 – 262.
32. A. P. Singh, M. P. Singh, J. B. Baruah, Changes in the proportions of an active pharmaceutical through cocrystals, *Drug Dev. Res.*, 2021, 1 – 10.
33. S. A. Dalrymple and G. K. H. Shimizu, Crystal Engineering of a Permanently Porous Network Sustained Exclusively by Charge-Assisted Hydrogen Bonds, *J. Am. Chem. Soc.*, 2007, **129**, 12114 – 2116.
34. (a) B. Lou, S. R. Perumalla, C. C. Sun, Significant expansion of the solid state landscape of salicylic acid based on charge-assisted hydrogen bonding interactions, *Cryst. Growth Des.*, 2015, **15**, 24 – 28. (b) A. Tarai, J. B. Baruah, Quaternary and senary sub-assemblies in cocrystals and

TH-3622_196122001

salts of quinoline-4-carbaldoxime with aromatic carboxylic acids, *CrystEngComm*, 2016, **18**, 9095 – 9102.
35. V. Chandrasekhar, P. Thilagar, A. Steiner, Guest-assisted self-assembly of organostannoxane nanotubules on a mica surface, *Cryst. Growth Des.*, 2011, **11**, 1446 – 1449.
36. D. Singh, J. B. Baruah, Solid state assemblies of cyclic imides tethered hydroxy benzoic acids with pyridine and quinoline : toward the formation of channels and cavities, *Cryst. Growth Des.*, 2012, **12**, 3169 − 3180.
37. L. Sun, K. Hu, S. Jin, Y. Lu, C. Xu, B. Liu, D. Wang, G. Xia, Single-crystal and molecular structures of five hydrogen-bonding supramolecular salts based on 4-aminobenzoic acid, 2-aminobenzoic acid and acidic components, *J. Mol. Struct.*, 2019, **1178,** 229 – 241.
38. G. Smith, D. E. Lynch, K. A. Byriel, C. H. L. Kennard, Molecular cocrystals of carboxylic acids. XX. the crystal structures of 3,5-dinitrosalicylic acid and its adducts with the isomeric monoaminobenzoic acids, *Aust. J. Chem.*, 1995, **48**, 1133 – 1149.
39. A. O. L. E. vora, C. E. S. Bernardes, M. F. M. Piedade, A. C. L. Conceic, da M. E. M., Piedade, Energetics of glycine cocrystal or salt formation with two regioisomers: fumaric acid and maleic acid, *Cryst. Growth Des.*, 2019, **19**, 5054 – 5064.
40. J. B. Baruah, Inorganic molecular-complexes: potential for growth of a new subject-area in self-assembly, *Topics in Current Chem.*, 2020, **378**, 30.
41. C. R. Taylor, G. M. Day, Evaluating the energetic driving force for cocrystal formation, *Cryst. Growth Des*., 2018, **18**, 892 − 904.
42. S. P. Yelgaonkar, D. Kiani, J. Baltrusaitis, L. R. MacGillivray, Superstructural diversity in salt-cocrystals: higher-order hydrogen-bonded assemblies formed using U-shaped di-cations and with assistance of π-π stacking, *Chem. Commun.*, 2020, **56**, 6708 – 6710.
43. J. Sendh, M. P. Singh, J. B. Baruah, 5-[(Pyren-9-ylmethyl)amino]isophthalic acid with nitrogen containing heterocylces: stacking, N-H···π interactions and photoluminescence, *CrystEngComm*, 2021, **23**, 6952 – 6966.
44. Y. Cui, R. Liu, F. Ye, S. Zhao, Single-excitation, dual-emission biomass quantum dots: preparation and application for ratiometric fluorescence imaging of coenzyme A in living cells, *Nanoscale*, 2019, **11**, 9270 – 9275.
45. M. L. Liu, B. B. Chen, J. H. He, C. M. Li, Y. F. Li, C. Z. Huang, Anthrax biomarker: An ultrasensitive fluorescent ratiometry of dipicolinic acid by using terbium(III)-modified carbon dots, *Talanta*, 2019, **191**, 443 – 448.
46. J. Yuan, X. Dong, B. Zhang, Q. Zhou, S. Lu, Q. Wang, Y. Liao, Y. Yang, H. Wang, Tunable dual emission of fluorescence-phosphorescence at room temperature based on pure organic supramolecular gels, *Dyes Pig.*, 2020, **181**, 108506.
47. A. Tarai, J. B. Baruah, A solution and solidstate study on the recognition of hydroxyaromatic aldoximes by nitrogen containing compounds, *Cryst. Growth Des.*, 2016, **16**, 126 – 135.
48. H. Dong, J. Zhao, H. Yang, Y. Zheng, The mechanism of ratiometric fluoride sensing and the ESIPT process for 2,6-dibenzothiazolylphenol and its derivative, *Org. Chem. Front.*, 2018, **5**, 1241–1247.
49. Y. Chen, Y. Yang, Y. Zhao, S. Liu, Y. Li, The effect of different environments on excited-state intramolecular proton transfer in 4′-methoxy-3-hydroxyflavone, *Org. Chem. Front.*, 2019, **6**, 218 – 225.
50. A. Kaur, P. Kaur, S. Ahuja, Forster resonance energy transfer (FRET) and applications thereof, *Anal. Methods*, 2020, **12**, 5532 – 5550.

TH-3622_196122001

51. S. K. Behera, S. Y. Park, J. Gierschner, Dual emission: classes, mechanisms, and conditions, *Angew. Chem. Int. Ed.* 2021, **60**, 22624 – 22638.
52. C. I. Yeo, Y. S. Tan, H. C. Kwong, V. S. Lee and E. R. T. Tiekink, I···N halogen bonding in 1 : 1 co-crystals formed between 1,4-diiodotetrafluorobenzene and the isomeric *n*-pyridinealdazines (*n* = 2, 3 and 4): assessment of supramolecular association and influence upon solid-state photoluminescence properties, *CrystEngComm*, 2022, **24**, 7579 – 7591.

TH-3622_196122001

Appendix: Chapter 2

Physical Measurements: Infrared spectra of the solid samples were recorded on a Perkin-Elmer Spectrum-Two FT-IR spectrophotometer in the region 4000-400 cm^{-1} using attenuated total reflectance method. Powder X-ray diffraction patterns were recorded using Bruker powder X-ray diffractometer D2 phaser. ^{1}H-NMR spectra of ligands were recorded on a BRUKER Ascend-600 MHz NMR spectrometer using TMS as internal standard. The ESI-mass spectrum of was recorded on an Agilent QTOF 6520 mass spectrometer. Perkin Elmer Lamda-750 spectrometer was used to record the solid state UV-visible spectra by diffuse reflectance. Fluorescence emissions were measured in a Horiba Jobin Yvon Fluoromax-4C spectrofluorometer or Horiba Jobin Yvon Fluoromax-4P spectrofluorometer by taking specified amount of solutions as described in each Figure captions given in the text or solid sample (20 mg- 30 mg) and exciting at required wavelength. Life-time decay profiles of the solid sample (finely ground) were measured on an Eddinburg Instrument, Model: FSP920. The samples for scanning electron micrographs were prepared by drop-cast method by placing a drop of the salt dissolved in DMSO and allowed to slowly evaporate. The FESEM were measured by a FESEM Gemini 300. The melting points were recorded on a Buchi melting point B-540 apparatus. The thermogravimetric analyses were done on PerkinElmer TGA 4000, at a heating rate 10 °C per minute under nitrogen gas flow.

Computational method: All theoretical calculations, including optimization, energy calculation, and HOMO-LUMO energy gaps, were performed by using the B3LYP[A.1], functional with 6-311++G (d,p)[A.2] as a basis set in Gaussian 09W software.[A.3] The structure was generated using the Gauss View program by swapping the positions of the labile protons in the CIF file. To create new assemblies from the CIF file, Gauss View was utilized to exclude the molecules that were not needed for generating the new assembly.

Crystallographic Study: The X-ray single crystal diffraction data for the salts were collected by Oxford SuperNova and Bruker D8 Quest diffractometers at room temperature. Data refinement and cell reductions were carried out by CrysAlisPro.118 SMART software. Data reduction and cell refinements were performed using SAINT and XPREP software. Structures were solved by

TH-3622_196122001

direct methods using SHELXS-14 and were refined by full-matrix least-squares on F^2 using SHELXL-14 and OLEX2. All non-hydrogen atoms were refined in anisotropic approximation against F^2 of all reflections. Hydrogen atoms were placed at their geometric positions by riding and refined in the isotropic approximation. The crystallographic parameters are listed in the Table A1 and A2.

Table A1: Crystallographic parameters of the salt and the ionic-cocrystals of H**anthraimmida** and **Chloroanthraimmida**.

Parameters	**2[(H_3anthraimmida)]$^{2+}$[(26pdc)$^{2-}$·2(H26pdc)$^{-}$]·($H_2$26pdc)·CH_3OH (2.1)**	**(H_3anthraimmida)$^{2+}$(35pdc)$^{2-}$·4H_2O (2.2)**	**[(H_3anthraimmida)]$^{2+}$[(26pdc)]$^{2-}$·resorc·CH_3OH. H_2O (2.3)**	**2[(H_3anthraimmida)]$^{+}$[(35pdc)]$^{2-}$·2resorc (2.4)**
Formula	$C_{71}H_{66}N_{10}O_{17}$	$C_{28}H_{34}N_4O_8$	$C_{35}H_{38}N_4O_8$	$C_{61}H_{59}N_7O_8$
CCDC	2099505	2099935	2099504	2099936
Mol.wt.	1331.33	554.59	642.69	1018.15
Crystal system	triclinic	triclinic	triclinic	triclinic
Space group	$P\bar{1}$	$P\bar{1}$	$P\bar{1}$	$P\bar{1}$
a(Å)	8.9684(14)	10.541(5)	10.662(8)	10.8880(9)
b(Å)	14.022(2)	10.714(5)	12.684(9)	12.0827(10)
c (Å)	26.653(4)	13.132(7)	14.241(11)	20.6944(19)
α (°)	101.059(5)	89.016(14)	110.387(13)	91.546(3)
β (°)	94.792(5)	70.669(13)	111.87(3)	92.109(3)
γ (°)	95.101(5)	81.670(14)	92.60(2)	107.956(3)
V (Å^3)	3259.2(9)	1384.0(12)	1641(2)	2586.0(4)
Density, g cm^{-3}	1.357	1.331	1.301	1.308
Abs. coeff., mm^{-1}	0.099	0.098	0.093	0.088
F (000)	1396	588	680	1076
Total no. of reflections	11550	4899	5778	9156
Reflections, I > 2σ(I)	7298	2414	3886	5940
Max. θ/°	25.048	25.049	25.048	25.050
Ranges (h, k, l)	$-10 \le h \le 10$	$-12 \le h \le 12$	$-12 \le h \le 12$	$-12 \le h \le 12$
	$-16 \le k \le 16$	$-12 \le k \le 12$	$-15 \le k \le 15$	$-14 \le k \le 14$
	$-31 \le l \le 31$	$-15 \le l \le 15$	$-16 \le l \le 16$	$-24 \le l \le 24$
Complete to 2θ (%)	100	99.8	99.6	100
Data/restraints/parameters	11550/4/905	4899/0/361	5778/4/436	9156/5/692
GooF (F^2)	1.258	1.050	1.044	1.034
R indices [I > 2σ(I)]	0.0659	0.1004	0.0742	0.0637
wR_2 [I > 2σ(I)]	0.1769	0.2063	0.2108	0.1606
R indices (all data)	0.1119	0.1917	0.1051	0.1030
wR_2 (all data)	0.2174	0.2439	0.2390	0.1849

TH-3622_196122001

Parameters	**Chloroanthraimmida or Clanth**	[(H_2**chloroanthraimmida**)$^{2+}$][2(H**35pdc**)$^-$]·4H_2O **(2.5)**	[(H_2**chloroanthraimmida**)$^{2+}$][2(H**35pdc**)$^-$]·(**IFbenz**)·4H_2O **(2.6)**	[(H_2**chloroanthraimmida**)$^{2+}$(**35pdc**)$^{2-}$]·(**IFbenz**)·2CH_3OH **(2.7)**
Formula	$C_{21}H_{20}ClN_3$	$C_{35}H_{38}N_5O_{12}Cl$	$C_{38}H_{38}N_5O_{12}ClF_2I$	$C_{36}H_{33}N_4O_6ClF_4I_2$
CCDC	2385089	2396359	2396360	2403207
Mol.wt.	349.85	756.15	957.08	982.91
Crystal system	triclinic	monoclinic	triclinic	Monoclinic
Space group	$P\bar{1}$	P $2_1/c$	$P\bar{1}$	P $2_1/n$
a(Å)	8.256(5)	11.0457(16)	8.8096(5)	13.111(6)
b(Å)	8.510(5)	31.235(4)	11.2696(6)	15.861(8)
c (Å)	13.138(8)	11.3942(17)	21.1324(12)	18.599(9)
α (°)	86.269(2)	90	85.724(2)	90
β (°)	72.619(2)	117.679(5)	81.896(2)	90.667(14)
γ (°)	85.562(2)	90	72.086(2)	90
V (Å^3)	877.5(9)	3481.3(9)	1975.30(19)	3867(3)
Density, g cm^{-3}	1.324	1.443	1.609	1.688
Abs. coeff., mm^{-1}	0.226	0.183	0.958	1.764
F (000)	368	1584	970	1936
Total no. of reflections	3301	6122	7768	8453
Reflections, I > 2σ(I)	2859	4999	6522	7028
Max. θ/°	25.681	24.999	26.018	25.242
Ranges (h, k, l)	$-10 \le h \le 10$	$-13 \le h \le 13$	$-10 \le h \le 10$	$-16 \le h \le 16$
	$-10 \le k \le 10$	$-37 \le k \le 37$	$-13 \le k \le 13$	$-20 \le k \le 20$
	$-16 \le l \le 16$	$-13 \le l \le 13$	$-26 \le l \le 26$	$-23 \le l \le 23$
Complete to 2θ (%)	99.3	99.9	99.8	99.6
Data/restraints/parameters	3301/0/230	6122/0/494	7768/0/545	8453/0/486
GooF (F^2)	0.935	1.098	1.122	1.038
R indices [I > 2σ(I)]	0.0666	0.0832	0.0408	0.0422
wR_2 [I > 2σ(I)]	0.1732	0.2077	0.0775	0.1053
R indices (all data)	0.0764	0.0957	0.0551	0.0543
wR_2 (all data)	0.1835	0.2147	0.0852	0.1187

TH-3622_196122001

Table A2: Hydrogen bond parameters of the salts and ionic-cocrystals.

Salts	D-H···A	d_{D-H} (Å)	$d_{H\cdots A}$ (Å)	$d_{D\cdots A}$ (Å)	∠D-H···A (º)
2.1	N(3) –H(3N')...O(13) [1-x,1-y,-z]	0.89	2.30	2.945(3)	130
	N(3) –H(3N')...N(10) [1-x,1-y,-z]	0.89	2.22	3.050(3)	155
	N(1) –H(1N)...N(5) [-1+x,y,z]	0.93(3)	2.22(3)	3.144(3)	176(3)
	N(8) –H(8N')...O(2) [x,y,z]	0.89	2.15	2.846(3)	135
	N(8) –H(8N')...N(4) [x,y,z]	0.89	2.23	3.018(3)	147
	N(3) –H(3N)...O(8) [x,y,z]	0.89	2.19	2.922(3)	139
	O(5) –H(5O)...O(1) [2-x,1-y,1-z]	0.82	1.69	2.472(4)	160
	N(6) –H(6N)...N(9) [1+x,y,z]	1.02(4)	2.02(4)	3.036(4)	176(4)
	N(8) –H(8N)...O(3) [x,y,z]	0.89	2.23	2.900(3)	132
	N(8) –H(8N)...O(9) [x,y,z]	0.89	2.48	3.151(3)	133
	O(10) –H(10O)...O(3) [x,y,z]	0.94(3)	1.53(3)	2.459(3)	169(4)
	O(14) –H(14O)...O(12) [1+x,y,z]	0.93(3)	1.58(3)	2.492(4)	163(4)
	O(15) –H(15O)...O(7) [1-x,1-y,-z]	0.94(3)	1.52(3)	2.449(3)	168(3)
	O(17) –H(17O)...O(11) [x,y,z]	0.82	2.07	2.808(5)	149
2.2	N(3) –H(3N')...O(3) [1-x,1-y,1-z]	0.89	2.01	2.803(6)	148
	N(1) –H(1N) ...O(1) [x,y,z]	0.86	1.79	2.650(7)	176
	O(5) –H(5O')...O(6) [x,y,z]	0.90	1.91	2.713(7)	147
	N(3) –H(3N)...O(4) [1+x,y,-1+z]	0.89	1.91	2.772(6)	162
	O(8) –H(8O')...O(7) [x,y,z]	0.85	2.01	2.783(12)	152
	O(7) –H(7O')...O(6) [x,y,z]	0.82	1.92	2.735(10)	169
	O(7) –H(7O)...O(8) [1-x,1-y,1-z]	0.99	1.96	2.903(11)	159
	O(8) –H(8O)...O(2) [1-x,1-y,1-z]	0.85	1.88	2.659(9)	152
2.3	N(3) –H(3N')...O(4) [1-x,-y,-z]	0.89	1.80	2.690(4)	176
	N(1) –H(1N)...O(1) [1-x,1-y,1-z]	0.86	1.79	2.612(5)	159
	O(7) –H(7O')...O(2) [x,y,z]	0.90(5)	1.75(5)	2.653(5)	173(5)
	N(3) –H(3N)...O(4) [x,y,z]	0.89	2.03	2.794(4)	143
	O(5) –H(5O)...O(7) [-x,1-y,1-z]	0.82	1.89	2.649(6)	153
	O(6) –H(6O)...O(3) [1-x,-y,1-z]	0.82	1.85	2.667(5)	173
	O(7) –H(7O)...O(1) [1-x,1-y,1-z]	0.93(4)	1.88(4)	2.805(5)	172(5)
	O(8) –H(8O)...O(3) [x,1+y,z]	0.82	2.17	2.904(9)	149
2.4	N(3) –H(3N')...O(2) [x,y,z]	0.89	1.90	2.729(3)	154
	N(7) –H(7N')...O(4) [1-x,1-y,-z]	0.89	1.88	2.694(3)	152
	N(3) –H(3N)...O(1) [1-x,1-y,1-z]	0.89	1.94	2.742(3)	148
	O(5) –H(5O)...O(2) [x,y,z]	1.03(6)	1.91(6)	2.769(4)	140(6)
	O(6) –H(6O)...N(4) [x,-1+y,z]	0.82	1.98	2.739(4)	154
	N(7) –H(7N)...O(3) [x,y,z]	0.89	1.89	2.698(4)	150
	O(7) –H(7O)...N(1) [1-x,-y,1-z]	0.82	1.92	2.734(4)	169
	O(8) –H(8O)...N(5) [1-x,-y,-z]	0.82	1.90	2.708(4)	169
2.5	N(1) –H(1)...O(5) [x,y,-1+z]	0.86	2.05	2.832(10)	150
	N(3) –H(3A)...O(7) [1-x,-y,1-z]	0.89	1.90	2.781(4)	168
	N(3) –H(3B)...O(1) [x,y,-1+z]	0.89	1.87	2.702(4)	156
	N(4) –H(4)...O(4) [x,1/2-y,1/2+z]	0.86	1.73	2.592(5)	178
	N(6) –H(6)...N(5) [x,1/2-y,1/2+z]	0.88(6)	1.70(6)	2.576(4)	173(6)
	O(9) –H(9A)...O(2) [x,y,z]	0.85	1.88	2.725(5)	171
	O(9) –H(9B)...O(8) [x,y,z]	0.85	2.09	2.929(7)	169
	O(10) –H(10A)...O(8) [x,y,z]	0.85	1.80	2.640(5)	170
	O(10) –H(10B)...O(9) [1-x,-y,1-z]	0.85	2.10	2.935(7)	166
	O(11) –H(11A)...O(10) [1-x,-y,1-z]	0.85	1.86	2.704(6)	173
	O(11) –H(11B)...O(2) [x,y,z]	0.85	1.92	2.750(6)	165
	O(12) –H(12A)...O(7) [x,y,z]	0.85	1.89	2.706(8)	159
	O(12) –H(12B)...O(11) [-1+x,y,z]	0.85	2.06	2.840(9	151

TH-3622_196122001

2.6	N(1) –H(1)...O(5) [-x,2-y,1-z]	0.86	2.03	2.868(4)	164
	N(3) –H(3A)...O(9) [-x,1-y,1-z]	0.89	2.06	2.933(4)	166
	N(3) –H(3B)...O(2) [x,y,z]	0.89	2.12	2.967(3)	159
	N(5) –H(5)...O(2) [x,y,z]	0.86	1.73	2.595(4)	179
	O(4) –H(4)...O(9) [1-x,1-y,1-z]	0.82	1.76	2.571(4)	171
	O(9) –H(9A)...O(10) [-x,1-y,1-z]	0.85	1.84	2.686(4)	175
	O(9) –H(9B)...O(8) [-x,-y,1-z]	0.85	1.77	2.604(3)	167
	O(10) –H(10A)...O(12) [1-x,1-y,1-z]	0.85	1.90	2.747(5)	175
	O(10) –H(10B)...O(5) [1-x,-y,1-z]	0.85	1.86	2.693(4)	167
	O(11) –H(11A)...O(6) [-x,1-y,1-z]	0.85	1.85	2.692(5)	172
	O(11) –H(11B)...O(6) [1+x,y,z]	0.85	1.94	2.727(5)	154
	O(12) –H(12A)...O(7) [x,y,z]	0.85	1.94	2.786(5)	172
	O(12) –H(12B)...O(11) [-1+x,y,z]	0.85	1.98	2.817(4)	166
2.7	N(1) –H(1N)...O(4) [3/2-x,-1/2+y,1/2-z]	0.80(5)	1.83(5)	2.626(4)	173(6)
	N(3) –H(3A)...O(1) [3/2-x,1/2+y,1/2-z]	0.89	1.86	2.705(4)	158
	N(3) –H(3B)...O(3) [x,y,z]	0.89	1.90	2.760(4)	161
	O(5) –H(5)...O(6) [x,y,z]	0.82	1.91	2.728(9)	175
	O(6) –H(6)...O(1) [1/2-x,1/2+y,1/2-z]	0.82	1.85	2.662(7)	170
	C(7) –H(7A)...F(4) [x,y,z]	0.97	2.35	3.307(5)	169

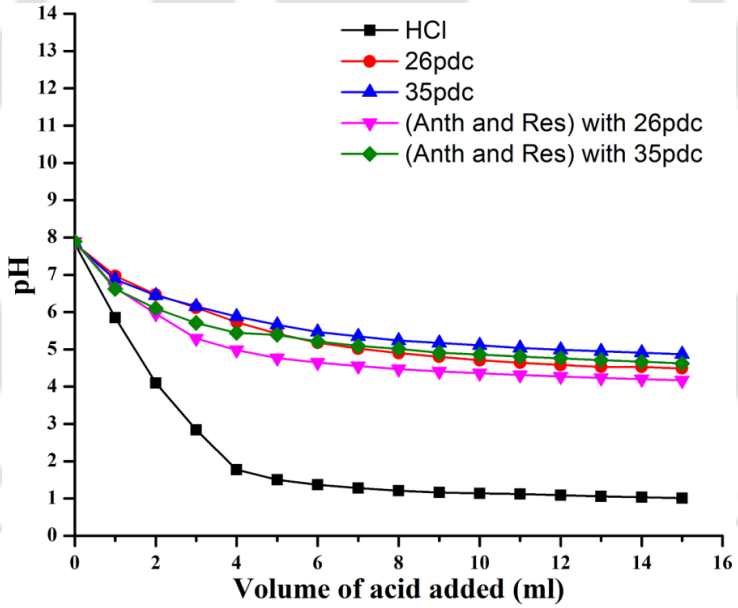

Figure A1: The pH titrations of H**anthraimmida** (4mL, 1mM in methanol) (i) with HCl (1 mM) (ii) with H_2**26pdc** (1mM in methanol) (iii) with H_2**35pdc;** (iv) and (v) are same titrations as (ii) and (iii) but each solution contained 1mM H**anthraimmida** with 1mM resorcinol.

TH-3622_196122001

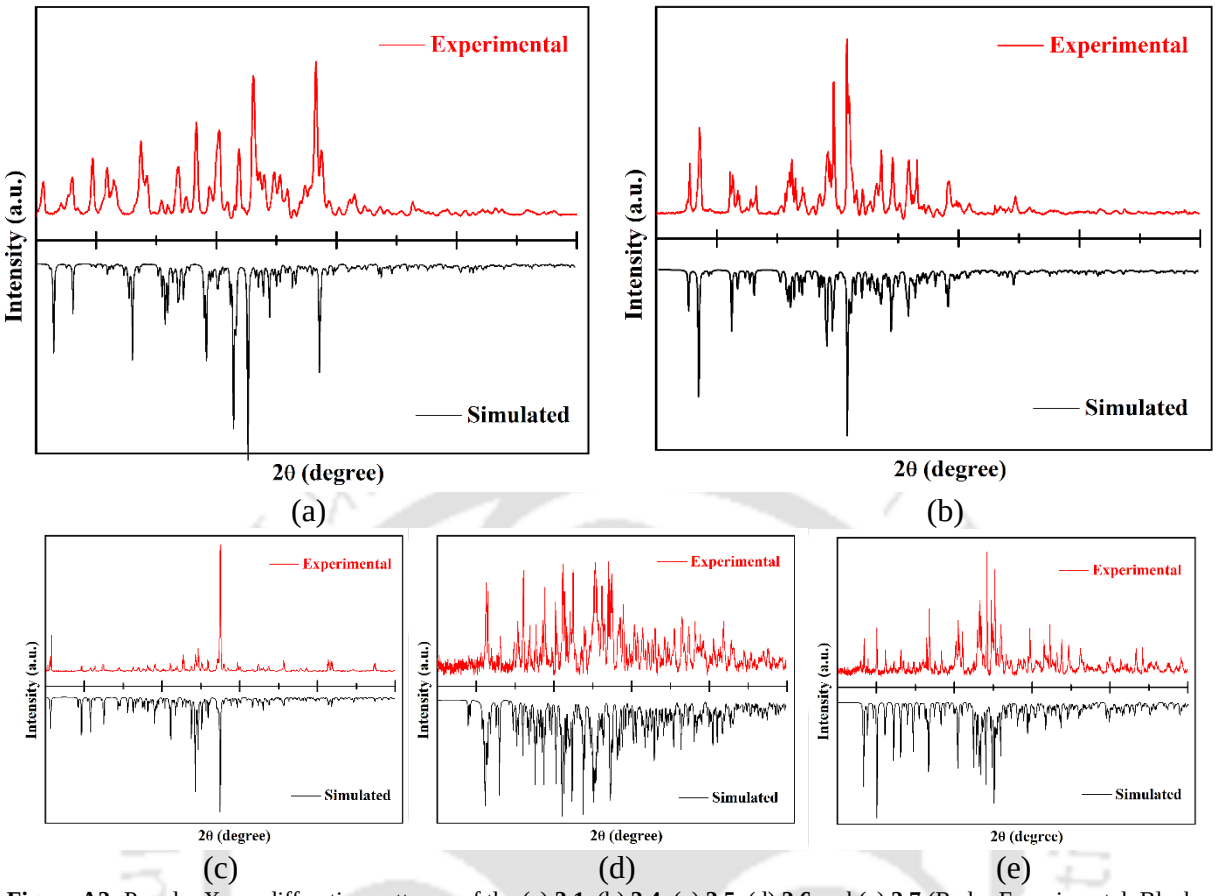

Figure A2: Powder X-ray diffraction patterns of the (a) **2.1**, (b) **2.4**, (c) **2.5**, (d) **2.6** and (e) **2.7** (Red = Experimental, Black = Simulated). Simulated pattern generated from CIF file).

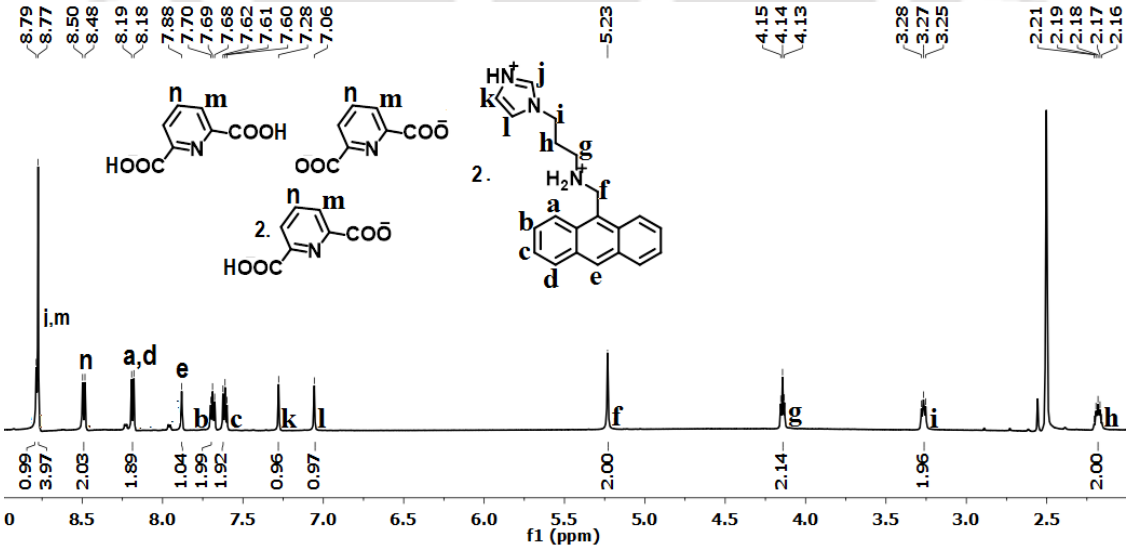

Figure A3: ^{1}H-NMR (600 MHz, DMSO-d$_6$) spectra of the **2[(H$_3$anthraimmida)]$^{2+}$[(26pdc)$^{2-}$·2(H26pdc)$^{-}$]·(H$_2$26pdc)·CH$_3$OH (2.1).**

TH-3622_196122001

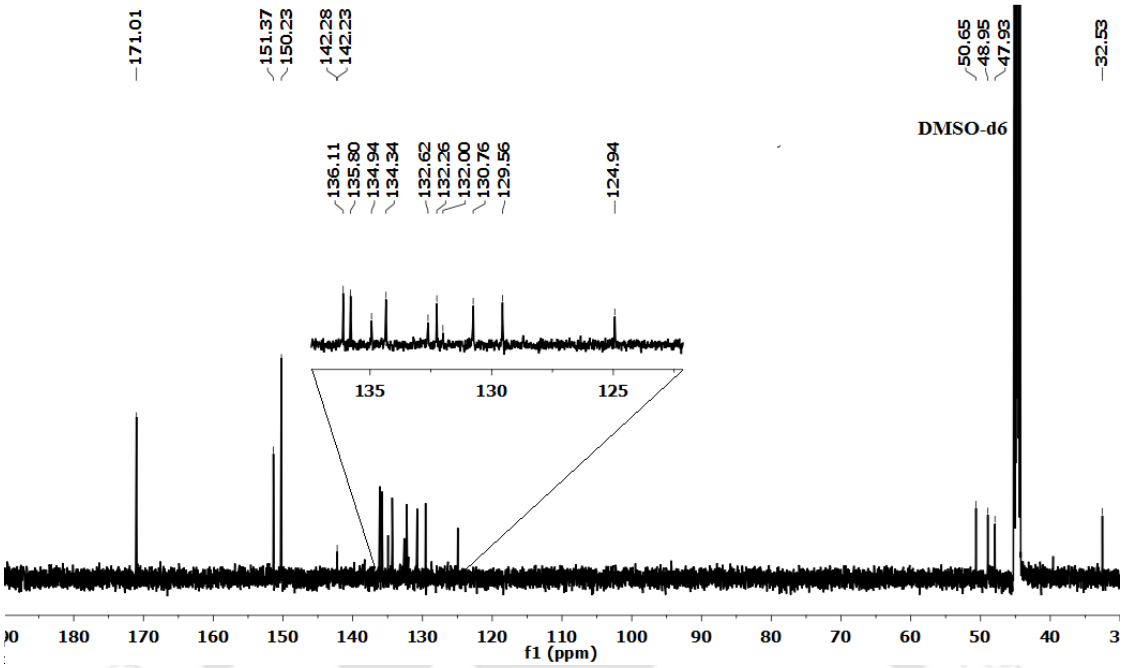

Figure A4: ^{13}C-NMR (125 MHz, DMSO-d$_6$) spectra of the **2[(H$_3$anthraimmida)]$^{2+}$[(26pdc)$^{2-}$·2(H26pdc)$^{-}$]·(H$_2$26pdc)·CH$_3$OH (2.1)**.

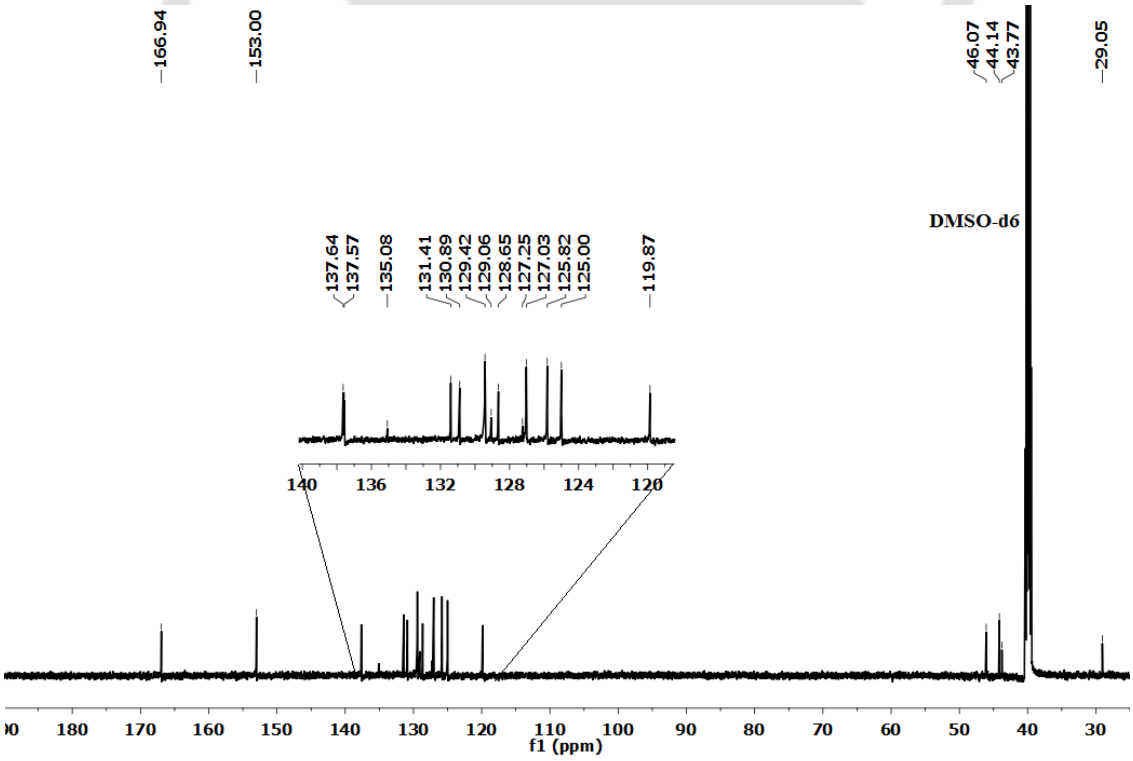

Figure A5: ^{13}C-NMR (125 MHz, DMSO-d$_6$) spectra of (**H$_3$anthraimmida)$^{2+}$(35pdc)$^{2-}$·4H$_2$O (2.2)**.

TH-3622_196122001

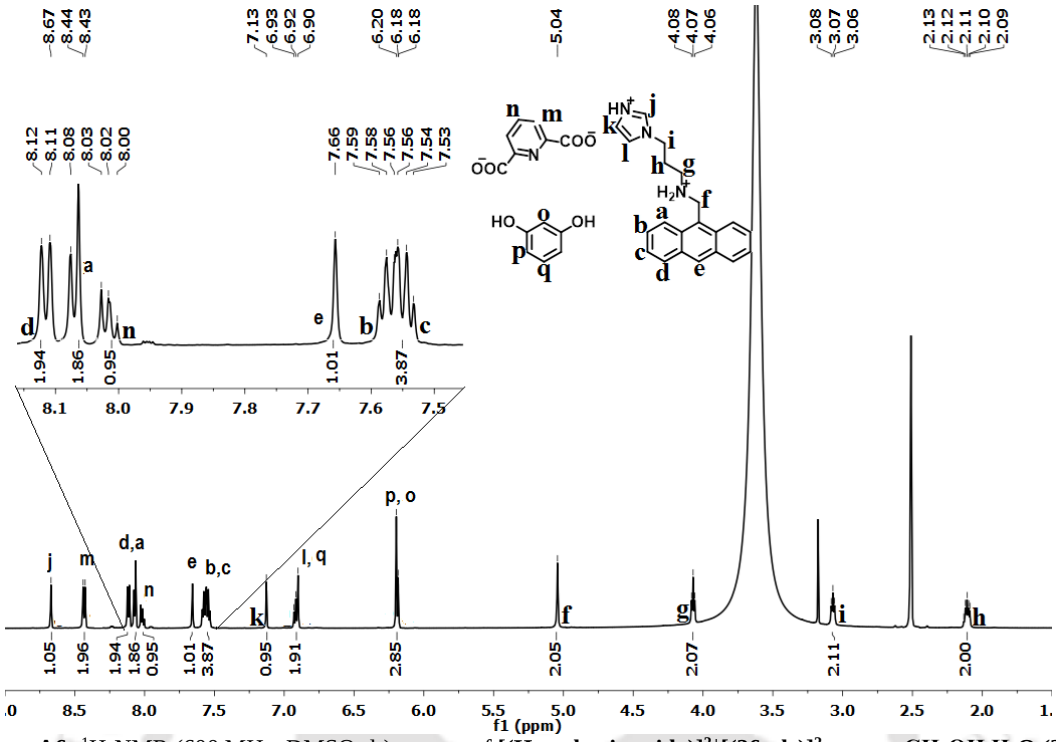

Figure A6: ^{1}H-NMR (600 MHz, DMSO-d$_6$) spectra of **[(H$_3$anthraimmida)]$^{2+}$[(26pdc)]$^{2-}$·resorc·CH$_3$OH·H$_2$O (2.3)**.

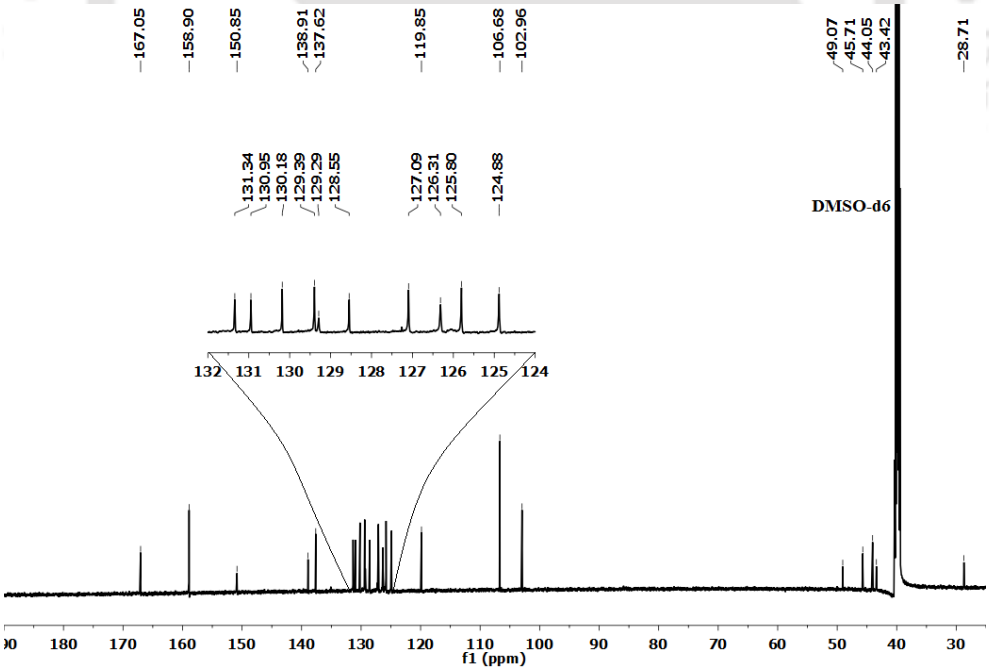

Figure A7: ^{13}C-NMR (125 MHz, DMSO-d$_6$) spectra of the **[(H$_3$anthraimmida)]$^{2+}$[(26pdc)]$^{2-}$·resorc·CH$_3$OH·H$_2$O (2.3)**.

TH-3622_196122001

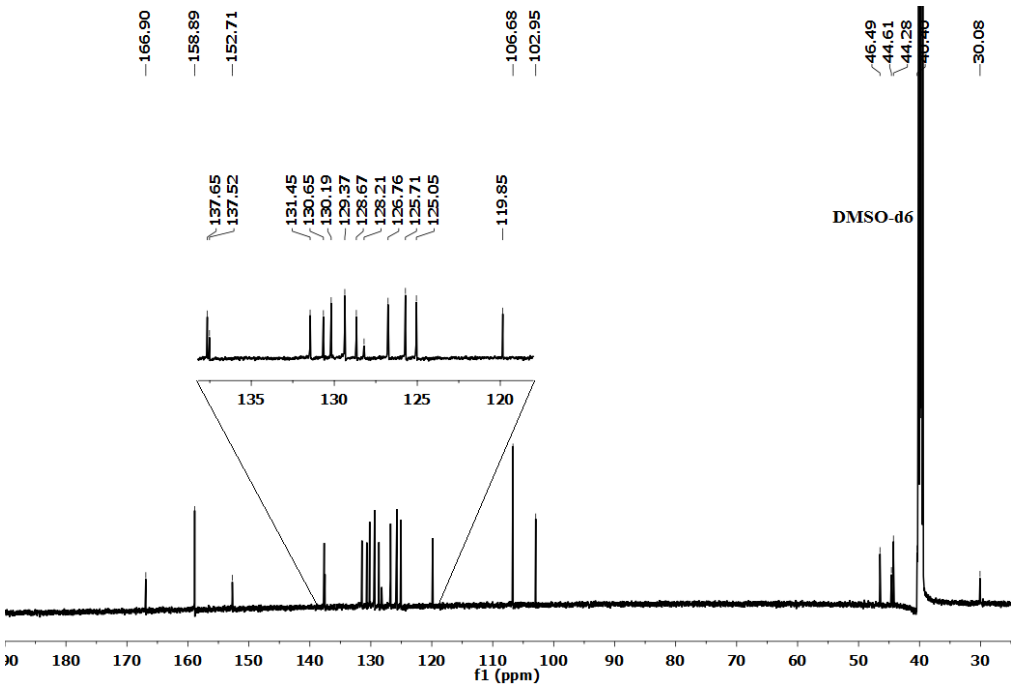

Figure A8: ^{13}C-NMR (125 MHz, DMSO-d_6) spectra of the **2[(H_2anthraimida)]$^+$[(35pdc)]$^{2-}$·2resorc (2.4)**.

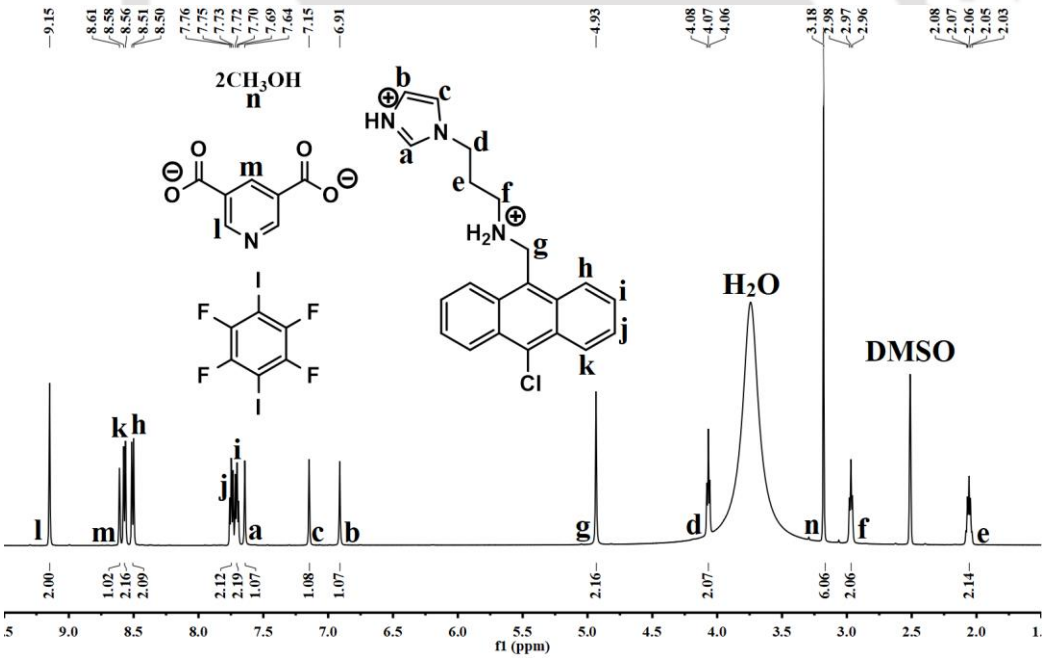

Figure A9: ^{1}H-NMR (600 MHz, DMSO-d_6) spectra of [(H_2**chloroanthraimmida)**$^{2+}$**(35pdc)**$^{2-}$]·**(IFbenz)**·2CH_3OH **(2.7)**.

TH-3622_196122001

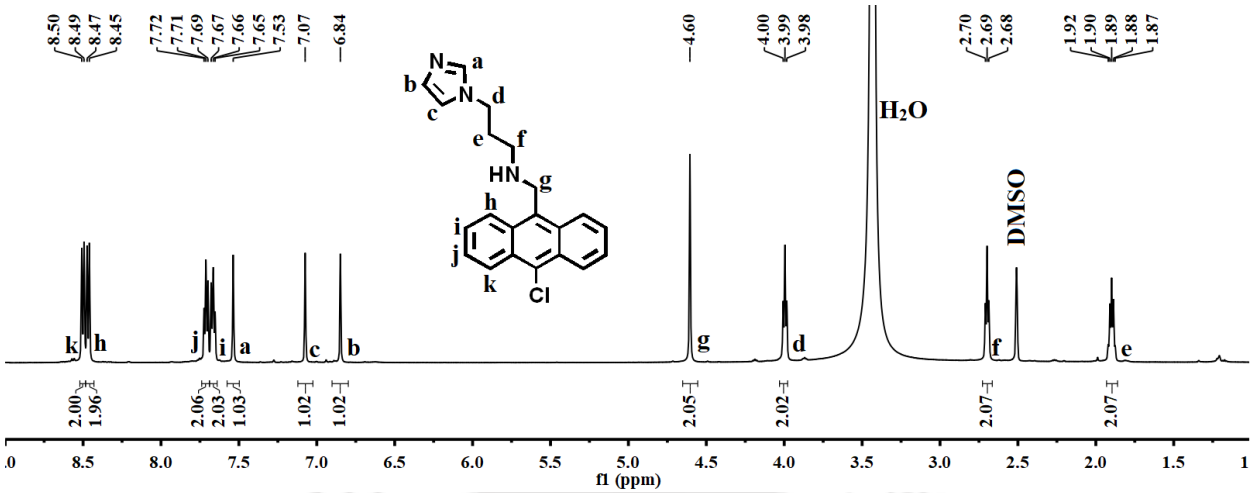

Figure A10: ^{1}H-NMR (600 MHz, DMSO-d_6) spectra of the **Chloroanthraimmida**.

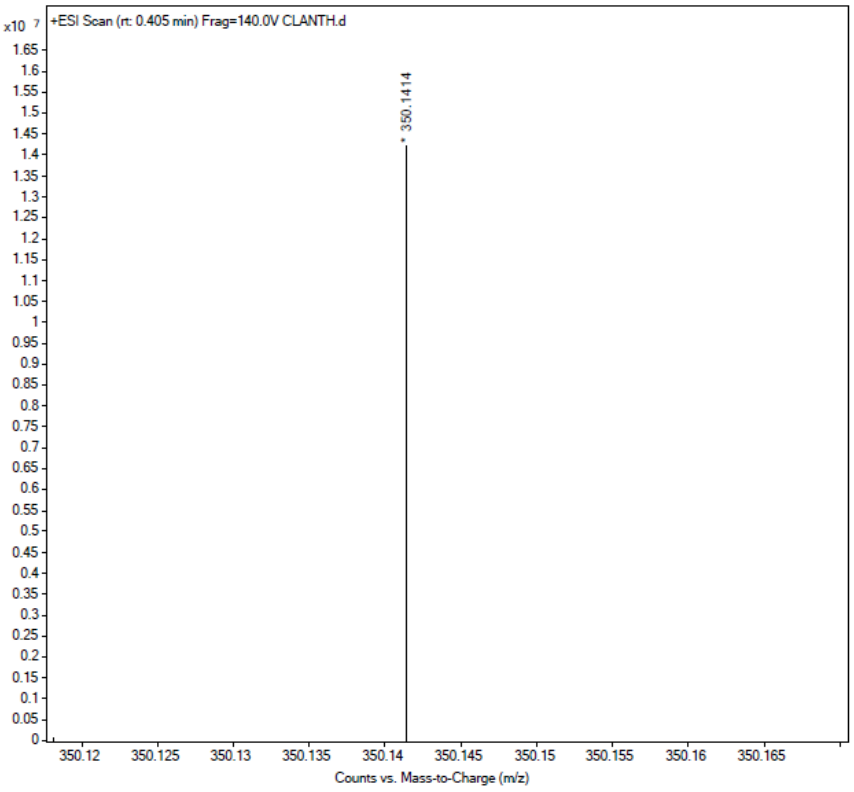

Figure A11: ESI mass spectrum of the **Chloroanthraimmida**.

TH-3622_196122001

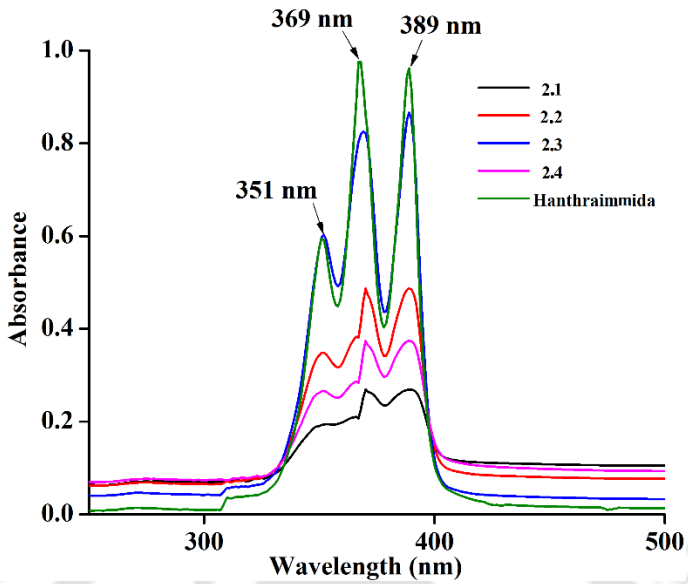

Figure A12: UV-vis spectra of the cocrystals **2.1-2.4** and H**anthraimmida** (10^{-6} M in DMSO).

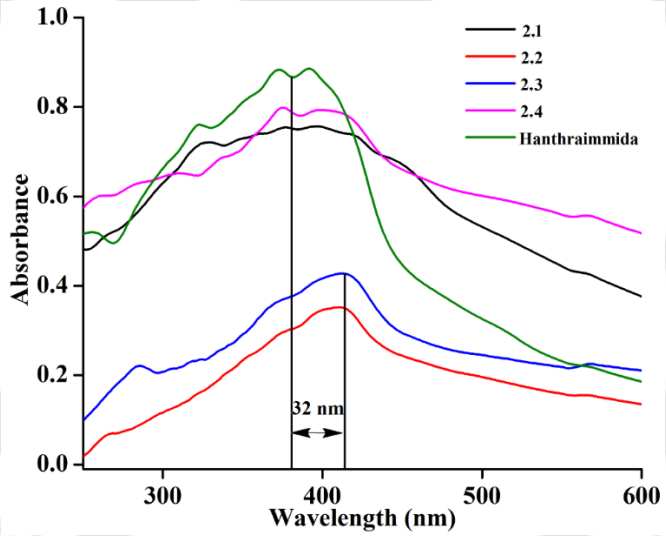

Figure A13: Solid state UV-visible spectra of the cocrystals **2.1-2.4** and H**anthraimmida**.

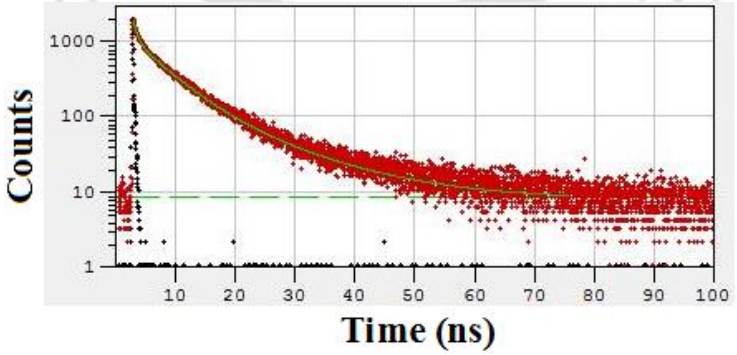

Exponential Components Analysis (Reconvolution)

TH-3622_196122001

Fitting range : [104; 3100] channels

□² : 1.089

	B_i	ΔB_i	f_i (%)	Δf_i (%)	τ_i (ns)	$\Delta\tau_i$ (ns)
1	0.2670	0.2200	24.540	22.096	0.654	0.050
2	0.0663	0.0070	48.925	5.189	5.252	0.005
3	0.0138	0.0016	26.534	3.103	13.706	0.003

Shift : -1.001 ns (± 22.392 ns)

Decay Background : 8.120 (± 0.298)

IRF background : 0.100

Figure A14: Time resolved fluorescence emission of solid sample of **2.1** (λ_{ex},405 nm; λ_{em},490 nm).

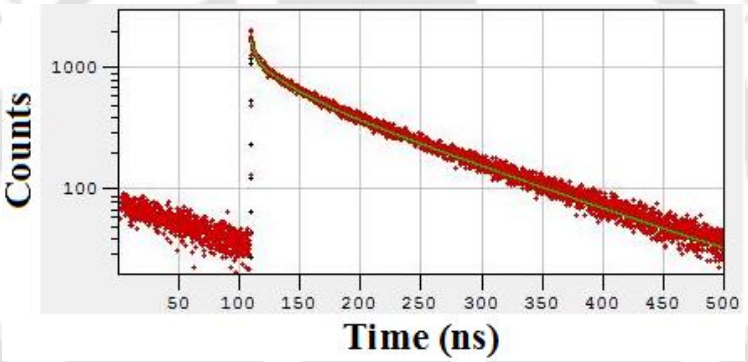

Exponential Components Analysis (Tail Fitting)

Fitting range : [880; 4096] channels

□² : 1.049

	B_i	ΔB_i	f_i (%)	Δf_i (%)	τ_i (ns)	$\Delta\tau_i$ (ns)
1	543.8052	17.3091	1.816	0.067	3.470	0.017
2	448.5926	11.2802	11.865	0.299	27.479	0.002
3	746.7656	12.5292	86.319	1.448	120.095	0.0001

Shift : 0 ns (± 0 ns)

Decay Background : 4.797 (± 1.259)

Figure A15: Time resolved fluorescence emission of solid sample of **2.2** (λ_{ex}, 405 nm; λ_{em},490 nm).

TH-3622_196122001

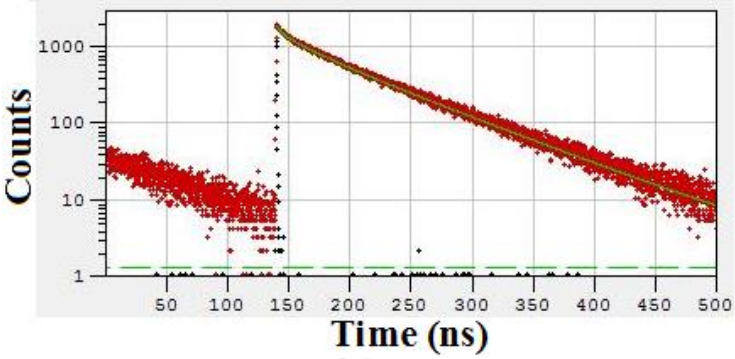

Exponential Components Analysis (Tail Fitting)

Fitting range : [1131; 4096] channels

χ^2 : 1.012

	B_i	ΔB_i	f_i (%)	Δf_i (%)	τ_i (ns)	$\Delta\tau_i$ (ns)
1	345.0226	18.4528	1.191	0.075	3.296	0.031
2	488.1303	22.6494	13.341	0.620	26.104	0.002
3	1138.4395	30.1089	85.468	2.261	71.705	0.0002

Shift : 0 ns (± 0 ns)

Decay Background : 1.191 (± 0.428)

Figure A16: Time resolved fluorescence emission of solid sample of **2.3** (λ_{ex}, 405 nm; λ_{em},480 nm).

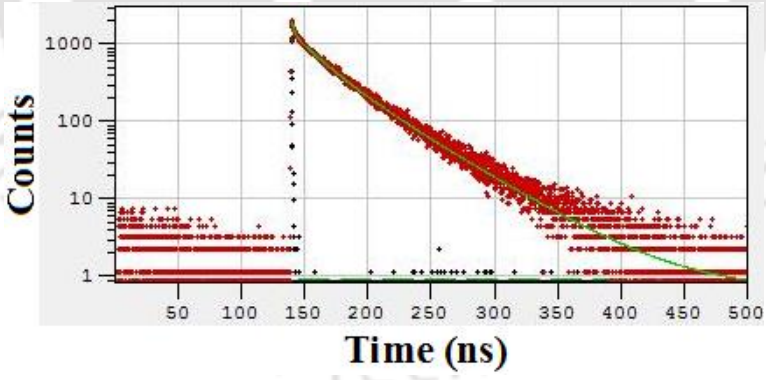

Exponential Components Analysis (Tail Fitting)

Fitting range : [1130; 4096] channels

χ^2 : 1.018

	B_i	ΔB_i	f_i (%)	Δf_i (%)	τ_i (ns)	$\Delta\tau_i$ (ns)
1	656.2955	16.9560	3.017	0.111	2.062	0.022
2	719.9695	28.0951	33.634	1.315	20.959	0.002

TH-3622_196122001

3	628.1241	33.4922	63.349	3.378	45.248	0.0004

Shift : 0 ns (± 0 ns)

Decay Background : 0.675 (± 0.106)

Figure A17: Time resolved fluorescence emission of solid sample of **2.4** (λ_{ex},405 nm; λ_{em}, 480 nm).

References:

A.1. E. A. Amin and D. G. Truhlar, *J. Chem. Theory Comput.*, 2008, **4**, 75–85.
A.2. Joshua A. Plumley, J. J. Dannenberg, *Journal of Computational Chemistry*, 2011, **32**, 1519-1527.
A.3. M. Frisch, G. Trucks, H. Schlegel, G. Scuseria, M. Robb, J. Cheeseman, G. Scalmani, V. Barone, G. Petersson, H. Nakatsuji, *Gaussian 09, Revision A.02*; Gaussian, Inc.: Wallingford, CT, 2016.

TH-3622_196122001

CHAPTER 3

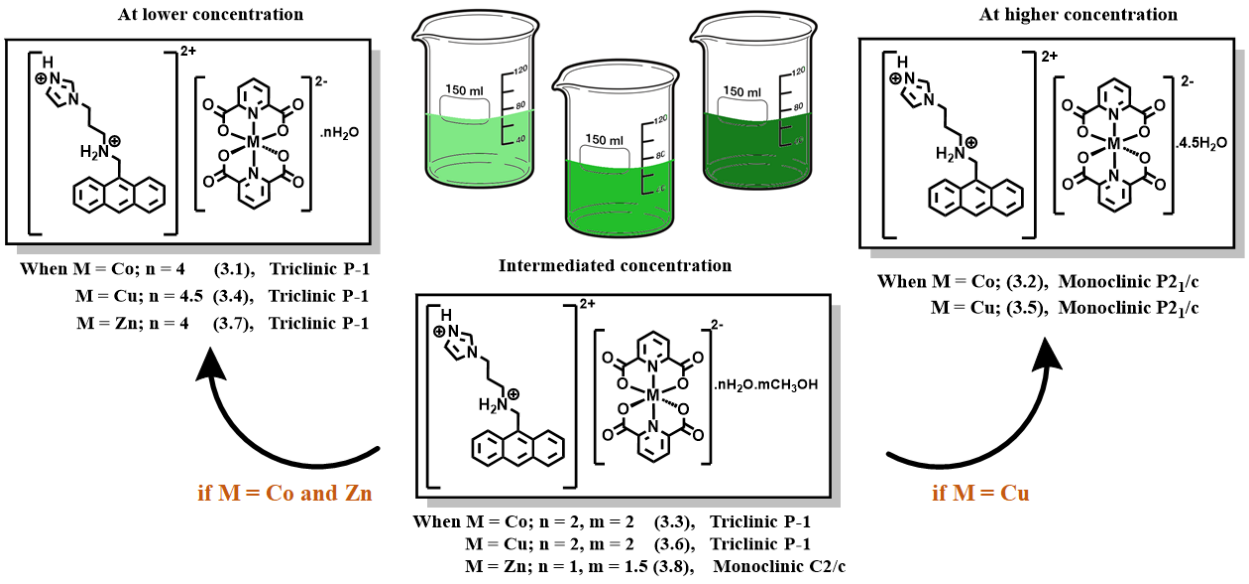

TH-3622_196122001

Chapter 3

Polymorphic hydrates of bivalent cobalt, copper and zinc 2,6-pyridinedicarboxylate complexes having metastable intermediate: characterisations and interconversions

3.1. Design principle

It was shown in the earlier chapter that the fluorescence intensity of N-(anthracen-9-ylmethyl)-3-(1H-imidazol-1-yl)propan-1-amine (H**anthraimmida)** was enhanced upon interactions with 2,6-pyridinedicarboxylic acid. Based on this result, we were interested to prepare different assemblies of protonated (H**anthraimmida**) to organize stacking among the anthracenyl part to create herringbone or lamellar structures by stacking them between layered structures of bis-pyridinedicarboxylate metal complex anions as illustrated in the Figure 3.1.

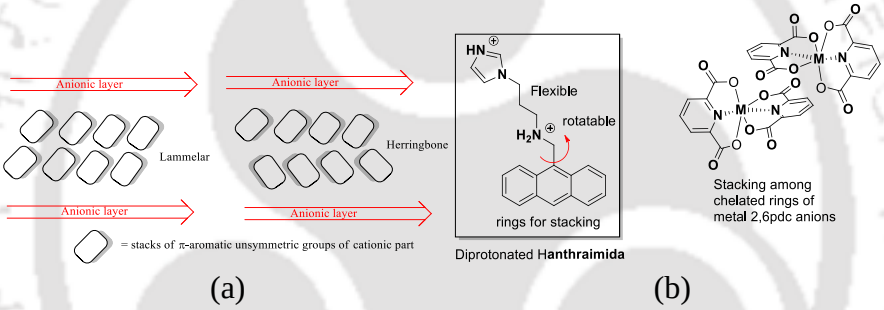

Figure 3.1: (a) Design principle for lamellar and Herringbone arrangements, (b) The structure of dication from H**anthraimmida** and the chelate-chelate stacks between 2,6-pyridinedicarboxylate in its metal complex anion.

The interest to have such a design scheme to explore, arose from the fact that metal-bis-2,6-pyridinedicarboxylate complexes form layered structures, where imidazolium cations could be organized in between the layers.[1] Furthermore, the anionic part from metal-2,6-pyridinedicarboxylate complexes also assemble as chelate-chelate stacks (Figure 3.1b) to form anionic 1D-layer-like arrangements.[2] Hence, the cation such as H**anthraimmida** anchored in such layers of anions will provide avenues for the 1D arrangement of anthracenyl group in different manners with the layer. The flexible tether of the anthracenyl unit of H**anthraimmida** would allow the anthracenyl unit to settle and adopt different spatial orientations through interplay of weak interactions or a stimuli. While attempting to prepare these forms through crystallization from different solutions, we found that copper-2,6-pyridinediarboxylate complex possessing dication of N-(anthracen-9-ylmethyl)-3-(1H-imidazol-1-yl)propan-1-amine from methanol solution had serendipitously provided three different forms of hydrates. Standardization of crystallization

TH-3622_196122001

conditions had showed that three different forms of hydrates could be crystallized from same solution but with different concentrations. This serendipitous discovery had led us to follow up such crystallizations and allowed us to characterize all the forms of those hydrates and their transformations. Based on such an observation, we had optimized the crystallization conditions, it paved way to obtain different hydrates starting from same reactants but at differently concentrated solutions. We extended this to other two metal 2,6-pyridinedicarboxylate namely cobalt and zinc complexes. These aspects are illustrated in the following section of this chapter.

3.2. Crystallization of different hydrates and interconversions

In the literature, there are examples where hydrates or multi-component crystals are obtained in crystalline form by choosing a suitable crystallization condition.[3-9]

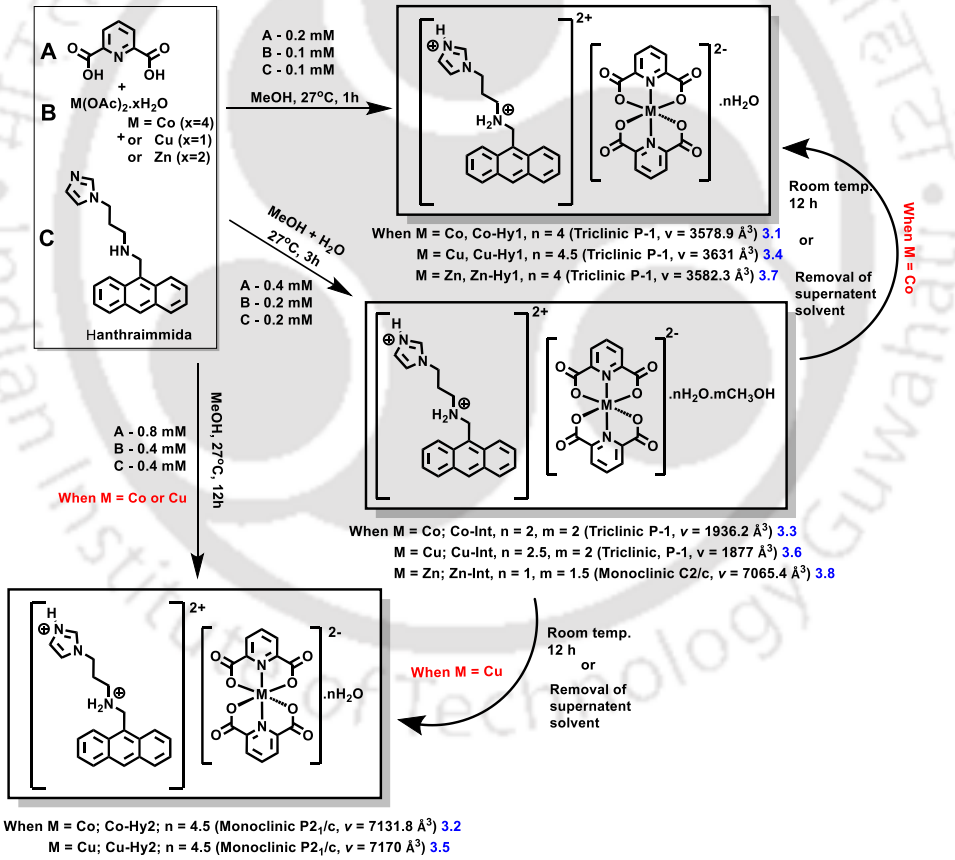

Scheme 3.1: Different hydrates of cobalt (II), copper (II) and zinc (II) complexes.

In the present study, different forms of hydrates of H**anthraimmida** containing cobalt(II), copper(II) and zinc-2,6-pyridinedicarboxylate were obtained from the solution containing the

TH-3622_196122001

corresponding metal (II) acetate, H**anthraimmida** together with 2,6-pyridinedicarboxylic acid in 1:1:2 molar ratio but at different concentrations of methanol as illustrated in the scheme 3.1.

As the crystals were unstable, they were taken out and placed in paraffin oil and the suitable crystals were selected and mounted in X-ray and with fast data collection the structure was determined. The crystal structure of the same was determined at liquid nitrogen temperature to check the integrity of the structure. The crystallising conditions of the hydrates are listed in table 3.1. There are examples of coordination polymers possessing methanol or water molecules transforming reversibly between solvated and desolvated forms.[10] In this case there was no crystal to crystal transformation, but it was solvent mediated crystal transformation.

Table 3.1: Concentrations of reactants in methanol to crystallize the hydrates

Hydrate	$M(OAc)_2 \cdot xH_2O$ (mmol)	2,6-H_2pdc (mmol)	Solvent (mL)	Hanthraimmida (mmol)	Time of stirring	Time for crystallization
3.1/3.4/3.7	$0.1^{@\#\$}$	0.2	Methanol (20mL)	0.1	1 h	6-7 days
3.3/3.6/3.8	$0.2^{@\#\$}$	0.4		0.2	3 h	2 days
3.2/3.5	$0.4^{@\#}$	0.8		0.4	12 h*	3-4 days

@ M = Co. x = 4, # M= Cu, x = 1; $ M = Zn, x = 2; * = 2 mL water was added after appearance of precipitate after 12hrs

Similarly three different forms of hydrates, among which two were polymorphs of the hydrate of the complex $[(H_3$**anthraimmida**$)Cu(26pdc)_2]_2 \cdot 9H_2O$ {**Cu-P1** and **Cu-P2**} (**3.4** and **3.5**) and an intermediate hydrate $[(H_3$**anthraimmida**$)Cu(26pdc)_2] \cdot 2.5H_2O \cdot 2CH_3OH$ {**Cu-Int**} (**3.6**) were obtained. A crystallization from a reaction occurring at a relatively short duration (1hr) and at low concentration (Table 3.1) yielded the polymorph (**3.4**). Whereas, the reaction with the same reactants continued for longer time (12hrs) at a relatively higher concentrations of the reactant, resulted in the formation of another polymorph (**3.5**). At an intermittent concentration the polymorphs in approximately three hours provided **Cu-Int** (Scheme 3.1). In this case the transformation of the **Cu-Int** to the crystals of **Cu-P2** was observed. The transformation could be monitored by placing on a glass-plate and observing under a microscope. It showed that it agglomerates initially and then transformed to another form (The URL link attached here shows the video of transformation from **Cu-Int** to **Cu-P2** https://pubs.acs.org/doi/suppl/10.1021/acsomega.3c05132/suppl_file/ao3c05132_si_002.mp4). Adequate care in handling the crystals had to be taken to get the data in a similar way as that of the **Co-Int**.

TH-3622_196122001

Two hydrates of zinc(II)2,6-pyridinedicarboxylate [(H_3**anthraimmida**) $Zn(26pdc)_2$]·$4H_2O$ **{Zn-Hy1} 3.7** and [(H_3**anthraimmida**)$Zn(26pdc)_2$]·H_2O·$1.5CH_3OH$ {**Zn-Int**} **3.8** were crystallized by changing the concentrations of the reactant in same volume of solvent at room temperature listed in the Table 3.1 similar to the preparation of hydrates of cobalt and copper complexes. The lower concentrated solution required more time to reach super saturation to yield the crystals of the stable hydrate **3.7**. Whereas, from higher concentrated solution, resulted a metastable hydrate **3.8**. As this methanol hydrate was also unstable, we had to store it immediately putting the crystals in paraffin oil, and then mount the crystal for fast data collections.

3.3. Self-assemblies of different hydrates of cobalt complex (3.1-3.3)

The crystal structure of the three hydrates of the cobalt complex showing the hydrogen bonded water molecules in **3.1**, **3.2** and methanol and water molecules in **3.3** are shown in the Figure 3.2. The differences among the structures arose from the water molecules or water and methanol solvent of crystallization. The **Co-Hy1** (**3.1**) had a dication H_3**anthraimmida**, a dianion **[**$Co(26pdc)_2$**]$^{2-}$** and four water molecules of crystallization. In the asymmetric unit of the unit cell of the crystals of this hydrate, there were two symmetry independent cations and also two symmetry independent anions. There are examples of solvates of 1,10-phenanthroline with different π-stacks, certain ones among them were transient species, and after removal from the mother liquor they also forms a hydrate with three symmetry independent molecules in asymmetric unit.[11] The solvates having different solvent of crystallization also provide systems with symmetry independent molecules.[12] In the solid-state self-assembly of **3.1**, each symmetry non-equivalent molecules had four water molecules. Among them, a pair of water molecules were connected by O18-H···O19, {$d_{D\cdots A}$, 2.721(6) Å, <D-H···A 165°} hydrogen bonds (Figure 3.2a); they linked the two symmetry non-equivalent anions in the assembly. Accordingly, two independent anions of different molecules were hydrogen bonded to the pair of water molecules by O19-H···O12 {$d_{D\cdots A}$, 2.769(5) Å, <D-H···A 158°} and O18-H···O7 {$d_{D\cdots A}$, 2.841(5) Å, <D-H···A 172°} hydrogen bonds (Figure 3.2a). The $^{+}$N-H bond of the imidazolium part of the cation was hydrogen bonded to O18 atom {$^{+}$N4-H···O18, $d_{D\cdots A}$, 2.692(7) Å, <D-H···A 167°} of one of the water molecules. There was no direct connectivity between the anions and cations utilizing the $^{+}$N-$H_{imidazole}$ bond, but they were linked together by intervening water molecules. On the other hand, $^{+}$N-H_{amine} bond was also

TH-3622_196122001

involved in hydrogen bond by linking the anion through $^{+}$N3-H$_{amine}$···O16 bond {d$_{D}$···$_{A}$, 2.771(4) Å, <D-H···A 168°}.

Additionally, there was a cyclic structure formed by hydrogen bonding of carbonyl oxygen (O14) with two water molecules having oxygen atoms (O23 and O24) as the intervening hydrogen bonding molecules anchored to O9 oxygen atom of carboxylate of the same anion. The hydrogen bond sequence for this cyclic structure was O14···H-O23···H-O24···O9 (hydrogen bond parameters are listed in hydrogen bond table A2 in the Appendix). There was also another pair of water molecule bearing the O20 and O22 atoms were hydrogen bonded to each other and the hydrogen bonded dimer was responsible to hold two symmetry independent anions by forming hydrogen bonds with oxygen atoms of the carbonyl and carboxylate of the anions. The O17 and O21 atoms bearing water molecules were also forming hydrogen bonded dimer and these linked anions as well as cations through hydrogen bonds. The imidazole nitrogen $^{+}$N1-H was hydrogen bonded to O21 of water. There were direct hydrogen bonds between the cations and anions, through $^{+}$N6-H$_{amine}$···O6$_{carbonyl}$ and $^{+}$N3-H$_{amine}$···O16$_{carbonyl}$ hydrogen bonds. The symmetry independent anions present in the crystal lattice were located next to each other, and they had chelate-chelate stacking among them to provide a one- dimensional chain-like arrangement. This is not unusual as there are large numbers of chelate complexes where stacking among the coordinated ligands form assemblies[12] and 2,6-pyridinedicarboxylate complexes[1-2] are not exception to those. The imidazole parts of the cations were held on the chain and the anthracenyl units projected away as illustrated from the chain as in Figure 3.2d. All the anthracenyl units of a chain were projected in one direction of the chain, and the chain next to each other had a similar arrangement and the face having the anthracenyl units projected face to face with the other chain so that the π-stacks of anthracenyl parts are formed. These double chains were organized parallel each having the anthracenyl part embedded between two chains and the double chains were held together by water molecules to make an extended two-dimensional structure. This provided a lamellar arrangement, where each double chained portion were related to the neighbor double chain by a mirror plane reflection. Stacking among the phenyl-rings are well known to occur in edge to face, face to face or oblique manners,[13] while in the layers of the layer like structures had only face to face stacked anthracenyl units. The anthracenyl units from each symmetry independent molecules were in pairs and there were three centroid to centroid distances between these units. The two distances between the planes

TH-3622_196122001

of anthracenyl rings of the pairs comprising of same symmetry independent cations were 4.220 Å and 4.139 Å, while between the two anthracenyl rings with independent symmetry, the distance was 3.763 Å. Generally, the stacking interactions within 3.5 Å are significant, hence having a separation of 3.763 Å showed a significant contribution of stacking effect. The π-stacking among aromatic units have profound interest in fundamental,[14] biological[15] and material sciences.[16] The magnitude of aromatic π-stacking interactions is very small (~2 kJ mol^{-1}). [17] Yet, those contribute to design catalysts[18] and magnetic,[19] optical, [20] high energy materials. [21] Aromatic π-stackings in a self-assembly influence physical property such as conductance, proton transfer etc.[22] In the present example, the stacking arrangements were based on a imidazole containing cation and the complex was formed at ambient temperature under neutral conditions with a biologically benign metal ion. The hydrate was stable in open air and retains its crystallinity for more than two weeks and the physical properties remain intact adds further advantage.

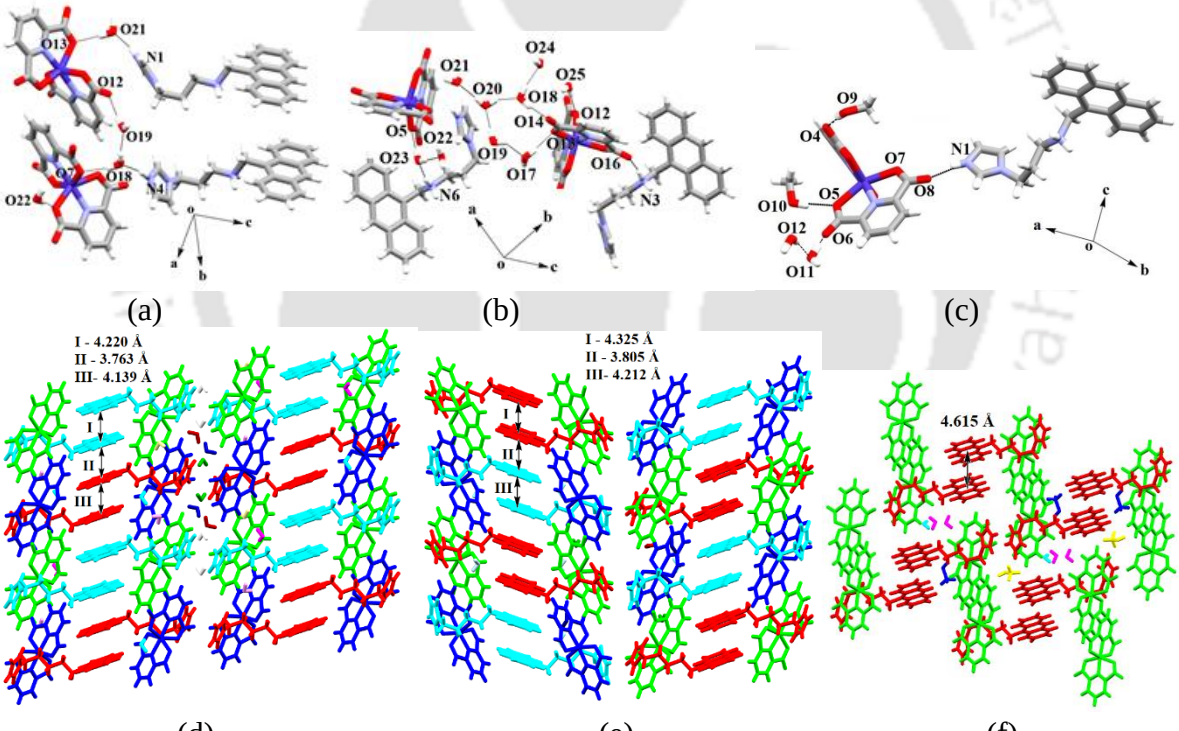

Figure 3.2: Hydrogen-bonded water or methanol molecules in the crystal structures of the hydrates of the cobalt complex (a) **3.1**, (b) **3.2** and (c) **3.3**. The different packing orientations of π-stacks in the hydrates (d) **Co-Hy1** (**3.1**) along *ac*-crystallographic plane, (e) **Co-Hy2** (**3.2**) and (f) **Co-Int** (**3.3**) along *bc*-crystallographic plane.

The asymmetric unit of hydrate **Co-Hy2 (3.2)** also had two symmetry independent cations and also two symmetry independent anions. It had nine water molecules of crystallization shared by two symmetry independent complexes, hence per complex, had 4.5 water molecules. The self-

TH-3622_196122001

assembly of the **3.2** had four water molecules connected to one of the symmetry independent anion, forming a ring-like cyclic structure. The cycle consist a sequence O14···H-O18···H-O20···H-O19-H···O17-H···O13 of hydrogen bonds (Figure 3.2b). The oxygen atoms of the carboxylate O13 and O14 of anion had served as the pivots to form the cyclic structure. The oxygen atom O21 of the water molecule of the hydrate (which was shared by two molecules) was located outside the cyclic structure, and it had trifurcated hydrogen bonding to link the cyclic structure by O20-H…O21 and another carboxylate by O20-H···$O10_{carbonyl}$ and $^{+}$N4-$H_{(imidazole)}$···O20 hydrogen bonds. The other four water molecules possessing the O22, O23, O24 and O25 were involved with another symmetry independent part (hydrogen bond parameters are listed in table A2). The two water molecules having O22 and O23 oxygen atoms on this part of the asymmetric unit, were hydrogen bonded to form dimer. The O23 of the dimer was held to O5 of a carboxylate and $^{+}$N-$H_{(amine)}$, whereas the O22 was hydrogen bonded to carbonyl oxygen O4 of a carboxylate. The water molecule possessing O18 atom was serving as hydrogen bond donor as well as acceptor and was linking the symmetry independent parts in the asymmetric unit. There was O18-H···O24 hydrogen bond ($d_{D}\cdots_{A}$, 2.822(6) Å, <D-H···A 161°) between two water molecules and served as acceptor through O18···H-O20 and as acceptor for O18-H···$O14_{carbonyl}$ independent units. The oxygen atom O21 of water molecule of cyclic water structure also provided the knitting between the symmetry independent units by forming hydrogen bonds with an intervening water molecule that was hydrogen bonded to an oxygen (O3) of nearby carboxylate anion. This sharing resulted in the 4.5 numbers of water molecule and carboxylates per molecule of the complex. The cation was held to the cyclic water assembly by $^{+}$N1-$H_{imidazole}$···O19 charge-assisted hydrogen bond ($d_{D}\cdots_{A}$, 2.700(8) Å, <D-H···A 163°). In the self-assembly of this hydrate there were two symmetry non-equivalent anions and cations. The packing pattern of **Co-Hy2** (**3.2**) had similar chains of anions as observed in the other hydrate **Co-Hy1** (**3.1**) and also had analogous chain to each other. But there was no mirror plane reflection symmetry relation, it had a Herringbone type structure; where the of anthracenyl rings of symmetry non-equivalent cations were found at similar positions in the two neighboring double chains (Figure 3.2e). The structure of **Co-Hy2** (**3.2**) had a Herringbone cross-bedding structure, which relates to the structures of sediments formed on the sea-shores by tides. Those structural patterns have a look of the structural arrangements of the bones of a fish. Such patterns on the soil in a sea-shore occurs due to periodic flows of water during the forward and

TH-3622_196122001

backward movement of water in tide and ebb. Those periodic patterns have the fore-sets in successive parallel structured arrangements in opposite directions.[23] There are also examples of self-assemblies where changes in the stacking among the molecules caused gate opening and enabled to design in artificial ion channel by externally adding a π-stacking component.[24]

Herringbone arrangement is a term used for organized π-stacks, has broad dimensions for material design.[25] Herringbone structures are formed by solvent guided synthesis,[26] host-guest interactions,[27] effect of substituents[28] and stimuli. [29] The hydrate **Co-Hy2** (**3.2**) differed from **Co-Hy1** (**3.1**) in the amounts of water molecules, structurally also they had very close similarity, but the translation of layers being different made the former less symmetric. In this case also there were three π-separation distances between the parallel rings, the ones with symmetry equivalent pairs were 4.325 Å and 4.212 Å. Whereas, the distance between the centroids of the rings from symmetry independent cations was 3.805 Å. These separtions are slightly longer than the similar one found in **Co-Hy1** (**3.1**), hence the **Co-Hy2** (**3.2**) has lesser π-stacking effect on the electrostatically guided assembly. Comparing two hydrates it may be suggested that the **Co-Hy1** (**3.1**) had direct hydrogen bonding between anions and cations and they had also shorter distance of separtion between the aromatic stacks as compraed to the **Co-Hy2** (**3.2**).

The asymmetric unit of the methanol hydrate **Co-Int** (**3.3**) had a cation and anion, these were connected directly by N1-H···O8 [$d_{D\cdots A}$, 2.628(4) Å, <D-H···A 164(5)°] hydrogen bond (Figure 3.2c). The methanol molecules were hydrogen bonded to the oxygen atom (oxy) of the anion. Two water molecules formed hydrogen bond pair through O11-H···O12 and was linked to a carbonyl oxygen through O11-H···O6 hydrogen bond. This pair of water molecule served as linker for two neighboring complex and contributed to expand the self-assembly. The structure was further stabilized by very weak C-H···π and C-H···O interactions. The anions were present in the lattice as discrete pairs assembled through chelate-chelate stacking. (Figure 3.2f). The anthracenyl unit had projected out in each molecule of the complex and two independent molecules were held together through stacking between the anthracenyl rings. The distance between the two parallel stacks was 4.615 Å, this distance had suggested that there were very weak interactions between the rings. Overall, it formed channel-like arrangement, in the interstices at independent voids water or methanol molecules were located. The structural analysis have shown that the extensive hydrogen bonding due to water molecules and extensive π-stacks were not present in the methanol hydrate.

TH-3622_196122001

Hence, there was easy exchange of methanol molecules by water molecules from the hydrates or vice-versa to maximize the number of hydrogen bonds in getting the intermediate, which then transformed to have a structure with effective π-staking among the aromatic units. Stacking among chelates is an important factor to guide assemblies of metal complexes.[30] Solvents guiding to crystallize a particular form of hydrate depends on the ability of the solvent to disrupt or reconstruct the sub-assemblies within a supramolecular system.[31-32] In the present example, transformations between the intermediate hydrate to the stable form of hydrate required reorganization of structures to provide new stacking arrangements from an original one. The transformation from **Co-Int** (**3.3**) to **Co-Hy1** (**3.1**) took place but not **Co-Hy2** (**3.2**); as the **Co-Hy1** (**3.1**) had electrostatically guided assembly and had better stacking than the latter.

3.4. Self-assemblies of different hydrates of copper complex (3.4-3.6)

The asymmetric units of the two polymorphic hydrates **Cu-P1** (**3.4**) and **Cu-P2** (**3.5**) had two symmetry independent cations as well as anions in their respective asymmetric unit along with nine water molecules each. As per the compositions, each complex had 4.5 molecules of water. Each organic cation in the structures of the **Cu-P1** (**3.4**) and **Cu-P2** (**3.5**) had independent orientations of imidazole unit with respect to the anthracenyl group; and conformation of those organocations were not equivalent. The structure of the two polymorphs omitting the water molecules are shown in the Figure 3.3a and 3.3b. The coordination environment around copper(II) ion of the both polymorphs were identical having two 2,6-pyridinedicarboxylates coordinated to copper(II) ion, each providing NO2 type of coordination. The metal-ligand bond parameters are listed in Table A4. The symmetry independent anions were found as stacked dimers. The distance between the two planes of stacked dimers of the anions in **Cu-P1** (**3.4**) and **Cu-P2** (**3.5**) was 3.676 Å and 3.601 Å respectively.

The imidazolium portion of the organic dication H**anthraimmida** of the **Cu-P1** (**3.4**) were involved in the formation of charge-assisted hydrogen bonds. The eight molecules of water located at different portion of the lattice were found as four independent hydrogen bonded pairs and three discrete water molecules (Figure 3.3c). The water pairs held together by O17-H···O18, O19-H···O20, O21-H···O22; O23···H-O24 served as hydrogen bonded intervening units to assemble four independent anions. The discrete water molecules served as hydrogen bonded bridges to

TH-3622_196122001

connect the cations and anions. For example, the $^{+}$N6-H$_{amine}$···O25$_{water}$ hydrogen bond and O25-H$_{water}$···O7$_{carboxylate}$ held an anion with the cation through intervening water.

In the self-assembly of the **Cu-P2** (**3.5**), there were five water molecules (bearing O19, O20, O21, O22, O24) hydrogen bonded to each other as shown in the Figure 3.3d and these knitted three neighboring anions by hydrogen bonding to oxygen atoms of the neighboring carboxylates. The discrete water molecule bearing O17 served as source for hydrogen bonded bridge to hold a cation and anion with carboxylate oxygen (O9) of anion and $^{+}$N3-H of a cation. The two symmetry-independent cations were involved in hydrogen bonds in a different manner, they had $^{+}$N-H$_{imidazole}$···O$_{water}$ and $^{+}$N-H$_{imidazole}$···O$_{carboxylate}$ hydrogen bonds contributing to the assembly. The hydrogen bond parameters are listed in the Table A2.

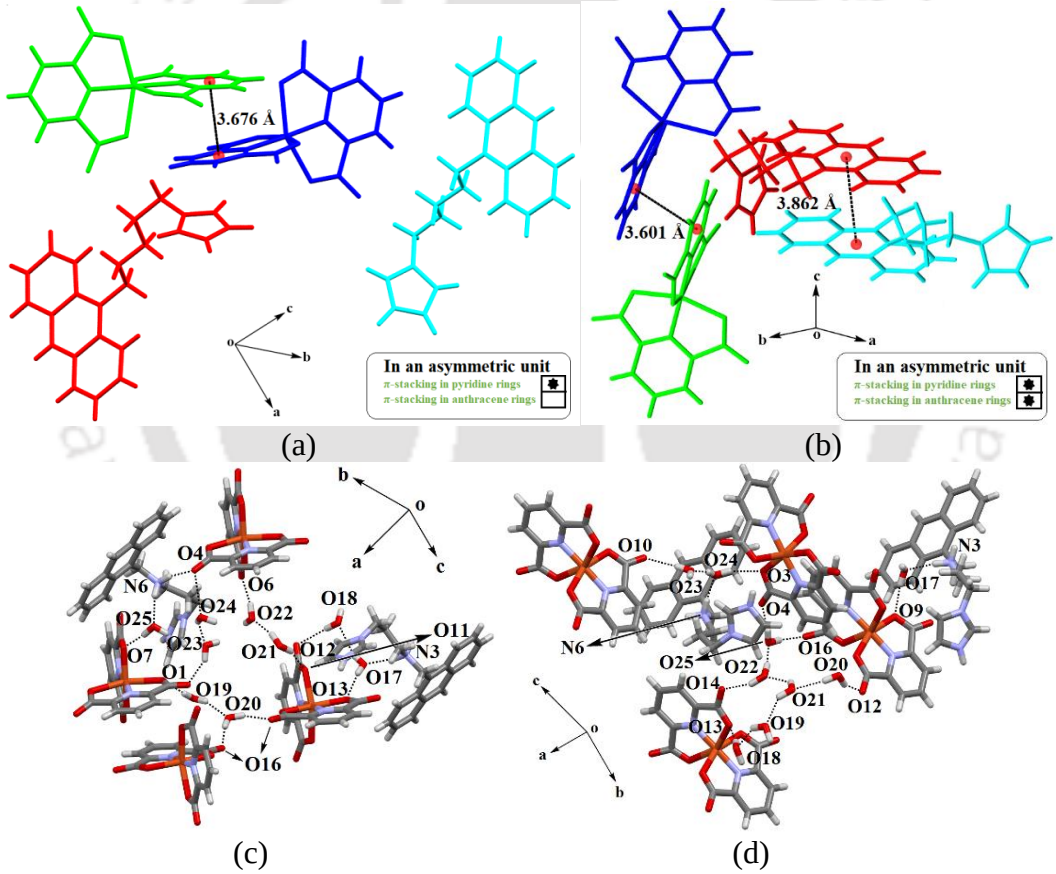

Figure 3.3: The crystal structure of (a) **Cu-P1 (3.4)** and (b) **Cu-P2** (**3.5)** (Water molecules are omitted for clarity); and the packing patterns of the (c) **Cu-P1 (3.4)** and (d) **Cu-P2 (3.5)** showing the orientations of π-stacks in the two polymorphs.

Both the polymorphs had independent types of chain-like arrangements among the cations and anions; these chains were organized in such a way that anthracene rings form two independent chains. These chains are assembled in face to face stacking to form layer-like arrangements. The

TH-3622_196122001

rings were inclined with respect to the anionic chains (Figure 3.4). Those bilayers of **3.4** were oriented in same direction providing a lamellar structure; whereas, in the case of **3.5**, the layers were organized in the opposite directions as alternate bilayers to provide herringbone structure. These arrangements provided differences in the packing of the two polymorphs. Flexible dyads such as of monoalkoxynaphthalene–naphthalimide undergoes thermochromic transformation due to changes in the π-stacks.[33] In such systems, the flexible alkyl chains had a role to guide the stacks. In the present example, we had $(CH_2)_3$- tether linking the anthracenyl group with the imidazolium cation. Thus, there were various conformations to guide the orientations of those rings and to bring variety in the self-assemblies.

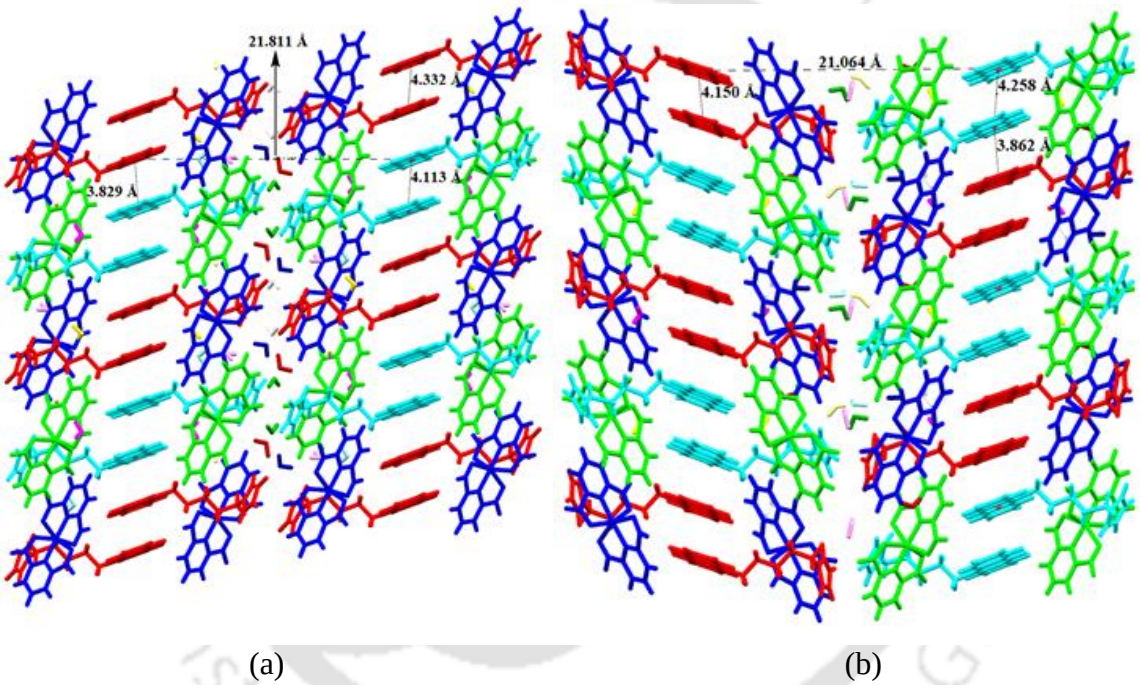

Figure 3.4: The crystal packing patterns of the (c) **Cu-P1** (**3.4)** and (d) **Cu-P2 (3.5)** showing the orientations of π-stacks in the two polymorphs along *ac*-crystallographic plane.

It may be noted that the bisphosphoramidites and its methanol solvate was reported to have single and two molecules in the asymmetric units; in that case the packing patterns were guided by edge to face C-H···π interactions.[34] Our examples had two symmetry independent molecules with lamellar and Herringbone arrangements has provided avenues for a new polymorphic compound of such a kind. The two distances between the planes of anthracenyl rings of the pairs comprising of same symmetry independent cations were 4.113 Å and 4.332 Å for **Cu-P1** (**3.4**); and 4.150 Å and 4.258 Å for **Cu-P2** (**3.5**), similar distance between the two anthracenyl rings with independent symmetry were 3.829 Å for **3.5** and 3.862 Å for **3.5**. But, the interlayer separation in the case **3.5**

TH-3622_196122001

was 21.811 Å and same for the **3.5** was 21.064 Å (Figure 3.4). This showed that there were balances between the stackings, and direct comparison could not be made. Hence, the two polymorphs were reversibly formed.

In the crystal structure of the **Cu-Int** (**3.6)**, the asymmetric unit had a $[Cu(26pdc)_2]^{2-}$ anion and a H_3**anthraimmida** cation (Figure 3.5a). One of the carbonyl oxygen atom (O8) of the anion was hydrogen bonded to a hydrogen bonded water dimer (Fig 3.5b). The water dimer was formed by O9-H···O12 hydrogen bond. This compound had also anthracene rings in parallel positions, but those were located at translated positions. The oxygen atom of one of the methanol molecules served as bridge to anchor the cation and anion by O10-H···O7 and N3-H···O10 hydrogen bonds. In addition, other methanol molecule was held to anion by O11-H···O4 hydrogen bond. Thus, the two methanol molecules had distinguishable hydrogen bond environments. The cations and anions were also linked together by $^{+}N1\text{-}H_{imidazole}\cdots O6_{carboxylate}$ hydrogen bonds.

In the structure of the **3.6**, there were parallel but non-eclipsing rings of the anthracenyl units as pairs along the *b*-crystallographic direction of the crystal lattice of **Cu-Int** with centroid to centroid distance 4.56 Å. This distance suggested no stacking interactions among the anthracenyl units. In the lattice, four neighboring cations were organized by hydrogen bonds of the oxygen atoms of C=O of the anions with N-H bond of $-^{+}NH_2-$ unit of the cation to provide channels in which the pairs of anions were held (Figure 3.5c). Imidazole based copper complex upon spontaneous desolvation of acetonitrile solvent to provide coordination polymers.[35] In the present case, crystals of the anhydrous form could not be obtained upon heating. The lattice had laterally embraced enclosures of anthracenyl groups encapsulating two $[Cu(26pdc)_2]^{2-}$ anions (Figure 3.5c) within each void. A view along *b*-crystallographic axis showed these enclosures as channel like arrangements. The anions were encapsulated in these cations embraced channel-like structure. Packing diagram of the **Cu-Int** (**3.6**) showing the encapsulated anions in cationic enclosures is shown in Figure 3.5c. Hirshfeld surface analyses of **3.4**, **3.5** and **3.6** were performed and the respective surfaces are shown in the Figure 3.5d and 3.5f. The red-spots on the surfaces are indicative of the contacts having hydrogen-bonds. The prominent hydrogen bonds could be seen in the Figures indicate the assigned hydrogen bonds in the self-assembly. A view from *bc*-plane showed that the anions were found as pair due to two chelated ligands having chelate-chelate

TH-3622_196122001

stacking. Those stacked ligands of the $[Cu(26pdc)_2]^{2-}$ were separated by a centroid to centroid distance 3.55 Å.

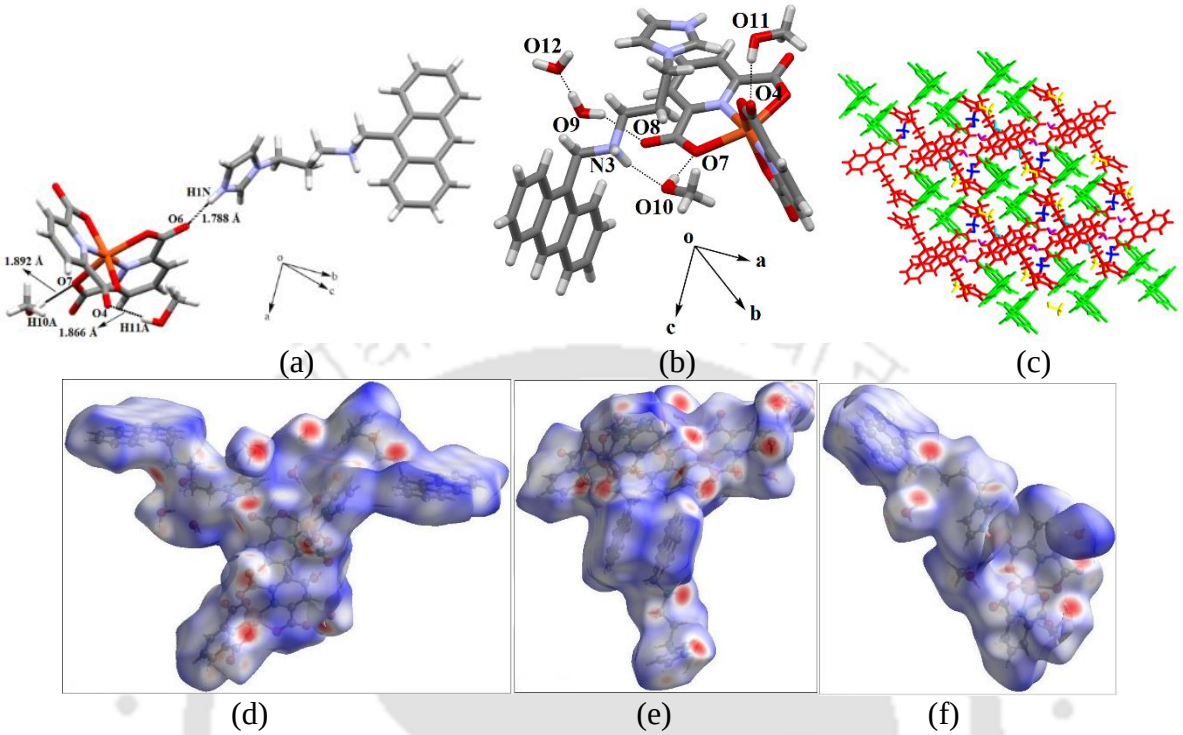

Figure 3.5: (a) The crystal structure of **Cu-Int (3.6)**, showing hydrogen bonds of the anion with methanol molecules and cation, the water molecules are omitted for clarity, (b) The hydrogen bonds of the solvent molecules. (c) The channels in the crystal lattice of **Cu-Int (3.6)** and inclusions of the water and methanol molecules. Hirshfeld diagram of crystal structures of the copper hydrates (d) **Cu-P1** (**3.4**), (e) **Cu-P2 (3.5)** and (f) **Cu-Int (3.6)**.

The intermediate **Cu-Int** (**3.6)** was an assembly of anion encapsulated in a cationic non-covalent enclosure; there are examples of such class of structures reported in literature.[36-37] The channel-like arrangements of non-covalent structures are useful to assemble and disassemble to facilitate ion transport. In our case we found that structure **3.6** was very unstable and turned to π-stacked structure. Accordingly, the loss of methanol solvent molecule, the molecule reorganizes to form stacking among the planar portions of the anions as well as among the cations. This process is favorable as methanol is a low boiling solvent and escapes easily from lattice due by capturing moisture which has higher hydrogen bonding abilities. Attempted synthesis of methanol solvate of the complex by performing crystallization from a solution prepared in dry methanol and in inert atmosphere, was not successful. The polymorph **3.5** had 4.5 water molecules per complex; though crystallography suggests there were 9 molecules per unit cell that has two complex molecules in the unit cell holding them. Theoretically at ambient condition the volume of a molecule of

TH-3622_196122001

methanol is 6.9×10^{-23} cm^3 and volume of a water molecule is 2.98×10^{-23} cm^3. There were 4.5 molecules of water of the polymorph **3.5** (per complex) that has a volume of 12.06×10^{-23}. Whereas, **3.6** has two and half water molecules together with two methanol molecules has a volume 21.25×10^{-23} cm^3. As replacement of methanol by water will require lesser volume, hence replacement of water is possible. Furthermore the water molecules has much higher numbers of hydrogen bond sites of methanol to provide a stable structure. Accordingly, the incorporation of water molecule to expel out the methanol molecules of **3.6** was feasible with a minimal volume change. From earlier research, it is a fact that hydrates having lower amount of water molecules provide channel like structures[38] and we do find a similar aspect having channel-like structure in **3.6**. The structure of **3.6** was also determined at low temperature (120 K, the CCDC No. 2265340), in this case, it had 2.5 water molecules and two methanol molecules in the complex as solvent of crystallization. We could not resolve the crystallographic disorder in the water molecules in the structure. Hence, the structure was solved by squeezing the water molecules and the structure is enclosed as supporting information. There was least change in the unit cell parameters with respect to the unit cell parameters at room temperature, confirming it to be the same structure. These discussions as well as the observations relating to the channel suggested its propensity to form stacked structures through easy loss of the methanol molecules from the channels. The transformation took place by accepting water molecules from solvent (99% methanol) to replace methanol; as the water is a better hydrogen bond forming species than methanol to utilize higher numbers of hydrogen bonds than methanol to provide stability.

3.5. Self-assemblies of different hydrates of zinc complex (3.7-3.8)

Similar to the hydrates of the cobalt and copper complexes, the two hydrates of the zinc complex namely **Zn-Hy1 (3.7)** and **Zn-Int (3.8**) were having extensive hydrogen bonds in their respective assembly. The self-assemblies are shown in the Figure 3.6.

The hydrate **3.7** had two symmetry independent molecules in asymmetric unit, thus had eight water molecules in the asymmetric unit. The water molecules were held as four pairs at different locations and knitted the self-assembly by serving as bridging units. Out of these, the two water molecules were connected to each other by O23-H···O19 {$d_{D\cdots A}$, 2.718(4) Å, <D-H···A 156°} hydrogen bond had served as bridge to hold an anion on one side by O19-H···O2 {$d_{D\cdots A}$, 2.758(7)

TH-3622_196122001

Å, <D-H···A, 167°} and cation by $^{+}$N4-H$_{(imidazole)}$···O23 {$d_{D···A}$, 2.685(5) Å, <D-H···A 165(4)°} (Figure 3.6a), similar water dimer was formed by O21-H···O22 was responsible to hold an anion and a cation by hydrogen bonding at its distal ends. Two other water molecules (O20, O24) were held together by O20-H···O24 provided support to hold two anions at two ends as illustrated in the Figure 3.6a and finally the pair formed by O18-H···O17 hydrogen bond was held intra- and inter-molecularly to anions to strengthen the self-assembly. In the self-assembly of **3.8** the cations were linked to the anions by $^{+}$N3-H···O4$_{carbonyl}$, whereas, the methanol molecule was held to the $^{+}$N-H$_{amine}$ by $^{+}$N-H$_{amine}$···O10 and oxygen atom of carboxylate of neighboring molecule by O10-H···O7 {$d_{D···A}$, 2.764(4) Å, <D-H···A 170°} hydrogen bonds (Figure 3.6b).

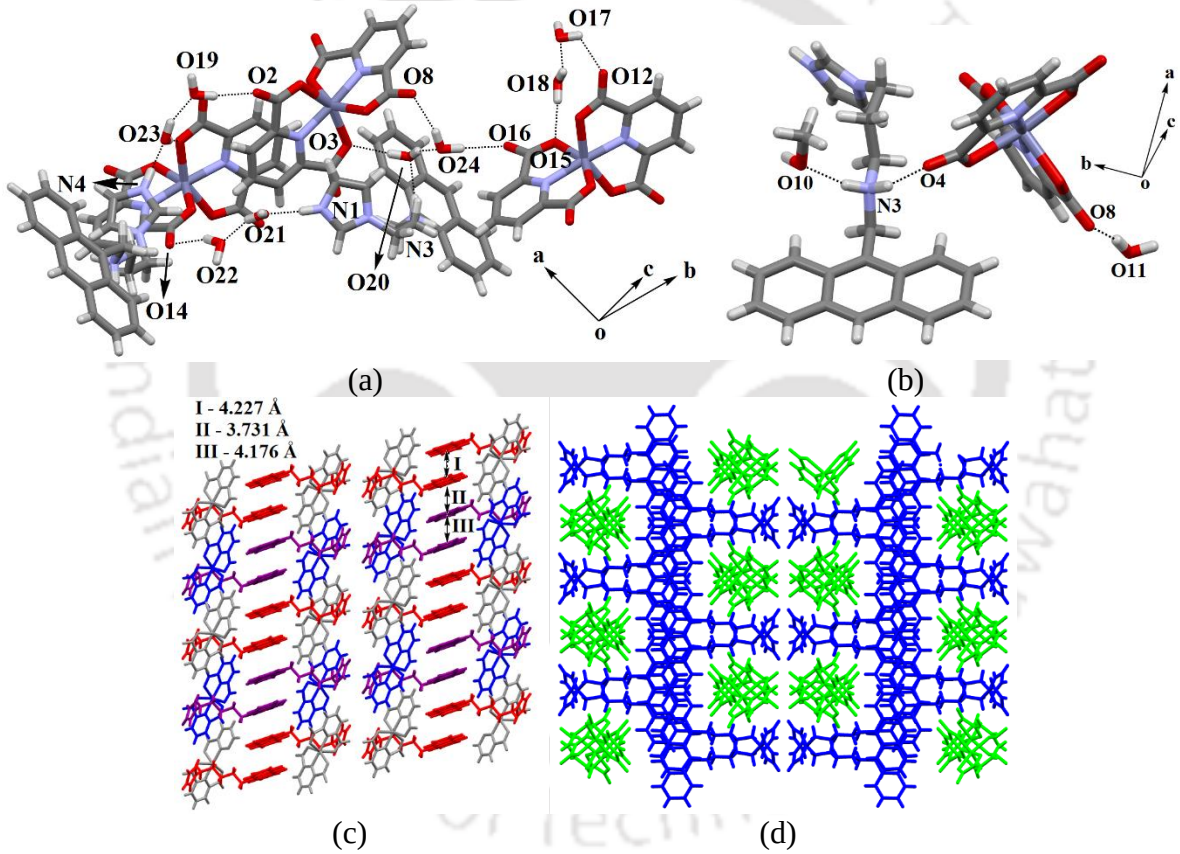

Figure 3.6: Hydrogen-bonded water or methanol molecules in the crystal structures of the zinc hydrates (a) **Zn-Hy1** (**3.7**) and (b) **Zn-Int (3.8)**.The different packing orientations of π-stacks in the hydrates (c) **3.7** along *ac*-crystallographic plane, (d) **3.8** along *bc*-crystallographic plane.

A water molecule was hydrogen bonded to carbonyl oxygen atom by {O(11)–H···O(8), $d_{D···A}$, 2.804(7) Å, <D-H···A 163°}. The hydrogen bond parameters are illustrated are listed in Table A2. The **Zn-Hy1 (3.7)** had a lamellar structure that was similar to the found in one such structures in

TH-3622_196122001

copper and cobalt hydrates. The distances between the planes of anthracenyl rings of the pairs comprising of same symmetry were 4.227 Å and 4.176 Å and between two symmetry different anthracenyl parts was 3.731Å (Figure 3.6c). These distances are comparable to corresponding cobalt complex, but copper complex of similar kind had relatively weaker stacking interactions. On the other hand, the **Zn-Int (3.8)** had a channel like packing along the *bc*-crystallographic plane. The stacking among the anthracenyl units provide chains and the embrace to include chains of anions in relatively large voids and the two sets of independent anions were accommodated in the channels of one void.

3.6. Comparisons of stacking interactions among the hydrates

The hydrates described here of the cobalt (II) complex had a very close structural relation between the corresponding different forms of the copper (II) complex. In the series of hydrates, structure of **Co-Hy1** (**3.1**) was isomorphous to that of the **Cu-P1** (**3.4**) and **Zn-Hy1** (**3.7**) (similarity index, 0.0006).

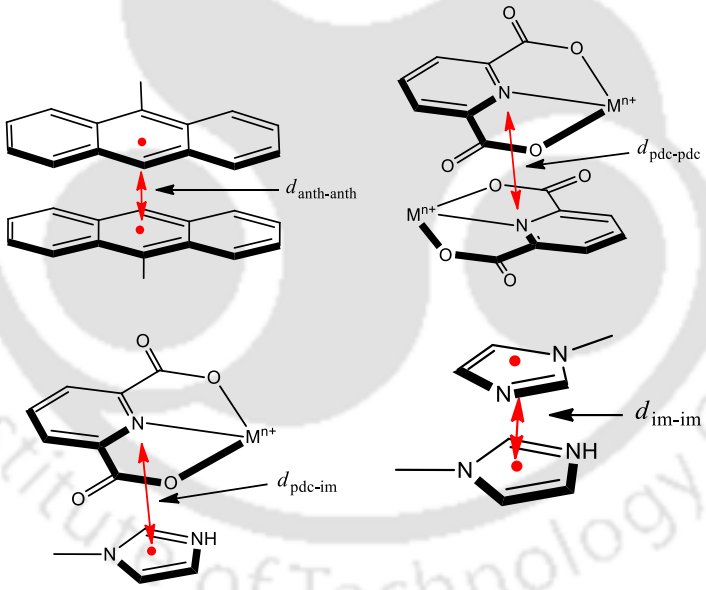

Figure 3.7: Different π-stacks observed in the hydrates.

The cationic as well as anionic parts of the complexes **3.1-3.8** had planar units, namely anthracenyl, imidazole and 2,6-pyridinediarboxylate parts as shown in the Figure 3.7. Each has scope to stack among themselves or form stacks with one another. From the charge point of view, the imidazolium and imidazolium cation would not be favorable, whereas an anthracenyl-anthracenyl stacking will contribute to stability.

TH-3622_196122001

Hence, the centroid to centroid distances of the parallel rings at the closest proximity of four types were found in different hydrates, namely, anthracenyl-anthracenyl ($d_{anthra\text{-}anthra}$), 26pdc-26pdc ($d_{pdc\text{-}pdc}$), 26pdc-imidazolium ($d_{pdc\text{-}im}$) imidazolium-imidazolium ($d_{im\text{-}im}$) illustrated in the Figure 3.7 were examined in each assembly. The observed distances between parallel planar units are tabulated in the Table 3.2. The distances of separation of the stacking listed in Table 3.2 of these hydrates were similar and there were substantial amounts of stacking interactions contributing to their self-assemblies. The lower stability of **Co-Hy2** (**3.2**) than **Co-Hy1** (**3.1**) was supported by the fact that the intermediate **Co-Int** (**3.3**) was transformed only to **Co-Hy1** (**3.1**) but not to **Co-Hy2** (**3.2**). While in case of copper intermediate **Cu-Int** (**3.6**) transforms to **Cu-P2** (**3.5**), showed the higher stability of **Cu-P2** (**3.5**) than **Cu-P1** (**3.4**).

Table 3.2: List of centroid-centroid distances among different parallel rings in the closest vicinity with a referral ring.

Hydrate	$d_{anthra\text{-}anthra}$ (Å)	$d_{pdc\text{-}pdc}$ (Å)	$d_{pdc\text{-}im}$ (Å)	$d_{im\text{-}im}$ (Å)
Co-Hy1 (3.1)	3.763, 4.139, 4.220	3.647, 3.651	4.225, 5.232	_
Co-Hy2 (3.2)	3.805, 4.212, 4.325	3.593, 3.643	4.248, 4.304	4.021
Co-Int (3.3)	4.615	3.565,	3.895	3.561
Cu-P1 (3.4)	3.753, 4.200, 4.392	3.676	4.181, 4.203, 5.229, 5.314	_
Cu-P2 (3.5)	3.803, 4.196, 4.344	3.601, 3.659	4.305, 4.283,	4.113
Cu-Int (3.6)	4.586	_	3.867	3.534
Zn-Hy1 (3.7)	3.731, 4.176, 4.277,	3.647, 3.650	4.233, 5.246	_
Zn-Int (3.8)	6.621	3.710	4.016	3.391

The intermediate **Zn-Int** (**3.8**), had a larger distance among the anthracenyl units ($d_{anthra\text{-}anthra}$) as well as between the chelated *pdc* rings ($d_{pdc\text{-}pdc}$). It had two imidazolium placed in face to face manner, which offered repulsive interactions. The lack of adequate stacking patterns in the **Zn-Int** (**3.8**) had suggested that it was a kinetic product, it underwent facile conversion to **Zn-Hy1** (**3.7**) to have superior π-stackings among the rings.

A comparison among the bond-distances of the coordinated bonds in the anions of the hydrates of the Co, Cu and Zn had showed that the M-N distances were 2.01 Å and 2.02 Å (when M = Co); 1.94 Å and 1.96 Å (when M = Cu) and approximately 2.01 Å (when M = Zn). The differences were insignificant, whereas, the M-O bond distances were 2.12 Å - 2.19 Å (M = Co); 2.08 Å - 2.22 Å (M = Cu) and 2.17Å - 2.25Å (M = Zn), respectively. The order was as per the increasing trend of the ionic radii from Co^{2+} to Zn^{2+} ions. The metal-ligand bond parameters for different hydrates

TH-3622_196122001

are listed in Table A3-A5. The relative degree of distortion from octahedral geometry of the anions of the hydrates were evaluated by calculating the octahedral distortion parameter [39] $\Delta O_h = 1/6\sum[(d_n-d)/d]^2$, where d_n is the nth metal-ligand bond distance and d is the average metal-ligand bond distance. The parameters are listed in Table 3.3. For the hydrates having two symmetry independent anions (**Co-Hy1**, **Co-Hy2**, **Cu-P1**, **Cu-P2** and **Zn-Hy1**) per unit cell, the distortions at both the anions were calculated. Each anion had deviation from an ideal octahedral geometry. The anions of the **Co-Int** and **Co-Hy1** had less deviation from octahedron geometry. On the other hand, the zinc hydrates had showed relatively larger deformation. The polymorphic copper(II) hydrates had larger deviation obviously from Jahn-Teller distortions.

Table 3.3: Relative distortions of the anions from octahedral geometry in different hydrates

Hydrate	ΔO_h (10^{-3})	Hydrate	ΔO_h (10^{-3})	Hydrate	ΔO_h (10^{-3})
Co-Hy1	0.96 and 1.09	**Cu-P1**	3.54 and 4.47	**Zn-Hy1**	1.43 and 1.66
Co-Hy2	1.09 and 1.28	**Cu-P2**	3.79 and 5.75	**Zn-Int**	1.79
Co-Int	1.03	**Cu-Int**	3.19		

The extents of distortions were metal dependent. Hence, one of the possible effects to cause the relative difference of distortions among the anions within the same complexes was from the packing patterns.

3.7. Analysis on the transformation among hydrates by comparison of unit-cells

It is well known fact that during crystal growth changes across a crystallographic plane[40-46] and synthons[47] occur. As an example, 5-methyl-2-[(2-nitrophenyl)amino]-3-thiophenecarbonitrile commonly known as ROY forms large numbers of polymorphs,[48] several forms have counterparts that have double or triple unit cell volume with respect to another one. The occurrence of such unit cell sizes in the polymorphs of ROY is graphically shown in the Figure A1. There are also numbers of examples on polymorphs[49-55] where the ratios of unit-cell volumes are related by integral numbers. There are certain examples of single- or multi-component polymorphs[38,56] where the unit-cell dimensions are as integral multiples. The examples on the changes of one form of unit cell to another in a crystal to crystal transformation by loss of smaller components (which may be

TH-3622_196122001

solvent/gas etc.) are also known.[10,33,57] Thus we examined the unit-cell volumes of each of the hydrates to examine if there is a correlation among them and whether the transformations could be understood in terms of change in one unit cell to another.

The space groups of the three hydrates **Co-Hy1** (**3.1**), **Co-Hy2** (**3.2**), **Co-Int** (**3.3**) were triclinic $P\bar{1}$, monoclinic $P2_1/c$ and triclinic $P\bar{1}$ respectively. The respective unit-cell volumes were 3578.9(11) $Å^3$, 7131.7(19) $Å^3$ and 1936.2(2) $Å^3$, respectively and their ratios were 1.84:3.68:1. Whereas, the ratio of unit cell volumes of **Co-Hy1** (**3.1**), **Co-Hy2** (**3.2**), is 1:1.99 (~2), that means **Co-Hy2** (**3.2**) had a unit-cell volume twice of the unit-cell volume of **Co-Hy1** (**3.1**). The unit-cell of the **Co-Hy1** (**3.1**) had orientations of the anthracenyl units projecting outwards, favorable to form π-stacks to form the combination between two unit cells as shown in the Figure 3.8a. A combination of two unit-cells of the **Co-Hy1** (**3.1**) would provide a new unit-cell with double the volume; that is the unit-cell of **Co-Hy2** (**3.2**). Despite having the conducive arrangement to transform the unit cells of **Co-Hy1** (**3.1**) to the unit-cell of **Co-Hy2** (**3.2**), we did not observe a direct crystal to crystal transformation.

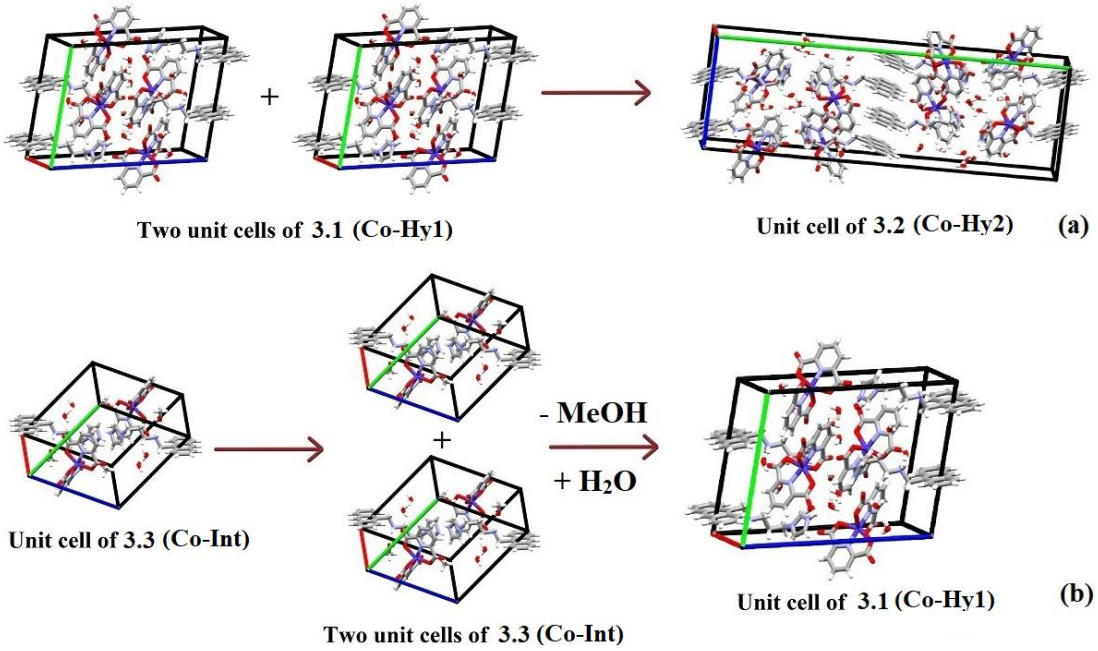

Figure 3.8: Plausible routes for coalescence of unit-cells of different hydrates to provide unit-cell of another hydrate of the cobalt (II) complex causing an effective π-stacking.

This transformation was feasible as triclinic crystal system permitted any angle between the edges, whereas, a monoclinic unit-cell has two axes at right angles to a third axis, which also permits a two-fold rotation or mirror reflection. It is not necessary that a volume change of unit cell occurs

TH-3622_196122001

during the changing of space group such as monoclinic $P2_1/c$ to triclinic $P\bar{1}$. For example, during reversible phase transition observed in the case of 2,6-dichloro-p-benzoquinone no volume change took place.[58] Temperature dependent phase-transition of $Na_3Bi(IO_3)_6$ changes between triclinic $P\bar{1}$ to triclinic P1 occurred by translation increase along *b*-crystallographic axis, which resulted in doubling of volume of unit cell.[59] But we could crystallize from same component in solution but starting with different concentrations of solutions from same volume of solvent, which had suggested that there was a synergy in solution to form one from other. The transformations of two hydrates required changes in the amounts of water molecules and relocation of positions of molecules and also hydrogen bond schemes. Such requirements inhibited direct conversion of these two forms of the crystals of the hydrates. In the unit-cell of the **Co-Int** (**3.3**), the projections of the anthracenyl units were suitable to cause coalescence between two unit-cells to reconstruct another by an approach from the *ab*-crystallographic plane. The crystals of the hydrates **Co-Hy1** (**3.1**) and **Co-Int** (**3.3**) belonged to triclinic $P\bar{1}$ space group, coalescence of two unit-cells of **Co-Int** (**3.3**) with a translation along the c-axis followed by rearrangements of the unit-cell angles and of the other two axes was possible. Hence, a conversion took place by replacing methanol molecules from the unit cell of **Co-Int** (**3.3**) by water molecules, followed by internal adjustment of orientations among the molecules had provided the unit cell of the **Co-Hy1** (**3.1**). Accordingly, while doubling the original unit-cell axes of the **Co-Int** (**3.3**) as well as the angles underwent reorganization, and the unit cell volume corresponded to approximately double from the original one.

The crystals of the **Cu-P1** (**3.4**) belonged to triclinic $P\bar{1}$ space group, whereas the crystals of the **Cu-P2** (**3.5**) belonged to monoclinic $P2_1/c$. The unit cell volume of the polymorphs, **Cu-P1** (**3.4**) had a volume 3631(4) $Å^3$, whereas the **Cu-P2** (**3.5**) had a volume about twice of this, precisely 7170(4) $Å^3$. There was a large difference in the length of the *b*-crystallographic axis, for **Cu-P1** (**3.4**), which was 15.195(10) Å and for **Cu-P2** (**3.5**) it was 41.360(12) Å. Crystal densities of the polymorphs were similar. The **Cu-Int** (**3.6**) was crystallized in triclinic $P\bar{1}$ space group and had a unit cell volume 1877(7) $Å^3$ which was about four times smaller than the respective volume in **Cu-P2**, but about half the volume of the **Cu-P1**. On the other hand, the two symmetry independent molecules in the unit cell of each polymorph were with different torsion angles (Table A7).

TH-3622_196122001

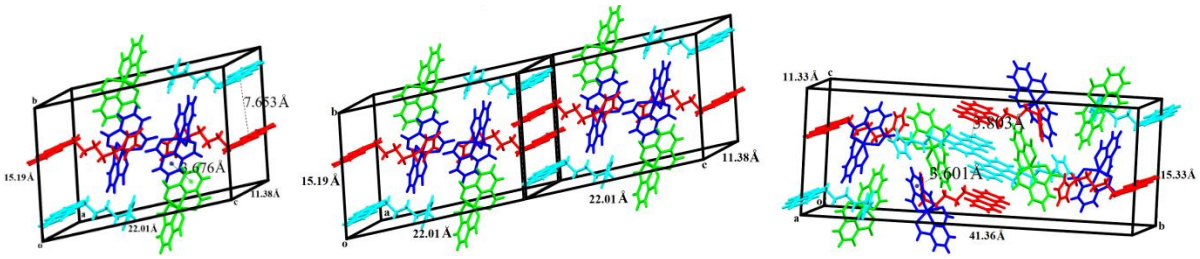

(a) (b) (c)

Figure 3.9: different unit cells to show the doubling of unit cell volume through π-stacking, (a) Unit cell of the **Cu-P1 (3.4)** and (b) Coalescence of *ab*-crystallographic faces of two unit cells of **Cu-P1**, (c) the unit cell of **Cu-P2 (3.5)**.

The **Cu-P1** and **Cu-P2** had same numbers of symmetry independent molecules same compositions but the unit cells were different in space group and volume. The analysis on the unit cell had suggested that once two faces unit cells of **Cu-P1** were overlapped along *ab*-crystallographic plane, it would provide similar packing to the **Cu-P2** (Fig 3.9b). This coalescence would accommodate the required π-stacking among the anthracenyl groups that was present in the **Cu-P2** (Fig 3.9b). In this case, the polymorph **Cu-P1** (triclinic, $P\bar{1}$) got converted to polymorph **Cu-P2** (monoclinic, $P2_1/c$). This was possible because of the symmetry were conducive as discussed in the case of transformations of the hydrates of cobalt complex. The doubling of unit cell volumes occurs in inorganic compounds due to electronic effect[60] and deformation of geometry.[61] Doubling and quadruplet increase in volumes of unit cell among polymorphs without conformational changes of the molecules were reported earlier.[62] We also had reported the extended domain as a factor to enhance unit cell volumes in polymorphic solvates.[63] The evaporation rates of solvents also provide time dependent π-stacks among donors and acceptor molecules,[64] and our results showed this aspect as a new example. In this study, the additional point is on the role of concentration dependence together with time dependence in the formation of the three forms of the complex. Indeed, we observe a similar propensity to form stacks among the planar units. Switching between π-systems from one form to other;[65] their property changes[66] and desolvation leading to isostructural forms[67] are well known. The hydrolysis of ester containing complex in solid state converting to crystalline carboxylate compound was reported by us.[68] In the present case, the formation of the **Cu-P2** from the **Cu-Int** involved very small amount of mass loss, but it caused a change to form new unit cell with about 4-times increase in the unit cell volume from **Cu-Int**, hence it was not a single crystal to single crystal transformation, which was also revealed in real time conversion recorded under microscope.

TH-3622_196122001

The unit-cell volume of **Zn-Int** (**3.8**) (monoclinic, Z = 8) was 3.76 times higher than the unit cell volume of **Zn-Hy1** (**3.7**) (triclinic Z = 4). This difference was apparently from the eight and four molecules of the complexes present in the respective unit-cell. A closer examination had showed that the central portion of the unit cell of **Zn-Int** (**3.8**) had very close similarity to the overall packing arrangements found in the unit-cell of **Zn-Hy1** (**3.7**). Hence, the arrangements of this portion of the unit cell of **Zn-Int** (**3.8**) may be visualized to be a replica content of **Zn-Hy1** (**3.7**) that was covered by additional molecules on the two sides of an embedded unit cell of **Zn-Hy1** (**3.7**) with aid of solvent molecules (Figure 3.10) along the relatively longer *a*-crystallographic axis. Furthermore, the crystals of **Zn-Int** (**3.8**) were belonged to triclinic ($P\bar{1}$) space group, whereas, the crystals of **Zn-Hy1** (**3.7**) were from monoclinic C2/c space group. As for a transformation of the monoclinic space group to triclinic space group the three angles between the unit-cell axes had to reorganize without setting a fixed condition. Hence, the cell reduction from unit cell with Z = 8 to Z = 4 had resulted the transformation (Z is the numbers of molecules in unit cell). The respective reduction by the transformation to the triclinic cell from the monoclinic unit cell involved changes in the α, β, γ angles by ~10°, ~17° and ~1° respectively. During the course of the transformation, the length of the *a*-crystallographic axis of the unit-cell of the parent ($P\bar{1}$) was decreased by four-folds.

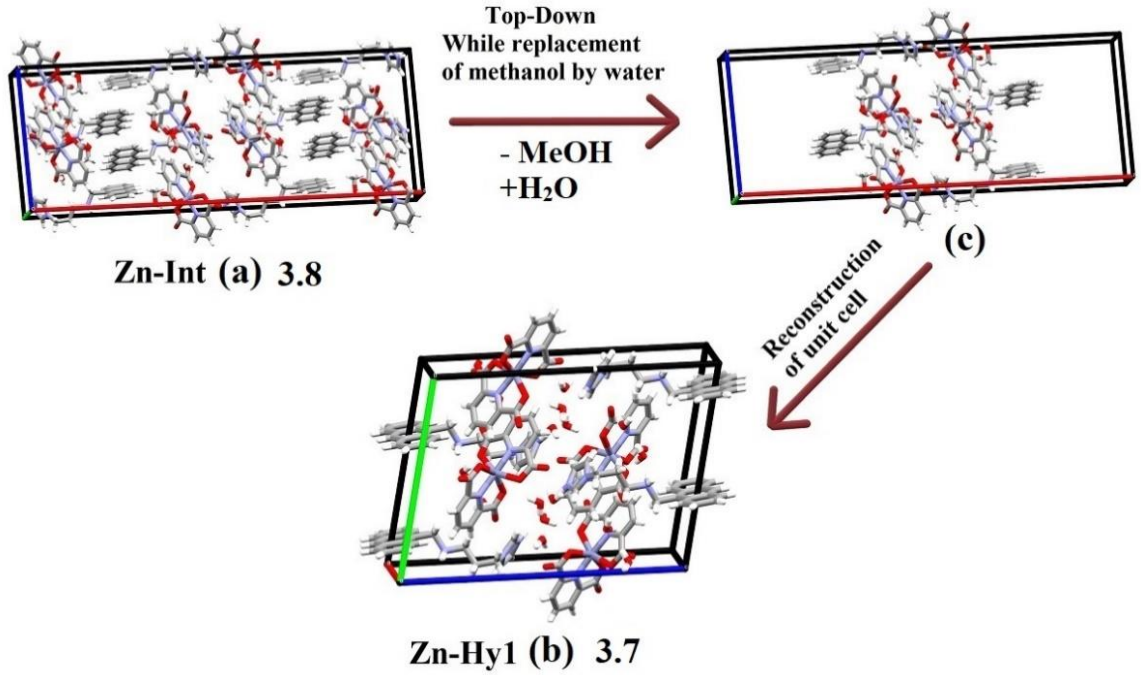

Figure 3.10: Top-down approach from unit-cell of **3.8** to generate unit-cell of **3.7**.

TH-3622_196122001

Thus, this crystallographic axis was affected significantly by the transformation. While this transformation of the unit cell to another unit cell of another space group, unit-cell angles got readjusted. The *b*-axis of the newly formed unit-cell was increased by ~5 Å from the unit cell axis of **Zn-Int** (**3.8**), whereas *c*-axis was shortened by ~6 Å. Thus, a top-down approach by segmenting the outer portions of the unit cell of **Zn-Int** (**3.8**) had provided the unit cell of the **Zn-Hy1** (Figure 3.10). The transformation process may be attributed to the consequence of Ostwald law. The law suggests that a metastable form in a solution transforms to a stable solid phase, and transforms until the most stable state is reached.[69-70] The proposition on the top-down and bottom-up approach of unit-cells are well be applied to other polymorphs found in literature where unit-cells volumes have integral difference. Two such examples namely in the polymorphs of 4-aminobenzoic acid,[71-72] or in gallic acid[73] where doubling of unit cell through a top-down approach were examined are shown in the Appendix (Figure A2 and A3). These transformations were also due to the fact that symmetry relation between the two unit-cells were permissible for the reconstruction of corresponding space-groups and transformations required minimum relocation of the molecules.

3.8. Powder X-ray diffraction study of 3.1-3.8

In the present examples, in each crystallization no co- or post-crystallization was considered, it was necessary to find out the bulk purity of the samples after crystallization, and to provide yield of the individual forms. The powder-X-ray diffraction pattern have shown the phase of the crystalline hydrates were matched with the simulated from the crystallographic information files (CIFs) of the experimentally determined X-ray single-crystal structures. This suggested single phases of the recrystallized products. The powder X-ray diffraction of these hydrates **3.1**-**3.8** are shown in the (Figure A4-A6), it was not easy to get the patterns of the intermediate hydrates **Co-Int** (**3.3**), **Cu-Int** (**3.6**) and **Zn-Int** (**3.8**), a great amount of care and repeated experiments were required to get those patterns in place. When we compared the simulated powder patterns of these complexes with the experimental data, it was confirmed that the experimental diffraction patterns matched the simulated diffraction pattern obtained from single crystal diffraction data, indicating a high purity of the bulk materials.

As illustrative example, the experimentally determined powder XRD of the **Cu-P1** (**3.4**), **Cu-P2** (**3.5**) and **Cu-Int** (**3.6**) are shown in the {a, b and d of Figure 3.11 (i)}. The transformation of **3.6** to **3.5** was reflected in the instantaneously recorded PXRD of the freshly prepared **3.6** {b of Fig

TH-3622_196122001

3.11 (i)}, it had matching peak with the PXRD generated from its CIF, showing only one form in the crystals. Once the PXRD of the same sample was re-recorded {c of Fig 3.11 (i)}, it was found that the PXRD was matching with the PXRD of the **3.5** {d of Fig 3.11 (i)}.

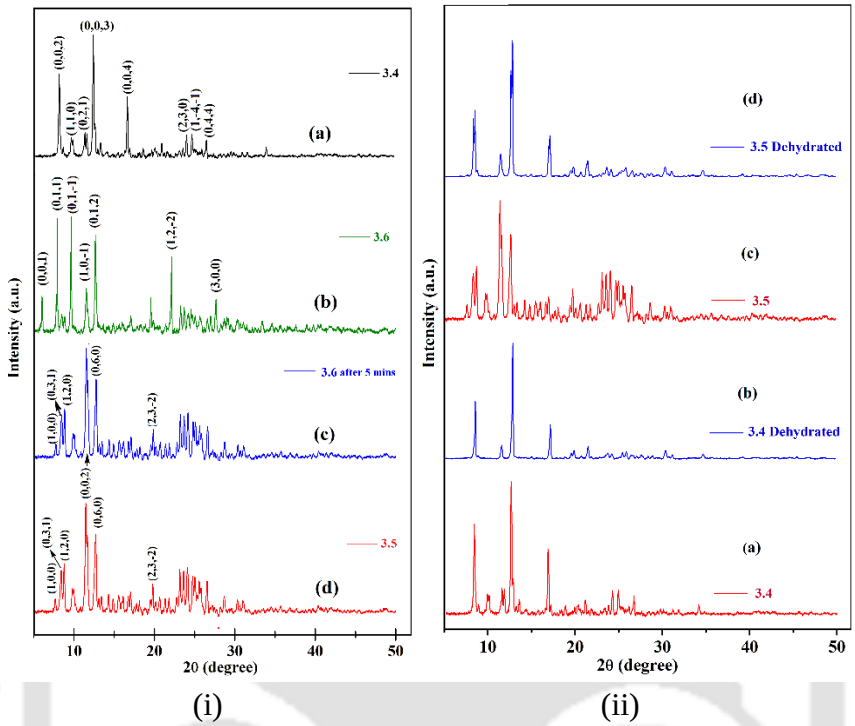

Figure 3.11: (i) PXRD patterns of (a) **Cu-P1**(**3.4**), (b) **Cu-Int** (**3.6**), (c) **3.6** after five minutes and (d) **3.5**; (ii) PXRD patterns of (a) **3.4**, (b) **3.4** after heating at 150 ˚C, (c) **Cu-P1** (**3.5**) and (d) **3.5** after heating at 150˚C.

The textures of the crystals of **Cu-Int** were also changed immediately. This occurred due to the replacements of the methanol molecules from the crystals by incorporation of water molecules. The **3.4** and **3.5** were independently desolvated each by heating at 150 °C for two hours in an oven. The PXRD patterns of both the samples were recorded and both transformed to a common form. It was found that anhydrous form of the **3.4** had similar pattern as that of the **3.5** {Fig 3.11 (ii)}.

3.9. FT-IR spectra of the hydrates

The O-H stretches in each case of cobalt hydrates **Co-Hy1** (**3.1**) and **Co-Hy2** (**3.2**) were observed as broad peak in the range of 3318-3375 cm^{-1} {Figure 3.12 (i)}. The IR spectra of the solvate **Co-Int** (**3.3**) had showed sharp peak at 3368 cm^{-1}. This peak was used as to demarcate the instability of the **3.3** crystals. After five minutes the crystals lose the strong broad absorption at 3368 cm^{-1} {b of Figure 3.12 (i)}, and the IR spectra {c of Figure 3.12 (i)}, showed the peaks of the **3.1**. The IR spectra of the fresh sample of **3.3** had C-H stretches of the methanol at 2944 cm^{-1} and 2826 cm^{-1},

TH-3622_196122001

These peaks had disappeared upon standing and showed a broad peak at 3374 cm^{-1} (ν_{OH}) due to replacement of methanol by water. The IR spectra {a and d of Figure 3.12 (ii)} and the elemental analysis of the **Cu-P1** (**3.4**) and **Cu-P2** (**3.5**) had close resemblances between them. Both the polymorph had the characteristic IR-peaks from the carboxylate of the 26pdc at 1614 - 1619 cm^{-1}.

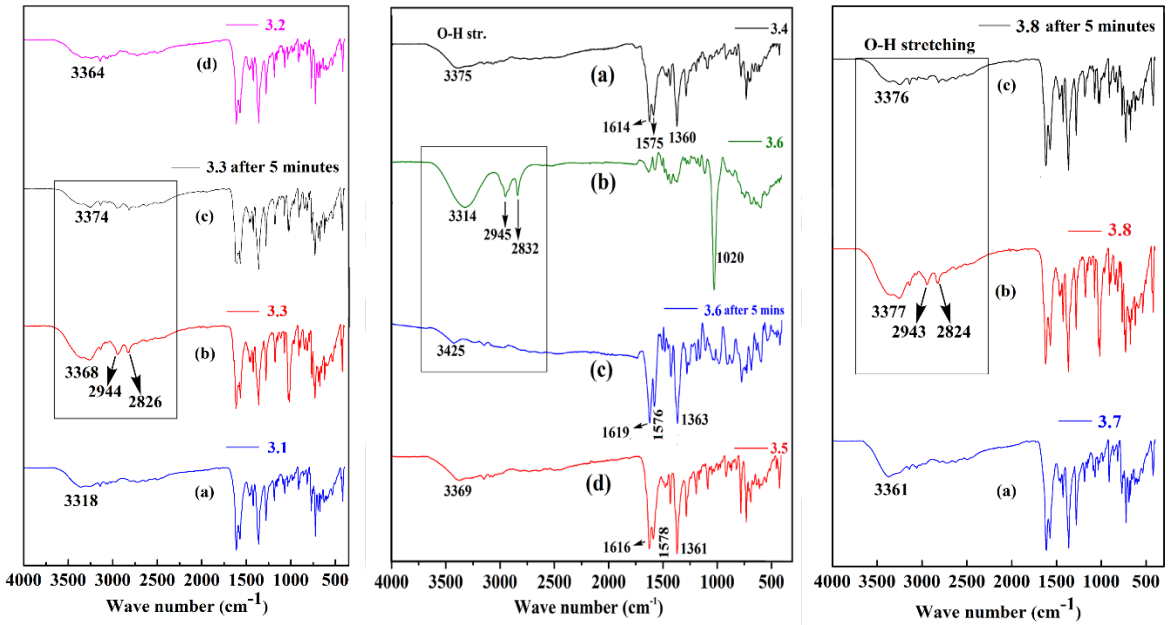

Figure 3.12: IR spectra of different cobalt hydrates **(i)**, copper hydrates **(ii)** and zinc hydrates **(iii)**.

The O-H stretches was observed as broad peak in the range of 3315-3375 cm^{-1}. The IR spectra of the solvate **Cu-Int** (**3.6**) had differences from the polymorphs, it showed sharp peak at 3314 cm^{-1}. This IR-peak was used also used to demarcate the instability of the **3.6** crystals. The crystals after five minutes lose the strong broad absorption at 3314 cm^{-1} {b of Figure 3.12 (ii)}, and the IR spectra {c of Figure 3.12 (ii)}, showed the IR peaks of the polymorph **3.5**. The IR spectra of the fresh sample of **3.6** has the methanol C-H stretches at 2945 cm^{-1} and 2832 cm^{-1} which disappeared upon standing and shows a broad peak at 3425 cm^{-1} (ν_{OH}) due to replacement of methanol by water. Fresh sample of **Zn-Int** (**3.8**) showed a large difference in the O-H stretching region of IR-spectra from spectra of **Zn-Hy1** (**3.7**). The solvate **3.8** had a broad peak for the O-H stretching at 3377 cm^{-1} {b of Figure 3.12 (iii)}. Whereas, in the hydrate **3.7** this O-H stretch was observed as a very weak peak at 3361 cm^{-1} {a of Figure 3.12 (iii)}. The IR spectra of **3.8** recorded after five minutes from a sample taken out from mother liquor, resembled the IR spectra of **3.7** {a of Figure 3.12 (iii)}.

TH-3622_196122001

3.10. TGA and DSC of the hydrates

The thermogram of **Co-Hy1** (**3.1**) had showed 9.14 % weight loss for water molecules around 50°-80°C (Figure 3.13a). This loss of weight was in an agreement with the calculated loss of four water molecules (9.24%). The **Co-Hy2** (**3.2**) had lost the water molecules in two steps, one set of water molecule was lost at 50°-80 °C and other at 100 °C (Figure 3.13b), The overall loss of weight for the water molecules was 10.20 % which tallied with calculated weight loss of 10.28 % for loss of 9 water molecules of the complex.

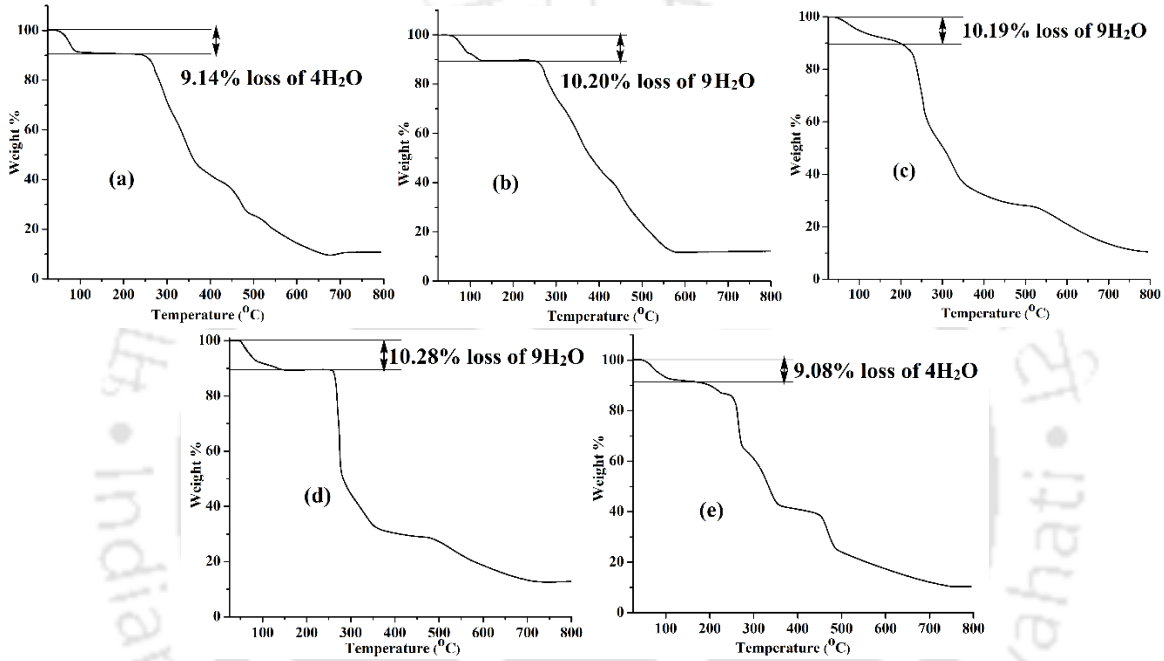

Figure 3.13: Thermogram of (a) **3.1**, (b) **3.2**, (c) **3.4**, (d) **3.5** and (e) **3.7** (heating rate 10°C/min) under nitrogen atmosphere.

The thermogram of **Cu-P1** (**3.4**) showed 10.19 % weight loss for water molecules around 60°-140°C (Figure 3.13c) was in an agreement with the theoretical value calculated for loss of four water molecules (10.22 %). The **Cu-P2** (**3.5**) had lost the water molecules in two steps, one set of water molecule was lost at 50°-100°C and other at 120 °C (Figure 3.13d), The overall loss of weight for the water molecules was 10.28 % which tallies with calculated weight loss of 10.22% for loss of 9 water molecules of the complex. The thermal stability of two polymorphs of copper **3.4** and **3.5** were checked by recording their individual thermogram (c and d of Figure 3.13) and differential scanning calorimetry (DSC) (Figure A7). The weight loss of the water of crystallization observed in thermogram of the polymorphic and the intermediate hydrate of the copper complex were also reflected in the corresponding differential scanning calorimetry {Figure

TH-3622_196122001

A7 (a)}, whereas, the polymorph **Cu-P2** (**3.5**) had lost the water molecules at 104°C {Figure A7 (b)}. The polymorph **3.4** was decomposed above 242°C; and the **Cu-P2** (**3.5**) was decomposed above 264°C.

As the polymorphs were decomposed above 242 °C, DSC plots of the polymorphs of the hydrates of copper complex were recorded between 30° to 120°C (Figure A9), followed by cooling in a cyclic manner. The **3.4** showed broad endothermic peak at 54° - 93°C, whereas, the **3.5** had showed multiple endothermic peaks in the range 60° - 111°C due to loss of water molecules (Figure A7). Both the polymorphs in their respective cooling cycle did not show the original peak observed in the first cycle in this temperature range; showing no absorption of water by the dehydrated sample. The DSC curve of **Cu-Int** (**3.6**) was {Figure A7 (c)} similar to that of the DSC of the **Cu-P2** (**3.5**) {Figure A7 (b)}. The thermogram of **Cu-Int** (**3.6**) showed approximately 13.29 % weight loss, indicating the loss of the two methanol and two and half water molecules {Figure A8 (b)}. To ensure the TG measurement **Cu-Int** (**3.6**), it was conducted at a heating rate of 50 °C/min.

The thermogram of the **Zn-Hy1** (**3.7**) (Figure 3.13e) showed the loss of the four water molecules at 50º - 100°C that corresponded to 9.08 % loss of weight, which was consistent with the calculated value (9.17 %). The water molecules in the complex were in two different environments, this was reflected in the thermogram, the weight loss for the water molecules in the region 50º-100°C was occurred in two independent steps (Figure 3.13e). By examining the crystal structure these steps were attributed, where two water molecules formed hydrogen-bonded cyclic structure, whereas other two discrete water molecules were connected to such dimer at two sides (Figure 3.6a).

3.11. EPR of the copper hydrates

The ESR spectra of **Cu-P1** (**3.4**) had characteristic peaks of perpendicular and parallel component of g_{av} = 2.18 of copper(II) in distorted octahedral geometry (Figure 3.14). The **Cu-P2** (**3.5**) had showed a broad peak for the perpendicular component of g_{av} = 2.21 and the parallel component was not distinct, and the **Cu-Int** (**3.6**) showed peak at g_{av} = 2.19. The ESR peak of the **Cu-Int** (Figure 3.14) observed in fresh sample immediately transformed to show the peak of the polymorph **Cu-P2**. This have showed that the intermediate and polymorphic hydrates had independent ESR signatures and distinguishes each form in solid state.

TH-3622_196122001

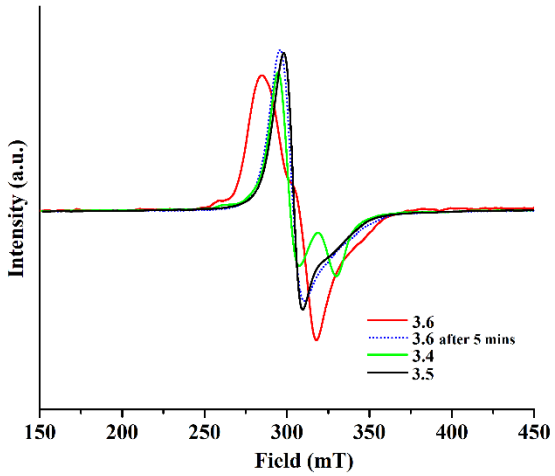

Figure 3.14: Overlaid X-band ESR spectra of the solid samples of **3.4**, **3.5**, **3.6** and **3.6** after five minutes at 297 K.

3.12. Aggregation and emission study

The aggregation behavior of the hydrates in solutions were studied by measuring the average particle sizes by dynamic light scattering (DLS) for the solution of two intermediate hydrates at different concentrations of water in methanol (Figure 3.15a). At higher concentartion of water added, the particle size changes drastically and precipitation occurs. Hence the change in photoluminescence profile can be seen, that is caused by nitrogen atom acting as hydrogen bond donor with water. The **Zn-Int** (**3.8**) had average particle size 2033 nm in pure methanol. Upon addition of water the particle size decreased to reach the size 1175 nm which is close to half of the original size.

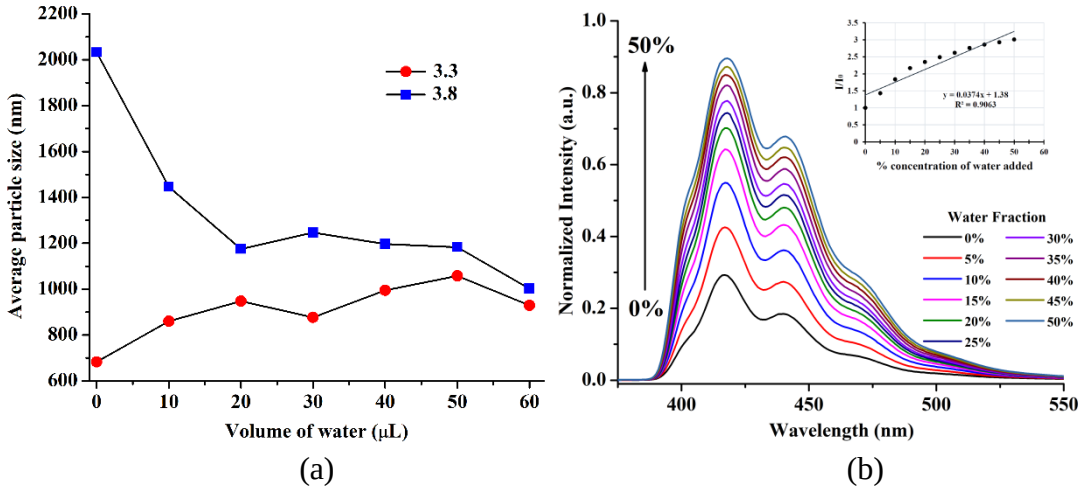

(a) (b)

Figure 3.15: (a) Plot of average particle size measured by dynamic light scattering from solution of **3.3** and **3.8** with different amounts of water (1 mL, 10^{-5}M in methanol upon addition of 10μL of water in aliquots). (b) Spectrofluorimetric titration (excitation at 300 nm) of a solution of **3.8 (**2 mL, 10^{-5}M in methanol) by varying percentage of water in solution from 0-50 % (v/v). Inset is the changes in fluorescence intensity at 415 nm from the titration.

TH-3622_196122001

Then it followed the trend and remained nearly of similar size. In the crystallographic study the unit cell volume of the **Zn-Int** (**3.8**) was twice as that of the **Zn-Hy1** (**3.7**). These trends supported that the **3.8** was transformed to **3.7** through disaggregation. On the other hand, the average particle sizes of the **Co-Int** (**3.3**) was smaller, it was 683 nm. In this case the size was increased by addition of water and increased to 1058 nm (Table A6). Thus, the transformation of **3.3** was through aggregation as observed in the increase in the unit cell volume. The **Zn-Int** (**3.8**) as well as the **Zn-Hy1** (**3.7**) showed similar emission spectra at emission maxima at 436 nm upon excitation at 300 nm. The differences observed in the two cases were in the relative intensities of the peaks and vibrational features seen as three anthracenyl-based emission peaks at 415 nm, 436 nm and 464 nm. The emission peak was assigned to the π*-π transitions based on analogous anthracenyl based peaks observed in the similar wavelengths. Anthracenyl based compounds are well known to show aggregation of the ground state as well as excited state impacting emission spectra.[74]

In the event of latter, a shift in emission peak from the original position of the S_1-S_0 transition was observed. Based on those values, in the present case the solution of zinc hydrates had showed excimer emissions. Upon addition of water to a methanol solution of the **Zn-Int** (**3.8**) (Figure 3.15b) or **Zn-Hy1** (**3.7**) (Figure A10) the emission intensity of those peaks was enhanced without shifting the emission wavelength. The increase in the intensity with concentration of water as illustrated in the inset of the Figure 3.14b could be fitted to a linear plot. The increase in intensity upon water was due to the changes in π-stacks by water, showing an aggregation induced emission enhancement.[11 75] Different hydrates of same compound showing different emissions are reported in literature[94 76] and our present observations are in accordance to such results in a new system but authenticated by study on aggregation and isolated crystalline compounds.

3.13. Conclusions

Concentration dependent crystallization of complexes starting from same volume of solutions of same components had enabled us to isolate and structurally characterize stable as well as metastable hydrates of bivalent zinc and cobalt complexes. Different hydrates were crystallized from same volume of solutions starting with different concentrations; as the time required for super-saturation by slow evaporation to crystallize in each solution was different. Halving of unit cell volume occurred by the transformation of metastable hydrate of zinc complex to provide the

TH-3622_196122001

stable tetrahydrate that had better π-stacks. Whereas, the metastable hydrate of the cobalt complex underwent association of two unit cells. The metastable hydrate of cobalt and zinc complexes were not iso-structural, but once they were converted to corresponding stable tetrahydrate, the tetrahydrates of the two metal complexes were iso-structural. Two polymorphs of copper having lamellar or Herringbone arrangements of the anthracenyl groups were formed under different crystallization conditions due to the propensity to maximize π-stacks among planar anthracene rings. In these examples, the copper-pdc anions served as hinges to the cations in different ways to influence the spatial orientations of the anthracenyl groups deciding the extent of face to face π-stacking among them. The most important aspect observed in this study was the **3.5** having double the unit cell volume that of **3.4** that occurred due to assembling of two unit cells along *ab* crystallographic faces through π-stacking. In this study, the coalescence of two independent unit cells of a polymorph through π-stacking converting to another polymorph is unprecedented and open a new avenue for understanding. This study also have illustrated the fact that assemblies in solution at different concentration could provide crystallization of mixed solvate as intermediate **3.6,** which transformed to **3.5** by replacement of methanol from channel-like enclosures of the **3.6** to maximize hydrogen bonds and π-stacking. The aggregation studies by DLS had provided evidences on the metal ion dependent segregated or aggregated (top-down or bottom-up) assembled particles in methanol upon addition of water. It was also found that as a consequence of aggregation, there was systematic enhancement of emission intensities of the hydrates of the zinc complex. The proposition on top-down and bottom-up building of unit-cells provided an open-ended avenue to understand the assemblies and transformations among hydrates.

3.14. Experimental Section

The instrumental details and crystallographic parameters are provided in Appendix section at the end of this chapter. In the FT-IR spectra, following abbreviations were used to describe strength of the absorption bands: s = strong, w = weak, br = broad, m = medium. Dynamic light scattering (DLS) and photoluminescence studies were done taking 10^{-5} M solution of compounds in methanol administering change in particle size and fluorescence intensity upon addition of 10μL of water in aliquots respectively. The ESR spectra of solid samples of copper hydrates were taken by wrapping it in Teflon tape and putting into ESR tube. The hirshfeld surface diagrams were generated by

TH-3622_196122001

using Crystal Explore software. The thermogravimetric analyses (TGA) were done using silica crucible, while aluminum pans were used for differential scanning calorimetric (DSC) analysis.

[(H$_3$anthraimmida)Co(26pdc)$_2$]·4H$_2$O {**Co-Hy1**} (**3.1**)**:** To a well stirred solution of 2,6-pyridinedicarboxylic acid (33.42 mg, 0.20 mmol) and cobalt(II) acetate tetrahydrate (24.95 mg, 0.10 mmol) in methanol (20 mL), H**anthraimmida** (31.54 mg, 0.10 mmol) was added. The resulting solution was stirred for about 1 hour and kept undisturbed for crystallization, provided the crystals of **3.1**. Isolated yield = 87%. IR (Neat, cm^{-1}): 3318 (br, s), 2723 (w), 1612 (s), 1572 (s), 1464 (m), 1423 (m), 1363 (s), 1307 (w), 1279 (s), 1185 (m), 1158 (w), 1088 (w), 1068 (m), 1034 (w), 982 (w), 912 (m), 858 (w), 816 (m), 769 (m), 723 (s), 692 (m), 673 (m), 681 (w), 627 (m), 601 (w), 534 (w), 417 (s).

[(H$_3$anthraimmida)Co(26pdc)$_2$]·4.5H$_2$O {**Co-Hy2**} (**3.2**)**:** To a well stirred solution of 2,6-pyridinedicarboxylic acid (133.68 mg, 0.80 mmol) and cobalt(II) acetate tetrahydrate (99.80 mg, 0.40 mmol) in methanol (20 mL), H**anthraimmida** (126.16 mg, 0.40 mmol) was added. The resulting solution was stirred for about 12 hours and it resulted in the formation of brown precipitate that was dissolved in 2mL of water and kept undisturbed for crystallization, provided the crystals of **3.2**. Isolated yield = 85%. IR (Neat, cm^{-1}): 3364 (br, s), 3140 (w), 1617 (s), 1571 (s), 1465 (m), 1422 (m), 1361 (s), 1279 (s), 1185 (m), 1158 (w), 1069 (m), 1033 (w), 913 (m), 857 (w), 816 (m), 769 (m), 723 (s), 692 (m), 673 (m), 582 (w), 534 (w), 416 (s).

[(H$_3$anthraimmida)Co(26pdc)$_2$]·2H$_2$O·2CH$_3$OH {**Co-Int}** (**3.3**)**:** To a well stirred solution of 2,6-pyridinedicarboxylic acid (66.84 mg, 0.40 mmol) and cobalt(II) acetate tetrahydrate (49.90 mg, 0.20 mmol) in methanol (20 mL), H**anthraimmida** (63.08 mg, 0.20 mmol) was added. The resulting solution was stirred for about 3 hour and kept undisturbed for crystallization, provided the crystals of metastable hydrate **3.3**. Estimation of yield in this case is not possible as the crystals formed are not stable after removal from solvent. IR (Neat, cm^{-1}): 3368 (br, s), 3285 (br, s), 2944 (s), 2826 (s), 1614 (s), 1567 (s), 1464 (m), 1450 (m), 1423 (m), 1361 (s), 1279 (s), 1177 (m), 1148 (w), 1113 (w), 1028 (m), 1016 (w), 963 (w), 910 (m), 845 (w), 816 (m), 789 (w), 765 (s), 742 (s), 728 (s), 690 (m), 675 (m), 657 (w), 621 (m), 585 (w), 530 (w), 420 (s).

TH-3622_196122001

[(H_3anthraimmida)Cu(26pdc)$_2$]·4.5H_2O {Cu-P1} (3.4): The similar procedure as **3.1** was followed in the synthesis of **3.4**, but copper (II) acetate monohydrate (19.96 mg, 0.10 mmol) was used in the place of cobalt salt. Isolated yield: 80 %. IR (Neat, cm^{-1}): 3375 (br, s), 2723 (w), 1614 (s), 1575 (s), 1464 (w), 1423 (w), 1360 (s), 1309 (m), 1278 (s), 1178 (m), 1108 (w), 1081 (w), 1065 (w), 960 (w), 910(m), 857 (w), 818 (m), 769 (m), 722 (s), 689 (m), 672 (m), 680 (w), 623 (m), 602 (w), 531 (w), 418 (s).

[(H_3anthraimmida)Cu(26pdc)$_2$]·4.5H_2O {Cu-P2} (3.5): The similar procedure as **3.2** was followed in the synthesis of **3.5**, but copper (II) acetate monohydrate (79.84 mg, 0.40 mmol) was used in the place of cobalt salt. Isolated yield: 75 %. IR (Neat, cm^{-1}): 3369 (br, s), 2723 (w), 1615 (s), 1574 (s), 1463 (w), 1420 (w), 1362 (s), 1307 (m), 1277 (s), 1179 (m), 1101 (w), 1082 (w), 1064 (w), 963 (w), 911 (m), 851 (w), 811 (m), 767 (m), 721 (s), 688 (m), 671 (m), 623 (m), 611 (w), 538 (w), 417 (s).

[(H_3anthraimmida)Cu(26pdc)$_2$]·2.5H_2O·2CH_3OH {Cu-Int} (3.6): The similar procedure as **3.3** was followed in the synthesis of **3.6**, but copper (II) acetate monohydrate (39.92 mg, 0.20 mmol) was used in the place of cobalt salt. This compound is as unstable as **3.3**. IR (Neat, cm^{-1}): 3368 (br, s), 3314 (br, s), 2945 (s), 2832 (s), 1621 (m), 1567 (m), 1511 (m), 1450 (m), 1423 (m), 1361 (w), 1148 (w), 1113 (w), 1020 (s), 963 (w), 910 (w), 845 (w), 816 (m), 765 (s), 690 (w), 675 (w).

[(H_3anthraimmida)Zn(26pdc)$_2$]·4H_2O {Zn-Hy1} (3.7): The similar procedure as **3.1** was followed in the synthesis of **3.7,** but zinc (II) acetate dihydrate (21.95 mg, 0.10 mmol) was used in the place of cobalt salt. Isolated yield = 83%. IR (Neat, cm^{-1}): 3361 (br, s), 2723 (w), 1613 (s), 1572 (s), 1451 (w), 1427 (m), 1364 (s), 1279 (s), 1187 (m), 1158 (w), 1088 (w), 1070 (m), 963 (w), 911 (m), 860 (w), 817 (m), 770 (m), 724 (s), 691 (m), 674 (m), 652 (m), 625 (w), 538 (w), 422 (s).

TH-3622_196122001

[(H_3anthraimmida)Zn(26pdc)$_2$]·H_2O·1.5CH_3OH {Zn-Int} (3.8): The similar procedure as **3.3** was followed in the synthesis of **3.8**, but cobalt acetate tetrahydrate was replaced by zinc (II) acetate dihydrate (43.90 mg, 0.20 mmol). This compound is as unstable as **3.3** and **3.6**. IR (Neat, cm^{-1}): 3377 (br, s), 3259 (br, s), 2943 (s), 2824 (s), 1620 (s), 1568 (s), 1465 (3), 1451 (m), 1426 (s), 1367 (s), 1281 (s), 1176 (m), 1149 (w), 1114 (w), 1175 (m), 1028 (s), 1016 (s), 963 (w), 910 (m), 896 (w), 845 (w), 817 (m), 789 (m), 767 (s), 742 (s), 728 (s), 689 (m), 675 (s), 657 (m), 621 (w), 586 (w), 537 (s), 501 (w), 420 (s).

3.15. References

1. J. C. MacDonald, P. C. Dorrestein, M. M. Pilley, M. M. Foote, J. L. Lundburg, R. W. Henning, A. J. Schultz, J. L. Manson, Design of layered crystalline materials using coordination chemistry and hydrogen bonds, *J. Am. Chem. Soc.*, 2000, **122**, 11692–11702.
2. K. Shankar, A. Kirillov, J. B. Baruah, A modular approach for molecular recognition by zinc dipicolinate complexes, *Dalton Trans.*, 2015, **44**, 14411–14423.
3. T. Threlfall, *Crystallisation of polymorphs: thermodynamic insight into the role of solvent*, *Org. Process Res. Dev.*, 2000, **4**, 384–390.
4. A. Berziņs, A. Trimdale-Deksne, S. Belyakov and J. H. ter Horst, *Switching nitrofurantoin polymorphic outcome in solvent-mediated phase transformation and crystallization using solvent and additives*, *Cryst. Growth Des.*, 2023, **23**, 5469–5476.
5. S. Chen, H. Xi and L. Yu, *Cross-nucleation between ROY polymorphs, J. Am. Chem. Soc.*, 2005, **127**, 17439–17444.
6. Y. Yan, B. M. Kariuki, C. E. Hughes, A. J. Logsdail and K. D. M. Harris, *Polymorphism in a multicomponent crystal system of trimesic acid and t-butylamine, Cryst. Growth Des.*, 2020, **20**, 5736–5744.
7. P. K. Thallapally, R. K. R. Jetti, A. K. Katz, H. L. Carrell, K. Singh, K. Lahiri, S. Kotha, R. Boese and G. R. Desiraju, *Polymorphism of 1,3,5-trinitrobenzene induced by a trisindane additive*, *Angew. Chem. Int. Ed. Engl.*, 2004, **43**, 1149–1155.
8. S. Aitipamula, P. S. Chow and R. B. H. Tan, *Dimorphs of a 1:1 cocrystal of ethenzamide and saccharin: solid-state grinding methods result in metastable polymorph, CrystEngComm*, 2009, **11**, 889–895.
9. A. Bajpai, H. S. Scott, T. Pham, K.-J. Chen, B. Space, L. Ma, M. L. Perry and M. J. Zaworotko, *Towards an understanding of the propensity for crystalline hydrate formation by molecular compounds*, *IUCrJ*, 2016, **3**, 430–439.
10. J. S. Costa, S. Rodriguez-Jimenez, G. A. Craig, B. Barth, C. M. Beavers, S. J. Teat and G. Aromi, Three-way crystal-to-crystal reversible transformation and controlled spin switching by a nonporous molecular material, *J. Am. Chem. Soc.*, 2014, **136**, 3869–3874.
11. D. E. Braun, A. Schneeberger, U. J. Griesser, Understanding the role of water in 1,10-phenanthroline monohydrate, *CrystEngComm*, 2017, **19**, 6133 – 6145.

TH-3622_196122001

12. D. N. Sredojević, Z. D. Tomić, S. D. Zarić, Evidence of chelate-chelate stacking interactions in crystal structures of transition-metal complexes, *Cryst. Growth Des.*, 2010, **10**, 3901–3908.
13. (a) F. Yao, J. Y. Wang, J. Pei, Control of π–π stacking via crystal engineering in organic conjugated small molecule crystals, *Cryst. Growth Des.*, 2018, **18**, 7–15. (b) M. Moret, A. Gavezzotti, The crystalline state of rubrene materials: intermolecular recognition, isomorphism, polymorphism, and periodic bond-chain analysis of morphologies, *New J. Chem.*, 2022, **46**, 7626–7637. (c) T. Fukushima, H. Sakamoto, K. Tanaka, Y. Hijikata, S. Irle, K. Itami, Polymorphism of [6] cycloparaphenylene for packing structure-dependent host-guest interaction, *Chem. Lett.*, 2017, **46**, 855–857. (d) C. Lu, Y. Wei, E. Zhu, J. E. Reutt-Robey, B. Xu, Polymorphism in self-assembled structures of 9-anthracene carboxylic acid on Ag(111), *Int. J. Mol. Sci.*, 2012, **13**, 6836–6848. (e) I. H. Park, A. Dey, K. Sasaki, M. Ohba, S. S. Lee, J. J. Vittal, Disappeared supramolecular isomer reappears with perylene guest, *IUCrJ*, 2020, **7**, 324 – 330.
14. (a) C. R. Martinez and B. L. Iverson, Rethinking the term "pi-stacking", *Chem. Sci.*, 2012, **3**, 2191–2201. (b) C. Janiak, A critical account on π–π stacking in metal complexes with aromatic nitrogen-containing ligands, *J. Chem. Soc. Dalton Trans.*, 2000, **3885**, 3885–3896. (c) W. B. Jennings, B. M. Farrell, J. F. Malone, Attractive intramolecular edge-to-face aromatic interactions in flexible organic molecules, *Acc. Chem. Res.*, 2001, **34**, 885–894. (d) P. Bora, B. Saikia, B. Sarma, Regulation of π···π stacking interactions in small molecule cocrystals and/or salts for physiochemical property modulation, *Cryst. Growth Des.*, 2018, **18**, 1448–1458. (e) J. H. Deng, J. Juo, Y. L. Mao, S. Lai, Y. -N. Gong, C. Zhong, T. -B. Lu, π-π stacking interactions: Non-negligible forces for stabilizing porous supramolecular frameworks, *Sci. Adv.*, 2020, **6**, eaax9976. (f) S. E. Wheeler, J. W. G. Bloom, Toward a more complete understanding of noncovalent interactions involving aromatic rings, *J. Phys. Chem. A*, 2014, **118**, 6133–6147. (g) R. Thakuria, N. K. Nath, B. K. Saha, The nature and applications of π–π interactions: A perspective, *Cryst. Growth Des.*, 2019, **19**, 523–528. (h) A. Guijarro, J. A. Verges, E. San-Fabian, G. Chiappe, E. Louis, Herringbone pattern and CH-π bonding in the crystal architecture of linear polycyclic aromatic hydrocarbons, *ChemPhysChem*, 2016, **17**, 3548–3557.
15. (a) G. B. McGaughey, M. Gagne, A. K. Rappe, π-Stacking interactions, alive and well in proteins, *J. Biol. Chem.*, 1998, **273**, 15458–15463. (b) E. T. Kool, Hydrogen bonding, base stacking, and steric effects in DNA replication, *Ann. Rev. Biophys. Biomol. Struct.*, 2001, **30**, 1–22. (c) T. Chen, M. Li, J. Liu, π–π stacking interaction: A nondestructive and facile means in material engineering for bio-applications, *Cryst. Growth Des.*, 2018, **18**, 2765–2783. (d) V. R. Cooper, T. Thonhauser, A. Puzder, E. Schroder, B. I. Lundqvist, D. C. Langreth, Stacking interactions and the twist of DNA, *J. Am. Chem. Soc.*, 2008, **130**, 1304–1308. (e) R. Iwaura, H. Yui, Y. Someya, M. O. Kameyama, Construction of energy transfer pathways self-assembled from DNA-templated stacks of anthracene, *J. Photochem. Photobio. B: Bio.*, 2014, **130**, 199–204. (f) E. A. Meyer, R. K. Castellano, F. Diederich, Interactions with aromatic rings in chemical and biological recognition, *Angew. Chem., Int. Ed.*, 2003, **42**, 1210–1250. (g) J. Dhar, D. P. Karothu, S. Patil, Herringbone to cofacial solid state packing via H-bonding in diketopyrrolopyrrole (DPP) based molecular crystals: influence on charge transport, *Chem. Commun.*, 2015, **51**, 97–100.
16. (a) M. D. Curtis, J. Cao, J. W. Kamp, Solid-state packing of conjugated oligomers: From π-stacks to the herringbone structure, *J. Am. Chem. Soc.*, 2004, **126**, 4318–4328. (b) C. Sutton, C. Risko, J. -L. Brédas, Noncovalent intermolecular interactions in organic electronic materials: implications for the molecular packing vs electronic properties of acenes, *Chem. Mater.*, 2016, **28**, 3–16. (c) D. A. M. Egbe, S. Turk, S. Rathgeber, F. Kuhnlenz, R. Jadhav, A. Wild, E. Birckner, G.

TH-3622_196122001

Adam, A. Pivrikas, V. Cimrova, G. Knor, N. S. Sariciftci, H. Hoppe, Anthracene based conjugated polymers: Correlation between π−π-stacking ability, photophysical properties, charge carrier mobility, and photovoltaic performance, *Macromolecules*, 2010, **43**, 1261–1269. (d) J. Gierschner, J. Shi, B. Milian-Medina, D. Roca-Sanjuan, S. Varghese, S. Y. Park, Luminescence in crystalline organic materials: from molecules to molecular solids, *Adv. Opt. Mater.*, 2021, **9**, 2002251. (e) D. Hashizume, M. Nakano, T. Ogaki, H. Takenaka, K. Kawabata, K. Takimiya, "Disrupt and induce" intermolecular interactions to rationally design organic semiconductor crystals: from herringbone to rubrene-like pitched π-stacking, *Chem. Sci.*, 2020, **11**, 1573–1580. (f) V. Bhat, G. Gopan, N. G. Nair, M. Hariharan, γ-Herringbone polymorph of 6,13-bis(trimethylsilylethynyl)pentacene: A potential material for enhanced hole mobility, *Chem. Eur J.*, 2018, **24**, 8679–8685.
17. W. L. Jorgensen, D. L. Severance, Aromatic-aromatic interactions: Free energy profiles for the benzene dimer in water, chloroform, and liquid benzene, *J. Am. Chem. Soc.*, 1990, **112**, 4768–4774.
18. A. J. Neel, M. J. Hilton, M. S. Sigman, F. D. Toste, Exploiting non-covalent π interactions for catalyst design, *Nature*, 2017, **543**, 637–646.
19. (a) D. L. Reger, A. Debreczeni, B. Reinecke, V. Rassolov, M. D. Smith, F. R. Semeniuc, Highly organized structures and unusual magnetic properties of paddlewheel copper(II) carboxylate dimers containing the π−π stacking, 1,8-naphthalimide synthon, *Inorg. Chem.*, 2009, **48**, 8911–8924. (b) Y. Tsuji, K. Okazawa, K. Kurino, K. Yoshizawa, Topology dictates magnetic and conductive properties of a π-stacked system: insight into possible coexistence of magnetic and conductive systems, *J. Phys. Chem. C*, 2022, **126**, 3244–3256. (c) J. Huang, M. Kertesz, Intermolecular covalent π-π bonding interaction indicated by bond distances, energy bands, and magnetism in biphenalenyl biradicaloid molecular crystal, *J. Am. Chem. Soc.*, 2007, **129**, 1634–1643.
20. M. Y. Jin, Q. Zhen, D. Xiao, G. Tao, X. Xing, P. Yu, C. Xu, Engineered non-covalent π interactions as key elements for chiral recognition, *Nat. Commun.*, 2022, **13**, 3276.
21. (a) S. Li, R. Gou, C. Zhang, π−π Stacking in energetic crystals, *Cryst. Growth Des.*, 2022, **22**, 1991–2000. (b) C. Zhang, X. Wang, H. Huang, π-stacked interactions in explosive crystals: Buffers against external mechanical stimuli, *J. Am. Chem. Soc.*, 2008, **130**, 8359–8365. (c) R. Bu, Y. Xiong, C. Zhang, π–π Stacking contributing to the low or reduced impact sensitivity of energetic materials, *Cryst. Growth Des.*, 2020, **20**, 2824–2841.
22. (a) C. Zhang, J. Cheng, Q. Wu, S. Hou, S. Feng, B. Jiang, C. J. Lambert, X. Gao, Y. Li, J. Li, Enhanced π–π stacking between dipole-bearing single molecules revealed by conductance measurement, *J. Am. Chem. Soc.*, 2023, **145**, 1617–1630. (b) Y. Wang, L. Hu, R. J. Staples, S. Pang, J. M. Shreeve, Highly selective nitroamino isomerization guided by proton transport dynamics: Full-nitroamino imidazole[4,5-d]pyridazine fused-ring system, *ACS Appl. Mater. Interfaces*, 2022, **14**, 52971–52978. (c) M. Dharmarwardana, B. M. Otten, M. M. Ghimire, B. S. Arimilli, C. M. Williams, S. Boateng, Z. Lu, G. T. McCandless, J. J. Gassensmith, M. A. Omary, Strong π-stacking causes unusually large anisotropic thermal expansion and thermochromism, *PNAS*, 2021, **118**, e2106572118.
23. G. Nichols, *Sedimentology and Stratigraphy* (2nd ed.), John Wiley and Sons, 2009, p. 168.
24. P. Talukdar, G. Bollot, J. Mareda, N. Sakai, S. J. Matile, Synthetic ion channels with rigid-rod π-stack architecture that open in response to charge-transfer complex formation, *J. Am. Chem. Soc.*, 2005, **127**, 6528–6529.

TH-3622_196122001

25. M. Donoshita, Y. Yoshida, M. Hayashi, R. Ikeda, S. Tanaka, Y. Yamamura, K. Saito, S. Kawaguchi, K. Sugimoto, H. Kitagawa, Various stacking patterns of two-dimensional molecular assemblies in hydrogen-bonded cocrystals: Insight into competitive intermolecular interactions and control of stacking patterns, *Angew. Chem. Int. Ed.*, 2021, **60**, 22839–22848.
26. G. A. Breault, C. A. Hunter, P. C. Mayers, Influence of solvent on aromatic interactions in metal tris-bipyridine complexes, *J. Am. Chem. Soc.*, 1998, **120**, 3402-3410.
27. (a) Y. Liu, K. Liu, Z. Wang, X. Zhang, Host-enhanced π–π interaction for water-soluble supramolecular polymerization, *Chem. Eur. J.*, 2011, **17**, 9930–9935. (b) S. Kohmoto, R. Tsuyuki, Y. Hara, A. Kaji, M. Takahashi, K. Kishikawa, Dual-mode of assembly of anthracene-based imidazolium salts both in non-polar organic solvents and in aqueous solution, *Chem. Commun.*, 2011, **47**, 9158–9160.
28. (a) M. J. Rashkin, M. L. Waters, Unexpected substituent effects in offset π–π stacked interactions in water, *J. Am. Chem. Soc.*, 2002, **124**, 1860–1861. (b) H. J. Cho, S. W. Kim, S. Kim, S. Lee, J. Lee, Y. Cho, Y. Lee, T. W. Lee, H. J. Shin, C. Song, Suppressing π–π stacking interactions for enhanced solid-state emission of flat aromatic molecules via edge functionalization with picket-fence-type groups, *J. Mater. Chem., C*, 2020, **8**, 17289–17296. (c) Z. Y. Chen, Q. L. Hong, H. X. Zhang, J. Zhang, Induction of chirality in boron imidazolate frameworks: the structure-directing effects of substituents, *Inorg. Chem.*, 2022, **61**, 6861–6868.
29. B. Roy, M. C. Reddy, P. Hazra, Developing the structure–property relationship to design solid state multi-stimuli responsive materials and their potential applications in different fields, *Chem. Sci.*, 2018, **9**, 3592 – 3606.
30. D. P. Malenov, S. D. Zaric, Strong stacking interactions of metal-chelate rings are caused by substantial electrostatic component, *Dalton Trans.*, 2019, **48**, 6328 – 6332.
31. M. Allesøe, F. van Den Berg, C. Cornett, F. S. Joergensen, B. Halling-Soerensen, H. L. De Diego, L. Hovgaard, J. Aaltonen, J. Rantanen, Solvent diversity in polymorph screening, *J. Pharm. Sci.*, 2008, **97**, 2145 – 2159.
32. P. T. Cardew, R. J. Davey, The kinetics of solvent-mediated phase transformations, *Proc. R. Soc. London, Ser. A*, 1985, **398**, 415 – 428.
33. C. D. Wight, Q. Xiao, H. R. Wagner, E. A. Hernandez, E. Martin, V. M. Lynch, B. L. Iverson, Properties in symmetric and asymmetric monoalkoxynaphthalene–naphthalimide donor–acceptor dyads: influence of the alkyl side chain length on the assembly and thermochromic solid-state, *Cryst. Growth Des.*, 2022, **22**, 7363–7373.
34. K. Gholivand, M. Hosseini, A. A. E. Valmoozi, K. Farshadfar, Polymorphism, pseudo-polymorphism, and conformerism in the crystal structure of piperazine-N,N′-bis(N,O-diphenyl phosphoramidate), *CrystEngComm*, 2017, **19**, 2536–2548.
35. X. Wei, S. de Beer and L. J. Barbour, Single-crystal to single-crystal transformation of a 0D Cu(II) metallocycle into a 1D coordination polymer triggered by spontaneous desolvation in mother liquor, *Cryst. Growth Des.*, 2023, **23**, 6258–6262.
36. L. Chen, S. N. Berry, X. Wu, E. N. W. Howe, P. A. Gale, Advances in anion receptor chemistry, *Chem.*, 2020, **6**, 61–141.
37. M. Barboiu, Encapsulation versus self-aggregation toward highly selective artificial K+ channels, *Acc. Chem. Res.*, 2018, **51**, 2711–2718.
38. K. M. Steed and J. W. Steed, Packing problems: high Z′ crystal structures and their relationship to cocrystals, inclusion compounds, and polymorphism, *Chem. Rev.*, 2015, **115**, 2895–2933.

TH-3622_196122001

39. M. E. Fleet, Distortion parameters for coordination polyhedra, *Mineralogical Magazine*, 1976, **40**, 531–533.
40. A. S. Myerson and B. L. Trout, *Nucleation from solution, Science*, 2013, **341**, 855–856.
41. S. L. Price, *Predicting crystal structures of organic compounds, Chem. Soc. Rev.*, 2014, **43**, 2098–2111.
42. X. Li, J. Wang, T. Wang, N. Wang, S. Zong, X. Huang and H. Hao, *Molecular mechanism of crystal nucleation from solution, Sci. China Chem.*, 2021, **64**, 1460–1481.
43. J. V. Parambil, S. K. Poornachary and J. Y. Y. Heng, *Template-induced nucleation for controlling crystal polymorphism: from molecular mechanisms to applications in pharmaceutical processing, CrystEngComm*, 2019, **21**, 4122–4135.
44. R. M. L. Bhardwaj, S. Price, S. L. Price, S. M. Reutzel-Edens, G. J. Miller, I. D. H. Oswald, B. F. Johnston and A. J. Florence, *Exploring the experimental and computed crystal energy landscape of olanzapine, Cryst. Growth Des.*, 2013, **13**, 1602–1617.
45. T. Sakai, K. Katagiri, Y. Uemura, H. Masu, M. Tominaga and I. Azumaya, *Pseudopolymorphism and polymorphic transition behavior of N-(4'-methoxyphenyl)-2-naphthalenesulfonamide, Cryst. Growth Des.*, 2013, **13**, 308–314.
46. Y. Jing, J. Zhang, M. Wan, J. Xue, J. Liu, J. Qin, Z. Hong and Y. Du, *Distinguishing polymorphs of ethenzamide-saccharin cocrystal based on terahertz and Raman vibrational spectroscopic techniques, IEEE Trans. Terahertz Sci. Technol.*, 2024, **14**, 152–161.
47. B. R. Jali and J. B. Baruah, *Polymorphs and hydrates of 2-(1,4-dihydro-1,4-dioxonaphthalen-3-ylthio)benzoic acid, Cryst. Growth Des.*, 2012, **12**, 3114–3122.
48. G. J. O. Beran, I. J. Sugden, C. Greenwell, D. H. Bowskill, C. C. Pantelides and C. S. Adjiman, *How many more polymorphs of ROY remain undiscovered, Chem. Sci.*, 2022, **13**, 1288–1297.
49. C. J. Butler, M. Yoshida, T. Hanaguri and Y. Iwasa, Mottness versus unit cell doubling as the driver of the insulating state in 1T-TaS2, *Nat. Commun.*, 2020, **11**, 2477.
50. D. Andrault, G. Fiquet, M. Kunz, F. Visocekas and D. Hausermann, The orthorhombic structure of iron: an in-situ study at high-temperature and high-pressure, *Science*, 1997, **278**, 831–834.
51. K. Edkins, G. J. McIntyre, C. Wilkinson, V. Kahlenberg, D. Toobbens, U. J. Griesser, J. Bruning and M. U. Schmidt and J. W. Steed, Extensive sequential polymorphic interconversion in the solid state: two hydrates and ten anhydrous phases of hexamidine diisethionate, *Cryst. Growth Des.*, 2019, **19**, 7280-7289.
52. J. Nath and J. B. Baruah, Self-assemblies of hydrates, ionic-cocrystals, and a salt based on 4-{[(4-nitro phenyl)carbamoyl]amino}-N-(pyrimidin-2-yl)benzene-1-sulfonamide: study in the solid and solution states, *Cryst. Growth Des.*, 2021, **21**, 5325–5341.
53. A. L. Grzesiak, M. D. Lang, K. Kim and A. J. Matzger, Comparison of the four anhydrous polymorphs of carbamazepine and the crystal structure of form I, *J. Pharm. Sci.*, 2003, **92**, 2260 – 2271.
54. D. E. Braun, R. M. Bhardwaj, A. J. Florence, D. A. Tocher and S. L. Price, Complex polymorphic system of gallic acid five monohydrates, three anhydrates, and over 20 hydrates, *Cryst. Growth Des.*, 2013, **13**, 19 – 23.
55. J. F. B. Black, P. T. Cardew, A. J. Cruz-Cabeza, R. J. Davey, S. E. Gilks and R. A. Sullivan, Crystal nucleation and growth in a polymorphic system: Ostwald's rule, p-aminobenzoic acid and nucleation transition states, *CrystEngComm*, 2018, **20**, 768 – 776.

TH-3622_196122001

56. S. Aitipamula, P. S. Chow and R. B. H. Tan, Polymorphism in cocrystals: a review and assessment of its significance, *CrystEngComm*, 2014, **16**, 3451 – 3465.
57. M.-M. Liu, Y.-L. Bi, Q.-Q. Dang and X.-M. Zhang, *Reversible single-crystal-to-single-crystal transformation from a mononuclear complex to a fourfold interpenetrated MOF with selective adsorption of CO2, Dalton Trans.*,2015, **44**, 19796 – 19799.
58. R. Destro, E. Sartirana, L. Loconte, R. Soave, P. Colombo, C. Destro, L. Lo Presti, Competing C═O···C═O, C–H···O, Cl···O, and Cl···Cl interactions governing the structural phase transition of 2,6-dichloro-p-benzoquinone at Tc = 122.6 K, *Cryst. Growth Des.*, 2013, **13**, 4571 – 4582.
59. R. Turnbull, J. Gonzalez-Platas, A. Liang, D. Jiang, Y. Wang, C. Popescu, P. Rodriguez-Hernandez, A. Munoz, J. Ibanez and D. Errandonea, Pressure-induced phase transition and band-gap decrease in semiconducting $Na_3Bi(IO_3)_6$, *Results in Physics*, 2023, **44**, 106156.
60. C. J. Butler, M. Yoshida, T. Hanaguri, Y. Iwasa, Mottness versus unit cell doubling as the driver of the insulating state in 1T-TaS2, *Nat. Commun.*, 2020, **11**, 2477.
61. D. Andrault, G. Fiquet, M. Kunz, F. Visocekas, F. Hausermann, The orthorhombic structure of iron: an in situ study at high temperature and high pressure, *Science*, 1997, **278**, 831 – 834. 62. K. Edkins, G. J. McIntyre, C. Wilkinson, V. Kahlenberg, D. Toobbens, U. J. Griesser, J. Bruning, M. U. Schmidt, J. W. Steed, Extensive sequential polymorphic interconversion in the solid state: two hydrates and ten anhydrous phases of hexamidine diisethionate, *Cryst. Growth Des.*, 2019, **19**, 7280 – 7289.
63. J. Nath, J. B. Baruah, Self-assemblies of solvates, ionic-cocrystals, and a salt based on 4-{[(4-nitrophenyl)carbamoyl]amino}-N-(pyrimidin-2-yl)benzene-1-sulfonamide: study in the solid and solution states, *Cryst. Growth Des.*, 2021, **21**, 5325 – 5341.
64. C. Peebles, P. M. Alvey, V. Lynch, B. L. Iverson, Time-dependent solid-state polymorphism of a series of donor–acceptor dyads, *Cryst. Growth Des.*, 2014, **14**, 290 – 299.
65. S. Inoue, K. I. Nikaido, T. Higashino, S. Arai, M. Tanaka, R. Kumai, S. Tsuzuki, S. Horiuchi, H. Sugiyama, Y. Segawa, K. Takaba, S. Maki-Yonekura, K. Yonekura, T. Hasegawa, Emerging disordered layered-Herringbone phase in organic semiconductors unveiled by electron crystallography, *Chem. Mater.*, 2022, **34**, 72 – 83.
66. Y. Abe, V. Savikhin, J. Yin, A. C. Grimsdale, C. Soci, M. F. Toney, Y. M. Lam, Unique reversible crystal-to-crystal phase transition structural and functional properties of fused ladder thienoarenes, *Chem. Mater.*, 2017, **29**, 7686 – 7696.
67. L. Zhou, Q. Yin, S. Du, H. Hao, Y. Li, M. Liu, B. Hou, Crystal structure, thermal crystal form transformation, desolvation process and desolvation kinetics of two novel solvates of ciclesonide, *RSC Adv.*, 2016, **6**, 51037 – 51045.
68. J. Nath, A. Kirillov, J. B. Baruah, Unusual solvent-mediated hydrolysis of dicarboxylate monoester ligands in copper(II) complexes toward simultaneous crystallization of new dicarboxylate derivatives, *RSC Adv.*, 2014, **4**, 47876 – 47886.
69. W. Ostwald, Studien über die Bildung und Umwandlung fester Körper. 1. Abhandlung: Übersättigung und Überkühlung, *Z. Phys. Chem.*, 1897, **22**, 289 – 330.
70. J. F. B. Black, P. T. Cardew, A. J. Cruz-Cabeza, R. J. Davey, S. E. Gilks, R. A. Sullivan, Crystal nucleation and growth in a polymorphic system: Ostwald's rule, p-aminobenzoic acid and nucleation transition states, *CrystEngComm*, 2018, **20**, 768–776.
71. R. A. Sullivan, R. J. Davey, Concerning the crystal morphologies of the α and β polymorphs of p-aminobenzoic acid, *CrystEngComm*, 2015, **17**, 1015 – 1023.

TH-3622_196122001

72. A. J. Cruz-Cabeza, R. Davey, I. J. Iain, D. H. Oswald, M. R. Ward, I. J. Sugden, Polymorphism in p-aminobenzoic acid, *CrystEngComm*, 2019, **21**, 2034 – 2042.
73. D. E. Braun, R. M. Bhardwaj, A. J. Florence, D. A. Tocher, S. L. Price, Complex polymorphic system of gallic acid—five monohydrates, three anhydrates, and over 20 hydrates, *Cryst. Growth Des.*, 2013, **13**, 19 – 23.
74. X. D. Huang, X. F. Ma, T. Shang, Y. Q. Zhang, L. M. Zheng, Photocontrollable magnetism and photoluminescence in a binuclear dysprosium anthracene complex, *Inorg. Chem.*, 2023, **62**, 1864 – 1874.
75. Y. Hong, J. W. Y. Lam and B. Z. Tang, *Aggregation-induced emission: phenomenon, mechanism and applications*, *Chem. Commun.*, 2009, **4332** – 4353.
76. Y. Fan, Y. Zhao, L. Ye, B. Li, G. Yang, Y. Wang, Polymorphs and pseudo-polymorphs of N,N-di(n-butyl)quinacridone: structures and solid-state luminescence properties, *Cryst. Growth Des.*, 2009, **9**, 1421 – 1430.

TH-3622_196122001

Appendix: Chapter 3

Physical Measurements: Infrared spectra of the solid samples were recorded on a Perkin-Elmer Spectrum-Two FT-IR spectrophotometer in the region 4000-400 cm^{-1} using attenuated total reflectance method. Powder X-ray diffraction patterns were recorded using Bruker powder X-ray diffractometer D2 phaser. ^{1}H-NMR spectra of ligands were recorded on a BRUKER Ascend-600 MHz NMR spectrometer using TMS as internal standard. Fluorescence emissions were measured in a Horiba Jobin Yvon Fluoromax-4C spectrofluorometer or Horiba Jobin Yvon Fluoromax-4P spectrofluorometer by taking specified amount of solutions as described in each Figure captions given in the text and exciting at required wavelength. The thermogravimetric analyses were done on PerkinElmer TGA 4000, at a heating rate 10 ℃ per minute under nitrogen gas flow. Dynamic light scattering (DLS) Studies were done using Malvern Zetasizer Nano ZS90. The solvent used were from Merck, EMPLURA® grades. The DSC analyses were done on Mettler Toledo DSC 1 STAR System, under nitrogen gas flow. ESR studies were done using JEOL, JES-FA200 Electron Spin Resonance (ESR) Spectrometer. The optical images on the transformation were done under an optical microscope with magnification 1X at 50 mm resolution. The solvent used were from Merck, EMPLURA® grades, methanol used was 99 %.

Crystallographic Study: The diffraction data for the hydrates were collected by using a Bruker Bruker D8 Quest diffractometer at room temperature for all the crystals, but for crystal of **3.8** data were collected at room temperature as well as at 120K. The refinement of and cell reductions were carried out by using SAINT and XPREP software. Structures were solved by direct methods using SHELXS-97 and were refined by full-matrix least-squares on F^2 using SHELXL-14 and OLEX2 programs. All non-hydrogen atoms were refined in anisotropic approximation against F^2 of all reflections. Hydrogen atoms were placed at their geometric positions by riding and were refined in the isotropic approximation. The crystallographic parameters are listed in the Table A1.

Table A1: Crystallographic parameters of the hydrates **3.1**-**3.8**.

Parameters	**Co-Hy1 (3.1)**	**Co-Hy2 (3.2)**	**Co-Int (3.3)**	**Cu-Hy1 (P1) (3.4)**	**Cu-Hy2 (P2) (3.5)**
Formula	$CoC_{35}H_{37}N_5O_{12}$	$Co_2C_{70}H_{76}N_{10}O_{25}$	$CoC_{37}H_{41}N_5O_{12}$	$Cu_2C_{70}H_{76}N_{10}O_{25}$	$Cu_2C_{70}H_{76}N_{10}O_{25}$
CCDC No.	2291316	2291317	2291315	2250640	2250641

TH-3622_196122001

Mol.wt.	778.62	1575.26	806.68	1584.48	1584.48
Crystal System	Triclinic	Monoclinic	Triclinic	Triclinic	Monoclinic
Space group	$P\bar{1}$	$P2_1/c$	$P\bar{1}$	$P\bar{1}$	$P2_1/c$
a (Å)	11.236(2)	11.229(18)	9.738(6)	11.380(7)	11.338(4)
b (Å)	15.180(3)	41.319(6)	13.904(8)	15.195(10)	41.360(12)
c (Å)	21.958(4)	15.400(2)	14.895(9)	22.011(14)	15.328(5)
α (°)	80.201(5)	90	78.263(2)	79.784(17)	90
β (°)	75.925(5)	91.519(5)	79.452(2)	75.809(17)	94.020(9)
γ (°)	88.858(5)	90	83.793(2)	88.457(18)	90
V ($Å^3$)	3578.9(11)	7131.7(19)	1936.2(2)	3631(4)	7170(4)
Density, gcm^{-3}	1.445	1.467	1.384	1.449	1.468
Abs. coeff., mm^{-1}	0.550	0.554	0.511	0.673	0.682
F (000)	1620	3280	384	1648	3296
Total no. of reflections	12519	12557	6773	12769	12633
Reflections, $I > 2\sigma(I)$	9397	9492	5766	8107	8946
Max. θ/°	25.000	25.000	25.000	24.999	25.000
Ranges (h, k, l)	$-13 \le h \le 13$ $-18 \le k \le 18$ $-26 \le l \le 26$	$-13 \le h \le 13$ $-49 \le k \le 49$ $-18 \le l \le 18$	$-11 \le h \le 11$ $-16 \le k \le 16$ $-17 \le l \le 17$	$-13 \le h \le 13$ $-18 \le k \le 18$ $-26 \le l \le 26$	$-13 \le h \le 13$ $-49 \le k \le 49$ $-18 \le l \le 18$
Complete to 2θ (%)	99.3	99.9	99.3	99.9	99.9
Data / restraints / parameters	12519/0/973	12557/0/991	6773/0/507	12769/0/983	12633/1/986
GooF (F^2)	1.092	1.164	1.105	1.109	1.096
R indices $[I > 2\sigma(I)]$	0.0660	0.0582	0.0605	0.0833	0.0523
wR_2 $[I > 2\sigma(I)]$	0.1390	0.1173	0.1539	0.1713	0.1125
R indices (all data)	0.0936	0.0860	0.0735	0.1391	0.0881
wR_2 (all data)	0.1593	0.1372	0.1676	0.2102	0.1395

Parameters	**Cu-INT (3.6)**	**Cu-Int (120K) (3.6)**	**Zn-Hy1 (3.7)**	**Zn-Int (3.8)**	**Zn-Int (120K) (3.8)**
Formula	$CuC_{37}H_{41}N_5O_{12}$	$Cu\ C_{35}\ H_{29}\ N_5\ O_8$ [+solvent]	$ZnC_{35}H_{37}N_5O_{12}$	$ZnC_{36}H_{35}N_5O_{10}$ [+ solvent]	$ZnC_{36}H_{35}N_5O_{10}$ [+ solvent]
CCDC No.	2250642	2265340	291319	2291318	2291320
Mol.wt.	811.29	711.17	785.06	763.06	763.06
Crystal System	Triclinic	Triclinic	Triclinic	Monoclinic	Monoclinic
Space group	$P\bar{1}$	$P\bar{1}$	$P\bar{1}$	C2/c	C2/c
a (Å)	9.70(2)	9.70(11)	11.252(8)	43.075(4)	42.715(6)
b (Å)	13.71(3)	13.80(15)	15.170(11)	10.485(9)	10.448(14)
c (Å)	14.69(3)	14.71(16)	21.985(16)	15.658(14)	15.502(2)
α (°)	78.23(4)	78.05(4)	80.090(2)	90	90
β (°)	79.74(5)	79.45(4)	75.766(2)	92.545(5)	91.995(3)
γ (°)	83.84(7)	83.37(4)	88.980(2)	90	90
V ($Å^3$)	1877(7)	1891.8(4)	3582.3(4)	7065.4(11)	6914.4(16)
Density, gcm^{-3}	1.435	1.248	1.456	1.435	1.466
Abs. coeff., mm^{-1}	0.652	0.630	0.756	0.761	0.777
F (000)	846	734	1632	3168	3168
Total no. of reflections	6607	7646	12602	6236	8912
Reflections, $I > 2\sigma(I)$	5464	6956	9732	4600	7559
Max. θ/°	25.000	26.323	25.000	24.999	28.726
Ranges (h, k, l)	$-11 \le h \le 11$ $-16 \le k \le 16$ $-17 \le l \le 17$	$-12 \le h \le 12$ $-18 \le k \le 18$ $-19 \le l \le 19$	$-13 \le h \le 13$ $-18 \le k \le 18$ $-26 \le l \le 26$	$-51 \le h \le 51$ $-12 \le k \le 12$ $-18 \le l \le 18$	$-57 \le h \le 57$ $-14 \le k \le 14$ $-20 \le l \le 20$

TH-3622_196122001

Complete to 2θ (%)	99.6	99.4	99.8	99.9	99.6
Data / restraints / parameters	6607/0/500	7646/0/446	12602/0/983	6236/0/478	8912/0/474
GooF (F^2)	1.016	1.049	1.078	1.120	1.071
R indices [I > 2σ(I)]	0.0555	0.0421	0.0451	0.0473	0.0365
wR_2 [I > 2σ(I)]	0.1488	0.1148	0.1116	0.1070	0.0831
R indices (all data)	0.0704	0.0455	0.0657	0.0760	0.0483
wR_2 (all data)	0.1709	0.1166	0.1358	0.1377	0.0927

Table A2: Hydrogen bond parameters of the hydrates.

Hydrate	D-H···A	d_{D-H} (Å)	$d_{H\cdots A}$ (Å)	$d_{D\cdots A}$ (Å)	∠D-H···A (º)
3.1	N(3) –H(3N')...O(16) [x,y,z]	0.89	1.88	2.760(5)	168
	N(1) –H(1N)...O(21) [1-x,1-y,1-z]	0.86	1.83	2.677(6)	166
	N(6) –H(6N')...O(6) [2-x,-y,1-z]	0.89	1.91	2.783(5)	165
	N(3) –H(3N)...O(24) [x,y,z]	0.89	1.93	2.785(5)	161
	N(4) –H(4N)...O(18) [x,y,z]	0.86	1.85	2.692(7)	167
	N(6) –H(6N)...O(22) [1-x,-y,1-z]	0.89	1.93	2.787(5)	162
	O(17) –H(17A)...O(4) [2-x,-y,1-z]	0.99	1.92	2.758(4)	169
	O(17) –H(17B)...O(4) [x,y,z]	0.85	1.96	2.775(4)	159
	O(18) –H(18A)...O(19) [x,y,z]	0.85	1.89	2.721(6)	165
	O(18) –H(18B)...O(7) [x,y,z]	0.85	2.00	2.841(5)	172
	O(19) –H(19A)...O(12) [1-x,1-y,1-z]	0.85	1.92	2.763(5)	170
	O(19) –H(19B)...O(12) [x,y,z]	0.85	1.96	2.769(5)	158
	O(20) –H(20A)...O(10) [-x,1-y,1-z]	0.85	2.10	2.944(6)	176
	O(20) –H(20B)...O(8) [x,y,z]	0.85	2.06	2.863(6)	158
	O(21) –H(21A)...O(13) [x,y,z]	0.85	2.01	2.860(5)	177
	O(21) –H(21B)...O(17) [-1+x,y,z]	0.85	1.89	2.717(5)	166
	O(22) –H(22A)...O(1) [x,y,z]	0.85	1.95	2.798(5)	173
	O(22) –H(22B)...O(20) [x,y,z]	0.85	2.08	2.893(6)	161
	O(24) –H(24A)...O(9) [1+x,y,z]	0.85	1.92	2.764(5)	173
	O(24) –H(24B)...O(23) [x,y,z]	0.85	2.22	3.002(8)	153
3.2	N(1) –H(1)...O(19) x,y,z]	0.86	1.87	2.700(8)	163
	N(3) –H(3A)...O(16) [-1+x,y,z]	0.89	1.89	2.771(4)	168
	N(3) –H(3B)...O(25) [x,y,z]	0.89	1.95	2.811(5)	163
	N(4) –H(4)...O(21) [x,y,1+z]	0.86	2.24	2.959(7)	141
	N(6) –H(6C)...O(23) x,y,z]	0.89	1.92	2.788(5)	164
	N(6) –H(6D)...O(2) [1+x,y,z]	0.89	1.87	2.734(5)	163
	O(17) –H(17A)...O(13) [x,1/2-y,-1/2+z]	0.85	2.05	2.885(5)	166
	O(17) –H(17B)...O(8) [1+x,y,-1+z]	0.85	2.01	2.833(4)	164
	O(18) –H(18A)...O(24) [x,y,z]	0.85	2.00	2.822(6)	161
	O(18) –H(18B)...O(14) [x,y,z]	0.85	1.87	2.712(6)	168
	O(19) –H(19B)...O(20) [x,y,z]	0.85	1.98	2.757(8)	152
	O(20) –H(20B)...O(18) [x,1/2-y,-1/2+z]	0.85	1.89	2.672(8)	153
	O(21)–H(21A)...O(10)[-1+x,1/2-y,-1/2+z]	0.85	1.96	2.785(5)	161
	O(21) –H(21B)...O(7) [x,y,-1+z]	0.85	2.57	3.274(5)	141
	O(22) –H(22A)...O(12) [x,y,z]	0.85	2.01	2.849(5)	169
	O(22) –H(22B)...O(4) [x,y,-1+z]	0.85	2.09	2.893(5)	158
	O(23) –H(23A)...O(22) [x,y,1+z]	0.85	1.98	2.819(5)	172
	O(23) –H(23B)...O(5) [x,y,z]	0.85	1.97	2.814(4)	173
	O(24) –H(24A)...O(6) [x,y,z]	0.85	1.85	2.688(4)	172
	O(24) –H(24B)...O(16) [-1+x,y,z]	0.85	2.03	2.881(4)	176
	O(25) –H(25A)...O(11) [x,y,z]	0.85	1.89	2.742(5)	175

TH-3622_196122001

3.3	N(1) –H(1)...O(8) [-x,1+y,1/2-z]	0.83(6)	1.81(6)	2.607(6)	161(5)
	N(3) –H(3A)...O(2) [1+x,y,z]	0.89	1.92	2.807(4)	172
	N(3) –H(3B)...O(10) [x,y,z]	0.89	1.94	2.787(4)	159
	O(9) –H(9)...O(4) [x,y,z]	0.76(6)	1.97(6)	2.716(5)	167(5)
	O(10) –H(10A)...O(5) [x,y,z]	0.82	1.94	2.756(4)	170
	O(12) –H(12A)...O(11) [x,y,z]	0.85	2.07	2.884(14)	160
3.4	N(1) –H(1N)...O(21) [-x,1-y,1-z]	1.03(11)	1.67(11)	2.686(11)	167(9)
	N(3) –H(3N')...O(10) [1-x,-y,1-z]	0.89	1.88	2.753(8)	165
	N(3) –H(3N)...O(17) [x,-1+y,z]	0.89	1.95	2.823(8)	165
	N(4) –H(4N)...O(19) [1-x,1-y,1-z]	1.02(9)	1.65(9)	2.663(10)	172(7)
	N(6) –H(6N')...O(4) [-1+x,y,z]	0.89	1.88	2.755(7)	168
	N(6) –H(6N)...O(25) [x,y,z]	0.89	1.95	2.811(7)	162
	O(17) –H(17A)...O(18) [x,y,z]	0.86(9)	2.22(9)	2.992(14)	150(8)
	O(17) –H(17B)...O(13) [-x,1-y,1-z]	0.84(9)	2.00(9)	2.815(8)	163(9)
	O(18) –H(18A)...O(12) [-x,1-y,1-z]	0.85	2.16	2.893(13)	144
	O(18) –H(18B)...O(8) [x,y,z]	0.85	2.43	3.219(12)	154
	O(19) –H(19A)...O(20) [x,y,z]	0.85	1.91	2.710(8)	157
	O(19) –H(19B)...O(1) [x,y,z]	0.85	1.97	2.824(8)	176
	O(20) –H(20A)...O(16) [1-x,-y,1-z]	0.85	1.91	2.755(7)	169
	O(20) –H(20B)...O(16) [x,y,z]	0.85	1.98	2.777(7)	156
	O(21) –H(21A)...O(22) [-x,1-y,1-z]	1.00	1.72	2.697(8)	164
	O(21) –H(21B)...O(11) [-x,1-y,1-z]	0.85	2.00	2.805(8)	156
	O(22) –H(22A)...O(6) [1-x,1-y,1-z]	0.82	2.00	2.796(7)	166
	O(22) –H(22B)...O(6) [-1+x,y,z]	0.85	1.93	2.759(7)	163
3.5	N(1) –H(1N)...O(19) [-1+x,1/2-y,1/2+z]	0.86	1.85	2.689(6)	163
	N(3) –H(3N')...O(16) [x,y,z]	0.89	1.88	2.761(4)	168
	N(3) –H(3N)...O(17) [-1+x,y,z]	0.89	1.96	2.823(6)	162
	N(6) –H(6N')...O(6) [x,y,z]	0.89	1.86	2.720(5)	163
	N(6) –H(6N)...O(24) [1+x,y,z]	0.89	1.93	2.803(5)	165
	O(17) –H(17A)...O(9) [x,y,z]	0.85(7)	1.94(6)	2.782(5)	171(5)
	O(18) –H(18A)...O(13) [x,y,z]	0.85	1.99	2.829(4)	170
	O(18) –H(18B)...O(2) [x,1/2-y,1/2+z]	0.85	2.00	2.849(4)	173
	O(19) –H(19B)...O(18) [x,y,z]	0.85	1.97	2.714(6)	145
	O(20) –H(20A)...O(12) [x,y,z]	0.85	2.02	2.807(6)	154
	O(20) –H(20B)...O(21) [x,y,z]	0.85	2.07	2.866(7)	155
	O(21) –H(21A)...O(19) [-1+x,y,z]	0.89(7)	1.84(7)	2.694(7)	161(6)
	O(22) –H(22B)...O(25) [x,y,z]	0.87(8)	1.95(7)	2.814(6)	169(8)
	O(23) –H(23B)...O(10) [x,y,z]	0.85	2.08	2.870(5)	155
	O(24) –H(24A)...O(23) [-1+x,y,-1+z]	0.85	1.96	2.803(5)	169
	O(24) –H(24B)...O(3) [x,y,z]	0.85	2.04	2.864(4)	165
	O(25) –H(25C)...O(4) [x,y,z]	0.85	1.87	2.714(4)	173
	O(25) –H(25D)...O(16) [x,y,z]	0.85	1.98	2.827(4)	171
3.6	N(1) –H(1N)...O(6) [-x,1-y,1-z]	0.86	1.79	2.572(7)	151
	N(3) –H(3N') ...O(2) [1+x,y,z]	0.89	1.91	2.794(7)	172
	N(3) –H(3N) ...O(10) [x,y,z]	0.89	1.92	2.761(7)	158
	O(9) –H(9A)...O(8) [x,y,z]	0.85	2.14	2.819(14)	137
	O(9) –H(9B)...O(12) [x,y,z]	0.85	1.76	2.563(18)	157
	O(10) –H(10A)...O(7) [x,y,z]	0.82	1.89	2.705(7)	171
	O(11) –H(11A)...O(4) [x,y,z]	0.82	1.87	2.697(8)	171
3.7	N(6) –H(6N')...O(10) [x,-1+y,z]	0.89	1.88	2.753(3)	168
	N(1) –H(1N)...O(21) [1-x,1-y,1-z]	0.86	1.84	2.688(5)	167
	N(3) –H(3N')...O(6) [1+x,y,z]	0.89	1.90	2.773(3)	165
	N(3) –H(3N)...O(20) [x,y,z]	0.89	1.94	2.802(3)	161
	N(4) –H(4N)...O(23) [1-x,1-y,1-z]	0.90(5)	1.80(4)	2.685(5)	165(4)
	N(6) –H(6N)...O(18) [1-x,-y,1-z]	0.89	1.94	2.797(4)	160
	O(18) –H(18A)...O(15) [-x,1-y,1-z]	0.85	1.92	2.772(4)	175
	O(18) –H(18B)...O(17) [x,y,z]	0.85	2.20	3.004(6)	157

TH-3622_196122001

	O(19) –H(19A)...O(2) [-x,1-y,1-z]	0.85	1.92	2.758(4)	167
	O(19) –H(19B)...O(2) [x,y,z]	0.85	1.96	2.775(4)	160
	O(20) –H(20A)...O(3) [x,y,z]	0.85	1.95	2.800(3)	173
	O(20) –H(20B)...O(24) [x,y,z]	0.85	2.08	2.907(5)	164
	O(21) –H(21A)...O(22) [x,y,z]	0.85	1.91	2.721(4)	159
	O(21) –H(21B)...O(7) [x,y,z]	0.85	2.01	2.851(4)	172
	O(22) –H(22A)...O(14) [x,-1+y,z]	0.85	1.93	2.767(4)	169
	O(22) –H(22B)...O(14) [1-x,1-y,1-z]	0.85	1.97	2.779(4)	158
	O(23) –H(23A)...O(19) [-x,1-y,1-z]	0.85	1.92	2.718(4)	156
	O(23) –H(23B)...O(11) [x,y,z]	0.85	2.01	2.861(4)	177
	O(24) –H(24A)...O(8) [x,y,z]	0.85	2.04	2.864(4)	162
	O(24) –H(24B)...O(16) [1+x,y,-1+z]	0.85	2.09	2.941(4)	179
3.8	N(1) –H(1)...O(6) [-x,1+y,1/2-z]	0.86(5)	1.80(5)	2.628(4)	164(5)
	N(3) –H(3A)...O(10) [x,1-y,-1/2+z]	0.89	1.96	2.830(4)	167
	N(3) –H(3B)...O(4) [x,-y,-1/2+z]	0.89	1.85	2.709(4)	161
	O(10) –H(10A)...O(7) [x,y,z]	0.82	1.95	2.764(4)	170
	O(11) –H(11A)...O(8) [x,1-y,-1/2+z]	0.85	1.98	2.804(7)	163
	O(11) –H(11B)...O(2) [x,y,z]	0.85	1.95	2.799(7)	162

Table A3: Co-N and Co-O bond distances (Å) in hydrates of the cobalt(II) complex.

3.1		**3.2**		**3.3**	
Co1 – N7	2.021(3)	Co1 – N7	2.027(3)	Co1 – N4	2.014(3)
Co1 – N8	2.022(3)	Co1 – N8	2.025(3)	Co1 – N5	2.020(3)
Co1 – O1	2.155(3)	Co1 – O1	2.157(3)	Co1 – O1	2.128(3)
Co1 – O3	2.159(3)	Co1 – O3	2.165(3)	Co1 – O3	2.125(3)
Co1 – O5	2.156(3)	Co1 – O5	2.138(3)	Co1 – O5	2.190(3)
Co1 – O7	2.169(3)	Co1 – O7	2.148(3)	Co1 – O7	2.166(3)
Co2 – N9	2.023(3)	Co2 – N9	2.020(3)		
Co2 – N10	2.022(3)	Co2 – N10	2.027(3)		
Co2 – O9	2.162(3)	Co2 – O9	2.125(3)		
Co2 – O11	2.148(3)	Co2 – O11	2.169(3)		
Co2 – O13	2.175(3)	Co2 – O13	2.163(3)		
Co2 – O15	2.189(3)	Co2 – O15	2.228(3)		

Table A4: Cu-N and Cu-O bond distances (Å) in hydrates of the copper(II) complex.

3.4		**3.5**		**3.6**	
Cu1 – N7	1.953(5)	Cu1 – N7	1.926(3)	Cu1 – N4	1.938(5)
Cu1 – N8	1.930(5)	Cu1 – N8	1.959(3)	Cu1 – N5	1.965(5)
Cu1 – O5	2.130(4)	Cu1 – O5	2.226(3)	Cu1 – O5	2.222(4)
Cu1 – O7	2.130(5)	Cu1 – O7	2.284(3)	Cu1 – O7	2.257(4)
Cu1 – O1	2.271(5)	Cu1 – O1	2.134(3)	Cu1 – O1	2.101(4)
Cu1 – O3	2.303(5)	Cu1 – O3	2.122(3)	Cu1 – O3	2.088(4)
Cu2 – N9	1.936(5)	Cu2 – N9	1.970(3)		
Cu2 – N10	1.955(5)	Cu2 – N10	1.917(3)		
Cu2 – O13	2.146(5)	Cu2 – O13	2.285(3)		
Cu2 – O15	2.159 (5)	Cu2 – O15	2.370(3)		
Cu2 – O9	2.245(5)	Cu2 – O9	2.114(3)		
Cu2 – O11	2.247(4)	Cu2 – O11	2.076(3)		

TH-3622_196122001

Table A5: Zn-N and Zn-O bond distances (Å) in hydrates of the zinc complex.

3.7		**3.8**	
Zn1 – N7	2.023(2)	Zn1 – N4	2.014(3)
Zn1 – N8	2.021(2)	Zn1 – N5	2.018(3)
Zn1 – O1	2.197(2)	Zn1 – O1	2.175(3)
Zn1 – O3	2.186(2)	Zn1 – O3	2.251(2)
Zn1 – O5	2.200(2)	Zn1 – O5	2.186(3)
Zn1 – O7	2.189(2)	Zn1 – O7	2.193(3)
Zn2 – N9	2.014(2)		
Zn2 – N10	2.026(2)		
Zn2 – O9	2.231(2)		
Zn2 – O11	2.197(2)		
Zn2 – O13	2.188(2)		
Zn2 – O15	2.195(2)		

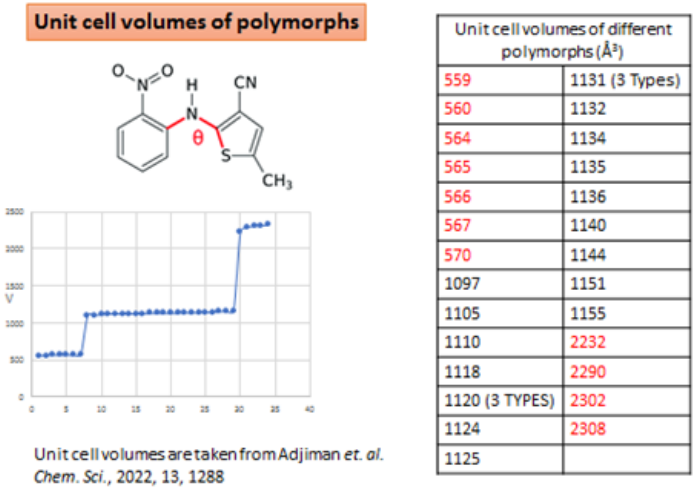

Unit cell volumes of different polymorphs (Å³)	
559	1131 (3 Types)
560	1132
564	1134
565	1135
566	1136
567	1140
570	1144
1097	1151
1105	1155
1110	2232
1118	2290
1120 (3 TYPES)	2302
1124	2308
1125	

Figure A1: A plot of showing different unit cell volumes of different polymorphs of ROY (Data are based on information provided in Chem. Sci., 2022, *13*, 1288-1297 and references therein).

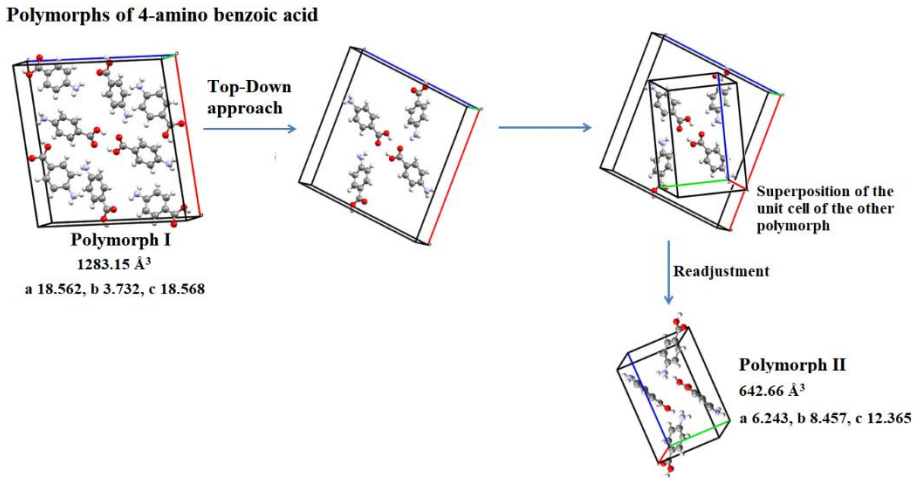

Figure A2: Illustration of top-down approach to generate unit cell contents of a polymorph of 4-aminobenzoic acid from contents unit cell another (the unit cells of the polymorphs analyzed from the CIF files adopted from CrystEngComm, 2015, *17*, 1015-1023 & CrystEngComm, 2018, *20*, 768-776).

TH-3622_196122001

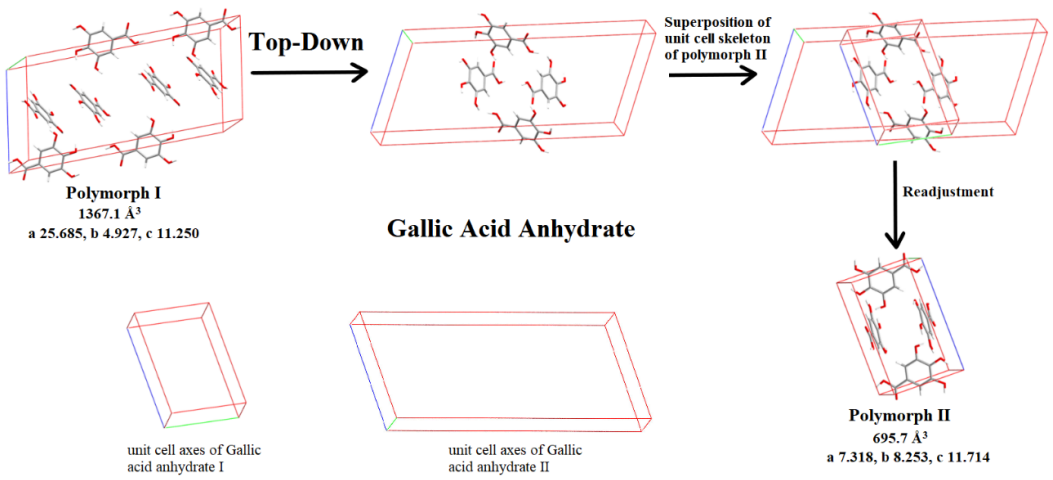

Figure A3: Illustration of a top-down approach to generate from contents of unit cell of a polymorph of gallic acid from unit cell of another form (the unit cells of the polymorphs analyzed from the CIF files adopted from Cryst. Growth Des. 2013, *13*, 19-23).

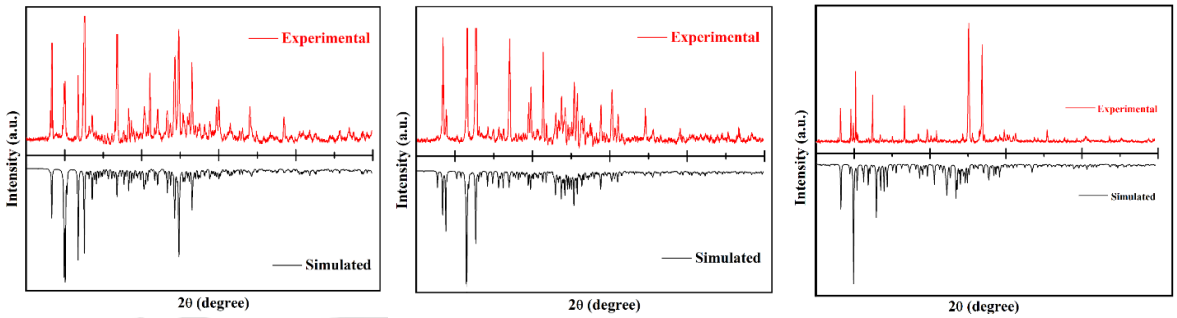

(a) (b) (c)

Figure A4: PXRD plot of (a) **3.1**, (b) **3.2** and (c) **3.3** (Red = Experimental, Black = Simulated). Simulated pattern generated from CIF file ($5^0 \leq 2\theta \leq 50^0$).

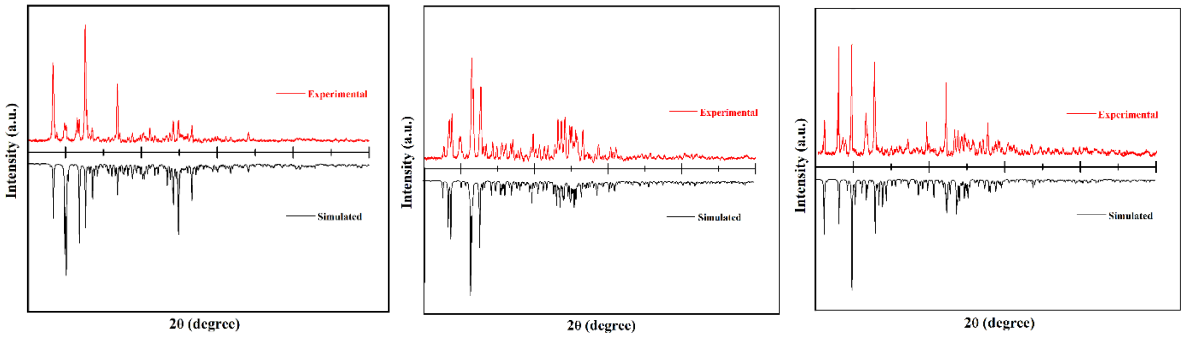

(a) (b) (c)

Figure A5: PXRD plot of (a) **3.4**, (b) **3.5** and (c) **3.6** (Red = Experimental, Black = Simulated). Simulated pattern generated from CIF file ($5^0 \leq 2\theta \leq 50^0$).

TH-3622_196122001

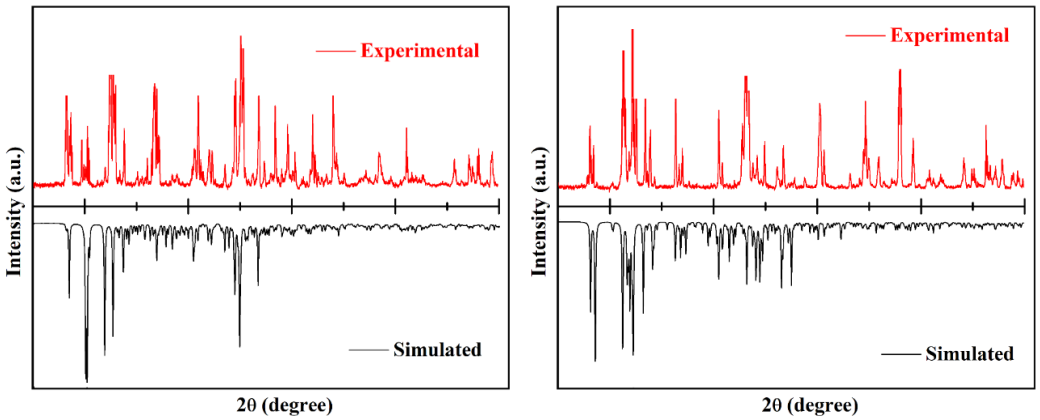

(a) (b)

Figure A6: PXRD plot of (a) **3.7** and (b) **3.8** (Red = Experimental, Black = Simulated). Simulated pattern generated from CIF file ($5^0 \leq 2\theta \leq 50^0$).

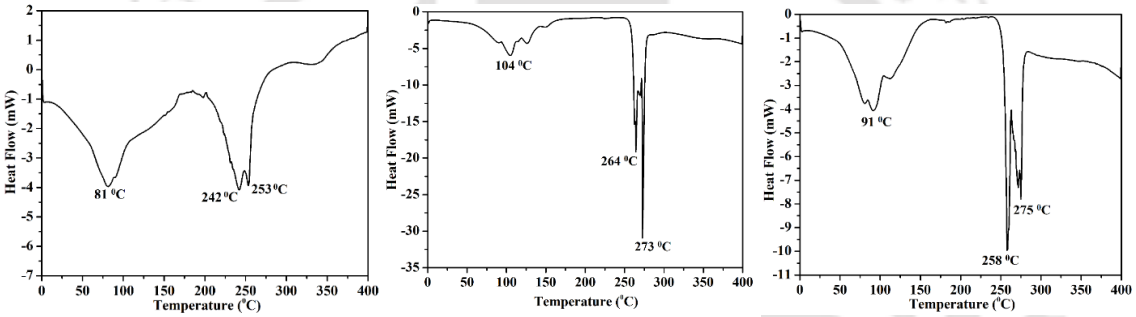

(a) (b) (c)

Figure A7: Differential scanning calorimetry plot of (a) **3.4**, (b) **3.5** and (c) **3.6** (Heating rate 10°C/min under nitrogen atmosphere).

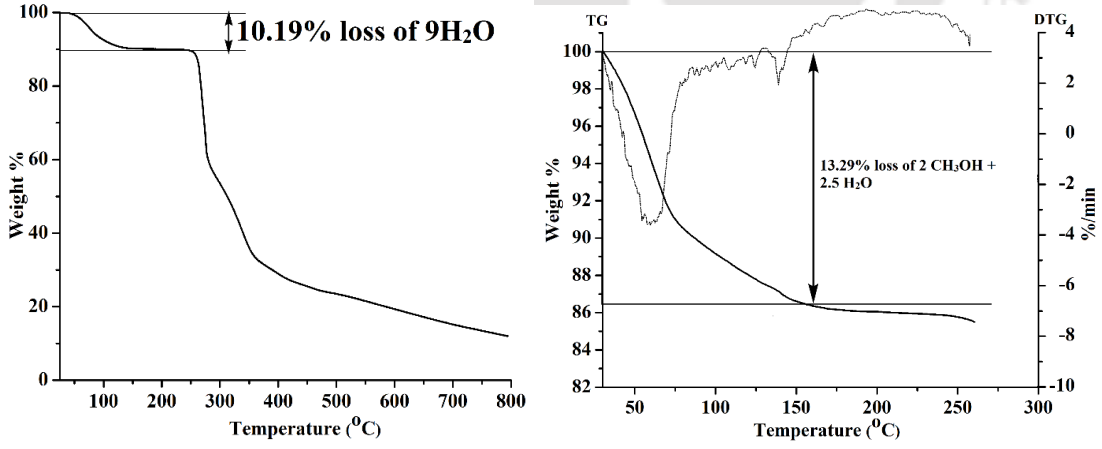

(a) (b)

Figure A8: Thermogram of **3.6**; (a) at heating rate 10°C/min under nitrogen atmosphere and (b) at heating rate 50°C/min under nitrogen atmosphere.

TH-3622_196122001

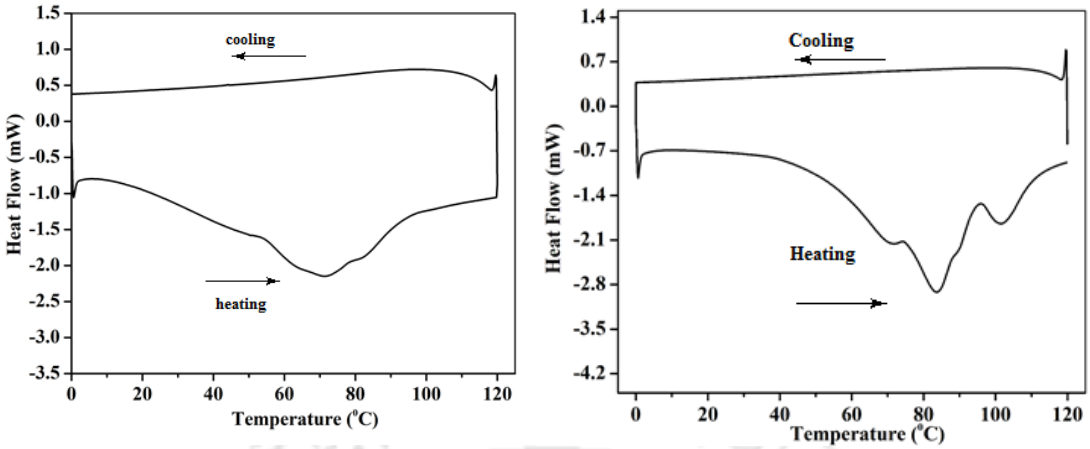

(a) (b)

Figure A9: Differential scanning calorimetry plot of (a) **3.4** and (b) **3.5** (heating and cooling cycle). (Heating rate 5°C/min under nitrogen atmosphere).

Table A6: Diameter of average particle sizes of two intermediates **3.8** and **3.3** in methanol **(**1 mL, 10^{-5}M) and after addition of each aliquot of water (10 µL).

Volume of water added (µL)	Diameter of average particle size (nm)	
	3.8	**3.3**
0	2033 ± 49	683 ± 52
10	1446 ± 87	860 ± 41
20	1175 ± 132	948 ± 22
30	1243 ± 83	877 ± 35
40	1197 ± 82	995 ± 26
50	1183 ± 87	1058 ± 40
60	1002 ± 53	929 ± 29

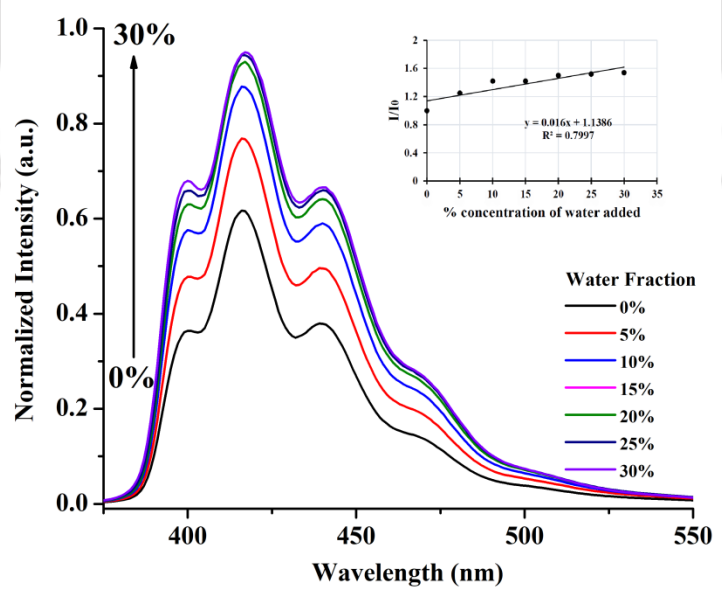

Figure A10: Spectrofluorimetric titration curves of **3.7** (2mL, 10^{-5} M in methanol), spectral changes during addition of 0-30% water. Inset: change in fluorescence intensity at 415 nm after systematic addition of water during titration (excitation at 300 nm).

TH-3622_196122001

Table A7: Torsion angles of the H_3**anthraimmida** present in the **3.4**, **3.5** and **3.6**.

Label of atoms of H_3**anthraimmida** representing torsion	Torsion	Torsion angle (^{0})		
		3.4	**3.5**	**3.6**
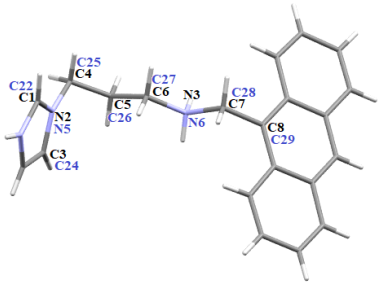	C6-N3-C7-C8	179.7(5)	177.1(3)	176.2(3)
	C5-C6-N3-C7	171.2(5)	171.6(3)	178.1(3)
	C4-C5-C6-N3	177.8(6)	-177.6(3)	-159.4(3)
	N2-C4-C5-C6	-69.4(8)	-65.7(5)	-67.3(4)
	C3-N2-C4-C5	-55.4(10)	-70.9(5)	80.6(5)
	C1-N2-C4-C5	131.5(7)	112.4(4)	-103.8(4)
	C27-N6-C28-C29	177.9(5)	179.4(3)	
	C26-C27-N6-C28	165.9(5)	164.2(4)	
	C25-C26-C27-N6	179.6(5)	164.2(4)	
	N5-C25-C26-C27	-67.0(8)	-71.2(6)	
	C24-N5-C25-C26	-55.9(9)	136.3(5)	
	C22-N5-C25-C26	132.6(7)	-48.1(6)	

TH-3622_196122001

CHAPTER 4

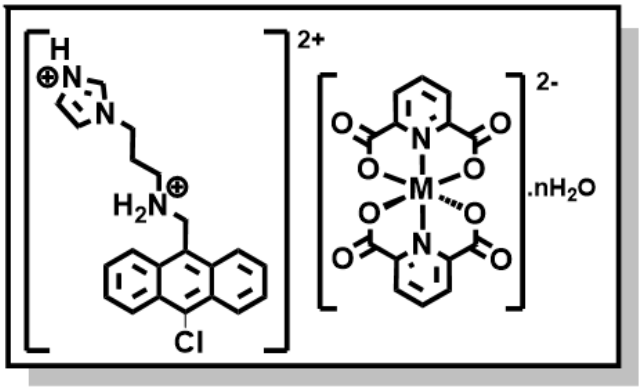

When M = Co, n = 5 (4.1), Monoclinic C2/c
M = Cu, n = 4 (4.3), Monoclinic C2/c
M = Zn, n = 4 (4.4), Monoclinic C2/c

Redesolving

Evaporation of solvent

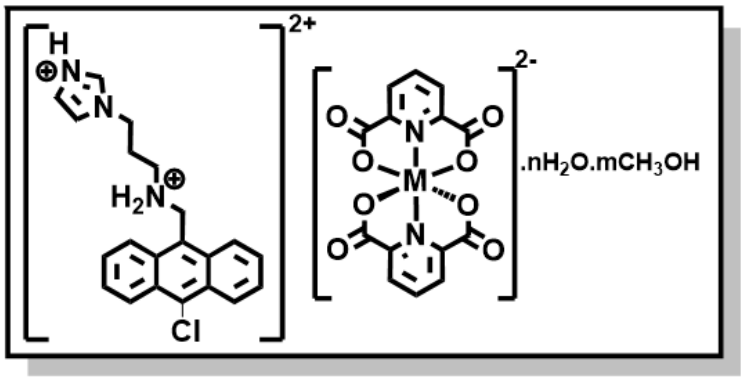

When M = Co; n = 1, m = 1 (4.2), Triclinic P-1
M = Cu; n = 1, m = 1.5 (4.4), Triclinic P-1

TH-3622_196122001

Chapter 4

Hydrates of Chloroanthracene tethered organo-cation and cobalt (II), copper (II) and zinc (II) 2,6-pyridinedicarboxylic acid complexes: reversible crystallization

4.1. Introduction

Based on the results presented in the previous chapter, it was necessary for us to explore the effect of a substituent of the cation on the crystallization of hydrates. For such a purpose we had chosen to study the chloro-substituted analogue N-{(10-chloroanthracen-9-yl)methyl}-3-(1H-imidazol-1-yl)propan-1-amine (abbreviated as **Clanth**), as the substrate to generate the organo-cation of analogous complexes as described in the chapter 3. The incorporation of a covalently linked chlorine atom would expected to provide structure where there will be competition of chlorine atoms in lattice to guide packing patterns and also possible halogen bonds.[1] It was also anticipated that chlorine atoms would occupy specific sites of the lattice and would avoid directly coming close to each other and such effect may allow easy conversion among the hydrates. It was our research endeavor to generate different stacking arrangements among chelate rings in different hydrates of metal-2,6-pyridinedicraboxylate (M-26pdc) with organic cation **Clanth**, which are shown in the Figure 4.1. The M-26pdc anions may guide the assemblies by being present as discrete or in dimeric, trimeric, polymeric forms through chelate-chelate stackings. In fact, these effects could be realized in various hydrates of cobalt, copper and zinc 2,6-pyridinedicarboxylates with organic cation **Clanth**, which were prepared by changing crystallization conditions. The results of these are presented in the following sections.

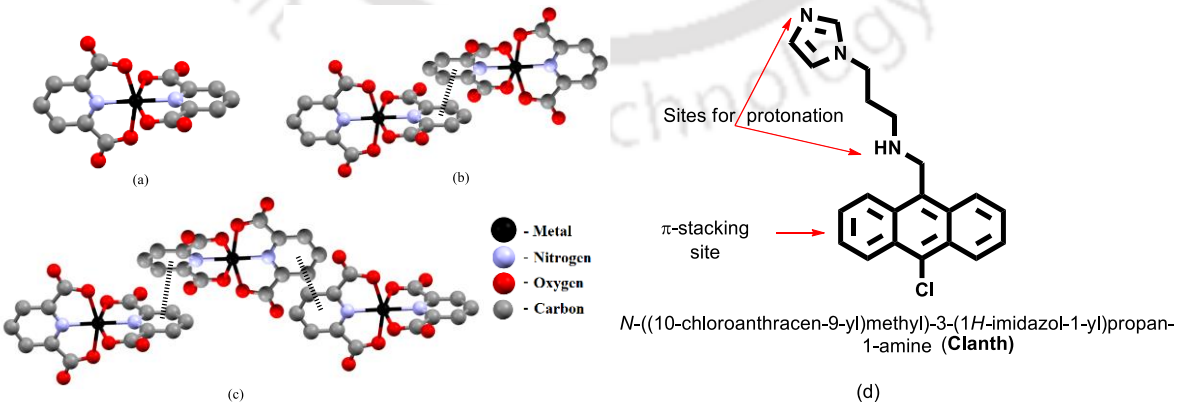

Figure 4.1: (a)-(c) The stacking among metal 2,6-pyridine-carboxylates. (d) The precursor (**Clanth**) of the cationic counterparts of the complexes.

TH-3622_196122001

4.2. Preparation of hydrates of H_2Clanth containing cobalt, copper and zinc 2,6-pyridinedicarboxylates

Different hydrates of bivalent cobalt, copper and zinc 2,6-pyridinedicarboxylate (26pdc) complexes having cation of N-{(10-chloroanthracen-9-yl)methyl}-3-(1H-imidazol-1-yl)propan-1-amine (dication abbreviated as **H_2Clanth**, Figure 4.2) were crystallised by concentration dependent crystallization. The crystals of the hydrates were obtained from closely similar crystallization procedures by varying the concentrations of the components in solution at fixed volume of solvent. The various hydrates prepared in these series were similar to the unsubstituted ones but the numbers of forms of hydrates were lesser in number. Two cobalt hydrates, **[(H_2Clanth)Co(26pdc)$_2$]·H_2O·CH_3OH** {**Co-H_2Clanth-Int**} (**4.1**) and **[(H_2Clanth)Co(26pdc)$_2$]·5H_2O** {**Co-H_2Clanth**} (**4.2**); two copper hydrates **[(H_2Clanth)Cu(26pdc)$_2$]$_2$·2H_2O·3CH_3OH** {**Cu-H_2Clanth-Int**} (**4.3**) and **[(H_2Clanth)Cu(26pdc)$_2$]·4H_2O** {**Cu-H_2Clanth**} (**4.4**) and one form of the zinc complex **[(H_2Clanth)Zn(26pdc)$_2$]·4H_2O** {**Zn-H_2Clanth**} (**4.5**) could be crystallized. Among these hydrates the one abbreviated with **Int**, were unstable and they had methanol along with water as solvent of crystallization. As all the preparations were similar, a typical description on the the crystallization of **Zn-H_2Clanth** is given here and the rest of the crystallization conditions are given in the Table 4.1. For its crystallization powdered solid sample of the **Clanth** (139.68 mg, 0.40 mmol) was added to a well stirred solution of 2,6-pyridinedicarboxylic acid (133.68 mg, 0.80 mmol) and zinc (II) acetate dihydrate (87.80 mg, 0.40 mmol) in methanol (20 mL). To the reaction mixture 2 ml of water was added to dissolve the off-white colored precipitate appeared after stirring the solution for about 12 hours. The homogeneous solution was kept undisturbed for 3 days, provided pale colored crystals of **Zn-H_2Clanth.**

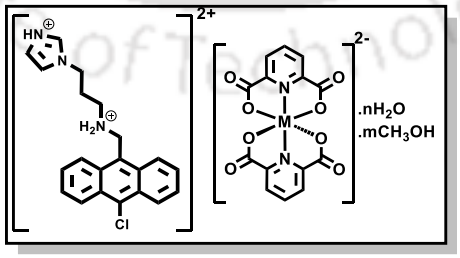

Co-H_2Clanth-Int, n = 1, m = 1 (Triclinic P-1, *V* = 1705.1 Å^3) 4.1
Co-H_2Clanth, n = 5, m = 0, (Monoclinic C2/c, *V* = 7108.7 Å^3) 4.2
Cu-H_2Clanth-Int, n = 1, m = 1.5 (Triclinic P-1, *V* = 3630.5 Å^3) 4.3
Cu-H_2Clanth, n = 4, m = 0, (Monoclinic C2/c, *V* = 7065.0 Å^3) 4.4
Zn-H_2Clanth, n = 4, m = 0, (Monoclinic C2/c, *V* = 7135.3 Å^3) 4.5

Figure 4.2 Hydrates of the cobalt, copper, zinc-26pdc complexes having **H_2chloroanthraimmida (H_2Clanth)** cation.

TH-3622_196122001

Table 4.1: Crystallization conditions for preparation of the hydrates.

Hydrate	$M(OAc)_2 \cdot xH_2O$[@](mmol)	H_2**26pdc** (mmol)	**Clanth** (mmol)	**Time for crystallization**
Co- H_2Clanth-Int (4.1)	0.2	0.4	0.2	2 days
Co- H_2Clanth[#] (4.2)	0.4	0.8	0.4	3-4 days
Cu- H_2Clanth-Int (4.3)	0.2	0.4	0.2	2 days
Cu- H_2Clanth[#] (4.4)	0.4	0.8	0.4	3-4 days
Zn- H_2Clanth[#] (4.5)	0.4	0.8	0.4	3-4 days

In each case 20 mL methanol was taken; M = Co, x = 4; M = Cu, x = 1 and M = Zn, x = 2.
[#] = 2 mL water was added after 12 hours to dissolve a precipitate formed and allowed to recrystallize.

During the course of complex formation, in all the cases the **Clanth** was protonated at -NH- and one of the nitrogen atoms of the imidazole by the in-situ abstraction of protons from the carboxylic acid groups of the H_2**26pdc**. Accordingly, each of the complex/hydrate had H_2**Clanth** dication as the cationic part. In general, protonation of such amine-based compounds is easily caused by a carboxylic acid.[2] The stable hydrates obtained for the copper and zinc complexes were tetra-hydrate whereas, the stable form of the hydrate of the cobalt complex had five water of crystallization molecules. The crystals of the stable hydrates were obtained when the reaction was performed at a relatively higher concentration as listed in the table 4.1. The stable hydrates were prepared by recrystallization of a precipitate formed during the reaction, which were dissolved in water and then allowed to crystallize.

4.3. Self-assemblies of the hydrates

The crystal structures of each hydrate were determined by single crystal X-ray diffraction. The hydrates without methanol molecules were stable, among these hydrates, there were three such stable hydrates one for each cobalt, copper and zinc complex.

In the self-assembly of the unstable transient hydrate, **[(H_2Clanth)Co(26pdc)$_2$]·H_2O·CH_3OH** {**Co-H_2Clanth-Int**} (**4.1**), the cation H_2**Clanth** was directly hydrogen bonded to the anions through hydrogen bonds between carboxylate oxygen atom and imidazolium by $^+$N-H by $^+$N1-$H_{(imidazole)}\cdots O2_{(carbonyl)}$ bond, {$d_{D\cdots A}$, 2.629(5) Å, <D-H···A 166(6)°}. (Figure 4.3a). The anions were also directly hydrogen bonded by $^+$N3-$H_{ammonium}\cdots O6_{carbonyl}$ {$d_{D\cdots A}$, 2.797(4) Å, <D-H···A 144°} and $^+$N3-$H_{ammonium}\cdots O5_{carboxylate}$ {$d_{D\cdots A}$, 2.807(4) Å, <D-H···A 159°} hydrogen bonds (Figure 4.3b). The methanol molecule acted as hydrogen bond donor to the oxygen atom (O9) of water {O10-

TH-3622_196122001

H···O9; $d_{D\cdots A}$, 2.751(7) Å, <D-H···A 172°} and same water molecule was hydrogen bonded to carbonyl of an oxygen atom by {O9–H···O8, $d_{D\cdots A}$, 2.964(5) Å, <D-H···A 173°} shown in the Figure 4.2a. This has terminated a hydrogen bonded chain, and the methanol and water remained in the interstices with the support of the assembled ions. The cations were present as discrete units and were held to anions on the two sides to provide a chain-like arrangements along *ab* crystallographic direction. The solvent molecules were held in the spaces between such layers (Figure 4.3d). The neighbouring anthracenyl-units were present as pairs of π-stacked aromatic rings with centroid to centroid distance 3.778 Å.

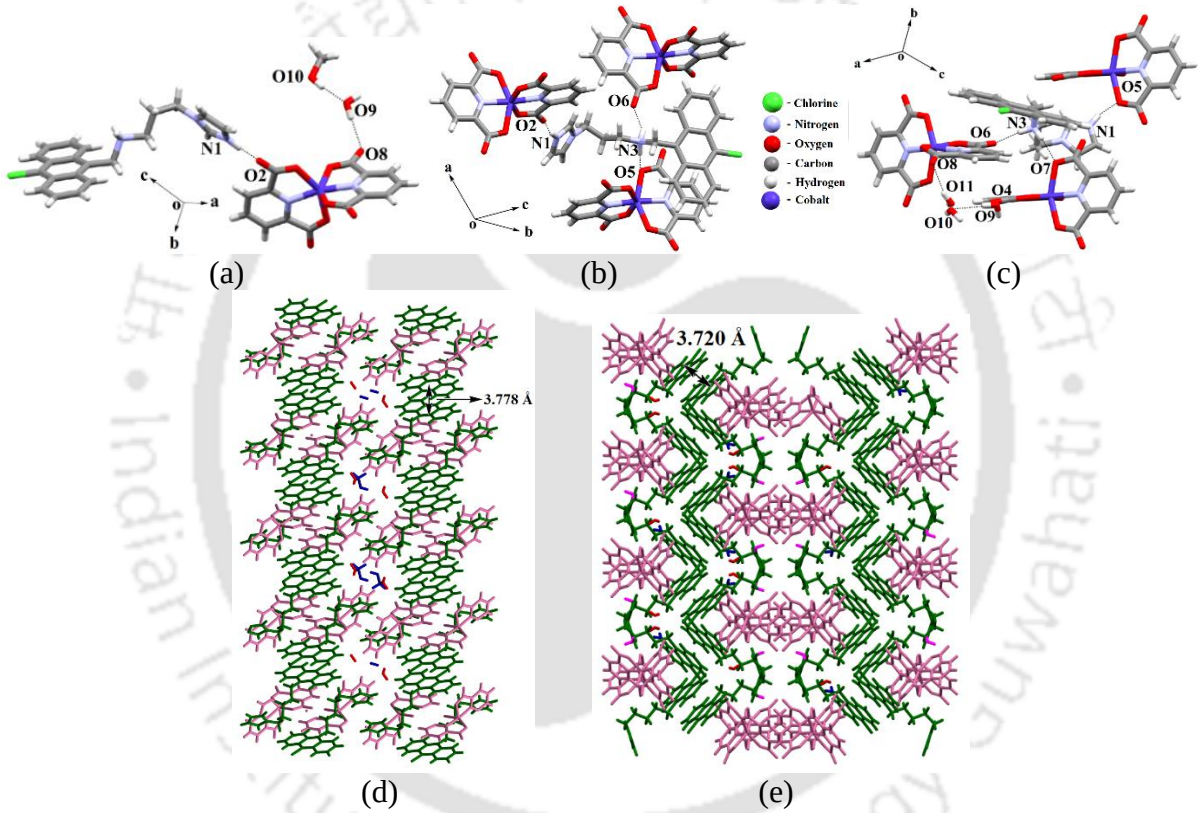

Figure 4.3: (a) The crystal structure of **Co-H_2Clanth-Int** (**4.1**), (b) The hydrogen bonded assemblies of **Co-H_2Clanth-Int** (**4.1**) showing hydrogen bond between the ions, (c) Self-assembly of **Co-H_2Clanth** (**4.2**) showing two rings of the anions eclipsing each other to have stacking interaction. The arrangements of the cations and anions in (d) **Co-H_2Clanth-Int (4.1)** and (e) **Co-H_2Clanth** (**4.2**) along crystallographic plane-*ab*.

In the self-assembly of the stable cobalt hydrate **[(H_2Clanth)Co(26pdc)$_2$]·5H_2O {Co-H_2Clanth}** (**4.2**), the cation was linked by $^{+}$N1-$H_{imidazole}\cdots O5_{carboxylate}$ {$d_{D\cdots A}$, 2.811(4) Å, <D-H···A 158°}, $^{+}$N3-$H_{ammonium}\cdots O7_{carboxylate}$ {$d_{D\cdots A}$, 2.808(4) Å, <D-H···A 165°} and $^{+}$N3-$H_{ammonium}\cdots O6_{carbonyl}$ {$d_{D\cdots A}$, 2.778(4) Å, <D-H···A 167°} interactions (Figure 4.3c). A water molecule was held by forming hydrogen bond with oxygen atom of another water molecule {O9-H···O10; $d_{D\cdots A}$, 2.942(6) Å, <D-

TH-3622_196122001

H···A 166°} and {O10-H···O11; $d_{D\cdots A}$, 2.872(6) Å, <D-H···A 162(8)°}. The water molecule having O11 was hydrogen bonded to carbonyl oxygen atom by {O10–H···O8, $d_{D\cdots A}$, 2.929(4) Å, <D-H···A 149(6)°}. Thus, in this case the -$^{+}NH_2$- as well as the hydrogen bonds of cation with anion and water molecules with anion had provided necessary linkages to have a stable structure. The anions of the **Co-H$_2$Clanth** (**4.2**) were present in the crystal lattice as pairs of $[Co(26pdc)_2]^{2-}$ located at close vicinity (Figure 4.3c). These anions were located at parallel position were not eclipsing each other but located at translated positions. Each pair was stabilized by N-$H_{(ammonium)}\cdots O_{(carbonyl)}$ and N-$H_{(ammonium)}\cdots O_{(carboxylate)}$ interactions; and also, by the two water molecules of the hydrate holding the same pair at other side. It is well established that chelate-chelate stacking interactions contribute to stability of assemblies.[3] The stacking interactions among coordinated pyridine rings in metal complex varies from 7 kcal/mol to 33 kcal/mol; and a stacking among two free pyridine rings provide a stability of ~4 kcal/mol. Whereas, a metal-pyridine bond provides stability of about 7 kcal/mol.[4] Hence, the coordinated pyridine of the **26pdc** and the stacking among the pyridine rings contributed to the stability of assemblies in the hydrates. There are also instances where other factors such as hydrogen bonds may be the prime factor over the stacking interaction.[5] In the present case, the $^{+}$N-H was involved in charge-assisted hydrogen bonds. The interactions of water molecules with two anions from one side and the $^{+}$N-H from another side held two anions together as pairs. Here, the assembled-portion formed by weak interactions to hold two anions at the closest vicinity shown in the Figure 4.2e, has a chloro-anthracenyl unit which is stacked with a plane of **26pdc** chelate. Concave shaped cations face opposite at alternate place and the cations located at alternate places had cation π-stacking between them. The distance between the centroids of the chloro-anthracenyl plane to the chelated **26pdc** ring was 3.720 Å; hence, showed stacking interactions between these sets of rings. The cations are organised as zig-zag chain and they form enclosures to embrace the anions. The higher stability of the hydrate was due to the hydrogen bonds holding the chelated anions in pairs and the stacking of chelate ring with the anthracenyl ring as illustrated in the Figure 4.2e.

The crystal lattice of the unstable form of the hydrate of the copper complex **[(H$_2$Clanth)Cu(26pdc)$_2$]$_2$·2H$_2$O·3CH$_3$OH** {**Cu-H$_2$Clanth-Int**} (**4.3**) had two symmetry independent molecules. The cation of the of the complex was hydrogen bonded to water by $^{+}$N4-$H_{imidazole}\cdots O21_{water}$ {$d_{D\cdots A}$, 2.662(6) Å, <D-H···A 171°} and $^{+}$N1-$H_{imidazole}\cdots O20_{water}$ {$d_{D\cdots A}$, 2.765(5)

TH-3622_196122001

Å, <D-H···A 165(4)°} interactions. It was also hydrogen bonded to the anions through an intervening water molecule {O20-H···O10$_{carbonyl}$; $d_{D\cdots A}$, 2.755(4) Å, <D-H···A 163°}. One methanol and two water molecules of crystallisation formed a hydrogen bonded chain holding two independent anions at two ends {O19-H···O5$_{carboxylate}$; $d_{D\cdots A}$, 2.668(6) Å, <D-H···A 175°} and {O21-H···O19; $d_{D\cdots A}$, 2.700(8) Å, <D-H···A 172°; O21-H···O20; $d_{D\cdots A}$, 2.758(6) Å, <D-H···A 144°} as show in the Figure 4.4a.

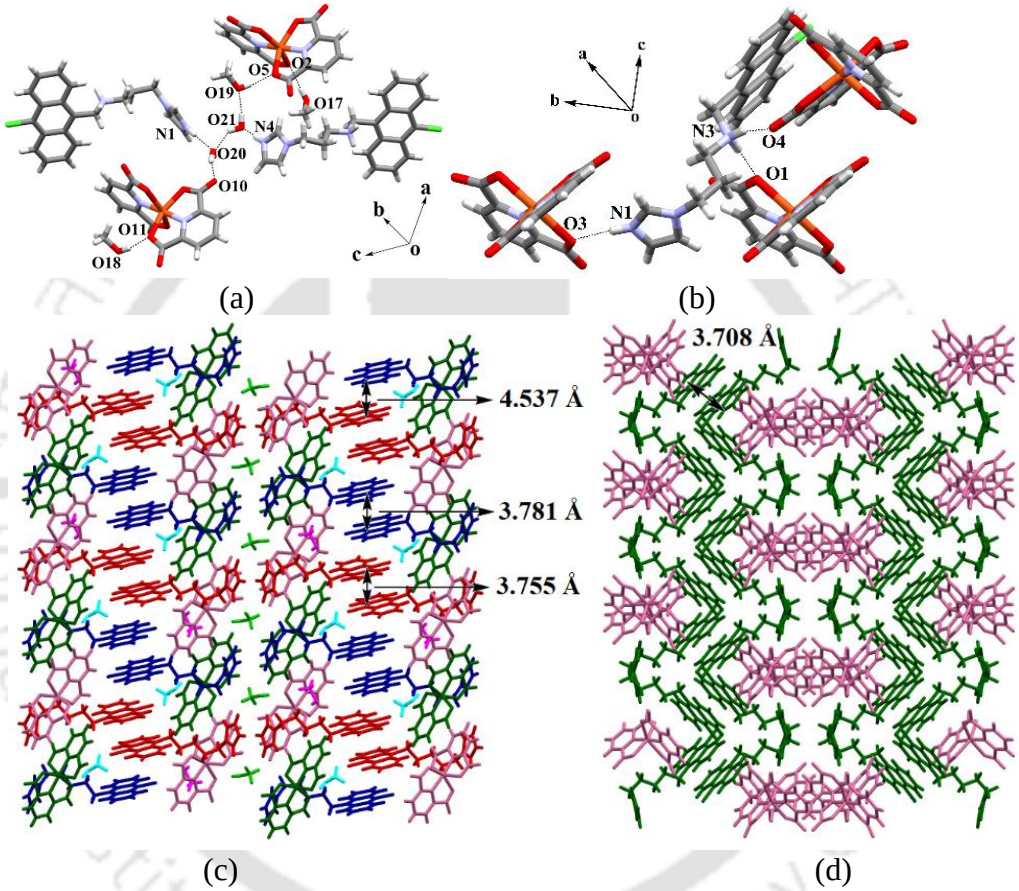

Figure 4.4: (a) The hydrogen bonded assembly of (a) **Cu-H$_2$Clanth-Int** (**4.3**), (b) **Cu-H$_2$Clanth** (**4.4**); The π-stacks and arrangement of cations and anions in (c) **Cu-H$_2$Clanth-Int** (**4.3**) along crystallographic plane-*bc* and (d) **Cu-H$_2$Clanth** (**4.4**) along crystallographic plane-*ab*.

It had a lamellar structure, in which the anions were in chain-like arrangement holding the cations. The anthracenyl units were projected one side of the layer. Two such layers come closer to have π-stacking among the anthracenyl groups. In this case the anthracenyl units were parallel but located at slightly translated position. The centroid to centroid distance between symmetry related pairs were 3.781Å, 3.755Å and between the symmetry independent pair was 4.537Å (Figure 4.4

TH-3622_196122001

c). Though they were not eclipsing yet there were stackings that have contributed to have a lamellar structure.

The crystal structure of the **Cu-H_2Clanth** (**4.4**) had highly disordered water molecules, to make a clear presentation, the water molecules were squeezed, and structure is presented without showing the water molecules. The cation of the hydrate complex was connected to the anion by $^{+}$N1-$_{Himidazole}$···O3$_{carboxylate}$ {$d_{D\cdots A}$, 2.782(5) Å, <D-H···A 175(5)°}, $^{+}$N3-H$_{ammonium}$···O1$_{carboxylate}$ {$d_{D\cdots A}$, 2.752(3) Å, <D-H···A 166°} and $^{+}$N3-H$_{ammonium}$···O4$_{carbonyl}$ {$d_{D\cdots A}$, 2.779(4) Å, <D-H···A 165°} hydrogen bonds (Figure 4.4b). In the crystal lattice of the **4.4**, the cations of the complex are concave shaped and each cation located at alternative concave face in opposite directions to each other. While doing so, the anthracenyl groups had appeared face to face with centroid to centroid distance 3.708 Å.

The only form of hydrate of the zinc complex was a tetrahydrate **[(H_2Clanth)Zn(26pdc)$_2$]·4H_2O** {**Zn-H_2Clanth**} (**4.5**). In the structure, the water molecules were highly disordered, hence could not be resolved. The structure was determined by squeezing the water molecules present in the hydrate. The amounts of water were estimated from the residual electron-density from the Fourier map of the X-ray single crystal diffraction data and were further confirmed by thermogravimetric analysis. The self-assembly of the **4.5** had the cation directly hydrogen bonded to anions through $^{+}$N1-H$_{imidazole}$···O1$_{carboxylate}$ {$d_{D\cdots A}$, 2.813(4) Å, <D-H···A 179(6)°}, $^{+}$N3-H$_{ammonium}$···O3$_{carboxylate}$ {$d_{D\cdots A}$, 2.794(3) Å, <D-H···A 167°} and $^{+}$N3-H$_{ammonium}$···O2$_{carbonyl}${$d_{D\cdots A}$, 2.777(4) Å, <D-H···A 167°} interactions (Figure 4.5a).

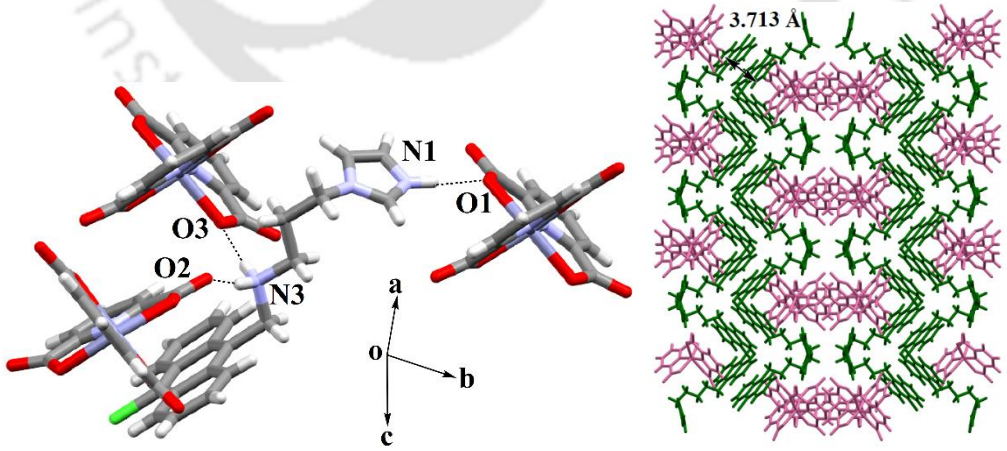

(a) (b)

Figure 4.5: (a) The hydrogen bonded assembly of (a) **Zn-H_2Clanth** (**4.5**) and (b) the π-stacks and arrangement of cations and anions in **4.5** along crystallographic plane-*ab*.

TH-3622_196122001

The packing pattern of the hydrate (Fig 4.5b) had similarity with the packing of the **Co-H_2Clanth** and **Cu-H_2Clanth**. All these had hydrates had concave shaped cations facing opposite face having stacking arrangements among the chloro-anthracenyl units. In the case of the **Zn-H_2Clanth** the π-separation between the two interacting parallel planes was 3.713 Å. Hence the common feature of these structurally similar stable hydrates were from the packing similarity, π-stackings, direct hydrogen bond between the anions and cations, and encapsulation of the anions in the embracing positions created by assembled cations. These structural analyses have showed that the packing patterns of the two less-stable hydrates **4.1** and **4.3** had large differences in the packings. Each of the hydrate had extensive stacking interactions, among same type or two different of planar units which are shown in the Figure 4.6 and are also listed in the Table 4.2. In the case of **4.1** the methanol molecules water terminated hydrogen bond with water; but, in the case of **4.3** it was a hydrogen bonded chain of anion···water···water···methanol···anion. The **4.1** had dimer of anions formed by eclipsing chelates with the centroid to centroid distance 5.098 Å (Figure 4.6a). It had two parallel imidazolium rings in a proximity of 3.975 Å, which provides repulsive interactions. The **4.3** had a lamellar structure (Figure 4.4c). In the packing, chloro-anthracenyl units were projecting in one direction, and the chains were arranged such that chloro-anthracenyl units of two chains at immediate neighbour were eclipsed (viewed along *ab*-crystallographic plane).

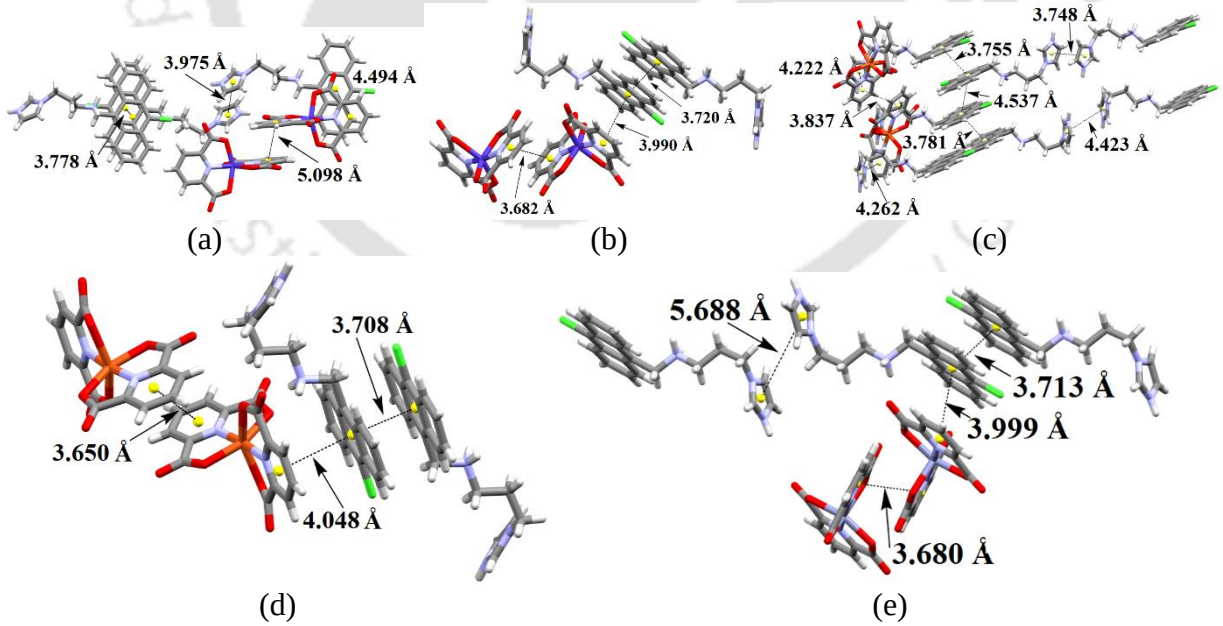

Figure 4.6: Stacking among cations and anions in the hydrates (a) **Co-H_2Clanth-Int (4.1)**, (b) **Co-H_2Clanth (4.2)** (c) **Cu-H_2Clanth-Int (4.3)** (d) **Cu-H_2Clanth (4.4)** and (e) **Zn-H_2Clanth (4.5)**.

TH-3622_196122001

The two chains had stacking interactions. The solvent molecules were located between the sides of the chain on the side having the hydrophilic part as shown in the Figure 4.4c. Whereas, the intermediate cobalt hydrate (**4.1**) had stacking among anions, but the distance between the eclipsing portions was 5.098 Å. This showed very weak interactions between them; and the distance of separation of chloro-anthracenyl···26pdc stack was 4.494 Å. The hydrate **4.3** also had stacks among the chloro-anthracenyl rings with chloro-anthracenyl or imidazolium with imidazolium units. The latter being repulsive interaction, the structure underwent facile change by solvent-solute interactions. The presence of this repelling stacks makes such systems helps to get converted to stable form, which increased the versatility for studying such reversible transformations suggested in other systems.[6,7] The intermolecular stacking interactions between chloro-anthracene rings and also between the 26pdc rings had dominated in the stable forms of the hydrates. The three stable hydrates had similar zigzag ladder-like arrangements from the arrangements of the cations constructed through the π-stacking.

Table 4.2: Centroid-centroid distances among eclipsing rings at the closest vicinity

Hydrate	$d_{\text{anthra-anthra}}$ (Å)	$d_{\text{pdc-pdc}}$ (Å)	$d_{\text{anthra-pdc}}$ (Å)	$d_{\text{im-im}}$ (Å)	$d_{\text{pdc-im}}$ (Å)
Co-H_2Clanth-Int (4.1)	3.778	5.098	4.494	3.975	-
Co-H_2Clanth (4.2)	3.720	3.682	3.990	-	-
Cu-H_2Clanth-Int (4.3)	3.781, 4.537, 3.755	3.837	-	4.423, 3.748	4.262, 4.222
Cu-H_2Clanth (4.4)	3.708	3.650	4.048	-	-
Zn-H_2Clanth (4.5)	3.713	3.680	3.999	-	-

The three stable hydrates (Co, Cu and Zn complexes) possessed assembled dimers of anions in their respective lattice. These stacked dimers were held together by hydrogen bond of bridging water molecules and $-^{+}NH_2$- part of the cation. In none of the example halogen bonds or C-H···chlorine interactions were observed. It was also found that the chlorine atoms were positioned away from each other. Thus, it may be suggested that the electrostatic and stacking interactions together with the electronic effect of chlorine atoms to remain away from each other had provided the propensity of the hydrates of the same metal complex for reversible transformations between them by changing the crystallisation conditions.

TH-3622_196122001

4.4. Unit cells of the hydrates

The crystals of all the stable hydrates were from monoclinic, C2/c space group. The unit-cell volumes of the single crystals of the stable hydrates followed an order zinc-complex > cobalt-complex > copper-complex. This trend was not found as per the order of the ionic radius, Zn(II) > Cu(II) > Co(II). It was due to the fact that the cobalt complex was a penta-hydrate and the other two were tetrahydrate. On the other hand, both the less-stable crystals of hydrate (alternatively, mixed solvate) belonged to triclinic, $P\bar{1}$ space group. The two less stable hydrates had different amounts of water with respect to methanol molecules of crystallization. The ratio of water to methanol in the less-stable hydrate of the cobalt complex was 1:1; whereas, similar less–stable hydrate of the copper complex had a ratio 1:1.5. In the case of cations without a substituent the less-stable form of hydrate had a water-methanol ratio 1:1.5.

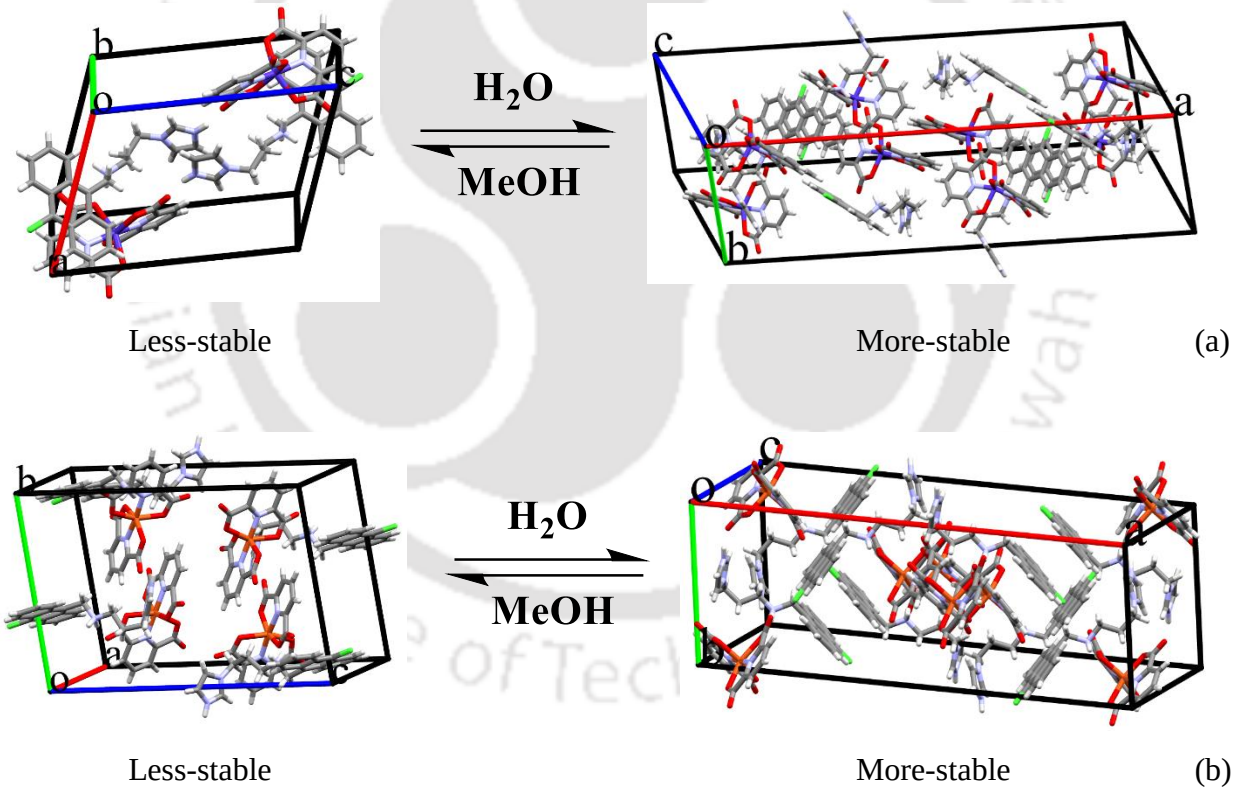

Figure 4.7: (a) and (b) are unit-cells of crystals of hydrates of the cobalt and copper complexes respectively that transformed in reversible manners.

The hydrates of the cobalt or copper complexes underwent reversible transformation upon changing recrystallization conditions. For example, the freshly prepared crystals of the intermediate mixed hydrates automatically got converted upon contact with moisture or water to

TH-3622_196122001

provide the stable hydrates; alternatively, the crystals of stable hydrate upon dissolution in the solvent from a concentration at which the intermediate was crystal was originally crystallised yielded the crystals of the less-stable form.This was an interesting point as the stoichiometry of the less-stable form with respect to a stable form were not identical, so as the Z values. Namely the less-stable form of the cobalt complex had unit cell volume 1705.1 (4) $Å^3$ (space group $P\bar{1}$, Z = 2), whereas, the stable form had unit cell volume 7108.7 (12) $Å^3$ (space group C2/c, Z = 8). Thus, for such a transformation, there has to be an increase in unit cell volume (Approx. 4 times) by changing in the numbers of molecules per unit cell (Z value). Whereas, analogous copper hydrates, less stable form had unit cell volume 3630.5(7) $Å^3$ (space group $P\bar{1}$, Z =2) and stable form had 7065(7) $Å^3$ (space group (C2/c, Z = 8) approximately double the volume of the less stable form. In each case there was a requirement of extra water molecules replacing by methanol or vice versa. From the point of internal structural changes, it may be viewed as a change in the domain of the less-stable cobalt complex to the new domain of the stable form with increment of four folds (Figure 4.7a). Whereas, the less stable hydrate of copper complex underwent doubling of the unit-cell volume to generate the unit-cell of the stable form (Figure 4.7b). Alternately, the stacking among the rings in different forms had to be reconstructed in each transformation, and it happened through the competitive effects of water and methanol to remain in the assembly within a unit cell. It has been reported in literature the exchange of water and methanol molecule affects the unit cell surface differently depending on the functional groups.[8] In accordance, the present results are different from the analogous systems not only from the fact that a cation has a chloro-substituent, but also in terms of transformations between space groups and reversibility in transformation. In those examples without a chloro-substituent, there were three different types of hydrates in each case; instead we have two types of hydrates in the present case. Furthermore in the present study, the space group transformation in one case required two fold or four fold increase in unit cell volume. The C2/c space-group and $P\bar{1}$ space-group transformation requires minimum changes and have been already found in pressure induced crystal to crystal transformations.[9,10] For example, pressure induced polymorphic transition of ferrous sulphate displacement of sulphate anions as well as FeO_6 units occurred.[9]

TH-3622_196122001

4.5. Powder X-ray diffraction and Scanning electron micrographs

The phase-purity of all the three stable hydrates (**Co-H_2Clanth**, **Cu-H_2Clanth** and **Zn-H_2Clanth**) were confirmed by recording powder XRD pattern of the respective samples and comparing with the simulated ones (Figure 4.8). The less stable ones (**Co-H_2Clanth-Int** and **Cu-H_2Clanth-Int**) could not be analysed due to their rapid conversion after removal from the solvent into the respective stable form. A great amount of care and repeated experiments were required to get those patterns in place. When we compared the simulated powder patterns of these with the experimental data, the experimental diffraction patterns matched the simulated diffraction patterns, indicating a high purity of the bulk materials.

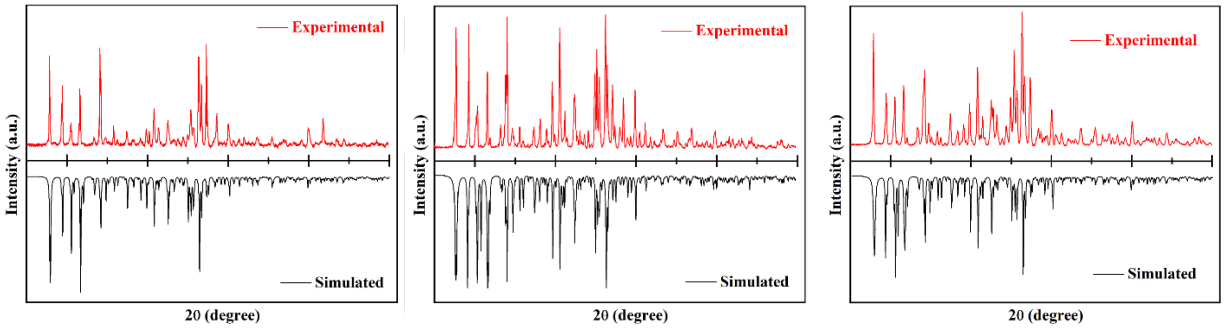

Figure 4.8: (i) PXRD patterns of (a) **Co- H_2Clanth** (**4.2**), (b) **Cu- H_2Clanth** (**4.4**) and (c) **Zn- H_2Clanth** (**4.5**) (Red = Experimental, Black = Simulated pattern generated from CIF file ($5^0 \leq 2\theta \leq 50^0$)**.**

The field emission scanning electron micrograph (FESEM) of the less-stable cobalt hydrate (**Co-H_2Clanth-Int**) as well as the stable form, we find that the less-stable form had nano-fibrous crystals (Figure 4.9) with about 200 nm width; and the stable form (**Co-H_2Clanth**) provided mesoscopic flakes {FigureA2(a)}.

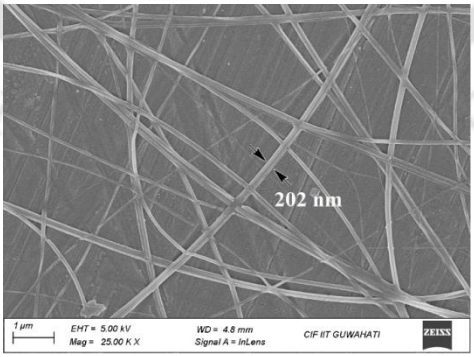

Figure 4.9: The FESEM image of **Co-H_2Clanth-Int** (**4.1**).

The SEM image of the lesser stable hydrate of the copper complex was not possible to record to get reproducible result, but the image revealed of the stable hydrate **Cu-H_2Clanth** had micron-

TH-3622_196122001

size rod shaped crystals which were about 2.6 µM × 54.0 µM sizes {Fig A2(b)}.The only form of zinc hydrate had dense cross-linked nano-fibrous structure with average breadth of about 182 nm {Fig A2(c)}.

4.6. FT-IR spectra of the hydrates

All the hydrates exhibited mostly similar IR peaks, as an illustrative example broad and strong O–H stretch around 3314-3391 cm^{-1}, indicative of hydrogen-bonded water molecules. There were weak at peak around 3107-3113 cm^{-1}, suggested the presence of C–H of aromatic or unsaturated systems, while a weak IR-absorption in the range of 2808-2824 cm^{-1} due to aliphatic C–H stretching was observed. The strong absorption peak in the range 1614-1621 cm^{-1} corresponded to the C=O stretching, typical of carboxylates or aromatic C=C stretching, complemented by another strong band at around 1574-1586 cm^{-1}, which was from asymmetric COO^- stretching or aromatic C=C vibrations.

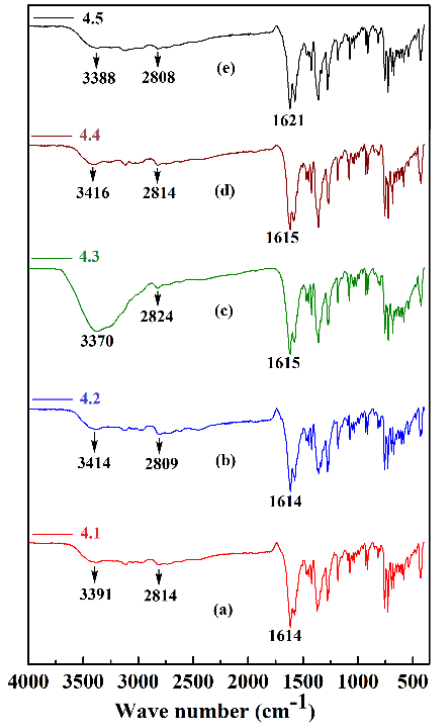

Figure 4.10: IR spectra of (a) **Co-H_2Clanth-Int (4.1)**, (b) **Co-H_2Clanth (4.2)**, (c) **Cu-H_2Clanth-Int (4.3)**, (d) **Cu-H_2Clanth (4.4)** and (e) **Zn-H_2Clanth (4.5)**.

Medium intensity peaks in the ranges 1448-1463 cm^{-1} and 1421-1425 cm^{-1} were associated with CH_2 bending or symmetric COO^- stretching. All the hydrates showed peaks at 603 cm^{-1} and 584

TH-3622_196122001

cm^{-1}, were from metal-oxygen (M–O) or bending modes of the anions. Finally, weak and strong peaks at 539 cm^{-1} and 429 cm^{-1}, respectively, indicated the M–O or M–N metal-ligand stretching of the complexes.

4.7. Thermogram of the stable hydrates

The thermogravimetric study was carried out to ascertain the amount of solvent loss and the ease of their loss from the respective complexes. The thermograms were also used to compare the thermal stability of the complexes. The thermogram of less stable hydrates **4.1** and **4.3** could not be recorded. In the case of **Co-H_2Clanth** (**4.2**), a weight loss of 10.48 % was observed, which corresponded to the loss of five water molecules (calculated 10.82 %) in the temperature range of 50ºC to 110ºC (Figure 4.11a). The decomposition temperature of the molecule was 294ºC.

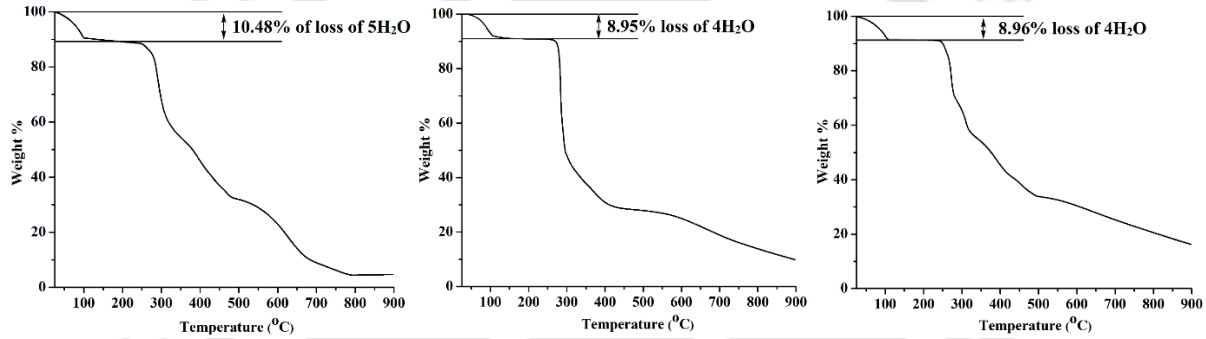

Figure 4.11: Thermogram of (a) **Co-H_2Clanth** (**4.2**), (a) **Cu-H_2Clanth** (**4.4**) and (a) **Zn-H_2Clanth** (**4.5**) (heating rate 10°C/min) under nitrogen atmosphere.

The thermogram of **Cu-H_2Clanth** (**4.4**) showed 8.95 % weight loss for water molecules around 70°C - 110°C (Figure 4.11b) was in an agreement with the theoretical value calculated for loss of four water molecules (8.80 %). The copper hydrate **4.4** decomposes at 280ºC. The thermogram of the **Zn-H_2Clanth** (**4.5**) (Figure 4.11c) showed the loss of the four water molecules at 70ºC - 110ºC that corresponds to 8.96 % loss of weight which was consistent with the theoretically calculated value (8.78 %). The hydrate **4.5** decomposed at 275ºC.

4.8. Aggregation and Fluorescence studies

In the case of zinc complex only the tetrahydrate was crystallised, many attempts to crystallise another form of hydrate was not successful. So, advantage of fluorescent nature of the cationic part was taken to find out if any feature of the intermittent species could be obtained.

TH-3622_196122001

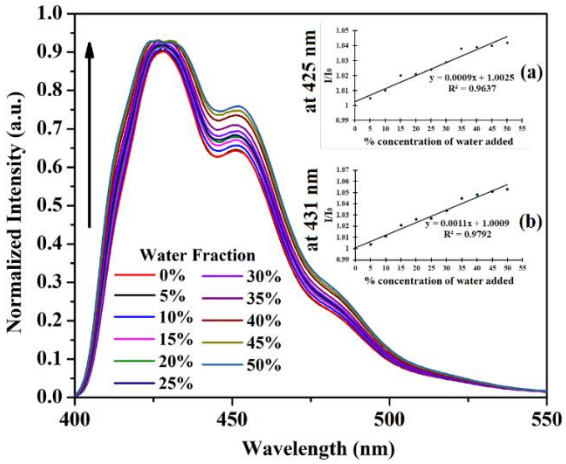

Figure 4.12: Spectrofluorimetric titration of a 2 mL solution taken from a bulk methanol solution containing zinc(II) acetate dihydrate (0.02 mM); 26-H_2pdc, (0.04 mM); **Clanth** (0.02mM) by adding 0-50 % water. Inset (a) and (b): change in fluorescence intensity at 425 nm and 431 nm after systematic addition of water during titration (excitation at 300 nm).

A solution was prepared at the concentration at which an unstable form would have formed (based on other analogues with cobalt and copper); the solution showed emission a peak at 428 nm upon excitation at 300 nm. This emission peak corresponded to the stable form of the hydrate as confirmed by recording emission spectra of a solution of **Zn-H_2Clanth** (**4.5**) in methanol from independent experiment (Figure A4). The emission peak originally present at 428 nm in the case of the titration with water was split into two new peaks appearing at 425 nm and 431 nm (Figure 4.12). The emissions at these wavelengths were increased with increase in amounts of water. This showed that in the case of the zinc complex there were also two aggregates in solution, but only one was crystallised out. Generally, H or J aggregates of π-stack show distinct emission peaks.[11]Dynamic light scattering study had showed that the addition of water to a dilute solution of the reaction mixture of the cobalt complex in methanol initially increases the particle sizes followed by decrease. In the case of copper, aggregation was decreased with water addition (Figure A5), these showed that with dilution of the reaction mixture with water the self-assembling in solution were changed, which had facilitated the transformation of one form to other.

4.9. Conclusions

The crystals of the stable hydrate of the cobalt and copper complexes belonging to monoclinic C2/c space groups were transformed to crystals of less-stable form of hydrates on dissolution in methanol (triclinic $\mathbf{P\bar{1}}$ space group). The crystals of the less-stable forms were formed easily as kinetic products, and got dissolved in solvent water new crystals having different amounts of water

TH-3622_196122001

molecules in the unit cells. These changes had provided higher amounts of hydrogen bonding sites and ways to gain higher stabilities. As a result, they were transformed to the stable form of hydrates. Accordingly, once less-stable form of crystals were exposed to moist condition, they underwent transformation to stable form. The stable forms had extensive stacking among the cations to form zig-zag ladder-like structure, assembling of which embraced the four anions with chelate-chelate stacking. Under sealed-condition the less -stable form could be stored for several days. Thus, it is not only the crystallization by concentration, but also the effect of water molecules replacing methanol and vice-versa contributed to the reversible crystallization. The stable forms of hydrates had extensive chelated anions at parallel positions suitable for coming close to stack; they were stabilized by hydrogen bonds of water and ammonium ion. Whereas, the less-stable forms had either stacked dimers or stacked chain of anions, which got dislodged to form stable forms by displacement among them. The reversible interconversion among the hydrates provided a new paradigm to undergo reconstructive non-covalent assemblies.

4.10. Experimental Section

The instrumental details and crystallographic parameters are provided in Appendix section at the end of this chapter. In the FT-IR spectra, following abbreviations were used: s = strong, w = weak, br = broad, m = medium intensity peaks.

[(H_2**Clanth)Co(26pdc)**$_2$**]·**H_2O**·**CH_3OH {**Co-**H_2**Clanth-Int**} (**4.1):** To a well stirred solution of 2,6-pyridinedicarboxylic acid (66.84 mg, 0.40 mmol) and cobalt(II) acetate tetrahydrate (49.90 mg, 0.20 mmol) in methanol (20 mL), **Clanth** (69.84 mg, 0.20 mmol) was added. The resulting solution was stirred for about 3 hours and kept undisturbed for crystallization, provided the crystals of **4.1**. Due to the unstable nature of the crystals it could not be stored and hence yield calculation was not possible. IR (Neat, cm^{-1}): 3391 (br, s), 3107 (w), 2814 (w), 1614 (s), 1574 (s), 1448 (m), 1421 (m), 1371 (s), 1277 (s), 1182 (s), 1091 (w), 1073 (m), 1034 (w), 927 (m), 912 (m), 817 (m), 756 (s), 727 (s), 692 (s), 675 (s), 646 (m), 623 (m), 603 (m), 584 (m), 539 (w), 429 (s).

[(H_2**Clanth)Co(26pdc)**$_2$**]·5**H_2O {**Co-**H_2**Clanth**} (**4.2):** To a well stirred solution of 2,6-pyridinedicarboxylic acid (133.68 mg, 0.80 mmol) and cobalt(II) acetate tetrahydrate (99.80 mg,

TH-3622_196122001

0.40 mmol) in methanol (20 mL), **Clanth** (139.68 mg, 0.40 mmol) was added. The resulting solution was stirred for about 12 hours and it resulted in the formation of brown precipitate that was dissolved in 2mL of water and kept undisturbed for crystallization, provided the crystals of **4.2**. Isolated yield = 45%. IR (Neat, cm^{-1}): 3391 (br, s), 3107 (w), 2809 (w), 1614 (s), 1574 (s), 1448 (m), 1421 (m), 1356 (s), 1277 (s), 1181 (s), 1091 (w), 1072 (m), 1034 (w), 928 (m), 913 (m), 817 (m), 756 (s), 727 (s), 692 (s), 674 (s), 603 (m), 589 (m), 431 (s).

[(H_2**Clanth)Cu(26pdc)**$_2$**]**$_2$**·2**H_2O**·3**CH_3OH {**Cu-**H_2**Clanth-Int**} (**4.3):** The similar procedure as **4.1** was followed in the synthesis of **4.3**, but copper (II) acetate monohydrate (39.92 mg, 0.20 mmol) was used in the place of cobalt salt. This compound is as unstable as **4.1**. IR (Neat, cm^{-1}): 3370 (br, s), 2824 (s), 1615 (s), 1574 (s), 1469 (m), 1448 (m), 1421 (m), 1359 (s), 1274 (s), 1266 (s), 1183 (m), 1092 (w), 1080 (m), 1037 (m), 1015 (w), 991 (w), 956 (w), 927 (m), 910 (m), 800 (w), 754 (s), 738 (w), 723 (s), 682 (s), 663 (w), 646 (w), 621 (w), 603 (m), 583 (w), 538 (w), 425 (s).

[(H_2**Clanth)Cu(26pdc)**$_2$**]·4**H_2O {**Cu-**H_2**Clanth**} (**4.4):** The similar procedure as **4.2** was followed in the synthesis of **4.4**, but copper (II) acetate monohydrate (79.84 mg, 0.40 mmol) was used in the place of cobalt salt. Isolated yield: 46 %. IR (Neat, cm^{-1}): 3416 (br, s), 3113 (w), 2814 (w), 1615 (s), 1586 (s), 1463 (w), 1448 (w), 1422 (m), 1359 (s), 1266 (s), 1183 (m), 1080 (w), 1037 (w), 928 (m), 910 (m), 851 (w), 814 (w), 755 (m), 723 (s), 683 (s), 663 (w), 647 (w), 623 (w), 584 (m), 425 (s).

[(H_2**Clanth)Zn(26pdc)**$_2$**]·4**H_2O {**Zn-**H_2**Clanth**} (**4.5):** The similar procedure as **4.2** was followed in the synthesis of **4.5**, but zinc (II) acetate dihydrate (87.80 mg, 0.40 mmol) was used in the place of cobalt salt. Isolated yield: 83 %. IR (Neat, cm^{-1}): 3388 (br, s), 3112 (w), 2808 (w), 1621 (s), 1574 (s), 1463 (w), 1425 (m), 1361 (s), 1278 (s), 1184 (m), 1101 (w), 1075 (w), 1034 (m), 927 (w), 911 (m), 818 (m), 756 (s), 727 (s), 692 (m), 676 (m), 584 (m), 543 (w), 431 (s).

TH-3622_196122001

4.11. References

1. G. Cavallo, P. Metrangolo, R. Milani, T. Pilati, A. Priimagi, G. Resnati and G. Terraneo, The Halogen Bond, *Chem. Rev.*, 2016, **116**, 2478−2601.
2. B. Lin, Y. Liu, M. W. Wang, Y. Wang, S. Du, J. B. Gong and S. Wu, Intermolecular interactions and solubility behavior of multicomponent crystal forms of orotic acid: prediction and experiments, *Cryst. Growth Des.*, 2021, **21**, 1473−1481.
3. D. N. Sredojevic, Z. D. Tomic, S. D. Zaric, Evidence of chelate-chelate stacking interactions in crystal structures of transition-metal complexes, *Cryst. Growth Des.*, **2010, *10***, 3901–3908.
4. D. B. Ninkovic, G. V. Janjic, S. D. Zaric, Crystallographic and ab-initio study of pyridine stacking interactions. Local nature of hydrogen bond effect in stacking interactions, Cryst. Growth Des., 2012, **12**, 1060–1063.
5. G. M. Kapteijn, D. M. Grove, G. van Koten, W. J. J. Smeets, A. L. Spek, A new mixed alkoxo aryloxo palladium complex with a bidentate nitrogen donor system, *Inorg. Chim. Acta*, 1993, **207**, 131–134.
6. T. Chen, M. Li, J. Liu, π–π Stacking interaction: a nondestructive and facile means in material engineering for bio applications, Cryst. Growth Des., **2018**, ***18***, 2765–2783.
7. B. Moulton, M. J. Zaworotko, From molecules to crystal engineering: supramolecular isomerism and polymorphism in network solids, *Chem. Rev.*, **2001, *101***, 1629–1658.
8. I. Weissbuch, V. Yu, T. L. Leiserowitz, M. Lahav, Solvent effect on crystal polymorphism: why addition of methanol or ethanol to aqueous solutions induces the precipitation of the least stable β form of glycine, *Angew. Chem. Int. Ed.*, 2005, **44**, 3226–3229.
9. J. M. Meusburger, M. Ende, D. Talla, M. Wildner, R. Miletich, Transformation mechanism of the pressure-induced C2/c to P1 transition in ferrous sulfate monohydrate single crystals, *J. Solid State Chem.*, 2019, **277**, 240–252.
10. M. Mączka, S. Sobczak, M. Krys, F. F. Leite, W. Paraguassu, A. Katrusiak, Mechanism of pressure-induced phase transitions and structure-property relations in methylhydrazinium manganese hypophosphite perovskites, *J. Phys. Chem. C*, 2021, **125**, 10121–10129.
11. S. Ma, S. Du, G. Pan, S. Dai, B. Xu, W. Tian, Organic molecular aggregates: from aggregation structure to emission property, *Aggregate*, 2021, **2**, e96.

TH-3622_196122001

Appendix: Chapter 4

Physical Measurements: Infrared spectra of the solid samples were recorded on a Perkin-Elmer Spectrum-Two FT-IR spectrophotometer in the region 4000 - 400 cm^{-1} using attenuated total reflectance method. Powder X-ray diffraction patterns were recorded using Bruker powder X-ray diffractometer D2 phaser. The ^{1}H-NMR spectra were recorded on a BRUKER Ascend-600 MHz NMR spectrometer using TMS as the internal standard. Microscopic images of crystal morphologies were recorded on Carl Zeiss Gemini 300 FESEM by drop-casting method. The thermogravimetric analyses were done on PerkinElmer TGA 4000, under nitrogen gas flow. Fluorescence emission spectra in solution were recorded on a Horiba Jobin Yvon Fluoromax-4 spectrofluorometer. The solvent used were from Merck, EMPLURA® grades. Dynamic light scattering (DLS) Studies were done using Malvern Zetasizer Nano ZS90.

Crystallographic Study: The diffraction data for the hydrates were collected by using a Bruker Bruker D8 Quest diffractometer at room temperature for all the crystals, The refinement of and cell reductions were carried out by using SAINT and XPREP software. Structures were solved by direct methods using SHELXS-97 and were refined by full-matrix least-squares on F^2 using SHELXL-14 and OLEX2 programs. All non-hydrogen atoms were refined in anisotropic approximation against F^2 of all reflections. Hydrogen atoms were placed at their geometric positions by riding and were refined in the isotropic approximation. The crystallographic parameters are listed in the Table A1.

Table A1: Crystal and refinement parameters of the Hydrates **4.1-4.5**.

Parameters	**Co-H_2Clanth-Int (4.1)**	**Co-H_2Clanth (4.2)**	**Cu-H_2Clanth-Int (4.3)**	**Cu-H_2Clanth (4.4)**	**Zn-H_2Clanth (4.5)**
Formula	$C_{36}H_{34}ClN_5O_{10}Co$	$C_{35}H_{34}ClN_5O_{11}Co$ [+ solvent]	$C_{73}H_{72}Cl_2N_{10}O_{21}Cu_2$	$C_{35}H_{28}ClN_5O_8Cu$ [+ solvent]	$C_{35}H_{28}ClN_5O_8Zn$ [+ solvent]
CCDC No.	2363160	2363161	2363162	2363163	2363164
Mol.wt.	791.06	795.05	1623.38	745.61	747.44
Crystal System	triclinic	monoclinic	triclinic	Monoclinic	monoclinic
Space group	$P\bar{1}$	C2/c	$P\bar{1}$	C2/c	C2/c
a (Å)	10.881(14)	40.171(4)	10.591(12)	40.23(2)	40.142(3)
b (Å)	10.909(14)	11.694(11)	14.981(17)	11.745(7)	11.730(8)
c (Å)	15.370(2)	16.270(16)	22.983(3)	16.106 (10)	16.302(11)
α (°)	92.594(5)	90	92.633(3)	90	90
β (°)	110.565(3)	111.556(3)	92.562(3)	111.810(17)	111.643(2)
γ (°)	91.135(4)	90	93.924(3)	90	90
V ($Å^3$)	1705.1(4)	7108.7(12)	3630.5(7)	7065(7)	7135.3(8)
Z	2	8	2	8	8

TH-3622_196122001

Density, gcm^{-3}	1.541	1.486	1.485	1.402	1.392
Abs. coeff., mm^{-1}	0.651	0.627	0.743	0.751	0.820
F (000)	818	3288	1680	3064	3072
Total no. of reflections	6919	7809	17273	6218	7863
Reflections, $I > 2\sigma(I)$	5588	5761	12104	4844	5966
Max. θ/°	25.242	25.242	25.242	25.000	25.242
Ranges (h, k, l)	$-13 \le h \le 13$ $-13 \le k \le 13$ $-19 \le l \le 19$	$-51 \le h \le 51$ $-14 \le k \le 14$ $-20 \le l \le 20$	$-13 \le h \le 13$ $-19 \le k \le 19$ $-30 \le l \le 30$	$-47 \le h \le 47$ $-13 \le k \le 13$ $-19 \le l \le 19$	$-51 \le h \le 51$ $-15 \le k \le 15$ $-20 \le l \le 20$
Complete to 2θ (%)	99.5	99.7	99.8	99.9	99.9
Data / restraints / parameters	6919/0/487	7809/0/483	17273/0/984	6218/0/455	7863/0/455
GooF (F^2)	1.174	1.056	1.127	1.095	1.151
R indices $[I > 2\sigma(I)]$	0.0680	0.0645	0.0673	0.0428	0.0601
wR_2 $[I > 2\sigma(I)]$	0.1145	0.1821	0.1308	0.0985	0.1094
R indices (all data)	0.0887	0.0894	0.1051	0.0621	0.0839
wR_2 (all data)	0.1230	0.2144	0.1504	0.1148	0.1214

Table A2: Hydrogen bond parameters of the Hydrates.

Hydrate	D-H···A	$d_{D\text{-}H}$ (Å)	$d_{H\cdots A}$ (Å)	$d_{D\cdots A}$ (Å)	∠D-H···A (º)
4.1	N(1) –H(1)...O(2) [1-x,1-y,1-z]	0.91(6)	1.74(6)	2.629(5)	166(6)
	N(3) –H(3A)...O(6) [1-x,1-y,-z]	0.89	2.03	2.797(4)	144
	N(3) –H(3B)...O(5) [x,y,z]	0.89	1.96	2.807(4)	159
	O(9) –H(9B)...O(8) [-1+x,y,z]	0.85	2.12	2.964(5)	173
	O(10) –H(10A)...O(9) [x,y,z]	0.82	1.94	2.751(7)	172
4.2	N(1) –H(1)...O(5) [x,1+y,z]	0.86	1.99	2.811(4)	158
	N(3) –H(3A)...O(7) [x,y,z]	0.89	1.94	2.808(4)	165
	N(3) –H(3B)...O(6) [x,-y,1/2+z]	0.89	1.90	2.778(4)	167
	O(9) –H(9B)...O(10) [x,y,z]	0.85	2.11	2.942(6)	166
	O(10) –H(10A)...O(11) [x,y,z]	0.70(8)	2.20(8)	2.872(6)	162(8)
	O(10) –H(10B)...O(8) [x,1-y,1/2+z]	0.83(6)	2.18(6)	2.929(4)	149(6)
4.3	N(1) –H(1)...O(20) [1+x,1+y,z]	0.92(6)	1.87(6)	2.765(5)	165(4)
	N(3) –H(3A)...O(17) [1+x,y,z]	0.89	1.95	2.813(4)	164
	N(3) –H(3B)...O(8) [x,y,z]	0.89	1.87	2.751(4)	168
	N(4) –H(4)...O(21) [x,y,z]	0.86	1.81	2.662(6)	171
	N(6) –H(6C)...O(18) [-1+x,y,z]	0.89	1.95	2.822(4)	166
	N(6) –H(6D)...O(16) [x,y,z]	0.89	1.86	2.723(4)	164
	O(17) –H(17A)...O(1) [x,y,z]	0.82	1.97	2.769(4)	163
	O(18) –H(18A)...O(11) [x,y,z]	0.82	1.84	2.651(4)	170
	O(19) –H(19A)...O(5) [1-x,1-y,1-z]	0.82	1.85	2.668(6)	175
	O(20) –H(20A)...O(10) [x,y,z]	0.85	1.93	2.755(4)	163
	O(20) –H(20B)...O(4) [1-x,1-y,1-z]	0.85	1.87	2.708(4)	169
	O(21) –H(21A)...O(20) [-x,1-y,1-z]	0.85	2.03	2.758(6)	144
	O(21) –H(21B)...O(19) [1-x,1-y,1-z]	0.85	1.86	2.700(8)	172
4.4	N(1) –H(1)...O(3) [x,-y,-1/2+z]	0.84(5)	1.95(5)	2.782(5)	175(5)
	N(3) –H(3A)...O(1) [x,1-y,-1/2+z]	0.89	1.88	2.752(3)	166
	N(3) –H(3B)...O(4) [x,1+y,z]	0.89	1.91	2.779(4)	165
4.5	N(1) –H(1)...O(1) [x,-y,-1/2+z]	0.87(5)	1.94(5)	2.813(4)	179(6)
	N(3) –H(3A)...O(2) [x,1+y,z]	0.89	1.90	2.777(4)	167
	N(3) –H(3B)...O(3) [x,1-y,-1/2+z]	0.89	1.92	2.794(3)	167

TH-3622_196122001

Table A3: Co-N and Co-O bond distances (Å) and Metal-ligand bond angles (º) in compounds of the cobalt(II) complex.

Co-H_2Clanth-Int (4.1)				**Co-H_2Clanth (4.2)**			
Bond distances (Å)		Bond angles (º)		Bond distances (Å)		Bond angles (º)	
Co1 – N4	2.030(3)	O7-Co1-O5	148.36(10)	Co1 – N4	2.034(3)	O3-Co1-O5	85.15(12)
Co1 – N5	2.027(3)	O7-Co1-O3	92.04(10)	Co1 – N5	2.016(3)	O3-Co1-O1	151.33(10)
Co1 – O1	2.161(3)	O7-Co1-O1	98.63(11)	Co1 – O1	2.186(3)	O3-Co1-O7	98.12(11)
Co1 – O3	2.167(3)	O5-Co1-O3	101.54(10)	Co1 – O3	2.134(3)	O5-Co1-O1	99.69(11)
Co1 – O5	2.164(3)	O1-Co1-O5	83.18(11)	Co1 – O5	2.177(3)	O5-Co1-O7	150.48(9)
Co1 – O7	2.161(3)	O1-Co1-O3	151.00(10)	Co1 – O7	2.186(3)	N5-Co1-O3	115.43(11)
		N5-Co1-O7	76.19(10)			N5-Co1-O5	75.88(10)
		N5-Co1-O5	75.18(10)			N5-Co1-O1	93.07(10)
		N5-Co1-O3	90.82(10)			N5-Co1-O7	76.28(10)
		N5-Co1-O1	117.86(11)			N5-Co1-N4	168.34(12)
		N5-Co1-N4	166.45(11)			O7-Co1-O1	91.39(11)
		N4-Co1-O7	102.79(10)			N4-Co1-O3	76.17(11)
		N4-Co1-O5	108.19(10)			N4-Co1-O5	107.47(10)
		N4-Co1-O3	75.67(11)			N4-Co1-O1	75.42(11)
		N4-Co1-O1	75.69(11)			N4-Co1-O7	101.77(10)

Table A4: Cu-N and Cu-O bond distances (Å) and Metal-ligand bond angles (º) in compounds of the copper(II) complex.

Cu-H_2Clanth-Int (4.3)				**Cu-H_2Clanth (4.4)**			
Bond distances (Å)		Bond angles (º)		Bond distances (Å)		Bond angles (º)	
Cu1 – N7	1.934(3)	O1-Cu1-O7	95.88(11)	Cu1 – N4	1.952(2)	O7-Cu1-O3	83.76(10)
Cu1 – N8	1.946(3)	O1-Cu1-O3	155.65(10)	Cu1 – N5	1.928(2)	O7-Cu1-O1	96.38(10)
Cu1 – O1	2.125(3)	O1-Cu1-O5	90.73(11)	Cu1 – O1	2.257(2)	O1-Cu1-O3	151.97(8)
Cu1 – O3	2.189(3)	O3-Cu1-O7	92.57(10)	Cu1 – O3	2.274(2)	O5-Cu1-O3	100.34(10)
Cu1 – O5	2.220(3)	O3-Cu1-O5	91.54(10)	Cu1 – O5	2.125(2)	O5-Cu1-O7	156.60(8)
Cu1 – O7	2.223(3)	O5-Cu1-O7	154.12(10)	Cu1 – O7	2.136(2)	O5-Cu1-O1	90.59(10)
Cu2 – N9	1.916(3)	N8-Cu1-O1	97.42(11)			N4-Cu1-O3	76.45(9)
Cu2 – N10	1.946(3)	N8-Cu1-O7	77.20(10)			N4-Cu1-O7	108.98(9)
Cu2 – O9	2.111(3)	N8-Cu1-O3	106.72(11)			N4-Cu1-O1	77.05(9)
Cu2 – O11	2.111(3)	N8-Cu1-O5	77.15(11)			N4-Cu1-O5	94.34(9)
Cu2 – O13	2.244(3)	N7-Cu1-O1	78.85(11)			N5-Cu1-O3	105.74(9)
Cu2 – O15	2.329(3)	N7-Cu1-O7	99.60(10)			N5-Cu1-O7	78.14(10)
		N7-Cu1-O3	77.25(10)			N5-Cu1-O1	101.68(9)
		N7-Cu1-O5	106.23(11)			N5-Cu1-O5	78.58(10)
		N7-Cu1-N8	174.89(11)			N5-Cu1-N4	172.82(10)
		O11-Cu2-O9.	158.10(10)				
		O11-Cu2-O15	95.87(11)				
		O11-Cu2-O13	90.30(11)				
		O9-Cu2-O15	88.14(11)				
		O9-Cu2-O13	95.69(11)				
		N10-Cu2-O11	98.91(11)				
		N10-Cu2-O9	102.95(10)				
		N10-Cu2-O15	76.17(10)				
		N10-Cu2-O13	77.38(10)				
		O13-Cu2-O15	153.46(9)				
		N9-Cu2-O11	78.88(12)				
		N9-Cu2-O9	79.31(11)				
		N9-Cu2-N10	177.18(12)				
		N9-Cu2-O15	105.72(10)				
		N9-Cu2-O13.	100.80(11)				

TH-3622_196122001

Table A5: Zn-N and Zn-O bond distances (Å) and Metal-ligand bond angles (º) in compound of the zinc(II)complex.

Zn-H_2Clanth (4.5)

Bond distances (Å)		Bond angles (º)	
Zn1 – N4	2.007(2)	O1-Zn1-O5	98.69(9)
Zn1 – N5	2.023(2)	O3-Zn1-O1	151.49(8)
Zn1 – O1	2.220(2)	O3-Zn1-O5	88.92(9)
Zn1 – O3	2.208(2)	O7-Zn1-O1	86.67(9)
Zn1 – O5	2.292(2)	O7-Zn1-O3	99.59(10)
Zn1 – O7	2.114(2)	O7-Zn1-O5	151.63(9)
		N5-Zn1-O1	106.28(9)
		N5-Zn1-O3	102.23(9)
		N5-Zn1-O5	73.89(9)
		N5-Zn1-O7	77.86(10)
		N4-Zn1-O1	75.87(9)
		N4-Zn1-O3	76.54(9)
		N4-Zn1-O5	91.24(9)
		N4-Zn1-O7	117.02(9)
		N4-Zn1-N5	165.12(10)

(a) (b) (c)

Figure A1: Optical images of (a) **Co-H_2Clanth**, (**4.2**) (b) **Cu-H_2Clanth** (**4.4**) and (c) **Zn-H_2Clanth** (**4.5**).

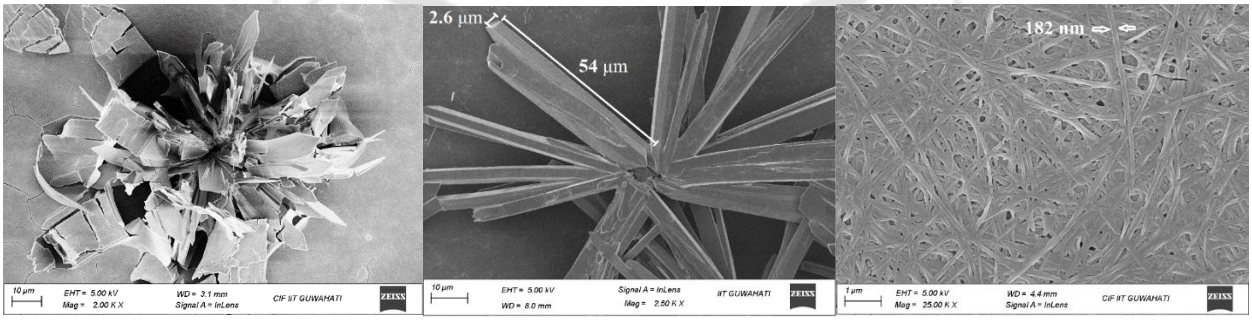

(a) (b) (c))

Figure A2: FESEM images of (a) **Co-H_2Clanth** (**4.2**), (b) **Cu-H_2Clanth** (**4.4**), and (c) **Zn-H_2Clanth** (**4.5**).

TH-3622_196122001

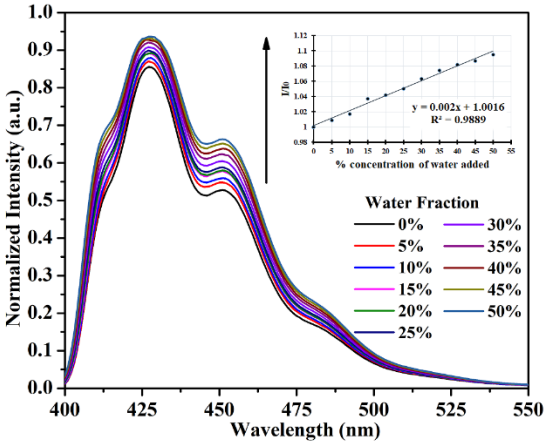

Figure A4: Spectrofluorimetric titration of **Zn-H$_2$Clanth (4.5)** (2mL, 10^{-5} M in methanol), by addition of 0-50% water. Inset: change in fluorescence intensity at 428 nm after systematic addition of w ater during titration (λ_{ex} 300 nm).

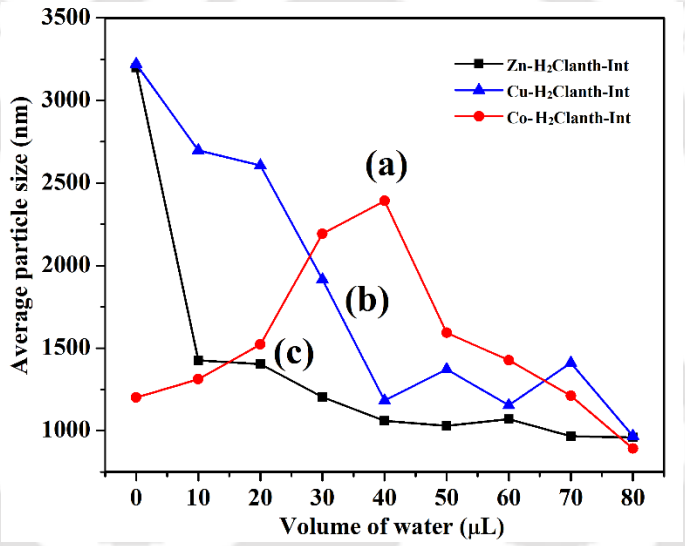

Figure A5: Plot of average particle sizes measured by dynamic light scattering 2 mL solution taken from a bulk methanol solution containing independent solution of (a) $Co(OAc)_2.4H_2O$ (0.02 mM); (b) $Cu(OAc)_2.H_2O$ (0.02 mM) or (c) $Zn(OAc)_2.2H_2O$ (0.02 mM) together with 26-H_2pdc, (0.04 mM); Clanth (0.02mM) upon addition of 10µL of water in aliquots.

Table A6: Diameter of average particle sizes from DLS experiment shown in Figure A5.

Volume of water added (µL)	Diameter of average particle size (nm)		
	Zn	**Co**	**Cu**
0	3200 ± 48	1201 ± 21	3221 ± 0
l10	1426 ± 118	1312 ± 41	2698 ± 4
20	1403 ± 177	1522 ± 14	2607 ± 3
30	1203 ± 82	2193 ± 0	1915 ± 9
40	1059 ± 92	2392 ± 6	1183 ± 18
50	1029 ± 66	1593 ± 15	1372 ± 13
60	1069 ± 48	1427 ± 24	1154 ± 25
70	965 ± 79	1211 ± 27	1411 ± 34
80	957 ± 132	891 ± 66	966 ± 39

TH-3622_196122001

CHAPTER 5

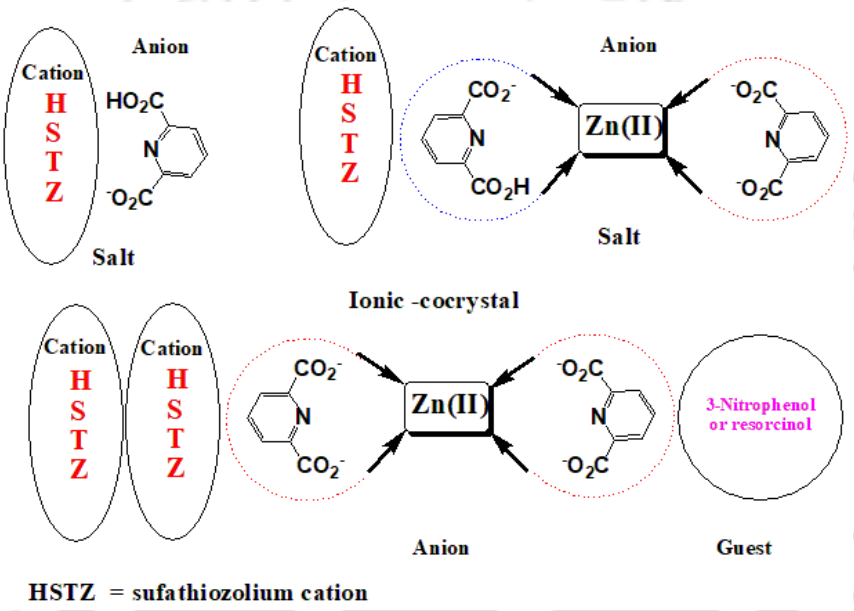

TH-3622_196122001

Chapter 5

Salts and ionic-cocrystals of 2,6-pyridinedicarboxylic acid and zinc complexes of it with cations of sulfa-drug

5.1. Introduction

Having established the numbers of multi-component cocystals of organo-ammonium based compounds with pyridinedicarboxylic acids as well as 2,6-pyridinedicarboxylic acid (H_2**26pdc**) in the earlier three chapters of this thesis, their possible utility in recognition and release of specific component of ionic-cocrystals were evident. 2,6-Pyridinedicarboxylic acid is a biocompatible compound.[1] It is a good coformer for API cocrystals[2-4] and it also forms various metal complexes.[5,6] Hence, it was felt that anion based on H_2**26pdc** or corresponding anionic complexes will serve or provide counterions to drug molecules such as sulfa-drugs having amine functionality. As a matter of fact, physical properties of active pharmaceutical ingredient (API) depend on properties of their partner components.[7-11] Use of inorganic salts as API provide new drug formulations.[12-14] The salts of amphoteric compounds are of interest as the partner molecule may also act as a guest molecule to provide different compositions. For example, salt of 4-aminobenzoic acid with dichloroacetic acid (A) has a dichloroacetic acid guest molecule;[15] whereas, salt of 2-aminobenzoic acid (B) with 2-hydroxy-3,5-dinitrobenzoic acid has protonated 2-aminobenzoic acid (B) as a guest (Figure 5.1).[16] Cocrystal C of Figure 5.1 has one protonated, two neutral 4-aminobenzoic acid molecules along with a 2-hydroxy-3,5-dinitrobenzoate anion.[16] Cocrystal or salt of regiomers such as maleic acid or fumaric acid with same coformer differ in stoichiometry.[17,18] These selected examples show that the stoichiometry of an adduct of conjugate acid-base may differ in an ionic-cocrystal. Such facts provided scopes to explore compositions of carboxylic acid salts of an API.

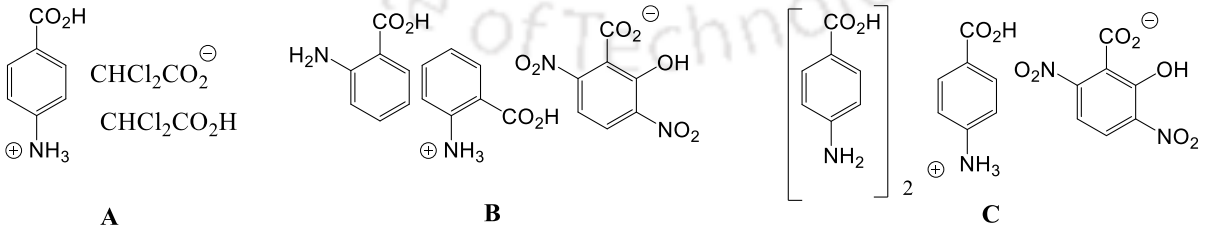

Figure 5.1: Some examples of ionic-cocrystals of carboxylic acids.

Due to low bio-availability and limited solubility of sulfa-drugs in water, some of those drugs are used in the form of their corresponding salts.[19-21] Cocrystals and salts of sulfathiazole drugs are

TH-3622_196122001

well studied.[22-27] Some sulfa-drugs show imine-amine tautomerism that influences nature of their cocrystals (Fig 5.2).[28,29] Self-assemblies of sulfathiazolium salt and zinc-26pdc complexes with different compositions are presented in this chapter to show varities in compositions.

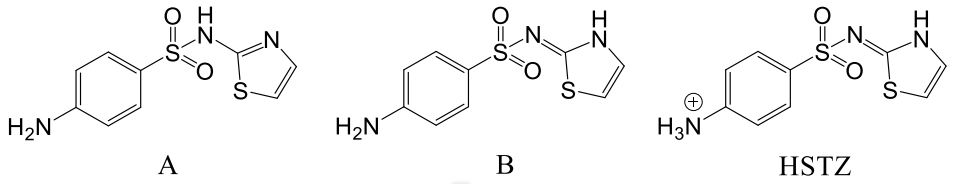

Figure 5.2: (A) Amine and (B) imine and HSTZ is protonated forms of sulfathiazole.

5.2. Synthesis and characterisation of the salt of 2,6-pyridinedicarboxylate with sulfathiazole

Sulfathiazole has two prontonation sites and has scope to form diprotonated species by recation with an acid, but the recation of 2,6-pyridinedicarboxylic acid (H_2**26pdc**) with sulfathiazole provided an 1:1 salt at ambient condition. The salt crystallised as hemihydrate had the composition [(HSTZ)(H**26pdc**)]·0.5H_2O (**5.1**). One of the carboxylic group was deprotonated and other remained as a free carboxylic acid in the pyridinedicarboxylic acid part. This composition offered as a new API salt to the vaious other salts listed for the drug molecule.[30-32] This salt had distinction of having a mono-deprotonated dicarboxylic acid and a mono-protonated sulfathiazole. It crystallised upon slow evaporation of the solvent of a solution containing the salt. The mono-deprotonated salt of 2,6-pyridinedicarboxylic acid (pKa = 2.6) with sulfathiazole (pKa = 7.2), hence the salt was formed due to large difference between the pKa of the acid with pKa of the base.[28] The salt was characterised by ^{1}HNMR and IR, followed by determining single crystal structure by X-ray diffraction. At room temperature we were not able to obtain crystalline product of dicarboxylate salt. Cationic part of the salt was protonated sulfathiazole in which phenylamino group was protonated. ^{1}HNMR of the salt had the proton-signals corresponding to cationic and anionic components as assigned in the Figure 5.8; the integrations of the signals of the protons from the anion and the cation were matching to an 1:1 ionic composition. Single crystal X-ray crystallographic study had revealed that unit cell of the crystal of the salt has HSTZ cation and H**26pdc** anion with half a molecule of water. The cation adopted imine form that is conventionally observed in the cocrystals of sulfathiazole.[28,29] However, there were examples in literature in related cocrystals or salts where both the tautomers namely imine or amine were also observed together in asymmetric unit determined by X-ray crystal structure.[29]

TH-3622_196122001

In the self-assembly determined by X-ray single crystal diffraction crystal structure, one N-H bond of the protonated amine group had participated in N1-H···O7 hydrogen bond with a bridging water molecule, which was further linked an oxygen atom of carboxylate anion through O7-H···O6 hydrogen bond. Another N-H of ammonium ion was found to form hydrogen bond with oxygen (of C=O) of a carboxylic acid group (Figure 5.3a).

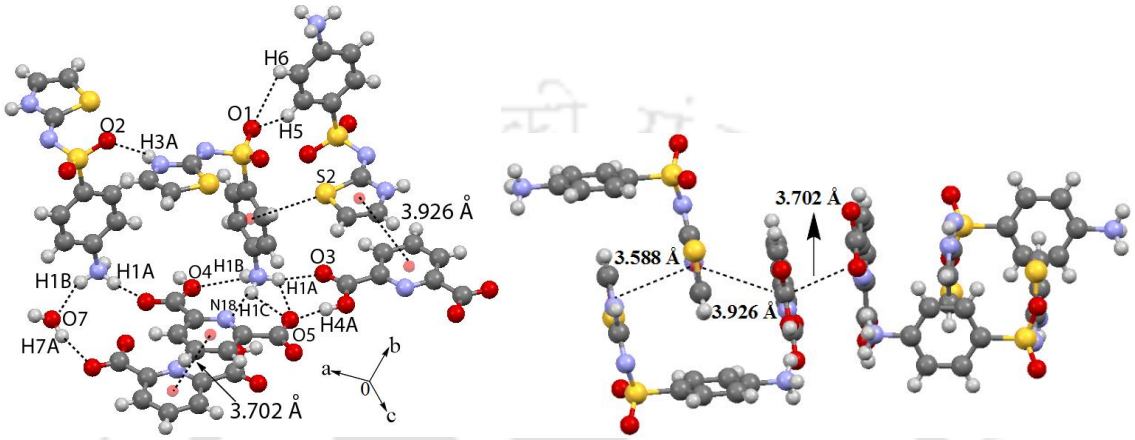

Figure 5.3: (a) Self-assemblies of (a) [(HSTZ)(H**26pdc**]·0.5H_2O (**5.1**), (b) Hydrogen bonded clips that encapsulate cation in the salt.

The hydrogen bond parameters are listed in Table A2 of the appendix secion. Oxygen atom of the oxy-anion of deprotonated carboxylic acid group formed O4-H···O5 hydrogen bond with O-H group of a carboxylic acid of a neighboring H**26pdc**. The self-assembly of the mono-anionic salt of 2,6-pyridinedicarboxylic acid with this particular organo-cation was of interest; as the corresponding sodium, potassium, cesium salts of 2,6-pyridinedicarboxylic acid were found to be multi-nuclear complexes or coordination polymers.[33] The self-assembly of the salt had C-H···O interactions involving C=O of carboxylate of the H**26pdc**, and S=O of the HSTZ. The C-H···O interactions were useful in self-assemblies to stabilize particular conformation of sulfa drugs.[34] In this case, these were inter-molecular interactions, which contributed to the interplay of weak interactions in the packing pattern and also had helped to form weakly bound dimeric units between cations within the assembly (Fig 5.3b). Water molecules had acted as hydrogen bond donor as well as hydrogen-bond acceptor holding the cationic and anionic counter parts together. Carboxylate group of the salt had participated in intermolecular hydrogen bonds with a free carboxylic acid group of neighbouring H**26pdc**. In general, aromatic stacking interactions are important in solid state packing of sulfa-drugs.[35,36] In the present example, thiazolium cation was

TH-3622_196122001

hydrogen bonded to H**26pdc** forming clip-like structure (Figure 5.3b) and the thiazole ring of another cation got sandwiched by the clip like arrangement to have shown the observed stacking interactions. H**26pdc** molecules of two such clips were co-facial neighbours, with a centroid to centroid distance 3.702 Å. One end of another cation, namely the thiazole ring was encapsulated into such a clip with 3.926 Å centroid to centroid distance with the H**26pdc** ring, whereas, the other face found the phenyl ring of phenylammonium cation parallel with a distance of separation 3.588 Å. These distances indicated aromatic stacking between these aromatic rings as important factor in the self-assembly which were also had charge-assisted hydrogen bonds[37] between cations and anions.

5.3. Synthesis and self-assemblies of the zinc complexes of 2,6-pyridinedicarboxylate with sulfathiazolium cation

As sulfadiazolium cation was associtaed with monodeprotonated 2,6-pyridinedicarboxylic acid, the result had encouraged to explore possible water soluble sulfathiazolium containing metal complexes of 2,6-pyridinedicarboxylate as illustrtated in the scheme 5.1.

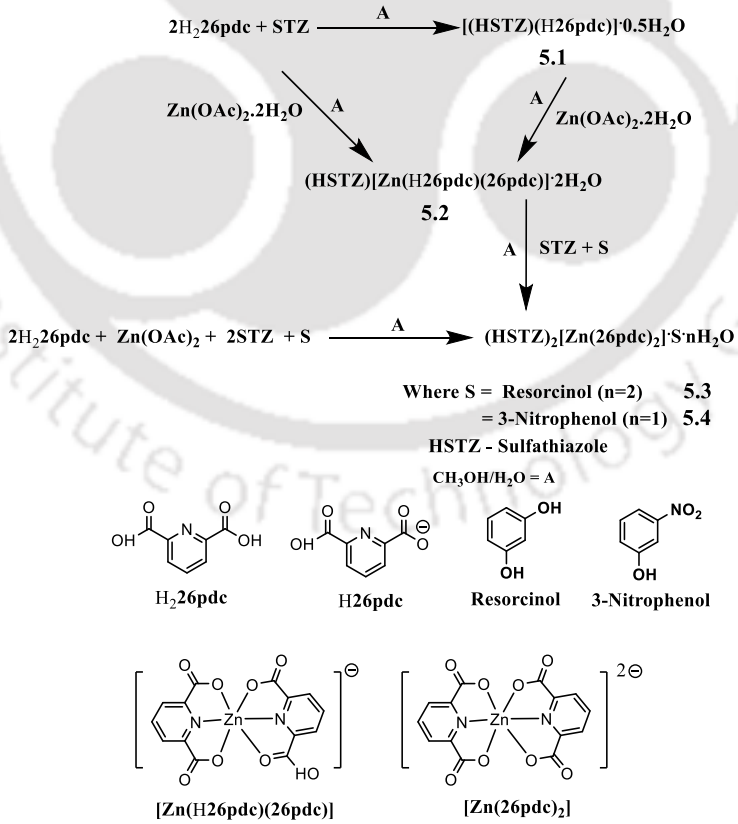

Scheme 5.1: Synthesis of salt **5.1** and complexes **5.2-5.4**.

TH-3622_196122001

In fact, the initial attempt to synthesize zinc-2,6-pyridinedicarboxylate by treatment of the salt [(HSTZ)(H**26pdc**)]·0.5H_2O with zinc(II) actetate salt had provided poor yield of a desired water soluble complex of the mono as well as di-deprotonated carboxylic acid, namely (HSTZ)[Zn(H**26pdc**)(**26pdc**)]·2H_2O (**5.2**) that had both mono and dianionic ligands.

The same complex could be prepared in good yield from a reaction of zinc(II) acetate with H_2**26pdc** in the presence of STZ. Excess amounts of sulfathiazole in the reaction also did not yield the corresponding dianionic zinc-pyridinedicarboxylate complex (HSTZ)$_2$[Zn(**26pdc**)$_2$]. The complex **5.2** was also characterised by recording IR, ^{1}HNMR and finally by determining crystal structure. Self-assembly of the complex dtermined from the X-ray crystal structure is shown in the Figure 5.4a. Complex had extensive hydrogen bonds involving water of crystallisation molecules in its self-assembly. Self-assembly had robust hydrogen bonded cyclic sub-assembly with graph set noation $R^5_6(16)$.[38] The robust sub-assemblies were formed by associations of four water molecules and two neighbouring two pdc of the anionic part as illustrated in Figure 5.4a. Two O-H bonds of two bridging water molecules of such a motif further formed O12-H···O2 hydrogen bonds with S=O of two independent cations. The pdc of the anionic part was engaged in hydrogen bond with cations forming cyclic $R^3_3(10)$ hydrogen bonded sub-assemblies. Due to this hydrogen bonded units, two neighbour cations were associated together through hydrogen bonds which were also held to an anion. The sulfathiazole is an unsymmetrical molecule, one end of it has a thiazole unit (denoted as head) and other end had aminophenyl unit (denoted as tail).

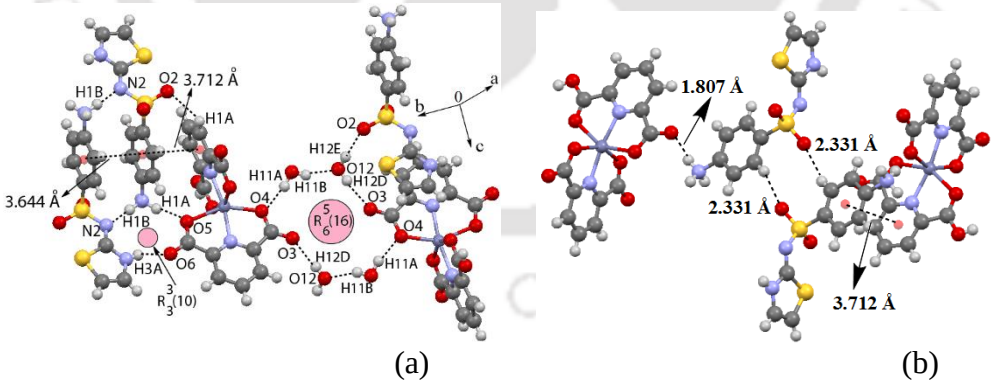

(a) (b)

Figure 5.4: (a) Self-assemblies of (HSTZ)[Zn(H**26pdc**)(**26pdc**)]·2H_2O (**5.2**), (b) Aromatic stacking interactions and C-H···O hydrogen bonds in self-assembly of **5.2**.

In the self-assembly the protonated cations were organised by hydrogen bonded dimers in head to tail manners. The dimers were held by N1-H···N2 hydrogen bonds. In the assembly phenyl rings of cations are located parallel to one set of pdc rings of anions, where the centroid to centroid

TH-3622_196122001

distance between the parallel rings is 3.712 Å. This distance between parallel planar π-rings suggested a strong aromatic stacking interaction between them. A close look at the arrangements of cations suggested that thiazole rings were also parallel to another set of pdc rings of anions. The co-facial distance of separation between such rings was found to be 4.123 Å. So, sulfathiazolium cations had served as bridge to hold two anions at two ends by weak aromatic stacking interactions. The cations in the assembly had C1-H···O2 interactions, contributed to overall scheme of hydrogen bonds.

When additional amounts of sulfathiazole was dissolved in methanol along with complex **5.2**, and to the same solution resorcinol or 3-nitrophenol was added, the respective solution provided ionic-cocrystals complex each having the dianionic-pdc as the only ligands to the zinc ion. The attempted crystallization by using 1,4-, 1,2- dihydroxy benzene or other positional isomers of nitro-phenols were not successful.

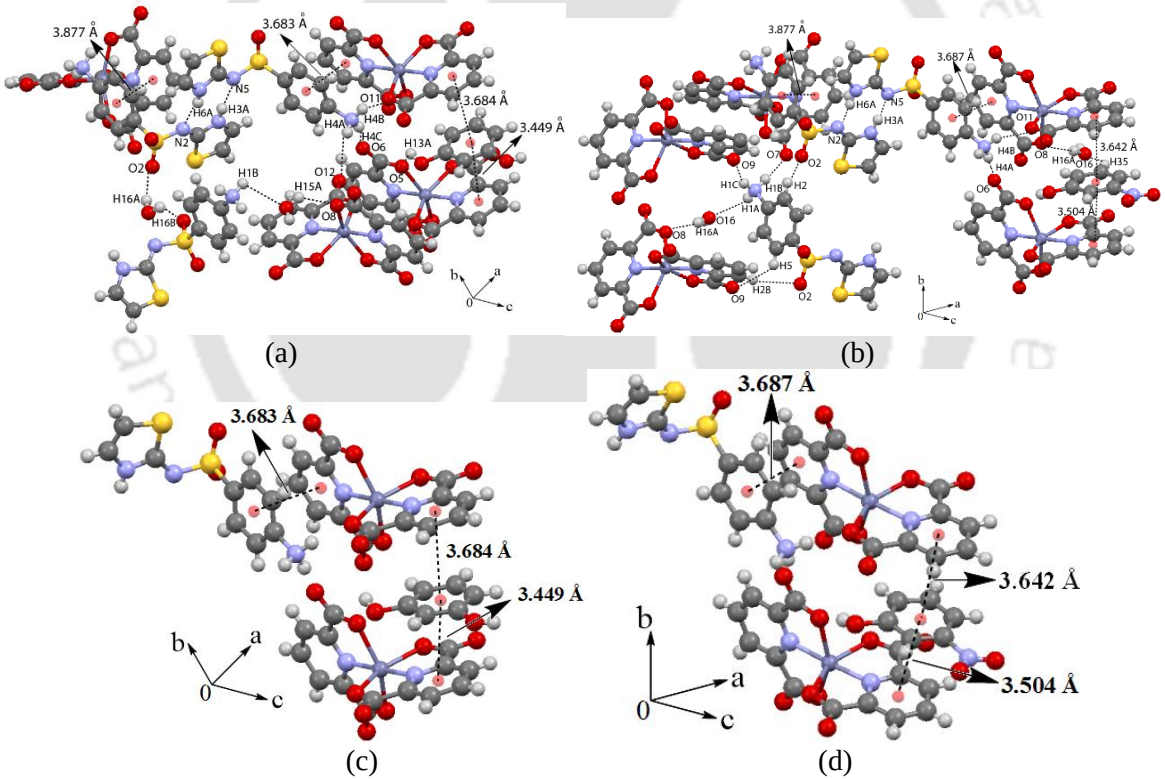

Figure 5.5: Self-assemblies of (a) $(HSTZ)_2[Zn(\mathbf{26pdc})_2]\cdot(resorcinol)\cdot 2H_2O$ (**5.3**) and (b) $(HSTZ)_2[Zn(\mathbf{26pdc})_2]\cdot(3\text{-}NP)\cdot H_2O$ (**5.4**). (c) and (d) are aromatic stacking among the ligands of the **5.3** and **5.4** respectively.

In the absence of the phenolic compounds, we could not crystallize the complex as $(HSTZ)_2[Zn(\mathbf{26pdc})_2]$. Ionic-cocrystal with resorcinol had a composition $(HSTZ)_2[Zn(\mathbf{26pdc})_2]\cdot(resorcinol)\cdot 2H_2O$ (**5.3**); whereas, the ionic-cocrystal with 3-nitrophenol had

TH-3622_196122001

a composition $(HSTZ)_2[Zn(\mathbf{26pdc})_2]\cdot(3\text{-nitrophenol})\cdot H_2O$ (**5.4**). Organocation containing zinc-pdc complexes possessing nitrophenolic guests have been well known in literature.[39] Both the complexes had conventional ONO-coordination modes of the pdc anion. Cations were formed by proton-transfer from the acid to the STZ. In each case, the nitrogen atom of aminophenyl unit of STZ molecule was protonated. The bond distances in the crystal structures of the complexes were supportive of imine form of the cations in the complexes. The self-assemblies of the two complexes (**5.3** and **5.4**) are depicted in Figure 5.5a and 5.5b. A characteristic feature of the self-assemblies of these two ionic-cocrystals was that, in both the cases cations were hydrogen bonded dimers having N3-H···N5 hydrogen bonds. Dimers had cations in head to tail arrangements. Each dimer had N-H···N hydrogen bonds between two similar rings, thereby forming $R^2_2(8)$ type units. Due to such sub-assemblies of the cations were located at translated positions, keeping the two heads close to each other but they maintained head to tail arrangements between the constituent cations. The N-H bonds of phenylammonium unit were involved in hydrogen bonds with oxygen atoms of coordinated **26pdc**. These hydrogen-bonded dimers acted as bridge by holding anions at two distal ends. The π-stackings between two phenylammonium ring of dimeric cations with two pdc rings from two independent anions occured at two ends of such a dimer. Distance of separation between co-facial rings of phenylammonium unit and chelated pdc ring in both the ionic-cocrystals **5.3** and **5.4** were very close, 3.683 Å and 3.687 Å respectively. These observations had suggested the presence of aromatic stacking interactions between the rings (Figure 5.5c and Figure 5.5d). Thiazole ring of cation of these ionic-cocrystals were not involved in stacking with pdc. As a consequence of stacking, each dimer acted as bridge to hold two anions at distal ends. Further to these, the hydroxyaromatic molecules were sandwiched between parallel pdc-rings of independent anions. Arrangement of anions in the lattice were influenced by aromatic stacking of the cations with anions as well as by the aromatic guests sandwiced between the anions. Since, stacking interactions of pdc with guest was the key factor in establishing the dianionic complexes. It was due to the ability of the pdc ligands of the complexes to involve in second coordination sphere interactions. In self-assembly of **5.3**, the centroid to centroid distance between parallel planes of pdc and resorcinol rings with respect to the independent faces of the resorcinol were 3.684 Å and 3.449 Å (Figure 5.5c). Whereas, such distances in **5.4** were 3.642 Å and 3.504 Å respectively (Figure 5.5d). **5.3** was dihydrate; where the molecules of water of crystallisation formed hydrogen

TH-3622_196122001

bonds with cations and anions. It may be mentioned that the pyridinedicarboxylate complexes had been well known to form layer-like structures through stacking interactions.[39] Presence of two relatively large size cations in lattice per anion, required bigger separation between the anions in respective crystal lattice. Stacking of hydroxyaromatics and dimers of the cations provided the necessary bridges among anions to keep the cation-cation contact well apart. On the other hand, the hydroxyaromatics getting sandwiched between the planes of chelated pdcs provided the required rigidity to the assembly and to maintain the directional nature of the self-assembly. Due to these reasons, dianionic complex without hydroxyaromatic guest could not be obtained. Alternatively, hydroxyaromatic guest molecules provided appropriate packing patterns in the respective ionic-cocrystal to accommodate two relatively big sized sulfathiazolium cations per dianion. Analysis of dimeric motifs of the cations revealed that, ways of association among cations depended on anions. Mono-deprotonated salt had dimeric motifs with very weak C-H···N interactions (Figure 5.6a) or they may be assumed as organised non-interacting monomers in the lattice. Self-assembly of **5.2** had hydrogen bonded dimers of cations formed through C-H···O interactions; whereas, the **5.3** and **5.4** had hydrogen bonded dimers formed by moderate N-H···N hydrogen bonds. As the hydrogen bond sites differed in each hydrogen bonded dimer, conformational adjustments of cation in the complex, as well as the translated position of a cation with respect to another cation in the self-assembly were different. Such motifs also had the cations arranged in a head to tail arrangement to reduce the inter-cationic repulsion. In general, multi-component APIs with different stoichiometric compositions by partner variations have been useful to modulate properties.[40-42] The examples shown here have different compositions which provided means to prepare API compositions with varied amounts of API with least invariance in the contents or by changing synthetic strategies.

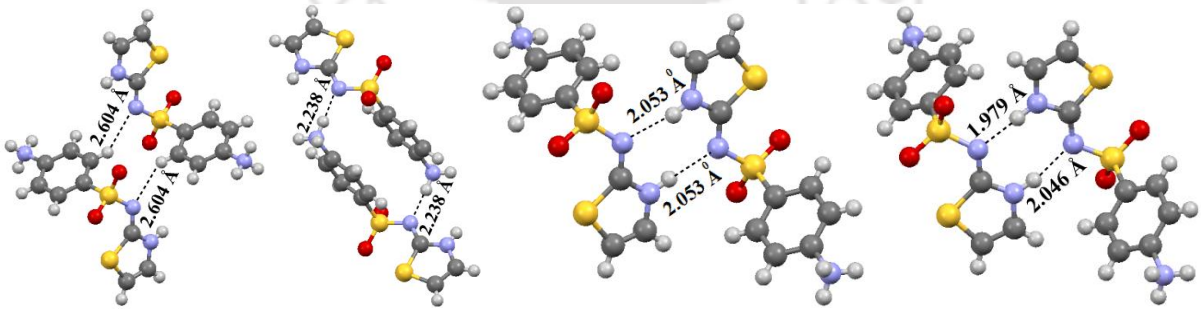

(a) (b) (c) (d)

Figure 5.6: Different hydrogen bonded cationic dimers found in self-assembly of (a) **5.1**, (b) **5.2**, (c) **5.3** and (d) **5.4**.

TH-3622_196122001

Generally, sulfa-drugs have poor solubility in water;[22-27,43] however, our sulfa drug containing zinc complexes reported here are highly soluble in water. The enhanced solubility was attributed to higher ionic character of the zinc complexes (Table 5.1).

Table 5.1: Molar conductance of salt and complexes

Compound	Molar Conductance ($S\ cm^2\ mole^{-1}$)
5.1	26
5.2	122
5.3	179
5.4	170

Molar conductance of the salt **5.1** is less than the complexes was suggestive of its less-ionic nature in water then the complexes. Molar conductance values of the complexes were in the order, **5.2** < **5.3** ~ **5.4** (Table 5.1). Molar conductance of the **5.2** confirmed it as 1:1 electrolyte (60 $S\ cm^2\ mole^{-1}$ per ion). Such values of **5.3** and **5.4** supported them to be 2:1 electrolyte. Guest molecules did not influence the ionizations.

5.4. Powder X-ray diffraction study of 5.1-5.4

In the present examples, there was the formation of only crystalline compounds, and thus, it was necessary to find out the bulk purity of the samples after crystallization, as the crystals observed are shown as the yield of the individual compounds. The phase of the crystalline compound matched the structure obtained from the single-crystal study. This suggested single phases of the recrystallized products.

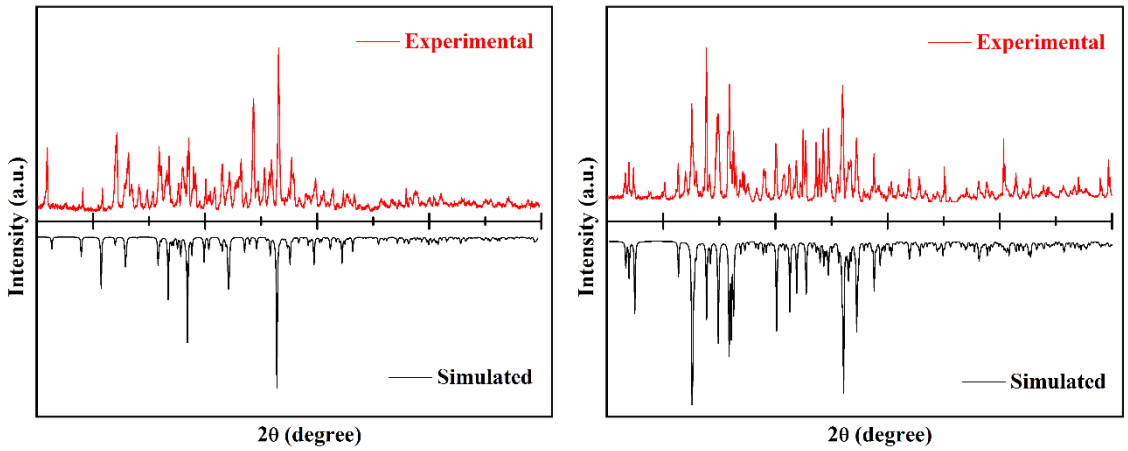

(a) (b)

TH-3622_196122001

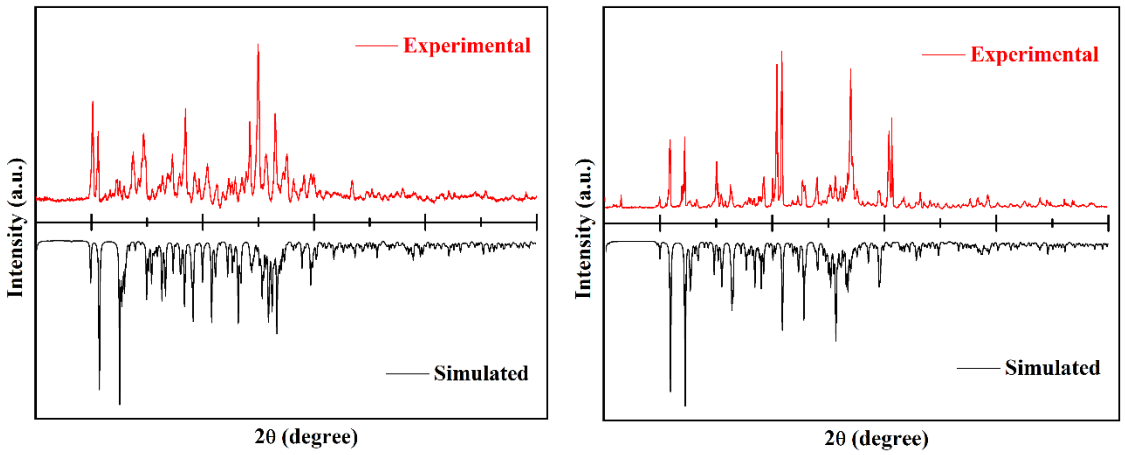

Figure 5.7: (i) PXRD patterns of (a) **5.1**, (b) **5.2**, (c) **5.3**, and (d) **5.4** (Red = Experimental, Black = Simulated pattern generated from CIF file ($5^0 \leq 2\theta \leq 50^0$).

The powder X-ray diffraction of these complexes **5.1-5.4** was recorded (Figure 5.7). When we compared the simulated powder patterns of these complexes with the experimental data, it was confirmed that the experimental diffraction patterns matched the simulated diffraction pattern obtained from single crystal diffraction data, indicating a high purity of the bulk materials.

5.5. NMR Spectra

All the compounds **5.1-5.4** were soluble in dimethyl sulfoxide (DMSO), which provided us the scope to study them in the solution phase. The ^{1}H-NMR spectra of the complexes were recorded and compared with the spectra of the parent compounds; the peak position and multiplicity confirms the composition of compounds. In all the cases broad peak in the range 12.45-12.50 ppm confirms the existence of sulfathiazole in its imine form (Figure 5.8).

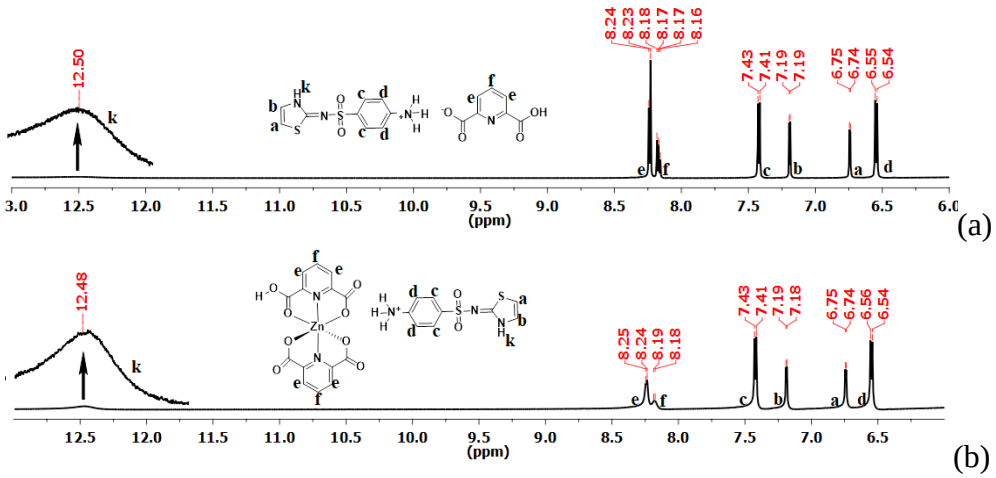

TH-3622_196122001

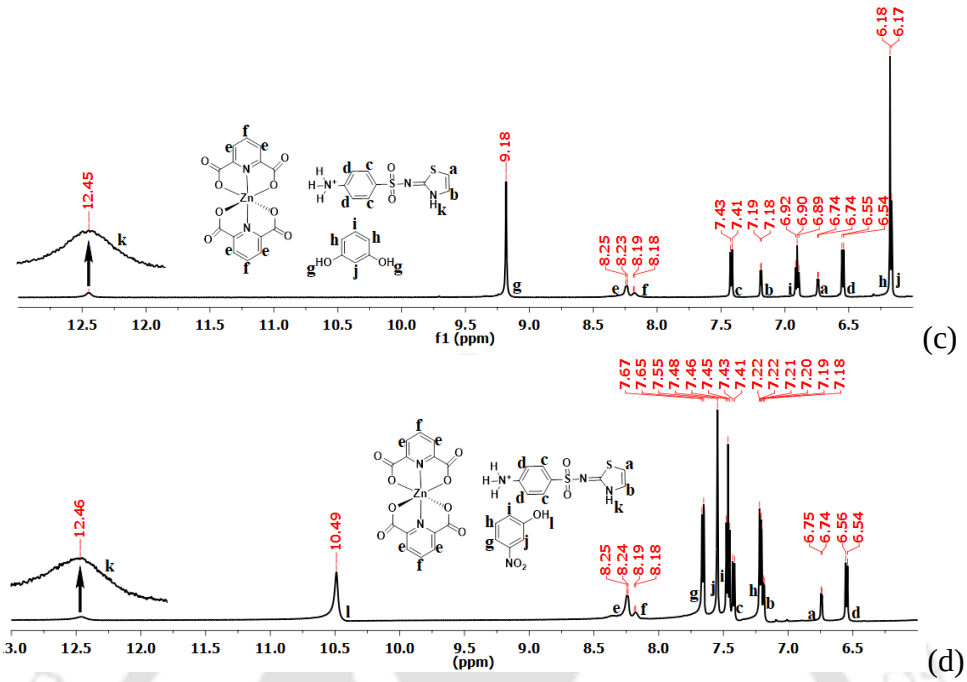

Figure 5.8: ^{1}H-NMR (600 MHz, DMSO-d_6) spectra of (a) **5.1**, (b) **5.2**, (c) **5.3** and (d) **5.4**.

The peaks due to aromatic -OH proton shows a singlet at 9.18 ppm and 10.49 ppm for resorcinol (Figure 5.8c) and 3-nitrophenol (Figure 5.8d) respectively. The peaks range from 6.17-8.25 ppm in all the cases corresponds to the aromatic protons.

5.6. UV-visible and Fluorescence spectra

Generally, nitro-aromatic compounds are quencher of emission of aromatic fluorophores; emission spectra of a solution of **5.2** in water showed a weak emission at 395 nm (Figure 5.9a). This emission peak in aqueous solution was quenched upon addition of 3-nitrophenol; whereas, upon addition of resorcinol to an aqueous solution of the **5.2** emission did not change (Figure 5.9b). Similarly, in the case of **5.3** quenching was administered during the titration against 3-nitrophenol (392 nm) and no change in fluorescence intensity was observed for the titration against resorcinol (Figure A3). However, no evident change can be observed in the fluorescence intensities for compound **5.4** (Figure A4). Hence, the examples showed here have their distinguishable characteristic optical features too. The solid state spectral (UV-visible and fluorescence) studies of the compounds **5.1-5.4** were also done to see their characteristic signature peaks. The λ_{max} of absorption spectra of solid compounds **5.1**, **5.2**, **5.3** and **5.4** was 340 nm, 310 nm, 370 nm and 333

TH-3622_196122001

nm respectively {Figure A3 (a)}. The emission spectra of solid samples corresponds to λ_{em} at 381 nm, 386 nm, 372 nm and 375 nm for compounds **5.1**, **5.2**, **5.3** and **5.4** respectively.

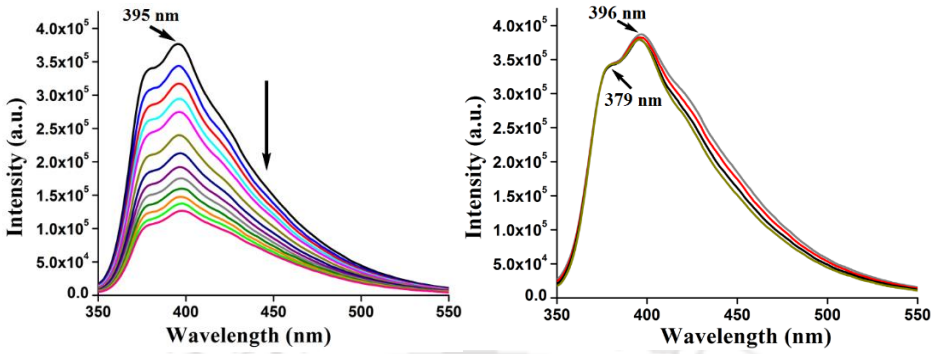

Figure 5.9: Fluorescence titration of **5.2** (10^{-4} M in water) with **(a)** 3-Nitrophenol and **(b)** Resorcinol, (10 µL aliquot of 10^{-3} M in water). (ex. 330 nm)

Due to the structural variation different emission spectra was observed, the ionic-cocrystal (**5.3**) consisting 3-nitrophenol as a guest shows the quenched fluorescence intensity even in the solid state spectra at 375 nm {Figure A3 (b)}.

5.7. Conclusions

The intrinsic acid-base property, stacking abilities and ligating properties of 2,6-pyridinedicarboxylic acid were used to regulate amounts of cationic form of sulfathiazole drug to prepare different self-assemblies of different compositions. Three different compositions of salts of sulfathiazole with pdc were used as examples to show varied drug compositions with minimum invariants through formation of self-assemblies. It was also shown that the despite $[Zn(\mathbf{26pdc})_2]^{2-}$ being the common species, an additional component was necessary as an exception to stabilize this as $(HSTZ)_2[Zn(\mathbf{26pdc})_2]$. It was not favored without a coformer due to the large size of the cations. Accordingly, self-assemblies with phenolic compounds were stabilized by aromatic stacking interactions. These aspects were important to modulate the proportions of drugs and in controlled release, as the 1:1 electrolyte released lesser amount of a component than a 2:1 electrolyte in solution. The antibacterial activities with *E. coli* DH5α have shown that the salt and the complexes have lower g/ml antibacterial activity than the parent drug (Table A4).

TH-3622_196122001

5.8. Experimental Section

The detailed synthetic methodologies for the synthesis of the salt and metal complexes are described. Analytical data are provided with each compound. The instrumental details, crystallographic parameters, and method used are provided in Appendix section at the end of this chapter. The following abbreviations are used for identification of spin multiplicities in 1H-NMR spectra: s = singlet, d = doublet, t = triplet, q = quartet, m = multiplet; and for FTIR spectra, following abbreviations were used to identify the absorption bands: s = strong, w = weak, br = broad, m = medium.

[(HSTZ)(H26pdc)] 0.5H_2O (5.1): A solution of sulfathiazole (255 mg, 1 mmol) in 10 ml methanol was mixed with solution of 2,6-pyridinedicarboxylic acid (167 mg, 1.0 mmol, 10 ml) in methanol and the stirred. The transparent solution thus obtained was left to slowly evaporate in air, giving crystals of salt in 3-days.

Isolated yield: 85 %. ^{1}HNMR (600 MHz, DMSO-d_6): 12.5 (s, 1H), 8.24 (d, J = 6 Hz, 2H), 8.18-8.16 (m, 1H), 7.42 (d, J = 12 Hz, 2H), 7.19 (d, J = 4.8 Hz, 1H), 6.74 (d, J = 4.2 Hz, 1H), 6.54 (d, J = 8.4 Hz, 2H). IR (KBr, cm^{-1}): 3051 (m), 1681 (s), 1642 (s), 1597 (w), 1566 (m), 1524 (s), 1495 (s), 1422 (s), 1348 (m), 1322 (s), 1285 (m), 1180 (w), 1166 (m), 1145 (s), 1114 (m), 1088 (m), 1071 (s), 1031 (w), 1017 (w), 933 (m), 915 (m), 851 (m), 835 (w), 767 (s), 732 (s), 680 (s), 636 (s), 613 (w), 568 (m), 551 (m), 495 (w), 438 (s), 417 (m).

(HSTZ)[Zn(H26pdc)(26pdc)].2H_2O (5.2): To a solution of 2,6-pyridinedicarboxylic acid (167 mg, 1.0 mmol) in methanol (10 ml), a solution of zinc(II) acetate dihydrate (109 mg, 0.5 mmol) in methanol (10 ml) was added. A white precipitate was obtained after stirring for half an hour. The precipitate was dissolved by adding 20 ml of water and to this solution sulfathiazole (127 mg, 0.5 mmol) was added. The reaction mixture was stirred for 2hrs at room temperature. Further standing for 4 days at room temperature resulted in crystals of complex **5.2**. Isolated yield: 69 %. ^{1}H NMR (600 MHz, DMSO-d_6): 12.48 (s, 1H), 8.25 (d, J = 6 Hz, 4H), 8.19 (m, J = 6 Hz, 2H), 7.42 (d, J = 12 Hz, 2H), 7.19 (d, J = 6 Hz, 1H), 6.75 (d, J = 6 Hz, 1H), 6.55 (d, J = 12 Hz, 2H). IR (KBr, cm^{-1}): 2962 (m), 1618 (s), 1571 (s), 1518 (s), 1427 (m), 1371 (s), 1261 (s), 1186 (w), 1133 (m), 1076

TH-3622_196122001

(s), 1019 (m), 931 (m), 856 (m), 798 (s), 772 (m), 727 (m), 675 (s), 636 (m), 564 (m), 545 (m), 435 (m).

$(HSTZ)_2[Zn(26pdc)_2].(resorcinol).2H_2O$ (5.3): Sulfathiazole (255 mg, 1 mmol) was added to a solution of complex **5.2** (688 mg, 1 mmol) in methanol (10 ml) and stirred; a homogeneous solution was obtained. To this solution the resorcinol (220 mg, 2 mmol) was added and stirred for one hour. The solution was allowed to concentrate by self-evaporation at room temperature for 3 to 4 days. Off-white crystals of the respective complex were collected by decanting off the supernatant liquor. Isolated yield: 73 %. ^{1}H NMR (600 MHz, DMSO-d_6): 12.45 (s, 1H), 9.18 (s, 2H), 8.24 (m, J = 12 Hz, 4H), 8.19 (J = 6 Hz, 2H), 7.43 (d, J = 12 Hz, 2H), 7.19 (d, J = 6 Hz, 1H), 6.90 (t, J = 6 Hz, 1H), 6.74 (m, 1H), 6.55 (d, J = 6 Hz, 2H). 6.18 (d, 2H), 6.17 (s, 1H). IR (KBr, cm^{-1}): 3182 (w, br), 1603 (s), 1540(m), 1488 (s), 1367 (s), 1278 (s), 1166(m), 1143 (s), 1075 (m), 959 (m), 938 (m), 846 (m), 771 (m), 758 (m), 729 (m), 674 (s), 632 (m), 604 (w), 544 (m), 499 (m), 459 (m), 431(m).

$(HSTZ)_2[Zn(26pdc)_2].(3\text{-}NP).H_2O$ (5.4): Sulfathiazole (255 mg, 1 mmol) was added to a solution of complex **5.2** (688 mg, 1 mmol) in methanol (10 ml) and stirred; a homogeneous solution was obtained. To this solution 3-nitrophenol (278 mg, 2 mmol) was added and stirred for one hour. The solution was allowed to concentrate by self-evaporation at room temperature for 3 to 4 days. Off-white crystals of the respective complex were collected by decanting off the supernatant liquor. Isolated yield: 75 %. ^{1}H NMR (600 MHz, DMSO-d_6): 12.46 (s, 1H), 10.49 (s, 1H), 8.25 (m, J = 6 Hz, 4H), 8.19 (m, J = 6 Hz, 2H), 7.66 (d, J = 12 Hz, 1H), 7.55 (m, 1H), 7.48 (t, 1H), 7.42 (d, J = 12 Hz, 2H), 7.22 (m, 1H), 7.19 (d, J = 6 Hz, 1H), 6.75 (d, J = 6 Hz, 1H), 6.55 (d, J = 12 Hz, 2H). IR (KBr, cm^{-1}): 3384 (w), 2962 (m), 1623 (m), 1572 (m), 1518 (s), 1491 (m), 1431 (m), 1391 (m), 1345 (m), 1298 (m), 1259 (s), 1212 (m), 1188 (w), 1142 (m), 1089 (m), 1074 (s), 1017 (s), 933 (m), 873 (m), 849 (m), 793 (s), 771 (w), 761 (w), 731 (m), 704 (m), 670 (s), 631 (m), 602 (m), 567 (m), 554 (m), 502 (m), 457 (w), 434 (w).

5.9. References

1. J. F. Powell, Isolation of dipicolinic acid (pyridine-2:6-dicarboxylic acid) from spores of Bacillus megatherium, *Biochem. J.*, 1953, **54**, 210–211.

TH-3622_196122001

2. B. Das and J. B. Baruah, Supramolecular synthons and hydrates in stabilization of multicomponent crystals of nicotinamide and isonicotinamide with N-containing aromatic dicarboxylic acids, *Cryst. Growth Des.*, 2011, **11**, 5522–5532.
3. B. Bankiewicz and S. Wojtulewski, Two new cocrystals of the dipicolinic acid: Hirshfeld atom refinement of crystal structures and quantum theory of atoms in molecules analysis of molecular complexes, *Cryst. Growth Des.*, 2019, **19**, 6860–6872.
4. J. W. Steed, The role of co-crystals in pharmaceutical design, *Trends Pharm. Sci.*, 2013, **34**, 185–193.
5. L. Yang, D. C. Crans, S. M. Miller, A. la Cour, O. P. Anderson, P. M. Kaszynski, M. E. Godzala, La T. D. Austin and G. R. Willsky, Cobalt(II) and Cobalt(III) Dipicolinate Complexes: Solid State, Solution, and in Vivo Insulin-like Properties, *Inorg. Chem.*, 2002, **41**, 4859–4871.
6. B. Das and J. B. Baruah, Assembling of copper(II) dipicolinate complexes, *Polyhedron*, 2012, **31**, 361–367.
7. M. Karimi-Jafari, L. Padrela, G. M. Walker and D. M. Croker, Creating cocrystals: a review of pharmaceutical cocrystal preparation routes and applications, *Cryst. Growth Des.*, 2018, **18**, 6370–6387.
8. P. Cerreia Vioglio, M. R. Chierotti and R. Gobetto, Pharmaceutical aspects of salt and cocrystal forms of APIs and characterization challenges, *Adv. Drug Delivery Rev.*, 2017, **117**, 86–110.
9. N. K. Duggirala, M. L. Perry, O. Almarsson and M. J. Zaworotko, Pharmaceutical cocrystals: along the path to improved medicines, *Chem. Commun.*, 2016, **52**, 640–655.
10. Z. Li and A. J. Matzger, Influence of coformer stoichiometric ratio on pharmaceutical cocrystal dissolution: three cocrystals of carbamazepine/4-aminobenzoic acid, *Mol. Pharmaceutics*, 2016, **13**, 990–995.
11. X.-Q. Ma, C. Zhuang, B.-C. Wang, Y.-F. Huang, Q. Chen and N. Lin, Cocrystal of apigenin with higher solubility, enhanced oral bioavailability, and anti-inflammatory effect, *Cryst. Growth Des.*, 2019, **19**, 5531–5537.
12. D. Braga, F. Grepioni and O. Shemchuk, Organic–inorganic ionic co-crystals: a new class of multipurpose compounds, *CrystEngComm*, 2018, **20**, 2212–2220.
13. O. Shemchuk, D. Braga, F. Grepioni and R. J. Turner, Co-crystallization of antibacterials with inorganic salts: paving the way to activity enhancement, *RSC Adv.*, 2020, **10**, 2146–2149.
14. L. Casali, L. Mazzei, O. Shemchuk, K. Honer, F. Grepioni, S. Ciurli, D. Braga and J. Baltrusaitis, Smart urea ionic co-crystals with enhanced urease inhibition activity for improved nitrogen cycle management, *Chem. Commun.*, 2018, **54**, 7637–7640.
15. L. Sun, K. Hu, S. Jin, Y. Lu, C. Xu, B. Liu, D. Wang and G. Xia, Single-crystal and molecular structures of five hydrogen-bonding supramolecular salts based on 4-aminobenzoic acid, 2-aminobenzoic acid and acidic components, *J. Mol. Struct.*, 2019, **1178**, 229–241.
16. G. Smith, D. E. Lynch, K. A. Byriel and C. H. L. Kennard, Molecular cocrystals of carboxylic acids. XX. The crystal structures of 3,5-dinitrosalicylic acid and its adducts with the isomeric monoaminobenzoic acids, *Aust. J. Chem.*, 1995, **48**, 1133–1149.
17. A. O. L. E. Vora, C. E. S. Bernardes, M. F. M. Piedade and A. C. L. Conceic, da M. E. M. Piedade, Energetics of glycine cocrystal or salt formation with two regioisomers: fumaric acid and maleic acid, *Cryst. Growth Des.*, 2019, **19**, 5054–5064.
18. D. Kalita and J. B. Baruah, Visual distinction of dicarboxylic acids and their salts by 1-phenyl-3-(quinolin-5-yl)urea, *J. Mol. Struct.*, 2010, **969**, 75–82.

TH-3622_196122001

19. S. Ghosh, P. P. Bag and C. M. Reddy, Co-crystals of sulfamethazine with some carboxylic acids and amides: co-former assisted tautomerism in an active pharmaceutical ingredient and hydrogen bond competition study, *Cryst. Growth Des.*, 2011, **11**, 3489–3503.
20. S. Aitipamula, P. S. Chow and R. B. H. Tan, The solvates of sulfamerazine: structural, thermochemical, and desolvation studies, *CrystEngComm*, 2012, **14**, 691–699.
21. M. Oruganti and D. R. Trivedi, 4-Nitrobenzoic acid–sulfathiazole (1/1), *Acta Crystallogr.*, 2014, **E70**, o85–o86.
22. M. R. Caira, Sulfa drugs as model cocrystal formers, *Mol. Pharm.*, 2007, **4**, 310–316.
23. S. Domingos, A. Fernandes, M. T. Duarte, M. F. M. Piedade and M. Piedade, New multicomponent sulfadimethoxine crystal forms: sulfonamides as participants in supramolecular interactions, *Cryst. Growth Des.*, 2016, **16**, 1879–1892.
24. R. Samanta, S. Kanaujia and C. M. Reddy, New co-crystal and salt form of sulfathiazole with carboxylic acid and amide, *J. Chem. Sci.*, 2014, **126**, 1363–1367.
25. X. Pan, Y. Zheng, R. Chen, S. Qiu, Z. Chen, W. Rao, S. Chen, Y. You, J. Lü, L. Xu and X. Guan, Cocrystal of sulfamethazine and p-aminobenzoic acid: structural establishment and enhanced antibacterial, *Cryst. Growth Des.*, 2019, **19**, 2455–2460.
26. X. Zhang, L. Zhou, C. Wang, Y. Li, Y. Wu, M. Zhang and Q. Yin, Insight into the role of hydrogen bonding in the molecular self-assembly process of sulfamethazine solvates, *Cryst. Growth Des.*, 2017, **17**, 6151–6157.
27. S. M. Tailor and U. H. Patel, Hirshfeld surface analysis of sulfameter (polymorph III), sulfameter dioxane monosolvate and sulfameter tetrahydrofuran monosolvate, all at 296 K, *Acta Crystallogr.*, 2015, **71C**, 944–953.
28. T. Wang, J. S. Stevens, T. Vetter, G. F. S. Whitehead, I. J. Vitorica-Yrezabal, H. Hao and A. J. Cruz-Cabeza, Salts, cocrystals, and ionic cocrystals of a "simple" tautomeric compound, *Cryst. Growth Des.*, 2018, **18**, 6973–6983.
29. M. P. Singh and J. B. Baruah, Combinations of tautomeric forms and neutral-cationic forms in the cocrystals of sulfamethazine with carboxylic acids, *ACS Omega*, 2019, **4**, 11609–11620.
30. S. Mohamed, A. A. Alwan, T. Friscic, A. J. Morris and M. Arhangelskis, Towards the systematic crystallisation of molecular ionic cocrystals: insights from computed crystal form landscapes, *Faraday Discuss.*, 2018, **211**, 401–424.
31. L. Song, O. Shemchuk, K. Robeyns, D. Braga, F. Grepioni and T. Leyssens, Ionic cocrystals of ttiracetam and levetiracetam: the importance of chirality for ionic cocrystals, *Cryst. Growth Des.*, 2019, **19**, 2446–2454.
32. M. U. Faroque, A. Mehmood, S. Noureen and M. Ahmed, Crystal engineering and electrostatic properties of co-crystals of pyrimethamine with benzoic acid and gallic acid, *J. Mol. Struct.*, 2020, **1214**, 128183.
33. S. Santra, B. Das and J. B. Baruah, Assembly of dipicolinic acid by alkali-metal cations, *J. Chem. Crystallogr.*, 2011, **41**, 1981–1987.
34. A. Suhonen, I. S. Morgan, E. Nauha, K. Helttunen, H. M. Tuononen and M. Nissinen, Effect of a rigid sulfonamide bond on molecular folding: a case study, *Cryst. Growth Des.*, 2015, **15**, 2602–2608.
35. A. Z. El-Sonbati, M. A. Diab, M. M. El-Halawany and N. E. Salam, Polymer complexes: XLXII-interplay of coordination π–π stacking and hydrogen bonding in supramolecular assembly of [sulfa drug derivatives-N,S:N,O] complexes, *Spectrochim. Acta: Mol. Biomol. Spectrosc.*, 2010, **77**, 755–766.

TH-3622_196122001

36. R. Kumar, S. K. Rai, P. Singh, A. Gaurav, P. Yadav, R. S. Khanna, H. Gupta and A. K. Tewari, Face-to-face stacking in sulfonamide-based bisethylene bridged heteroaromatic dimers, *RSC Adv.*, 2015, **5**, 97205–97211.
37. G. Gilli and P. Gilli, *The Nature of the Hydrogen Bond – IUCr Monographs on Crystallography-23*, Oxford University Press, New York, 2009.
38. M. C. Etter, Encoding and decoding hydrogen-bond patterns of organic compounds, *Acc. Chem. Res.*, 1990, **23**, 120–126.
39. K. Shankar, A. Kirillov and J. B. Baruah, A modular approach for molecular recognition by zinc dipicolinate complexes, *Dalton Trans.*, 2015, **44**, 14411–14423.
40. Y. S. de Oliveira, W. S. Costa, P. F. Borges, M. S. A. de Santana and A. P. Ayala, The design of novel metronidazole benzoate structures: exploring stoichiometric diversity, *Acta Crystallogr. Sec. C Struct. Chem.*, 2019, **75**, 483–495.
41. S. Kumar and A. Nanda, Approaches to design of pharmaceutical cocrystals: a review, *Mol. Cryst. Liq. Cryst.*, 2018, **6671**, 54–77.
42. S. Domingos, A. Fernandes, M. T. Duarte and M. F. M. Piedade, New multicomponent sulfadimethoxine crystal forms: sulfonamides as participants in supramolecular interactions, *Cryst. Growth Des.*, 2016, **16**, 1879–1892.
43. S. Sareen, G. Mathew and L. Joseph, Improvement in solubility of poor water-soluble drugs by solid dispersion, *Int. J. Pharm. Investig.*, 2012, **2**, 12–17.
44. G. Vedantam, G. G. Guay, N. E. Austria, S. Z. Doktor, B. P. Nichols, Characterization of Mutations Contributing to Sulfathiazole Resistance in Escherichia coli, *Antimicrobial Agents and Chemotherapy*, 1998, **42**, 88-93.

TH-3622_196122001

Appendix: Chapter 5

Physical Measurements: Infrared spectra of the solid samples were recorded on a Perkin-Elmer Spectrum-Two FT-IR spectrophotometer in the region 4000 - 400 cm^{-1} using attenuated total reflectance method. Powder X-ray diffraction patterns were recorded using Bruker powder X-ray diffractometer D2 phaser. Perkin Elmer Lamda-750 spectrometer was used to record the solid state UV-visible spectra by diffuse reflectance. The ^{1}H-NMR spectra were recorded on a BRUKER Ascend-600 MHz NMR spectrometer using TMS as the internal standard. Fluorescence emission spectra in solution were recorded on a Horiba Jobin Yvon Fluoromax-4 spectrofluorometer. The solvent used were from Merck, EMPLURA® grades. Molar conductance values were measured by using an Elico conductivity meter model CM-180.

Crystallographic Study: The diffraction data for the hydrates were collected by using a Bruker APEX-II CCD diffractometer at room temperature for all the crystals. The refinement of and cell reductions were carried out by using SAINT and XPREP software. Structures were solved by direct methods using SHELXS-97 and were refined by full-matrix least-squares on F^2 using SHELXL-14 and OLEX2 programs. All non-hydrogen atoms were refined in anisotropic approximation against F^2 of all reflections. Hydrogen atoms were placed at their geometric positions by riding and were refined in the isotropic approximation. The crystallographic parameters are listed in the Table A1.

Table A1: Crystallographic parameters of the salt and complexes **5.1-5.4**.

Parameters	**5.1**	**5.2**	**5.3**	**5.4**
Formula	$C_{16}H_{15}N_4O_{6.50}S_2$	$C_{23}H_{21}N_5O_{12}S_2Zn$	$C_{38}H_{36}N_8O_{16}S_4Zn$	$C_{38}H_{33}N_9O_{16}S_4Zn$
CCDC	1994461	1994462	1994463	1994464
Mol.wt.	431.44	688.94	1054.36	1065.34
Space group	I 2/a	P$\bar{1}$	C 2/c	C 2/c
a(Å)	13.0836(4)	7.3895(3)	34.0593(12)	34.0920(13)
b(Å)	10.2432(3)	14.2721(9)	7.0748(2)	7.1324(2)
c (Å)	27.0497(10)	14.6812(7)	36.7179(11)	37.2876(13)
α (°)	90	111.373(5)	90	90
β (°)	99.431(4)	96.644 (4)	105.420(3)	108.600(4)
γ (°)	90	101.692(5)	90	90

TH-3622_196122001

V (Å^3)	3576.1(2)	1381.09(13)	8529.2(5)	8593.2(5)
Density, g cm^{-3}	1.603	1.657	1.642	1.647
Abs. coeff., mm^{-1}	0.346	1.114	0.856	0.851
F (000)	1784	704	4336	4368
Total no. of reflections	3161	4878	7556	7585
Reflections, I > 2σ(I)	2703	4173	6322	6205
Max. θ/°	25.048	25.048	25.049	25.049
Ranges (h, k, l)	−15 ≤ h ≤ 13	−8 ≤ h ≤ 8	−33 ≤ h ≤ 40	−40 ≤ h ≤ 28
	−12 ≤ k ≤ 11	−15 ≤ k ≤ 16	−8 ≤ k ≤ 8	−8 ≤ k ≤ 5
	−32 ≤ l ≤ 32	−17 ≤ l ≤ 15	−38 ≤ l ≤ 43	−41 ≤ l ≤ 44
Complete to 2θ (%)	99.9	99.8	99.9	99.5
Data/restraints/parameters	3161/2/275	4878/0/420	7556/4/622	7585/0/627
GooF (F^2)	1.018	1.010	1.170	1.066
R indices [I > 2σ(I)]	0.0360	0.0338	0.0925	0.0438
wR_2 [I > 2σ(I)]	0.0938	0.0812	0.2326	0.0967
R indices (all data)	0.0434	0.0417	0.1071	0.0567
wR_2 (all data)	0.1009	0.0888	0.2404	0.1043

Table A2: Hydrogen bond parameters of salt and complexes.

Salt/Complexes	D-H···A	d_{D-H} (Å)	$d_{H\cdots A}$ (Å)	$d_{D\cdots A}$ (Å)	∠D-H···A (°)
5.1	N(1) –H(1A)...O(3) [1/2+x,-y,z]	0.89	1.92	2.792(2)	165
	N(1) –H(1B)...O(7) x,-1+y,z]	0.89	1.98	2.837(2)	161
	N(1) –H(1C)...N(18) [x,y,z]	0.89	2.07	2.923(2)	161
	N(3) –H(3A)...O(2) [-1/2+x,-y,z]	0.80(2)	2.05(3)	2.800(2)	156(2)
	O(4) –H(4A)...O(5) [-1/2+x,-y,z]	0.90(3)	1.61(3)	2.508(2)	177(3)
	O(7) –H(7A)...O(6) [-1/2+x,1-y,z]	0.86(3)	1.85(3)	2.6820(19)	164(3)
5.2	N(1) –H(1A)...O(5) [-1+x,y,z]	0.89	1.84	2.726(3)	174
	N(1) –H(1B)...N(2) [-x,-y,1-z]	0.89	2.24	3.060(3)	154
	N(1) –H(1C)...O(8) [x,y,z]	0.89	1.81	2.691(3)	171
	N(3) –H(3A)...O(6) [1-x,-y,1-z]	0.79 (3)	1.94 (3)	2.705 (4)	165(3)
	O(9) –H(9A)...O(11) [1+x,y,z]	0.82	1.66	2.449(3)	161
	O(11) –H(11A)...O(4) [x,y,z]	0.87(4)	1.82(4)	2.673(3)	164(4)
	O(11) –H(11B)...O(12) [x,y,z]	0.79(4)	1.94(5)	2.690(4)	158(4)
	O(12) –H(12D)...O(3) [1-x,1-y,-z]	0.79(4)	2.00(4)	2.785(3)	175(3)
	O(12) –H(12E)...O(2) [-x,1-y,1-z]	0.96(4)	1.95(4)	2.893(4)	167(4)
5.3	N(1) –H(1A)...O(10) [1/2-x,-1/2+y,1/2-z]	0.89	1.91	2.786(8)	170
	N(1) –H(1B)...O(9) [x,2-y,1/2+z]	0.89	1.95	2.765(9)	152
	N(1) –H(1C)...O(7) [1/2-x,1/2+y,1/2-z]	0.89	1.85	2.726(9)	170
	N(3) –H(3A)...N(5) [x,y,z]	0.87(6)	2.05(6)	2.919(12)	173(7)
	N(4) –H(4B)...O(11) [-1/2+x,-1/2+y,z]	0.89	1.86	2.685(9)	153
	N(4) –H(4C)...O(6) [-1/2+x,-3/2+y,z]	0.89	1.87	2.744(9)	167
	N(6) –H(6A)...N(2) [x,y,z]	0.86(7)	2.05(8)	2.895(11)	167(8)
	O(13) –H(13A)...O(5) [1/2-x,3/2-y,-z]	0.82	2.31	2.702(8)	110
	O(14) –H(14A)...O(16) [x,y,z]	0.82	1.95	2.768(13)	173
	O(15) –H(15A)...O(8) [x,y,z]	0.85	2.34	2.854(10)	120
	O(15) –H(15B)...O(9) [1/2-x,3/2-y,-z]	0.85	2.26	2.923(9)	135
	O(16) –H(16A)...O(2) [1/2-x,1/2+y,1/2-z]	0.85	2.19	3.014(13)	163

TH-3622_196122001

	O(16) –H(16B)...O(1) [x,y,z]	0.85	2.17	2.870(12)	140
5.4	N(1) –H(1A)...O(10) [x,y,z]	0.89	1.88	2.761(3)	170
	N(1) –H(1B)...O(7) [x,1+y,z]	0.89	1.84	2.727(3)	171
	N(1) –H(1C)...O(9) [1/2-x,5/2-y,-z]	0.89	1.97	2.787(3)	153
	N(3) –H(3A)...N(5) [1/2-x,1/2+y,1/2-z]	0.85 (5)	2.05 (5)	2.909(5)	165 (5)
	N(4) –H(4A)...O(6) [-1/2+x,-3/2+y,z]	0.89	1.85	2.726(4)	169
	N(4) –H(4B)...O(11) [-1/2+x,-1/2+y,z]	0.89	1.87	2.704(3)	155
	N(6) –H(6A)...N(2) [1/2-x,-1/2+y,1/2-z]	0.92 (4)	1.98(4)	2.880(4)	166 (4)
	O(13) –H(13A)...O(5) [1/2-x,3/2-y,-z]	0.82	1.86	2.665(4)	168
	O(16) –H(16A)...O(8) [x,y,z]	0.85	2.01	2.836(5)	163
	O(16) –H(16B)...O(9) [1/2-x,3/2-y,-z]	0.85	2.19	2.920(4)	143

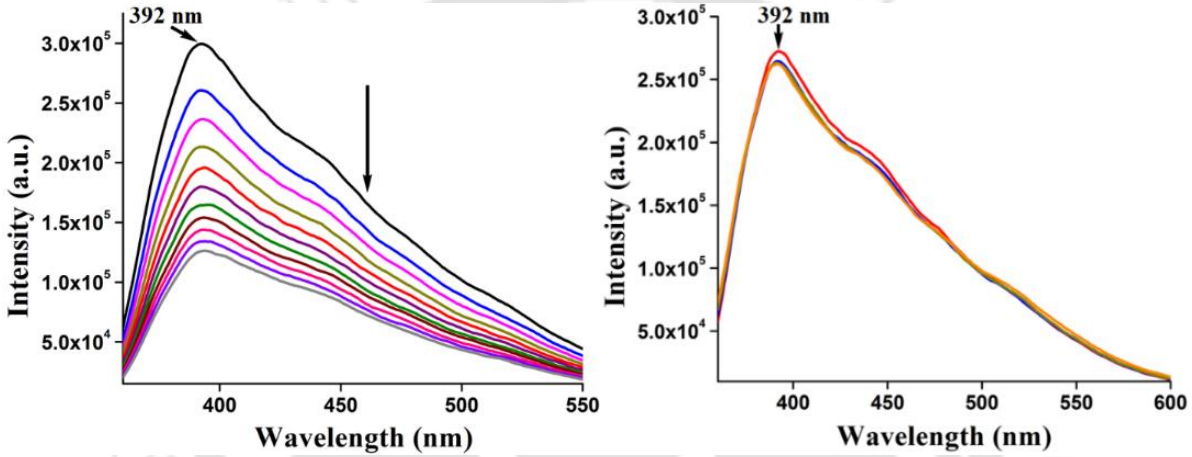

(a) (b)

Figure A1: Fluorescence titration of complex **5.3** (10^{-4} M in water) with **(a)** 3-Nitrophenol and **(b)** Resorcinol, (10 µL aliquot of 10^{-3} M in water). (ex. 330 nm)

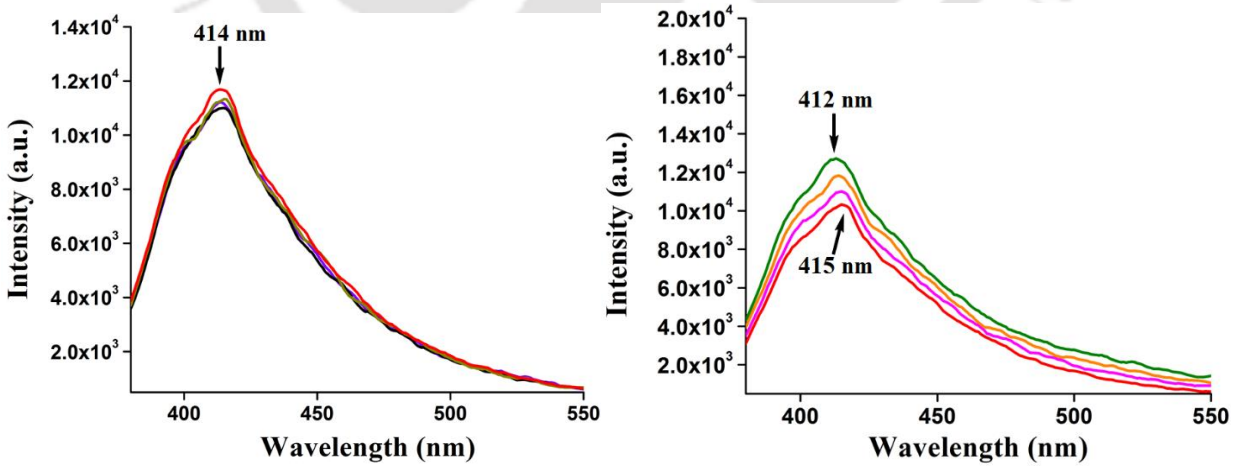

(a) (b)

Figure A2: Fluorescence titration of complex **5.4** (10^{-4} M in water) with **(a)** 3-Nitrophenol and **(b)** Resorcinol, (10 µL aliquot of 10^{-3} M in water). (ex. 330 nm)

TH-3622_196122001

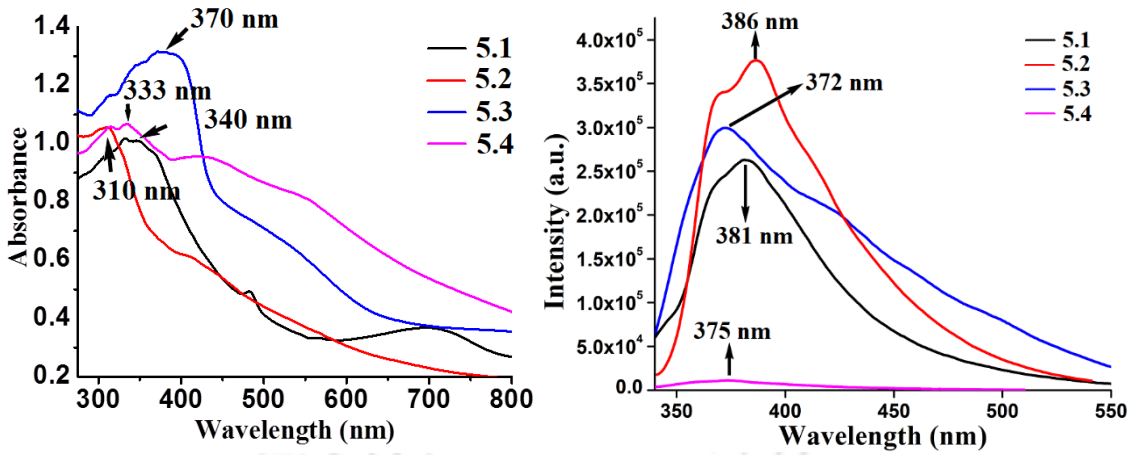

(a) (b)

Figure A3: (a) Solid state UV-spectra of compounds **5.1**- **5.4** and (b) solid state fluorescence spectra of compounds **5.1**- **5.4.**

Table A3: Excitation and emissions values of salt and complexes.

Salt/complexes	λ_{ex} (nm)	λ_{em} (nm)
5.1	320	381
5.2	330	386
5.3	340	372
5.4	360	375

Table A4: Colony forming unit count on *E. coli* DH5α by the API.

API[@]	Molecular wt. (in gms/mol)	Concentration (in µM)	% of sulfathiazole in compounds	Average % of relative CFU count/2.5 g	Average % of relative CFU count/µM
Sulfathiazole	255.3	9.79	100	23	2.34
5.1	431.5	5.79	59.2	59.5	10.27
5.2	689.0	3.62	37.0	65.2	18.01
5.3	1054.4	2.37	48.4	67.5	56.96
5.4	1065.3	2.34	47.9	58	49.57
Abbreviations: CFU, colony forming unit; @, 2.5 µg/ml of each API.					

TH-3622_196122001

Thesis Summary

The research work presented in the thesis has provided the salient features of various forms of ionic-cocrystals and hydrates of metal complexes derived from semi-flexible ditopic organic carboxylic acids with a flexible ditopic organic amine-base. The notable features were the isolation and characterization of compositionally different ionic-cocrystals formed by partial to complete proton transfer from acid to base. Having multiple numbers of differently protonated species and zwitterionic ions in cocrystals have opened a new dimension to explore. Depending on the local environment of the cations the solid-state fluorescence emission peaks were shifted to longer wave-lengths, which provided examples to shift the emission and to cause dual emissions. The conversion of mono-protonated species to diprotonated host-species in multi-component ionic-cocrystal is another significant finding in the course of the study. Structural variations in ionic-cocrystals highlighted distinctions in solvation environments, anion types, and intermolecular interactions.

Concentration-dependent crystallization enabled the isolation of stable and metastable hydrates of copper, cobalt and zinc complexes, with unit-cell transformations driven by π-stacking interactions. Uncommon observations of having four and half molecules of water of hydration and isolation of polymorphs of the same was significant and new observation. Polymorphs of the hydrate of this copper complex exhibited lamellar or Herringbone arrangements of anthracene groups due to π-stacking, and have opened up new possibility to study on the unit-cell coalescence to cause polymorphic transformations. Reversible transformations among the hydrates, transformations mediated by the solvent exchanges, had emphasized the role of hydrogen bonds, electrostatic interactions and π-stacking in structural stabilization. Dynamic aggregation studies revealed metal-ion-dependent assembling behaviors, influencing emission intensities in methanol-water mixtures. Additionally, the mono-deprotonated form Hpdc in cocrystals and complex having cation of sulfathiazole and the conversion of the complexes to metal-pdc complex by cocrystal formation have suggested the possibility of their modulation for drug availability in sulfathiazole derived complexes. Stabilization of self-assemblies with phenolic coformers through aromatic stacking allowed for tailored drug proportions and antibacterial activity.

TH-3622_196122001

List of Publications

1. **A. P. Singh**, M. P. Singh and J. B. Baruah, Changes in the proportions of an active pharmaceutical through cocrystals, *Drug Dev. Res.*, 2021, **1**, 1–10.

2. **A. P. Singh** and J. B. Baruah, Arrangements of fluorophores in the salts of imidazole tethered anthracene derivatives with pyridinedicarboxylic acids influencing photoluminescence, *Mater. Adv.*, 2022, **3**, 3513–3525.

3. **A. P. Singh** and J. B. Baruah, π-Stacking among the anthracenyl groups of a copper complex resulted in doubling of unit cell volume to provide new polymorphs, *ACS Omega*, 2023, **8**, 30776–30787.

4. **A. P. Singh** and J. B. Baruah, Lithium(I), cesium(I), barium(II) and cadmium(II) [2-(2,6-dichlorophenylamino)phenyl]acetate (diclofenac) complexes and coordination polymers, *Inorganica Chimica Acta*, 2024, **569**, 122131.

5. **A. P. Singh** and J. B. Baruah, Hydrates of N-(anthracen-9-ylmethyl)-3-(1H-imidazolium-1-yl)propan-1-ammonium zinc(II) or cobalt(II) 2,6-pyridinedicarboxylate: inter-conversions, assembling and utilities, *Inorg. Chem. Commun.*, 2024, **168**, 112883.

6. R. Brahma, **A. P. Singh** and J. B. Baruah, Synthesis and characterization of cis and trans cobalt(II) nalidixate complexes having 1-(4-chlorophenyl)-3-(pyridin-4-ylmethyl)urea ligand, *Dalton Trans.*, 2024, **53**, 14678–14691.

7. **A. P. Singh** and J. B. Baruah, Hydrates of N-((10-chloroanthracen-9-yl)methyl)-3-(1H-imidazol-1-yl)propan-1-ammonium cobalt(II), copper(II) and zinc(II) 2,6-pyridinedicarboxylate: reversible crystallization, *ACS Omega*, 2024, **9**, 47848–47856.

8. **A. P. Singh** and J. B. Baruah, Facts and reality of multi-component organic ionic-cocrystals of di-topic acid–base conjugates, *CrystEngComm*, 2025, **27**, 1701-1706.

TH-3622_196122001